Doping Approaches for Organic Semiconductors

Alberto D. Scaccabarozzi,[1†*] Aniruddha Basu,[1†] Filip Aniés,[3] Jian Liu,[2] Osnat Zapata-Arteaga,[4] Ross Warren, [5] Yuliar Firdaus,[1,7] Mohamad Insan Nugraha,[1] Yuanbao Lin,[1] Mariano Campoy-Quiles[4] Norbert Koch,[5] Christian Müller,[2] Leonidas Tsetseris,[6] Martin Heeney,[3] Thomas D. Anthopoulos[1*]

1. King Abdullah University of Science and Technology (KAUST), KAUST Solar Center (KSC), Thuwal 23955, Saudi Arabia

2. Department of Chemistry and Chemical Engineering, Chalmers University of Technology, Göteborg 412 96, Sweden

3. Department of Chemistry and Centre for Processable Electronics, Imperial College London, London, W12 0BZ , UK

4. Materials Science Institute of Barcelona, ICMAB-CSIC, Campus UAB, 08193 Bellaterra, Spain

5. Helmholtz-Zentrum Berlin für Materialien und Energie GmbH, Kekulé-Strasse 5, 12489 Berlin, Germany
Institut für Physik & IRIS Adlershof, Humboldt-Universität zu Berlin, 12489 Berlin, Germany

6. Department of Physics, National Technical University of Athens, Athens GR-15780, Greece

7. Research Center for Electronics and Telecommunication, Indonesian Institute of Science, Jalan Sangkuriang Komplek LIPI Building 20 level 4, Bandung 40135, Indonesia

† Authors contributed to this work equally
Corresponding authors: thomas.anthopoulos@kaust.edu.sa; alberto.scaccabarozzi@kaust.edu.sa

Abstract

Electronic doping in organic materials has remained an elusive concept for several decades. It drew considerable attention in the early days in the quest for organic materials with high electrical conductivity, paving the way for the pioneering work on pristine organic semiconductors (OSCs) and their eventual use in a plethora of applications. Despite this early trend, however, recent strides in the field of organic electronics have been made hand in hand with the development and use of dopants to a point that are now ubiquitous. This article attempts to provide an overview of all important advances in the area of doping of organic semiconductors and their applications. We first review the relevant literature with particular focus on the physical processes involved, discussing established mechanisms but also newly proposed theories. We then continue with a comprehensive summary of the most widely studied dopants to date placing particular emphasis on the chemical strategies towards the synthesis of molecules with improved functionality. The processing routes towards doped organic films and the important doping-processing-nanostructure relationships, are also discussed. We conclude the review by highlighting how doping can enhance the operating characteristics of various organic devices.

TOC Graphic

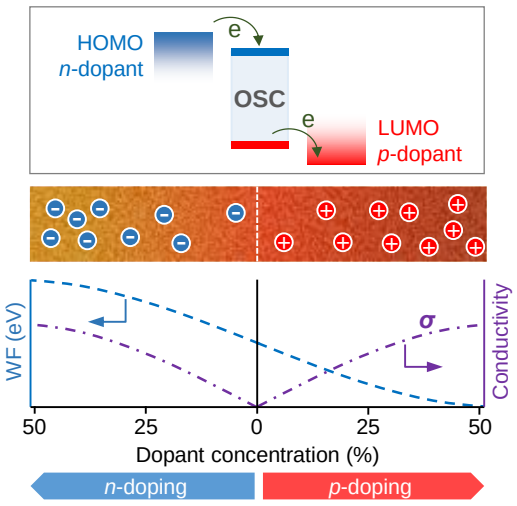

Table of Content

1. Introduction

The electronics revolution represents one of the major milestones of the 20th century with profound consequences on our society. To this end, organic electronics represent a new technological paradigm, similar to what the semiconductor industry achieved with the advent of silicon microelectronics.[1–5] Indeed, the deployment of organic semiconductors promises to widen the realm of electronics to countless new applications, thanks to their numerous advantageous properties.[6–8] A notable example is the organic light-emitting diode (OLED), that forged ahead since its discovery in 1987 and is now widely employed by the display and lighting industry, featuring devices that are light-weight and even flexible.[9–12] However, the exploitation of organic electronics in other applications, *e.g.,* thin-film transistors (TFTs) or photovoltaics (PVs), has been progressing slower than expected due to difficulties in delivering high performance and reliability.

A crucial element that unlocked the touted potential of organic electronics is electronic doping and here again, OLEDs serve as the prototypical example. It was only when doped charge transport layers were introduced in standard device architectures, that light-emitting diodes reached the performance and the technological maturity required for industrialization.[13,14] Furthermore, in recent years there has been a progressive transition from the straightforward use of dopants in highly conducting layers, to their incorporation into other fundamental parts of the devices. Active layers, for instance, have been almost entirely relying, until very recently, on pristine (*i.e.,* non-doped) organic semiconductors, in strong contrast to the typical approach exploited in classic inorganic semiconductors, *e.g.,* silicon. Indeed, the interaction between dopants and organic semiconductors typically occurs through weak interactions and therefore the fabrication of a stable doped junction, as in inorganics, is highly challenging. For instance, the fabrication approach employed in organic thin-film transistors (OTFTs) is commonly based on the use of a single component, pristine semiconductor that is used to bridge the source and drain electrodes to form the channel. Extensive efforts in optimizing structure-property relationships in these layers led to a level of device optimization that pushed this approach to its limits. In this context, the employment of multicomponent systems and in particular that of dopants, paved the way for new possibilities, enabling the demonstration of organic electronic devices with unprecedented performance.[15–21] Similarly, the recent use of molecular dopants in bulk heterojunctions (BHJs) of various organic photovoltaics (OPV) is paving the way to improved power conversion efficiencies (PCEs) that are projected to exceed the benchmark value of 20% for single-junction devices.[22–25] Moreover,

the ability to incorporate large amounts of dopants into organic semiconductors and thus achieve high electrical conductivity has been attracting a growing interest, owing to their potential use in new forms of thermoelectric generators.[26,27] However, as promising and fascinating as the doping strategy is, there are still a lot of unexplored paths, and despite the plethora of possible molecules that have been designed, most of the focus in device applications has been limited on a handful of material systems.

In this review article we discuss recent advances in the application of doping strategies for organic semiconductors. We will briefly review the fundamentals of doping in organics and the physical processes involved. We then address the relevant theoretical and computational work while highlighting the open questions related to the doping mechanisms. Further, we attempt to provide chemical insights, summarizing the most popular materials used as dopants and the novel molecular species that are emerging, with an emphasis on the chemical strategies towards the design of improved molecular dopants and their hosts. We then address the different processing methods for realizing doped films, discussing the routes towards high doping efficiency and the impact on the nanostructure of the host organic material(s). Finally, we highlight how doping has been exploited to control the operation of organic devices and in some cases to even enhance their performance. Full names of materials mentioned in this article and their chemical structures are given in the *Supporting Information* section, if not indicated.

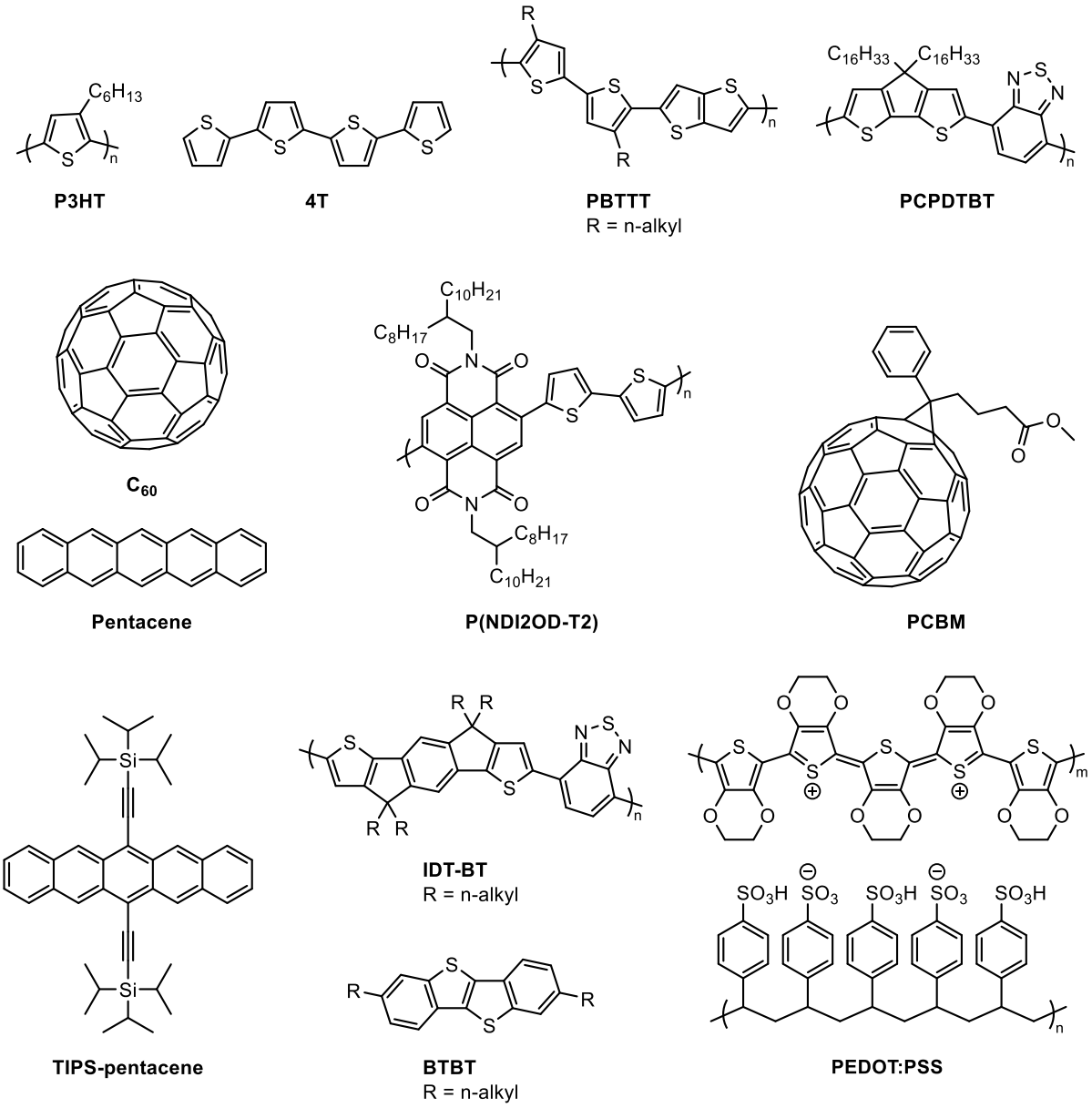

Figure 1: Chemical structure of selected OSCs.

2. Molecular doping of Organic Semiconductors

2.1. Physical Processes

In this section we discuss the physical processes relevant to doping of organic semiconductors (OSCs), starting from the orbital levels of single molecules and building up to the density of states for a thin film. We discuss the different doping mechanisms occurring in this class of materials and we cover the effect of doping on charge carrier density and transport in organic films. Finally, we provide a summary on the electrical contact formed between a metal and a doped organic semiconductor.

2.1.1. Density of states

2.1.1.1. Molecular orbital levels of a single molecule

The highest occupied molecular orbital (HOMO) and lowest unoccupied molecular orbital (LUMO) levels for molecular semiconductors and the valence band maximum and conduction band minimum for polymer semiconductors, play a key role in determining the electronic and optical properties of the materials, and are particularly important for the doping process. In the following, the terms HOMO/LUMO are used synonymously for valence/conduction bands, but it is pointed out that the reader should keep in mind the differences when considering a specific material. The localized electron wavefunctions of a molecule are in contrast to delocalized ones in polymers, which can result in one-dimensional dispersive electronic bands. For a single molecule in isolation, the energy of the HOMO level is considered equivalent to the vertical ionization energy (IE) - that is the energy required to remove an electron and place it at rest, in a vacuum, and infinitely far away from the molecule. Similarly, the electron affinity (EA), equivalent to the LUMO level for an isolated molecule, is defined as the energy gained by adding an electron to the molecule from infinitely far away.[28] The energy gap between the IE and EA defines the fundamental gap and can be measured experimentally for single molecules *via* a combination of gas-phase direct and inverse photoelectron spectroscopy (IPES).[29] The ionization energy and ionization potential are identical for an isolated molecule in vacuum, however, for solids, these two terms may take on different values. In a simple picture, the ionization potential is the energy difference between the HOMO level and the electrostatic potential at an infinite distance. The latter is often referred to as vacuum level and is commonly set to zero. The IE is the experimentally determined quantity, and can differ from the ionization potential if the electron removed from the HOMO level has to pass through a non-trivial electrostatic landscape. For example, this can be a surface dipole, requiring additional energy for electron removal compared to the ionization potential. As a final point regarding definitions, both the EA and IE have positive values below the vacuum level. Therefore, an increase of EA or IE signifies more tightly bound molecular energy levels.

2.1.1.2. Single molecules to thin films

While the IE and EA are well-defined values for a single or gas-phase molecule, environmental interactions in a condensed phase make measurements and calculations of these parameters dependent on the technique that is employed (see also section 2.5) and on the molecular organization within films. The IE and EA can be accurately determined through a combination of UPS and IPES. Alternatively, cyclic voltammetry (CV) is often used, where molecules in

solution or thin polymer films deposited on an electrode are electrochemically oxidized/reduced. It should be noted that CV only provides approximate values because it does not fully capture solid-state effects (cf. discussion below) and is sensitive to the precise experimental conditions.[30,31] For example, the IE of pentacene (cf. chemical structure in Figure 1) was found to be about 1.5 eV smaller in the solid phase as compared to gas phase.[32] Furthermore, variations by up to 1 eV in solid-state IE have been reported for films of the same compound but with different molecular orientation, e.g., edge-on *vs.* face-on with respect to the substrate.[33–35] These observations highlight the importance of carefully considering all solid-state effects that impact IE and EA, as briefly summarized in the following.

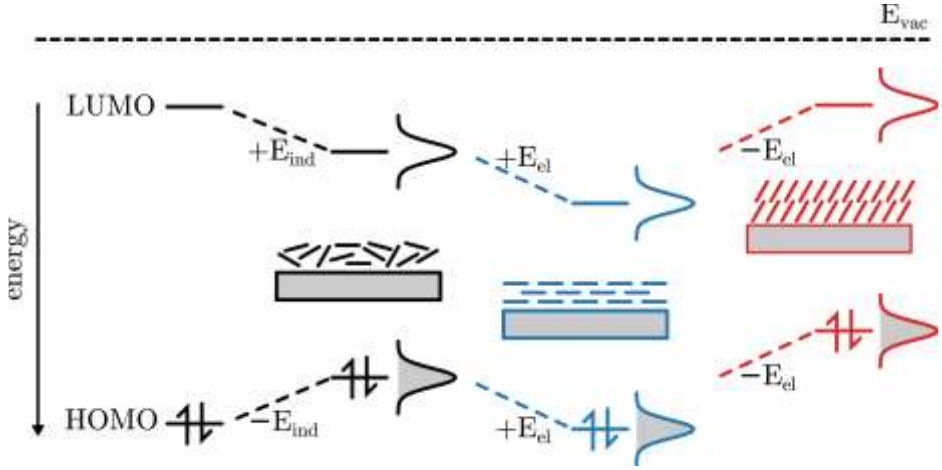

Figure 2: Drawing of the energy level shifts from single molecules to solids. The induction (or polarization) E_{ind} interactions act to stabilize the energy levels in a molecular solid with respect to the single molecule values. In crystalline or poly-crystalline films, the molecular ordering results in a further electrostatic shift labelled E_{el}. This interaction arises as a consequence of permanent charge distributions, resulting in the HOMO and LUMO manifolds shifting in the same direction, and by equal magnitude. The direction of the energy level shift depends upon the molecular orientation.

Figure 2 depicts the shift in HOMO and LUMO level energy upon going from a single molecule to a molecular solid. Firstly, induction interactions E_{ind} of a created charge with the surrounding molecules act to change the energy levels, with the IE decreasing and the EA increasing. Consequently, the fundamental gap becomes narrower. This electronic polarization by the dielectric environment[36,37] can be sizable (in the range of 1-2 eV), and it may even differ for an electron and a hole.[38] Secondly, collective electrostatic interactions E_{el} arising from permanent charge distributions of the molecule and its environment can lead to parallel shifts on the order of 1 eV of the IE and EA, i.e., the fundamental gap remains unchanged. This phenomenon is restricted to ordered molecular assemblies, e.g., crystalline films, as only the collective action of molecular bond-dipoles and quadrupoles,[35,39,40] as leading terms, give rise to electrostatic potential shifts in the far-field. Examples are rod-like molecules, such as many

oligomers and planar molecules, for which – in crystalline thin films – the EA and IE depend strongly on the molecular orientation with respect to surface,[35,38–41] and the same holds for ordered polymer films.[39] Further modification of the IE and EA of organic crystals can originate from a considerable overlap of HOMO and LUMO orbitals between neighboring molecules. In that case, delocalized and dispersive electronic bands emerge from the otherwise localized electronic states, and sizable bandwidths on the order of several 100 meV have been determined.[42]

In general, the energy levels of molecules in the solid are determined by the interactions with the environment, and thus strongly depend on the distance and mutual orientation of the molecules in the solid. To date, most studies on doped organic semiconductors are concerned with amorphous and polycrystalline materials. Studies on single crystals with low dopant concentration face the challenge of dispersing the dopants homogenously in the sample, but future efforts in this direction could be very rewarding. In the following sections, we focus on disordered systems described using Gaussian distributions. Readers interested in ordered materials, e.g. single crystals, and descriptions using alternative DOS distributions of the states relevant for charge transport, e.g. exponential, are referred to previous studies references [42–44].

In a disordered solid, the environmental interaction/parameters are randomly distributed, producing local energy level shifts with a similar random distribution. The Central Limit Theorem states that the sum of a group of random independent variables tends towards a normal distribution, even if the variables do not follow a normal distribution themselves. Therefore, the resulting spread of energy states per unit volume, termed the density of states (DOS), is described with a Gaussian function centered around a mean value with standard deviation σ_{DOS}, which can be thought of as a disorder parameter. Energetic disorder encompasses intermolecular effects, as well as on-site variations. Changes in conjugation length, configuration, conformation, the relative orientation of molecules, and the presence of chemical defects, all contribute to even greater disorder in the DOS.[45–47] The population of molecular vibrational and librational modes, as a function of temperature, impact the time-averaged DOS in an analogous manner.

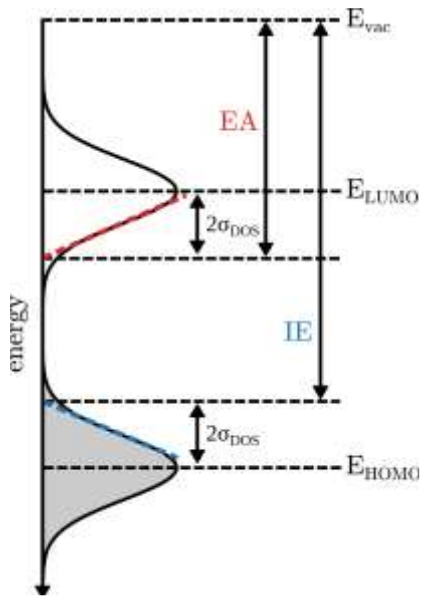

Figure 3: Gaussian approximation for the density of states (DOS) of a molecular solid. Two Gaussian distributions representing the occupied HOMO and unoccupied LUMO manifold are shown. They are centered around E_{HOMO} and E_{LUMO}, respectively. With this Gaussian approximation for the DOS, the IE and EA are commonly defined by linear extrapolation from the curve's inflection point towards zero, as shown, with the y-axis intercept at $2\sigma_{DOS}$ from the DOS centre.

Figure 3 shows Gaussian distributions representing the HOMO and LUMO manifolds in a molecular solid. The two distributions are centered around E_{HOMO} and $E_{LUMO,}$ and have an identical standard deviation σ. With this Gaussian approximation for the DOS, the IE and EA are commonly defined by linear extrapolation from the curve's inflection point towards zero, as shown, with the y-axis intercept at $2\sigma_{DOS}$ from the DOS center. It follows that in the disordered molecular solid, about 2.3 % of the molecules will have lower IE than determined *via* extrapolation, and likewise the same fraction of molecules will have a higher EA. Clear knowledge of the meaning of IE and EA is critical as these values often form the basis for selecting host and dopant combinations.

2.1.2. **Doping Processes**

Doping in OSCs is associated with complex mechanisms, many of which have been investigated using different approaches.[26,48–52] Yet, and despite the plethora of processes that have been reported, a complete understanding is still emerging. The large majority of molecular dopants are classified as neutral molecules that purely undergo an electron transfer with the OSC, without involving any chemical reaction. The electron transfer is believed to undergo two types of mechanisms: either ion-pair (IP) formation or charge-transfer complex (CTC) formation. Nevertheless, other dopants have been reported to undergo chemical reactions with

the OSC, and as a consequence, these systems are characterized by specific doping routes. In the following sections, we will discuss the different theories on doping of OSCs that have been reported, beginning with standard mechanisms and discussing the evolution of the dopants in that context.

2.1.2.1. Ion-pair formation

The basic doping mechanism in organic semiconductors is believed to undergo an electron transfer process from the OSC to the dopant (p-type doping) or from the dopant to the OSC (n-type doping).[13,26,57,58,48–51,53–56] Therefore, the IE and EA values of the OSC and the dopant play a major part in this process. For p-type doping, the EA of the dopant should ideally be equal or higher than the IE of the OSC, allowing the dopant to accept an electron into its LUMO from the HOMO of the OSC, resulting in a paired dopant anion and OSC cation.[48] For n-type doping, the opposite process occurs. That is, the OSC accepts an electron into its LUMO from the HOMO of the dopant and hence, the IP is formed between the dopant cation and OSC anion (Figure 4).

Spectroscopic evidence from several studies supports the formation of the IP in various systems.[48,49,56,57] The nature of the charge introduced into the OSC is not simply that of an excess electron or hole. Indeed, the charge formation is accompanied by a perturbation of the crystal lattice of the OSC, owing to the strong electron-phonon interactions in this class of materials, leading to an electronic charge dressed by phonon clouds. In condensed matter physics, this is defined as a quasi-particle, the polaron,[59] which in this case is localized on a single molecular site or conjugated polymer segment. During charge transport, the polaron, *i.e.*, the charge and its associated distortion, moves through other molecular locations, carrying the lattice distortion with itself. In the case of an amorphous OSC, the nature of the perturbation is associated with a structural distortions of the organic molecule. If a further charge is introduced into the semiconductor, two possibilities exist. The first is that a new polaron is formed in a different polymer segment or molecular site; the second is that the charge is added to an existing polaron. In the latter case, a new quasi-particle is formed, the bipolaron, which is defined as a pair of charges coupled with a strong distortion (a phonon cloud). The energetic condition for the formation of a bipolaron is that the Coulombic repulsion between the two charges needs to be smaller than the stability gained through nuclear reorganization.[60]

Following charge transfer, the hole on the host semiconductor must dissociate from the negatively ionized dopant in order to become a mobile carrier. The binding energy E_b of the IP

is approximated considering the Coulomb interaction between them (ignoring induction effects)

$$E_b(r) = \frac{e^2}{4\pi\varepsilon_0\varepsilon_r}\frac{1}{r} \tag{1}$$

where r is the charge-ionized dopant distance of separation. Taking a typical static dielectric constant of $\varepsilon_r \approx 3$ for apolar organic semiconductors[61,62] and an intermolecular distance of r ≈ 1 nm, yields a binding energy of $E_b \approx 0.5$ eV. As this approximate binding energy far exceeds the thermal energy at room temperature (kT = 25 meV), only a small fraction of charges will dissociate. However, this simple model neglects other effects, which reduce the barrier to dissociation, such as Coulomb potential overlap between nearby dopant ions,[52] energetic disorder,[63] and entropic contributions.[64]

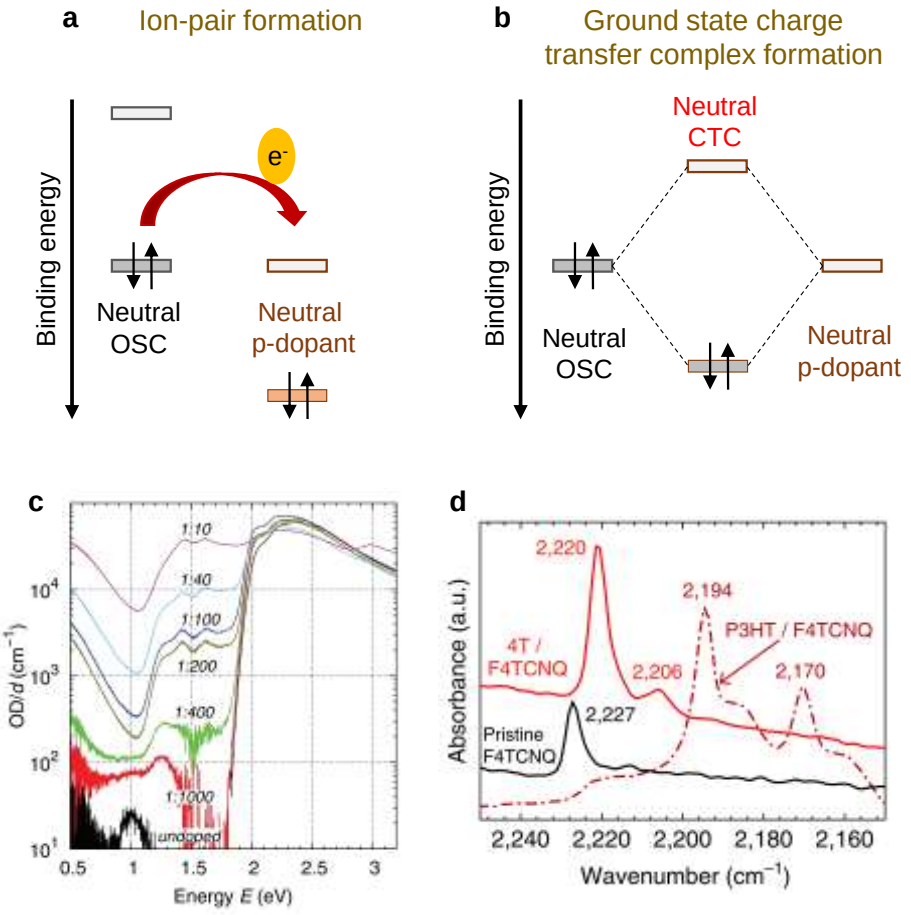

Figure 4: a) IP formation and b) ground state CTC formation. Adapted with permission from ref [48]. Copyright 2016 American Chemical Society. c) Absorbance spectra of undoped and F_4-TCNQ-doped P3HT films after thickness normalization (Reprinted with permission from ref [65]. Copyright 2013 American Physical Society). d) Infrared spectrum for F_4-TCNQ-doped 4T (solid line) and P3HT film (dot-dashed line). Reprinted with permission from ref [66]. Copyright 2015 Méndez et al. under Creative Commons Attribution 4.0 International License http://creativecommons.org/licenses/by/4.0/.

2.1.2.2. Charge-transfer complex formation

Another well-known mechanism for OSC doping involves the formation of CTCs. According to the latter, the frontier orbitals of OSC and dopant undergo hybridization to form a new set of occupied ($HOMO_{CTC}$) bonding and unoccupied ($LUMO_{CTC}$) antibonding orbitals.[26,48–51,67,68] In contrast with the IP mechanism, CTC formation can also form in systems having $EA_{dopant} << IE_{OSC}$ (for p-type doping) and $IE_{dopant} >> EA_{OSC}$ (for n-type doping).[48,66,69] The degree of hybridization and energy level splitting are concomitant with the extent of orbital overlap as well as with the energy level mismatch between OSC and dopant. The amount of charge transfer (δ) can be determined by the relative amplitude of these newly formed energy levels and can involve non-integer charge transfer.[48,66,69] Interestingly, a dopant can undergo both IP or CTC formation depending on the particular host semiconductor. For instance, in the case of F_4-TCNQ doping of a thiophene oligomer, quaterthiophene (4T, cf. chemical structure in Figure 1), Fourier transform infrared spectroscopy (FTIR) shows a redshift of the cyano (C≡N) peak of about 7 cm^{-1}, compared to the 30-33 cm^{-1} shift for the same dopant in P3HT, where IP formation is observed (Figure 4d).[66–68] These features indicate that a partial charge transfer (δ = 0.21-0.25) is involved for 4T owing to CTC, unlike IP. Although this partial charge transfer cannot produce charge carriers directly in the OSC, the partial charge transfer is achieved through an integer charge transfer (ICT) from the neutral OSC to CTC, where the CTC acts as a dopant for the undoped OSC.[66] However, the ICT is a non-spontaneous process that comprises substantial activation energy. Hence, not all CTCs are involved in the charge carrier generation, which eventually leads to lower carrier density and electrical conductivity compared to the IP mechanism. For example, under the same doping condition, the highest electrical conductivity (σ) of P3HT (IP mechanism) was observed to be 1 S cm^{-1} compared to 10^{-3} S cm^{-1} for 4T (CTC mechanism).[26,66] Nevertheless, due to the high complexity of the doping mechanism, it is still an open question to predict whether CTC or IP formation will take place in a given dopant/OSC system. Indeed, several factors dictate which mechanism would occur/prevail, such as dopant strength, charge carrier localization on OSCs, energy level offset, electron-hole interaction, spin relaxation, and disorder.[26] Therefore, further studies on the electronic structure of dopant/OSC systems and on hybridization effects are still required in order to advance our understanding of the relevant processes/relationships and as such improve our predictive power.

2.1.2.3. **Other doping processes**

Recently, non-conventional doping methods have been reported where the doping mechanism indeed undergoes an electron transfer process but no evidence for the formation of IP or CTC can be found. The chemical structures and a comprehensive discussion of the materials discussed hereafter are reported in Section 2.3. Goel *et al*. reported a p-doping route of a polymeric semiconductor (OSC-1) where a radical cation salt (OSC-2) is used as a dopant.[70] A similar process occurs when the polymer is doped with the strong oxidant tris(4-bromophenyl)ammoniumyl hexachloroantimonate (Magic Blue).[71,72] The doping occurs due to the electron transfer from the fully occupied $HOMO_{OSC\text{-}1}$ to the partially occupied $HOMO_{OSC\text{-}2}$. This process results in the reduction of OSC-2 and the resulting doped system becomes the mixture of both hole conductors.

Apart from the electron transfer processes, a few other doping mechanisms have also been reported for different dopant/OSC systems. The proton (H^+) related doping process is one of them, where the dopant introduces a proton to the OSC backbone to ionize the host. This charge is eventually redistributed via conjugation effects and the corresponding anion moiety enters into the system for electric neutrality.[26] The latter doping process is predominantly observed in polymeric OSCs due to the presence of extended conjugation in their backbones. For example, 4-ethylbenzenesulfonic acid (EBSA) has been used as a proton dopant in poly[2,5-bis(3-alkylthiophen-2-yl)thieno(3,2-b)thiophene] (PBTTT, cf. chemical structure in Figure 1) for thermoelectric applications, where a substantial improvement in the OSC conductivity was observed upon doping.[73] However, this type of doping is reversible and spontaneous de-doping occurs in presence of a base. In some cases, the acid does not lead to protonation of the conjugated backbone but mediates oxidation by O_2.[74–76] On the other hand, hydride (H^-) doping is an irreversible process, although the doping mechanism is still under debate. The doping reaction is believed to occur in the solution phase, either by hydride transfer or by electron transfer from the dopant to the OSC, both leading to the formation of CTC along with some byproducts (see Section 2.2.2).[77,78] As discussed earlier, the dissociation of the CTC is the key for the effective charge carrier generation and hence, CTC with lower binding energy favors an effective doping process. Zeng *et al*. used (4-(1,3-dimethyl-2,3-dihydro-1H-benzoimidazol-2-yl)phenyl)dimethyl-amine (N-DMBI) (cf. chemical structure in Figure 12) as a hydride dopant in two polymers with different EA values.[78] Spontaneous doping was found to happen in the polymer with a higher EA value at room temperature.

Lewis acid and base doping are also emerging doping methods recently explored in the area of OSCs (see Section 2.2.2). For example, boron trifluoride (BF_3), a non-oxidative Lewis acid, was used to p-dope poly(p-phenylene vinylene) (PPV) with the process argued to rely on the formation of a coordination bond between BF_3 and a vinyl group of PPV, which ultimately induces a positive charge in the backbone.[79,80] To gain a better understanding of the mechanism involved, Yurash *et al*. conducted a systematic study of the Lewis acid doping in organic semiconductors with strong (poly[2,6-(4,4-bis-(2-ethylhexyl)-4H-cyclopenta [2,1-b;3,4-b′]dithiophene)-alt-4,7(2,1,3-benzothiadiazole)] (PCPDTPT, cf. chemical structure in Figure 1)) and weak (poly[2,6-(4,4-bis-(2-ethylhexyl)-4H-cyclopenta [2,1-b;3,4-b′]dithiophene)-alt-4,7(2,1,3-benzothiadiazole)] (PCPDTBT)) Lewis basic sites and compared them with classic electron-transfer dopants and Brønsted dopants.[81] According to the suggested mechanism, doping occurs in three steps:

1) Formation of an acidic (Bronsted-type) tris(pentafluorophenyl)borane (BCF)-H_2O complex
2) Protonation of the polymer backbone with the formation of $[BCF:OH]^-$ complex,
3) Electron transfer from the neutral polymer chain segment to the protonated one resulting in the formation of a protonated radical species and a positively charged radical species, respectively. The positively charged radical species are attributed to being the free charge carriers in electrical measurements and the charge on it is effectively neutralized by $[BCF:OH]^-$ counterions.

Similarly, electron deficient OSCs can act as π-acids, facilitating n-type doping by interacting with Lewis bases.[80] An in-depth study by Guha *et al*. on Lewis base doping in naphthalenediimide (NDI) derivatives showed the π-acidity of the OSCs plays a crucial role along with dopant strength for effective n-type doping, where the Lewis base/π-acid interaction is the key factor for determining the doping magnitude in n-type semiconductors.[82] Recently, Lewis base containing tetrabutylammonium dopants have attracted much attention due to their unconventional doping mechanism. The latter has been described in the framework of a pure electron transfer process, from the anion, halogens (X^-) or hydroxide (OH^-), to the OSC (*e.g.*, Fullerene (C_{60}, cf. chemical structure in Figure 1)) which results in the formation of n-doped OSC radical anions (*e.g.*, $C_{60}^{\cdot-}$) and donor radicals (*e.g.*, $F^{\cdot}$ or $OH^{\cdot}$).[83] Yet, the high electronegativity of fluoride makes direct electron transfer thermodynamically unlikely, so a different mechanism has been proposed by Weber *et al*. who suggested that the presence of anions with strong nucleophilicity, such as F^- or OH^-, can introduce a more complex doping process. They proposed that instead of a direct electron transfer process, a nucleophilic addition

reaction occurs between the anion and the OSC forming a C_{60}-F^- adduct anion, which undergoes a subsequent electron transfer to a second C_{60} molecule.[84] For more detailed insight on the plausible mechanism involving Lewis bases, the readers are referred to Section 2.2.2 and a comprehensive review by Bridges *et al*.[80]

2.1.3. DOS of semiconductor and dopant

The following considerations are made for dopants that undergo electron transfer with the semiconductor, where the DOS of both compounds play a decisive role; for other doping mechanisms, *e.g.*, hydride transfer, this is not the case. Ideally, host and dopant materials that are to undergo electron transfer are paired based on securing a favorable energy offset to promote charge transfer between the frontier orbitals levels of adjacent host and dopant molecules. In practice, however, the position of the dopant's energy levels when placed within the host matrix is difficult to determine. Computational work has shown differences of up to 1 eV between a pure dopant crystal and a dopant impurity surrounded by a host semiconductor (Section 2.2), due to environmental interactions named above.[85] Shifts of 0.86 eV have been confirmed experimentally for the molecular p-dopant hexafluorotetracyanonaphthoquinodimethane (F_6-TCNNQ) with a phthalocyanine as the host[86].

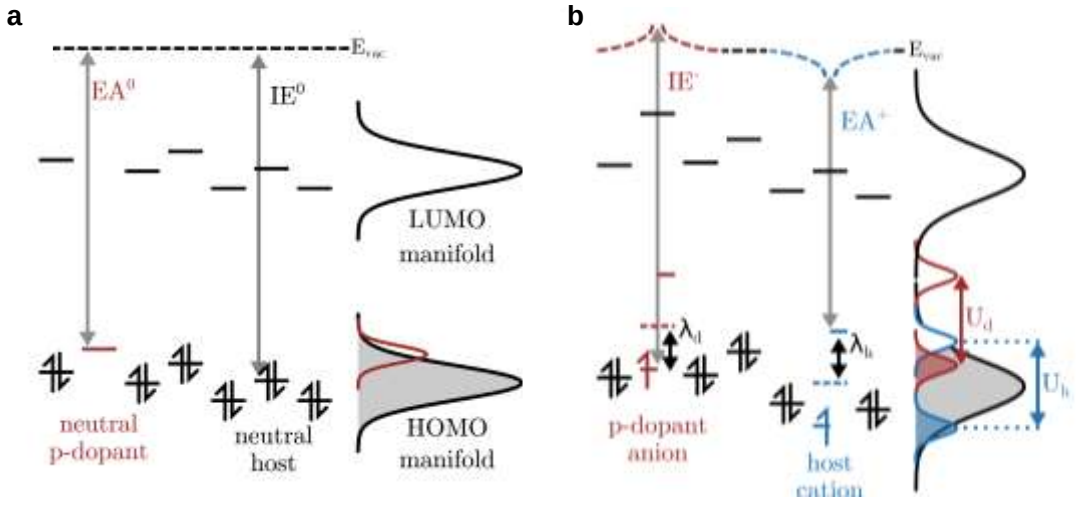

Figure 5: Illustration of the host and dopant DOS before (a) and after (b) charge transfer. (a) Energy levels of a neutral p-dopant within a matrix of the host semiconductor. The electron affinity of the neutral p-dopant is marked EA^0, as referenced from the vacuum level E_{vac}. Analogously, the neutral host's ionization energy is marked IE^0. The corresponding DOS is drawn on the right hand side, with the shaded area representing the occupied levels. (b) After charge transfer, the on-site Coulomb interactions split the anion's and cation's frontier orbitals in two, separated by the reorganization energy λ from their original

positions. EA^+ and IE^- mark the new levels of the host cation and dopant anion, respectively. Meanwhile, the intersite Coulomb interactions cause a shift in the neighboring molecule's energy levels, dependent on distance.

Figure 5a shows the DOS of a host and p-dopant *prior* to charge transfer. At zero temperature, the host semiconductor's HOMO manifold is fully occupied. The dopant's LUMO manifold, overlapping with the host's HOMO manifold, is unoccupied. The overlap between these two manifolds dictates the maximum charge transfer that can occur. In practice, many host and dopant states are spatially separated within the bulk material, reducing the likelihood of charge transfer. With increasing temperature, thermal fluctuations grant the opportunity for less-favorable configurations to result in charge transfer.[30]

After charge transfer, Figure 5b, Coulomb interactions both on-site (within the molecule) and off-site (acting on neighboring molecules), as well as molecular geometry changes, impact the shape of the DOS. Firstly, on-site Coulomb interactions split the former HOMO or LUMO level into two sub-levels for the ionized molecule, separated in energy by an amount commonly termed Hubbard (U_d or U_h).[87–89] The two sub-levels are single-electron levels, and define the EA and IE of the ionized molecule, $EA^{-/+}$ and $IE^{-/+}$ with "-" indicating the anion and "+" the cation state. Adding a charge to a molecule leads to changes in bond lengths and bond angles, which is associated with the reorganization energy λ.[90] This energy relates the neutral and charged molecule's energy levels, *i.e.*, the host cation's electron affinity EA^+ is lower than the neutral host IE^0 by λ_h, and the dopant anion's IE^- is higher than the neutral dopant's EA^0 by λ_d, as indicated in Figure 5b. Secondly, off-site Coulomb interactions shift the energy levels of nearby neutral molecules that sit within the Coulomb potential well generated by the ionized species, also shown in Figure 5b.

2.1.4. Charge carrier density *vs.* temperature

Mathematically, the description of organic semiconductors follows that established for inorganic semiconductors. Figure 6a displays the quantities needed to calculate the density of charge carriers in a p-doped semiconductor. The first panel shows the DOS for the host's HOMO and LUMO manifolds ($g_{HOMO}^{host}(E)$, and $g_{LUMO}^{host}(E)$), and the dopant's LUMO manifold $g_{LUMO}^{dopant}(E)$. The middle panel shows the Fermi-Dirac distribution function *f(E)* at $T = 4000$ K. The third and final panel shows the charge carrier densities per unit energy, at thermal equilibrium, of holes in the host HOMO manifold p(E), electrons in the host LUMO manifold n(E), and ionized p-dopants $n_{dopant}^{-}(E)$. From Figure 6a, p-doping is apparent from the

increased *p(E)* resulting from occupation of the dopant's LUMO manifold by electrons $n^{-}_{dopant}(E)$.

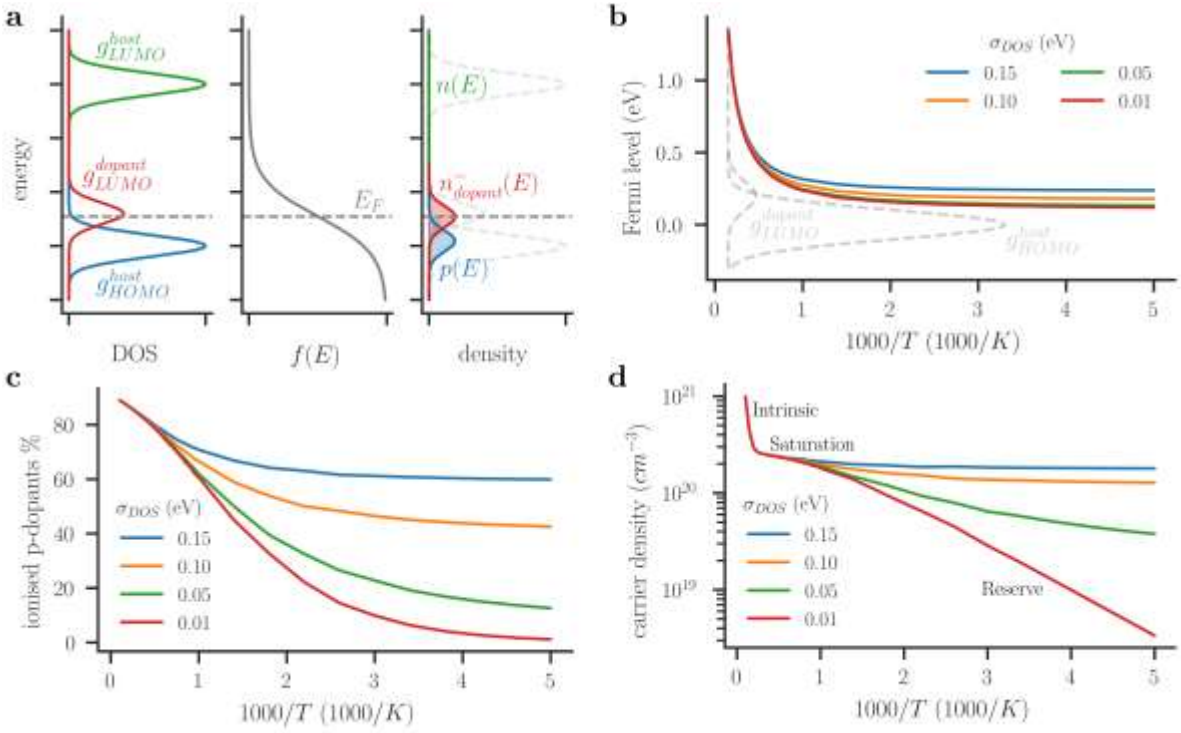

Figure 6: Plots of Fermi level, percentage of ionized p-dopants, and carrier density, against inverse temperature. (a) Graphical representation of the quantities needed to calculate charge carrier density in an organic semiconductor p-doped at a molar concentration of 40%. The first panel shows the Gaussian DOS for the host's HOMO g^{host}_{HOMO} (E), LUMO g^{host}_{LUMO} (E) and the dopant's LUMO g^{host}_{LUMO} (E). The second panel shows the occupation probability *f* (E), following Fermi-Dirac statistics, with the Fermi Level marked E_F. Finally, the third panel shows the charge carrier densities per unit energy of holes in the host HOMO manifold *p*(*E*), electrons in the host LUMO manifold *n*(*E*), and ionized p-dopants $n^{-}_{dopant}(E)$. (b) Fermi level against inverse temperature in a p-doped semiconductor. E_F quickly shifts toward the HOMO manifold with decreasing temperature, as intrinsic carriers are negligible and dopants fail to ionize. (c) The p-dopant ionization percentage as a function of inverse temperature. With lower temperature, only a fraction of the p-dopants can ionize. The disorder has a strong impact on how the ionization decreases with temperature. (d) Log plot of carrier density against inverse temperature. With low disorder (σ = 0.01 eV), the three regimes from inorganic semiconductor physics are visible - the intrinsic, dopant saturation, and dopant reserve regimes. With increasing disorder, it becomes difficult to distinguish between the dopant saturation and reserve regimes. For these simulations, the energy gap is E_{LUMO} - E_{HOMO} = 3 eV, the dopant's DOS is centered around E_{dopant} = 0.2 eV, the disorder is equal for all components in the mixture $\sigma_{DOS} = \sigma_{DOS}^{host} = \sigma_{DOS}^{dopant}$, and the molar doping concentration is 10%.

Figure 6b-d show the Fermi level position within the host semiconductor's gap, percentage of ionized p-dopants, and charge carrier density at a fixed molar dopant concentration of 10 % against inverse temperature. To visualize the effect of disorder, we vary the DOS standard deviation $\sigma_{DOS} = \sigma_{DOS}^{host} = \sigma_{DOS}^{dopant}$The respective values are determined by

Fermi-Dirac integrals, with the Fermi level set by numerically solving the neutrality condition $n_{free} = n^-_{dopant}$, where n^-_{dopant} is the number density of ionized dopants. The position of E_F varies generally little with σ_{DOS}. At temperatures relevant to organic semiconductors (ca. up to 500 K), E_F is found close to the HOMO manifold onset (IE as defined by extrapolation, *vide supra*), and only for excessively high T (where most organic semiconductors would decompose), the Fermi level moves towards mid-gap because thermally excited carriers of the host dominate and outweigh the effect of dopants. The impact of σ_{DOS} on the ionized dopant percentage (Figure 6c) is significant around room temperature. More dopants ionize with increasing disorder because of an increased overlap of $g^{host}_{HOMO}(E)$and $g^{dopant}_{LUMO}(E)$. Likewise, higher T makes more of the dopant LUMO's DOS accessible for the host's deeper lying HOMO levels and the ionized dopant percentage increases, but near room temperature the dependence is moderate.

The temperature dependence of charge carrier density, Figure 6d, can be split into three regimes, analogously to inorganic semiconductor physics textbooks, most clearly identifiable for the low disorder ($\sigma_{\mathrm{DOS}} = 0.01\ eV$). At low temperatures, p-dopants only partially ionize ($n < n_{dopant}$), corresponding to the dopant reserve or freeze-out regime. In this regime, the Fermi level sits within the p-dopant's LUMO manifold. With increasing temperature, a larger percentage of dopants ionized until the dopant saturation regime is reached ($n^-_{dopant} \approx n_{dopant}$). At very high temperatures, the contribution of intrinsic carriers (thermally excited across the host energy gap) exceeds those generated by the dopants (Figure 6c), and the Fermi level shifts towards its intrinsic position, at the center of the host's energy gap (Figure 6b).
Resolving the dopant reserve from the dopant saturation regime is difficult if the disorder is large. As the width of the Gaussian distributions increase, there is a greater overlap between the host and dopant manifolds, resulting in a larger fraction of ionized dopants already at T = 0 K. Therefore, the percentage of ionized p-dopants is less dependent on temperature for highly disordered systems. With this in mind, doped organic semiconductors are expected to operate in the reserve regime,[91,92] with dopant ionization below 100% unless the EA of p-dopants is much higher than IE of the host or the n-dopant IE is much lower than the host's EA.

2.1.4.1. **Charge carrier density *vs.* dopant concentration**

The Fermi level, percentage of ionized dopants, and charge carrier densities also depend on the dopant concentration present in the semiconductor. Here we express dopant concentration as the molar content of dopants divided by the total molar content of hosts and dopants in the

material mixture. We evaluate the Fermi-Dirac integrals at a fixed temperature (T = 300 K) over a range of dopant concentrations. At low dopant concentration (<< 1 %), the Fermi level, Figure 7a, resides within the host semiconductor gap with a high percentage of p-dopants ionized. As the dopant concentration increases, the Fermi level rapidly shifts to sit within the LUMO manifold of the dopant. Meanwhile, the percentage of ionized p-dopants, Figure 7b, plunges as the higher-lying dopant acceptor states are mostly inaccessible for electrons from the host's HOMO manifold. At this point, the doped semiconductor is operating in the reserve regime, and broadly encompasses the region of device-relevant doping concentrations.

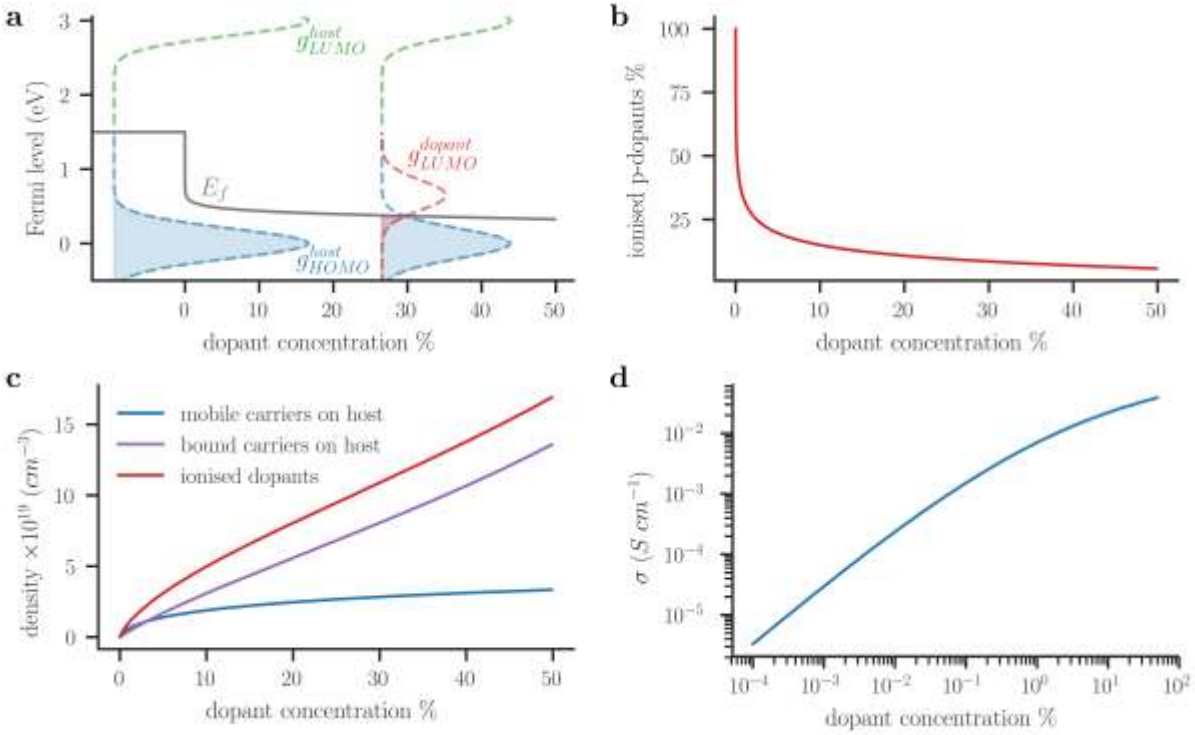

Figure 7: Plots of Fermi level, percentage of ionized p-dopants, carrier density, and conductivity against p-dopant molar fraction. (a) Fermi level shift as a function of dopant molar concentration, defined here as the molar content of dopants divided by the total molar content of hosts and dopants in the material mixture. The DOS before the addition of the dopant is overlayed, with the Fermi level sitting at its intrinsic position. At a dopant fraction of 25%, the DOS of the host and dopant are again overlayed, with the filled area representing occupied states. (b) Ionized dopant ratio as a function of dopant molar fraction. (c) Charge carrier density as a function of dopant molar fraction, given a molecular volume density of 3×10^{21} cm^{-3} and an integer charge transfer binding energy of E_B = 0.5 eV . (d) Log-log plot of conductivity against dopant molar fraction, assuming a constant mobility of 7.3×10^{-3} cm^2/Vs. The parameters used in all simulations are: E_{host} = 0 eV, E_{dopant} = 0.65 eV, T= 300 K and $\sigma = \sigma_{host} = \sigma_{dopant}$ = 0.2 eV.

Figure 7c plots the density of charge carriers, assuming a molecular volume density of 3×10^{21} cm^{-3}, as a function of dopant concentration. To separate mobile carriers from bound carriers, we have introduced an IP binding energy of 0.5 eV, in a similar manner to recently

published models.[63,86] The sum of mobile and bound carriers on the host is equal to the density of ionized dopants, also plotted in Figure 7c. At low doping concentrations, the charge carrier density increases quickly. At higher concentrations, in the dopant reserve regime, the rate of increase slows as fewer dopants are ionized. In this model, mobile charges are generated quickly at low doping concentrations before increasing comparably slowly beyond a doping concentration of around 10%.

2.1.4.2. **Doping Efficiency**

The doping efficiency describes the percentage of free charge carriers (or sometimes termed mobile charge carriers) that are generated per dopant in the semiconductor host material. Two processes must occur to generate a free charge carrier. First, the doping reaction must occur between the dopant and semiconductor host molecule, which ionizes the latter but leaves the resulting polaron Coulombically bound to the generated dopant counterion. The ionization efficiency can be defined as the ratio of the number of generated polarons $N_{polaron}$ and the total number of dopant molecules, N_{dopant}:

$$\eta_{ionization} = \frac{N_{polaron}}{N_{dopant}} \tag{2}$$

Secondly, the created polaron must dissociate from the dopant counterion, i.e., move sufficiently far away to be considered a free charge carrier. The dissociation efficiency can be defined *via* the number of free carriers N_{free} per total number of polarons:

$$\eta_{dissociation} = \frac{N_{free}}{N_{polaron}} \tag{3}$$

The doping efficiency is then given by the product of the ionization and dissociation efficiency:

$$\eta_{doping} = \eta_{ionization} \times \eta_{dissociation} = \frac{N_{free}}{N_{dopant}} \tag{4}$$

The distinction between bound and free charge carriers should not be considered as a static picture. Rather, averaged over a sufficiently long period of time, all polarons contribute to transport. At a given point in time, however, only a fraction of them contribute to charge transport.

Most dopants generate a maximum of one polaron in the organic semiconductor per dopant, meaning that $\eta_{ionization} \leq 100\%$, provided that the dopant/semiconductor pair undergo efficient ICT. If host and dopant form ground state CTCs, the frontier orbitals of the dopant and the host hybridize to form a new set of HOMO and LUMO levels of the complex, with a

narrower energy gap than its constituents. The resulting neutral CTC can act as a dopant, provided that the energy levels fulfill the requirements for a subsequent ICT process with surrounding host molecules.[66] The ionization efficiency is, therefore, reduced to significantly less than 100%, due to the additional step involved in this mechanism. Notably, CTC formation and ICT have been observed to occur simultaneously in some materials, for certain polymorphs[93,94] or depending on the doping method,[95] but a full understanding of its formation and effects on doping is yet to be developed.[48,66,93,94] In some cases, a dopant molecule is able to create two polarons in the semiconductor, i.e., $\eta_{ionization}$ can approach 200%. For p-type doping, this requires that the electron affinity of the dopant anion EA^- is still higher than the IE of the semiconductor, as was demonstrated for the prototypical electron acceptor F_4-TCNQ and a bithiophene–thienothiophene copolymer with tetraethylene glycol side chains [p($g_4$2T-TT)].[96]

If the dopant molecules are not well miscible with the host but phase separate, then the dopant molecules at the center of the resulting aggregates are unlikely to undergo a dopant reaction with the host, which also reduces $\eta_{ionization}$. Many semiconductor/dopant systems, therefore, first display a rapid increase in $N_{polaron}$ as an increasing amount of dopant is added, implying a high $\eta_{ionization}$. At higher dopant concentrations, however, $N_{polaron}$ increases less strongly with dopant concentration due to aggregation, and as a result, the electrical properties level out.[97] Most polarons remain within the Coulomb capture radius of their counterion and hence cannot freely move within an electric field. Only once a polaron dissociates from the corresponding counterion and takes up a position that is located sufficiently far away it becomes a free charge carrier. In the case of a low dopant concentration, a polaron can escape the Coulomb capture radius of a counterion with minimal chance of being captured by another counterion, and hence $\eta_{dissociation}$ can approach 100%. At intermediate dopant concentrations there are only a few positions within the host/counterion mixture where a polaron would not experience any Coulomb interaction with a counterion, and hence $\eta_{dissociation} << 100\%$. At very high doping levels the Coulomb capture radius of counterions starts to overlap, meaning that counterions partially screen each other, and as result, it becomes easier for a polaron to move, which can result in an increase in $\eta_{dissociation}$. As an example, at intermediate dopant concentrations for P3HT doped with F_4-TCNQ, in host/dopant rations between 5000 and 200, only 5% of the formed polarons were estimated to be mobile.[65]

Besides the dopant density, its size is also important to determine doping efficiency, since a larger dopant molecule size can help reducing the Coulomb interaction with polarons.

To continue with the same example, the distance between a polaron on the P3HT backbone and an F_4-TCNQ anion is thought to be about 5-9 Å,[98] but larger dopant molecules, such as molybdenum dithiolene complexes with a diameter of 11-14 Å [99,100] or dodecaborane-based dopants with a diameter of 20 Å,[101] give rise to a larger polaron/counterion distance, and hence polarons are less strongly bound. In fact, for P3HT doped with a dodecaborane-based dopant $\eta_{dissociation}$ = 100 % has been reported, i.e., all polarons are mobile charge carriers.[101]

In contrast, in the high dopant concentration regime, the counterion size will influence the maximum polaron density per unit volume. A small counterion will only occupy little space but a large counterion will occupy a considerable fraction of the available volume. For P3HT, we can estimate a theoretical maximum polaron density of ca. 1×10^{21} cm^{-3} (assuming that a polaron spreads over four repeat units[102]) . For larger dopants, such as molybdenum dithiolene complexes or dodecaborane-based dopants as mentioned above, the theoretical maximum polaron density in P3HT reduces to $0.2\text{-}0.7\times10^{21}$ cm^{-3}. Since, however, a larger dopant will improve $\eta_{dissociation}$, it can be anticipated that there is an optimal dopant size for which the maximum number of free charge carriers per unit volume can be obtained.

2.1.5. Charge carrier transport in doped semiconductors

Highly crystalline organic semiconductors with low density of crystal and interface defects can exhibit coherent band-like transport with charge carrier mobilities that decrease with increasing temperature, similar to crystalline inorganic semiconductors.[103,104] However, most organic semiconductor thin films are not single crystals but feature a complex nano- and microstructure (see Section 3) associated with a high degree of electronic disorder. Hence, under device-relevant conditions, transport is rate-limited by intermolecular charge transfer between weakly coupled electronic states, *via* thermally activated hops. Charge carriers are strongly localized due to the molecular reorganization upon charging. Therefore, a charge making a hop is accompanied by local structural distortion as well as polarization of its environment, which is collectively termed a polaron (see Section 2.1.2).

An important model used to describe hopping transport in molecular solids is Marcus theory, originally proposed to describe oxidation reactions between molecules in solution.[90,105] For a hop to occur, the molecules and their surrounding environment must reorganize, from their initial equilibrium position, through an unstable distorted state, to a final equilibrium position. In the high-temperature limit where vibrational modes can be treated classically, Marcus theory states an electron transfer rate in the weak coupling regime of

$$\Gamma_{if} = \frac{2\pi}{\hbar}|J_{if}|\frac{1}{\sqrt{4\pi\lambda kT}}exp\left(\frac{-(\Delta E+\lambda)^2}{4\lambda kT}\right) \quad (5)$$

where J_{if} is the intermolecular transfer integral, representing the electronic coupling strength between the states, ΔE is the energy difference between the final and initials states, and λ is the reorganization energy.

Considering a linear chain of identical states under a constant applied electric field, Equation (6) yields an expression for the charge carrier mobility

$$\mu = \frac{|J_{if}|}{\hbar}\sqrt{\frac{\pi}{\lambda kT}}exp\left(\frac{-\lambda}{4kT}\right)\frac{ea^2}{kT} \quad (6)$$

where a is the hopping distance between intermolecular sites. The mobility μ quantifies how fast a charge moves in response to an electric field F, and is a key parameter for electronic devices, for example, determining the ultimate switching speed in an organic field-effect transistor (OFET) attainable in the absence of any parasitic effects.[106] Using often encountered values of $J_{if} \approx 0.01$ eV, $\lambda \approx 0.5$ eV and $a \approx 10^{-9}$ m in Equation (2), the mobility is around $\mu \approx 7.3\text{x}10^{-3}$ $cm^2V^{-1}s^{-1}$, which, in general, is far lower than values displayed by many inorganic semiconductors. The mobility shows an Arrhenius-type temperature dependence at device-relevant temperatures, as the exponential term in Equation (6) dominates. The conductivity of a semiconductor σ can then be calculated as the product of the charge-carrier density p and the mobility μ,

$$\sigma = e\mu p \quad (7)$$

In contrast to inorganic semiconductors, where charge scattering effects lead to a decrease in conductivity with increasing temperature, the conductivity of organic semiconductors increases exponentially with temperature. This exponential increase is driven by the thermally activated hopping transport, as discussed previously. To show how the conductivity changes as a function of dopant concentration, we multiply the mobile charge-carrier density, as sketched in Figure 7c, by a constant charge-carrier mobility $\mu \approx 7.3\text{x}10^{-3}$ $cm^2V^{-1}s^{-1}$. We assume a constant mobility here for simplicity, however, scattering effects as the charge-carrier density increases lead to a decrease in mobility as a function of dopant concentration. The mobility then increases again at higher dopant concentrations due to screening/overlap. The product of the charge-carrier density and mobility, Figure 7 demonstrates that through the introduction of dopants, the conductivity can be enhanced over many orders of magnitude. At low dopant concentrations, the increase in conductivity with dopant concentration c_{dop} follows a monomial relationship of the $\sigma \propto c_{dop}^{y}$, with a constant

exponent *y*. At higher dopant concentrations, *y* reduces as the percentage of ionized dopants decreases and fewer mobile charge carriers are generated.

Experimental studies on varying dopant concentration usually observe a monomial dependence of the form $\sigma \propto c_{dop}^{y}$, however with $y > 1$. This super-linear conductivity increase is attributed to initial changes in mobility with doping concentration as a result of trap-filling,[107] and greater mobile charge-carrier generation when the Coulomb potentials of the ionized dopants overlap, reducing the barrier for IP dissociation.[52,63] Further deviations from the monomial dependence were reported at high dopant concentrations as a consequence of carrier-carrier scattering, in addition to carrier-ionized dopant scattering.[108] Saturation or even lowering of σ beyond a certain threshold of dopant concentration, typically in the range of 10-20 %, is often observed experimentally. In addition to the carrier-carrier scattering, serious disruption of the intrinsic semiconductor's packing and an increased density of grain boundaries (for crystalline materials) result in lowered charge carrier mobility and thus conductivity. So far, only one study on a polymeric semiconductor reported that σ decreased at high dopant concentration due to bipolaron formation instead of polarons.[109] Bipolarons are dicationic species and thus have doubly occupied/empty states, which are highly localized and do not effectively contribute to carrier transport.

2.1.6. Electrical contact to doped organic semiconductors

The electrical contact between a semiconductor and a conductive electrode can be either non-rectifying (Ohmic) or rectifying (Schottky contact). For most devices, unhindered non-rectifying carrier injection is desirable to minimize Ohmic losses. Figure 8a shows the energy level diagram for a conventional metal-semiconductor material system before contact. In this example, the metal work function Φ_m, i.e., the energy required to bring an electron from the metal Fermi level to the vacuum level E_{vac}, is lower than the p-doped semiconductor's work function Φ_s. The work function is always the energy difference between E_F and E_{vac}; for the metal, it is identical to its IE, and for the semiconductor, it is determined by the doping level. Upon contact (Figure 8b), holes transferred from the semiconductor to the metal side, create a depletion region and charge injection barrier on the semiconductor side of the interface. The barrier height Φ_b as seen by the majority carriers, holes in this example, moving from the metal to the semiconductor is given by $\Phi_b = \mathrm{IE} - \Phi_m$. The barrier seen by carriers moving from the semiconductor-side to towards the metal, is called the junction potential or built-in voltage V_{bi}, and is given by $V_{bi} = \Phi_s - \Phi_m$. The junction potential drives an exodus of mobile charge

carriers from a region on the semiconductor side of the interface. Assuming this region contains only charges generated by immobile ionized dopants N^-_{dopant}, and has an abrupt end, the depletion region width w is derived from Poisson's equation and is given by

$$w(V) = \sqrt{\frac{2\epsilon(V_{bi} - V)}{qN^-_{dopant}}} \tag{8}$$

The above equation is valid for applied voltages below the built-in voltage $V < V_{bi}$. This equation highlights two practical ways of avoiding rectifying contacts at metal-semiconductor interfaces; firstly, by matching the metal work function with the organic semiconductor's IE to minimize V_{bi}, secondly, through an increase in dopant concentration.

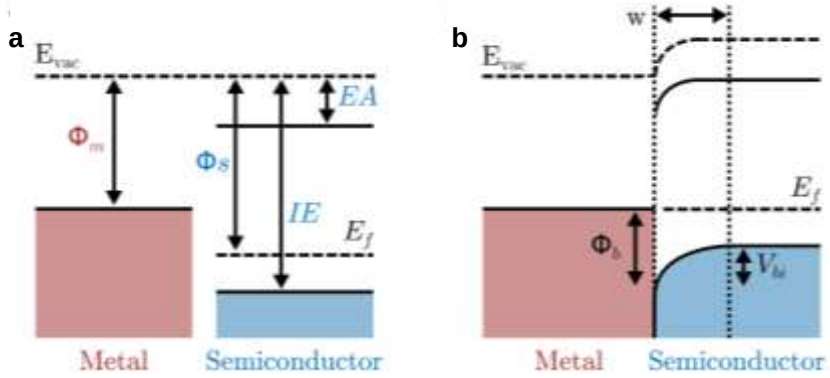

Figure 8: Schematic energy level diagram before and after contact at a metal-semiconductor interface. (a) Schematic before contact showing a metal with work function Φ_m and semiconductor with E_f at different potentials. (b) In equilibrium after contact, the metal work function and semiconductor Fermi level equilibrate, creating a barrier for majority carriers from the metal side of Φ_b and a barrier from the semiconductor side of V_{bi}.

The depletion region present between the metal and the semiconductor can be made narrower by doping of the semiconductor and/or the interface. This method is applicable in traditional semiconductors as well as organics, although major differences do exist. In the case of OSCs, for instance, the depletion region changes from hundreds of nanometers for undoped α-NPD to about 10 nm when p-doped with F_6-TCNNQ.[110] For undoped or lightly doped samples, the depletion region can extend far into the semiconducting layer. For example, the depletion width in fullerenes, C_{60}, deposited on gold, silver or copper, extends around 500 nm into the semiconductor.[111] If the film thickness is lower than the depletion region width, the Fermi level position will not be representative of its position in the bulk of the semiconductor far away from the contact. Rather, the Fermi level position varies with film thickness. In turn, a measurement of the depletion region width can give a good estimate of the density of mobile charge carriers, and with knowledge of N_{dopant}, the doping efficiency in a given doped organic

films.[112] Complications arise if the semiconductor contains states within its energy gap, which in real materials is practically unavoidable. Charges moving from the metal accumulate in the gap states, shielding the bulk semiconductor from the metal interface. Thus, the Fermi level pins to the energy position of the gap states, and is independent of the metal work function. For organic semiconductors, Fermi level pinning arises as a consequence of chemical impurities but also from structural imperfections.[113]

2.2. Atomistic Computational Studies

Doping of OSC is a complex task whose understanding and optimization should take into account many different mechanisms and factors. In this section we focus on how theoretical and computational studies, especially so-called atomistic studies, can elucidate key details and processes of doping and, by doing that, explain available experimental data or even guide materials synthesis and device engineering to novel doping routes. As discussed in the following, these studies can probe a wide range of aspects underlying the physics and chemistry of dopants and dopant-host systems. Examples include, but are not limited to, the energies of frontier orbitals, interactions between hosts and dopants or between dopants and solvents, dopant-induced changes in the microstructure of OSCs, and the effects of dopants on the optical, electronic, magnetic, or vibrational properties of a given sample.

The main approaches in atomistic studies can be categorized into three groups:

1) Quantum mechanical (QM) calculations which typically take into account in some approximate form the electronic many-body exchange-correlation (xc) effects
2) Classical Molecular Dynamics (MD) simulations which integrate the classical equations of motions for atoms/ions
3) Monte Carlo (MC) simulations

Given that these approaches probe different time and length scales (up to a few hundreds of atoms for QM calculations, thousands or even more atoms for MD and MC simulations), they are really complementary to each other. In fact, the comprehensive description of doping in OSCs requires ideally the combination of such different methods because it includes inherently multi-scale phenomena, such as the embedding of dopants in a large-scale host environment, the long-range transport of carriers in OSCs, and their release or scattering off dopant impurities.

The most common method in QM studies is Density Functional Theory (DFT) wherein many body effects are described through a so-called xc-functional. DFT and other electronic structure methods with post- or beyond-DFT corrections have become, through systematic

advances, a very useful and robust tool for the investigation of materials properties. However, it should be noted that certain calculated properties relevant to doping in OSCs often have a strong dependence on parameters of DFT studies, the most important of which are the xc-functional and the type of orbital basis used to describe the electronic wavefunctions. Likewise, the quality of MD simulations is largely controlled by the type of force-field parameters that represent the inter-atomic potentials. With these cautionary remarks in mind, the importance of atomistic studies in the modelling of novel dopants will certainly continue to grow as more powerful computer infrastructures and improved algorithms will make it possible to tackle phenomena which up to now have been intractable in practice. In addition, the identification of novel dopants with optimal performance in OSCs will take advantage of the wider use of computational screening with high-throughput calculations and machine-learning techniques.
In the next sections we present representative examples of achievements, challenges and opportunities in the modelling of OSC doping. The selection of these examples is not meant to be exhaustive and puts emphasis on relatively recent studies. For a more complete presentation of earlier pertinent works the reader can refer to previous review articles[48–50,114] about doping of OSCs.

2.2.1. Integer Charge Transfer and Charge Transfer Complexes

As we discussed earlier, in the simplest point of view, an extrinsic species can dope a host OSC with holes (electrons) if the LUMO (HOMO) of the former lies lower (higher) than the HOMO (LUMO) of the latter. In this case, electrons can hop from the dopant to a proximal OSC unit or vice versa, through ICT. Hence, the calculation of the energies of frontier orbitals is normally the first and rather straightforward step in assessing the suitability of a particular dopant vis-a-vis a certain OSC. It should be noted, however, that DFT results for HOMO and LUMO energies can show large variations[115] depending on the choice for the xc-functional and the orbital basis. For the "Becke, 3-parameter, Lee–Yang–Parr" (B3LYP)[116,117] xc-functional (one of the most popular xc-functionals), DFT HOMO energies tend to come up within a few tenths[118] of an electron-volt from experimental values, especially for a large enough orbital basis. LUMO DFT-B3LYP energies, on the other hand, typically turn up higher than experimental values.[118] However, when comparison is made to experimental LUMO values which are obtained by adding the optical gap to the HOMO energy, then the gap should be calculated with, e.g. Time-Dependent DFT (TDDFT).

Energies of frontier orbitals also have an intrinsic dependence on the interactions of dopants with their surrounding medium, namely the host OSC and possibly solvent molecules. At first approximation, these interactions can be taken into account through continuous polarizable or solvation models. With the availability of more computational power, however, explicit inclusion of the nearest neighbors becomes an option as well. Using this type of an approach, many-body GW studies[85] found that the electron affinity of p-type dopants (F_4-TCNQ, F_6-TCNNQ and hexacyaotrimethylene-cyclopropane (CN6-CP)) can shift lower by up to 1 eV when host-dopant interactions are part of the calculation. Such shifts are significant as they can alter completely the theoretical assessment with regard to the efficiency of a particular dopant. In addition, to decide whether a dopant molecule is capable of donating (or accepting) an electron to a proximal OSC unit and form a charge transfer complex (CTC) with the latter, the energy balance should include[119] the attractive interaction between the opposite charges of the CTC. In other words, even if the calculated HOMO or LUMO of a dopant molecule in the gas phase does not support the ICT scenario at first, the final verdict on the possibility of doping may change when environmental and excitonic effects are taken properly into account.

In most cases, dopant-host interactions have a purely non-bonding van der Waals and electrostatic character. There are, however, instances with non-negligible hybridization between the frontier orbitals of a dopant-host pair. The end result of this inter-molecular hybridization is the partial (i.e. non-integer) transfer of charge between the moieties of the complex. DFT studies[120] can access this scenario through the calculation of intermolecular binding energies (e.g. 0.87-0.94 eV for a F_4-TCNQ-Pentacene CTC), visualization of frontier orbitals and careful population analysis. Moreover, calculated reduced energy differences between the host-dopant hybrid HOMO-LUMO orbitals can account[66] for the sub-gap absorptions in UV/Visible/Near Infrared (UV-vis-NIR) spectroscopy.

More generally, a comparison between DFT-based and experimental UV-vis-NIR absorption spectra can clarify the degree of hybridization and of charge transfer since in the calculations one can adjust the charged state of dopants to ad hoc levels. In this way, DFT studies can give clear evidence[121] whether the doping mechanism in a particular case pertains to ICT with the presence of fully ionized dopants, or to the formation of CTCs with partial ionization. Furthermore, calculated frequencies for vibrational modes of dopants and their intensities in corresponding Infrared (IR) spectra show, respectively, distinct shifts and changes based on the level of ionization. For example, the calculated frequencies[121] of the cyano group of the F_6-TCNNQ dopant differ by 37-47 cm^{-1} between its neutral and anion forms, with the latter also having stronger IR intensities. Red shifts of the same order of magnitude were

obtained also when the F_6-TCNNQ dopant was simulated[121] in a complex with fragments of diketopyrrolopyrrole-based host polymers (DPP-TT-DPP and TT-DPP-TT).

Interestingly, DFT studies have found[121,122] that the degree of charge transfer depends also on the relative position of a dopant with respect to a host polymer chain. In particular, when an F_4-TCNQ dopant was stabilized[122] in a co-facial geometrical arrangement with the CPDT donor (D) moiety of the PCPDTBT co-polymer, DFT-based population analysis obtained an almost complete (0.93 e) charge transfer between the dopant and the polymer. Conversely, almost zero charge transfer was obtained when the dopant relaxed next to a BT acceptor (A) segment of the co-polymer. Similar results have been found by the DFT study[121] about the F_6-TCNNQ and the DPP-TT-DPP co-polymer with D-A alternation. These findings bear directly on the key issue of doping efficiency, as they reveal that the ionization of dopants may be suppressed by undesired host-dopant complex structures.

On the other hand, structural atomistic studies, based either on DFT or MD simulations, can probe conditions that enhance the efficiency of doping, e.g. by limiting dopant segregation. In this regard, coarse-grained molecular dynamics simulations[97] found that the replacement of apolar side alkyl chains in the D-A co-polymer P(NDI2OD-T2) (cf. chemical structure in Figure 1) with polar glycol-type groups enhanced the molecular dispersion of N-DMBI dopants (by trapping them between the side chains). Concomitantly, the tendency for clustering of dopants diminished and doping efficiency increased considerably.

Other key processes which should be a part of a comprehensive study of OSC doping and which could be examined in detail with atomistic studies are the chemical stability of dopants against degradation reactions, e.g., with oxygen or water, and dopant diffusion. Based on the above, the migration of dopants to different sites may switch on and off the degree of its ionization depending on the local environment,[122] while it can also lead to segregation or trapping at interfaces. Dopant clustering has also been indirectly probed in a recent study[123] with combined electron paramagnetic resonance (EPR) measurements and DFT calculations. In particular, pairs of F_6-TCNNQ dopants within a zinc phthalocyanine host were found to couple antiferromagnetically when placed at certain positions with respect to each other. In this way, the detection of spin adds another tool in the investigation of doping mechanisms.

The identification of stable charge transfer complexes can be the starting point for the study of their dissociation and the release of mobile carriers to the host OSC. To this extent, experiments can provide[63] valuable information on the binding energy of electrons and holes in the CTC. This quantity can, in principle, also be calculated with DFT, or in a mixed DFT/Molecular Mechanics scheme.[119] Analogous studies have been performed in the past, e.g.,

for the dissociation of charge transfer states between donors and acceptors in organic photovoltaic blends.[124] In the case of dopants, CTC dissociation efficiency has been shown with kinetic Monte Carlo[96] simulations to be sensitive also to the energetic disorder of states which are available for the release of carriers.

2.2.2. Hydride Transfer, Anion Doping and Lewis Acids

We now shift our attention to a broad class of dopants whose doping mechanisms cannot be accounted for (partly or fully) by the charge transfer process we discussed in the previous section. A prototypical member of this class is N-DMBI-H, an air-stable n-type dopant. The most widely held view[77,125] for this and other similar molecules is that they do not function as dopants via direct charge exchange with their hosts (although opposing evidence has been presented[125] as well up until recently). Indeed, DFT values[126] for the HOMO of N-DMBI-H (-4.44 eV) are lower than the LUMO energies of n-type OSCs, e.g. [6,6]-Phenyl C_{61} butyric acid methyl ester (PCBM, cf. chemical structure in Figure 1). On the other hand, if the hydrogen atom is removed from N-DMBI-H, then the calculated[126] energy of the singly Occupied Molecular Orbital (SOMO) of the remaining N-DMBI species is so high (-2.23 eV) so that it readily loses its highest lying electron.

In effect, the ionization of N-DMBI-H happens concurrently with the transfer of a hydride (H^-) anion to an adjacent molecule or polymer fragment, producing thus a radical host anion. The kinetics of this reaction is controlled by the corresponding energy barrier, which for the aromatic A-DCV-DPPTT (quinoid Q-DCM-DPPTT) n-type OSC is calculated[78] to be 26.3 kcal mol^{-1} (18.8 kcal mol^{-1}). Hence, this hydride transfer is a thermally activated process which requires annealing to moderately elevated temperatures, especially for A-DCV-DPPTT. The product of the reaction is a charge-transfer complex. Further DFT studies could probe the dissociation of this CTC, as well as obtain the quantitative details (reaction energy and barrier, binding energy of CTC) for other host-dopant systems for which hydride transfer has been suggested as the actual doping mechanism.

A mechanism akin to hydride transfer has been proposed for the so-called anion doping of organic semiconductors. A typical example of this case relates to doping of fullerenes,[84] polymers,[127] or non-fullerene acceptors[125] by tetrabutylammonium fluoride (TBAF). Although the mechanism of anion doping has been the subject of some debate (see section 2.1.2.3), in these examples, results from electron spin resonance, UV-vis-NIR absorption and ultraviolet spectroscopy suggest nucleophilic addition of the fluoride (F^-) anion of TBAF to C_{60} and

PCBM[84] or to the ClBDPPV[127] polymer. The resulting adduct is then proposed to undergo an electron transfer to neighboring fullerene molecules or polymer fragments resulting in the formation of neutral and charged radicals. Just like for the hydride transfer discussed above, the theoretical corroboration of the fluoride and, in general, anion transfer requires further careful computational analysis. For example, DFT calculations can, in principle, attempt to provide an unambiguous match between the proposed intermediate structures with specific features in the UV-vis spectra. Moreover, they can probe possible reaction pathways for the dissociation of certain radical products, a final step which is needed so that the whole process becomes exergonic. Preliminary results of a recent DFT study[128] for doping of a NDI co-polymer (P-90) by TBAF are consistent with the two-step process of fluoride addition to the polymer and subsequent release of an electron carrier.

In recent years there is a resurgent interest in the use of Lewis acids (organic or inorganic) as molecular dopants of organic semiconductors. The versatile chemistry of these compounds has already been demonstrated in applications such as organic photovoltaics and transistors.[17,21,80,129] The corresponding doping mechanism, however, remains under debate. For example, widely different scenarios have been reported for BCF, one of the most interesting members of this class at present. First, DFT and experimental LUMO energies for BCF seem[21] to preclude the case of p-doping through ICT, although we should mention that widely different values have been reported and more calculations and measurements are needed for this key quantity. A similar situation holds[17] (i.e. high LUMO energies are not compatible with ICT) for the Lewis acid acceptor bis(pentafluorophenyl)zinc (ZnCF) which has been shown to boost hole mobilities of organic transistors above 20 cm2 V-1 s-1.

Another possibility is that Lewis acids affect the properties of an OSC by reacting with any Lewis basic sites of the latter. Indeed, DFT studies have shown that it is energetically favorable for BCF to form adducts in several cases, e.g. with diF-TESADT, Tips-Pentacene (cf. chemical structure in Figure 1), and the C_{16}IDT-BT[21] and the PFPT[130] polymers. Likewise, ZnCF has been shown[17] to form adducts with C_{16}IDT-BT and stretched bonds with the C_8-BTBT small molecule (cf. chemical structure in Figure 1). These reactions change the energies of the frontier orbitals, albeit the calculated hybrid LUMOs are still not low enough to warrant a charge transfer effect. Nevertheless, experiments[17,21,128] have provided evidence that Lewis acids may affect the electronic properties of OSCs and improve thus the performance of pertinent devices not through direct electronic doping, but by changing the micro- or nano-structure of host polymers and small molecules. One way to do that is to induce[130] electric dipoles on the acceptor moieties of a blend. Although the functioning of Lewis acids as

structure modifiers is a plausible idea that could indeed explain several experimental observations, it has not attracted up to now focused and systematic computational investigations. In this respect, Molecular Dynamics (MD) simulations, either as a standalone study, or in combination with DFT calculations in a multi-scale scheme, can shed light to this key issue of how molecular dopants affect the local or long-range structure of embedding organic semiconductors.

While molecules such as BCF or ZnCF form readily adducts with certain molecules or polymers, their relatively bulky structure precludes this scenario in other cases. Nonetheless, even without direct binding to a host, they can form so-called frustrated Lewis pairs which are known to be sites of increased catalytic activity. Moreover, these and other Lewis acids are known to form stable complexes with ambient molecules, namely O_2 and H_2O molecules. For example, DFT calculations found[17] that a ZnCF molecule can bind an O_2 molecule and that the LUMO of the ZnCF-O_2 complex is low enough (-4.78 eV) that could possibly lead to doping through charge transfer. On the other hand, the ability of BCF to capture an H_2O molecule has been shown in a combined experimental and DFT study[81] to serve as the first step towards carrier doping of the PCPDTBT polymer. In particular, it was shown that the BCF-H_2O group can donate a proton to the polymer backbone, while the complex is transformed to a BCF-OH anion. DFT-calculated ^{1}H NMR spectra are in very good agreement with experimental data (as shown in Figure 9) and confirm thus that a proton has been transferred to the PCPDTBT polymer. The protonated site may then release a hole to the same or neighboring polymer chains. Overall, these findings put forward an additional BCF-induced doping mechanism which is consistent with prior knowledge on the catalytic efficiency of Lewis acids.

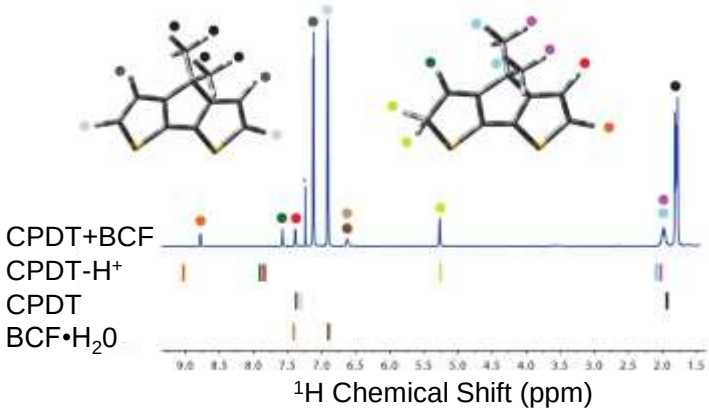

Figure 9: Comparison of DFT and experimental 1H NMR spectra for a fragment of a PCPDTBT polymer without (left) and with (right) a transferred proton (yellow-green site). Reprinted with permission from ref [81]. Copyright 2019 Springer Nature.

2.3. Dopant Materials

A wide variety of chemical species has been used as additives to dope organic semiconductors. This section provides a discussion on the chemical design and properties of the most significant examples, through the classification of different species by structural and mechanistic features. Those dopant classes which have already been extensively covered in previous review papers are briefly discussed in Sections 2.3.1 and 2.3.2 for context, followed by a more thorough description of doping and design strategies that have emerged over the past few years.[26,49,50,114,131] The effects and mechanisms of selected dopants in the context of devices are discussed in more depth in Section 4.

2.3.1. Inorganic species

Some of the earliest examples of doping of organic semiconductors relied on diatomic halogen species for the doping of polyacetylene.[132] In particular, diatomic iodine has been used for p-doping of a variety of organic semiconductors, including pentacene and different phthalocyanines.[133–136] Similarly, molecular oxygen can also lead to unintentional p-doping of organic semiconductors with low IE, such as polythiophenes.[137–141] However, oxygen typically acts as a source of electron traps, instead of improving electronic properties.[142,143] Metal oxides, such as MoO_3 and WO_3, have also been used for p-doping of a range of organic semiconductors, especially owing to the possibility to p-dope materials with high IE.[144,145] The limitations in the employment of these materials are related to the typically high temperatures of deposition, their tendency to form aggregates, and their instability. Inorganic salts – particularly oxidizing Lewis acids, such as $FeCl_3$, $AsCl_5$, or $SbCl_5$ – have also been shown to be efficient p-dopants.[146–149] However, they exhibit high reactivity, sensitivity to moisture, and the formation of side-products (such as HCl). Most Bronsted acids have also been used as p-dopants, particularly for polyanilines and polypyrroles.[49] Nitrosonium salts, e.g. $NOBF_4$, are another notable class of dopants that have also been used recently to achieve record-high conductivity, with their effectiveness partly driven by the reduction of nitrosonium to form gaseous nitric oxide.[150–153] For n-doping, alkali metals such as Li, Na, K, and Cs, have been applied, with the drawbacks of high chemical reactivity, and interdiffusion through organic layers owing to their small size.[154–156] Salts of alkali metals, particularly oxysalts, have also proven useful for n-doping.[157–160]

2.3.2. Molecular dopants

Various molecular dopants have frequently been the preferred choice over earlier alternatives such as alkali metals and elemental halogens. This owes primarily to their processing versatility as well as being less prone to diffusion within the doped organic layer, which has often been found to be a contributing factor to device performance degradation. Furthermore, the structure of molecular dopants can be readily modified for tuning of specific properties using relatively simple chemistry. Although the design of molecular dopants varies dramatically, they typically have in common that they promote efficient charge transfer between the dopant and the host semiconductor via the various mechanisms discussed earlier. As already mentioned, a prerequisite for that is that the frontier orbital energy levels of the dopant are at an appropriate level in relation to the host semiconductor (see section 2.1). Furthermore, a good dopant should ideally have good stability, be readily processable, and be compatible with the host material for efficient charge transfer without detrimental effects on other important properties, such as the ensuing layer morphology.

2.3.2.1. TCNQ derivatives

The most commonly applied p-type molecular dopant is F_4-TCNQ and its derivatives (Figure 10).[54,161,162] F_4-TCNQ is a volatile compound, which may lead to adverse effects such as uncontrolled dedoping– although the very same property has also been leveraged to control the doping level.[163,164] Extending the aromatic core (larger molecule) can reduce this volatility; for example, the naphthalene derivative F_6-TCNNQ has increased molecular weight, resulting in improved vacuum deposition control and reduced molecular diffusion.[165] Attempts to further reduce volatility by substitution of one fluorine of F_4-TCNQ with a bulky adamantanyl propyl chain led to a material which degraded before high vacuum sublimation.[166] However, the bulky group did facilitate solution processing. Moulé and co-workers further investigated solution processability by substituting one or two of the nitrile groups of F_4-TCNQ with alkyl esters. Significantly enhanced solubility was achieved, albeit with a slight upshift in the LUMO level.[167] The volatility of F_4-TCNQ was also lowered, along with the LUMO energy level, by substitution of two of the fluorine substituents with nitrile groups.[168]

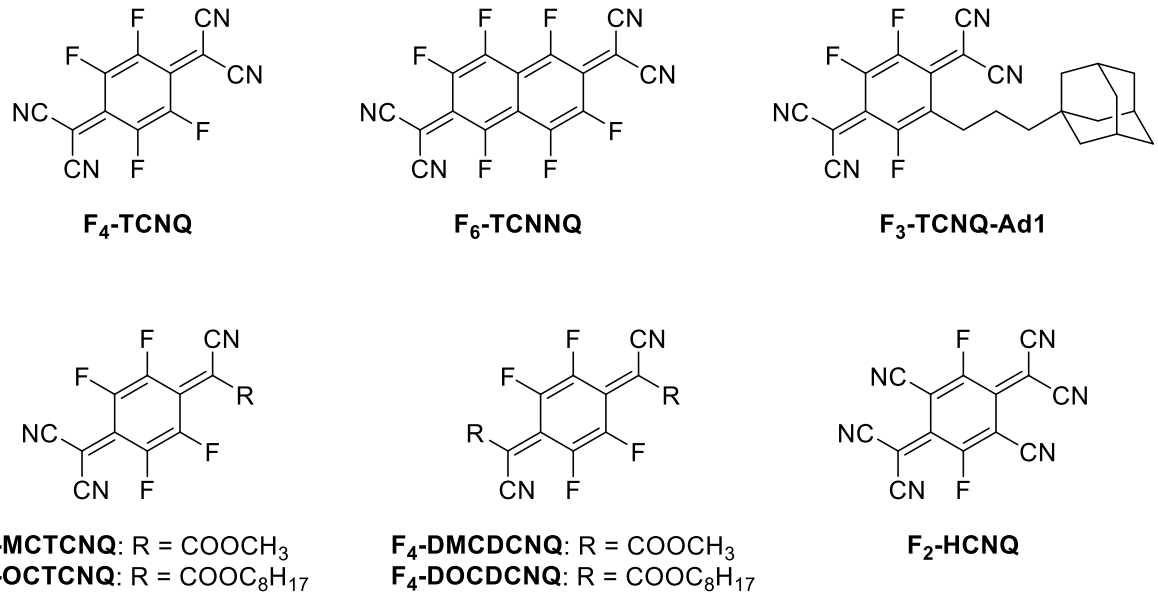

Figure 10: Structures of TCNQ-based molecular dopants.

2.3.2.2. **Fullerene dopants**

Fluorination has also been applied to fullerene-based p-dopants $C_{60}F_{36}$ and $C_{60}F_{48}$, significantly lowering the LUMO compared to C_{60}.[169,170] $C_{60}F_{36}$ was shown to have a doping efficiency similar to that of F_4-TCNQ – with the additional advantage of lower volatility and higher deposition control – whilst $C_{60}F_{48}$ have even stronger doping capabilities, doping materials with IE as high as 5.85 eV, as a result of the lower LUMO, and consequently a higher host/dopant energy offset.[171,172] Recently, a 1 mol% addition of $C_{60}F_{48}$ resulted in a 3-fold hole mobility improvement of a C_8-BTBT:C_{16}-IDT-BT blend, reaching charge carrier mobility values of 13 $cm^2V^{-1}s^{-1}$.[15] The bulky structure of fullerene derived dopants further provides an advantage of lesser diffusivity, and devices doped with fluorinated fullerenes have exhibited improved thermal and morphological stability.[15,171,173]

2.3.2.3. **Sulfur containing dopants and cationic dyes**

The design of suitable molecular n-type dopants has typically been more challenging, as the high-lying HOMO required for efficient doping results in high reactivity and instability in air. However, the major shortcomings of alkali metals as dopant species has prompted the search for molecular alternatives. In the early stages, molecules with relatively low-lying HOMOs, and therefore less efficient doping, were used, such as TTN, BEDT-TTF, and BTQBT.[174–176] A range of cationic dyes, either directly or via corresponding hydride precursors, were also trialed with some success (Figure 11).[177–179] Here the active dopant species is formed *in situ* during thermal evaporation. Lately, a couple of examples have emerged of dyes also being

used for p-doping, particularly with respect to conductivity improvement of polypyrrole through morphology guidance.[180–186]

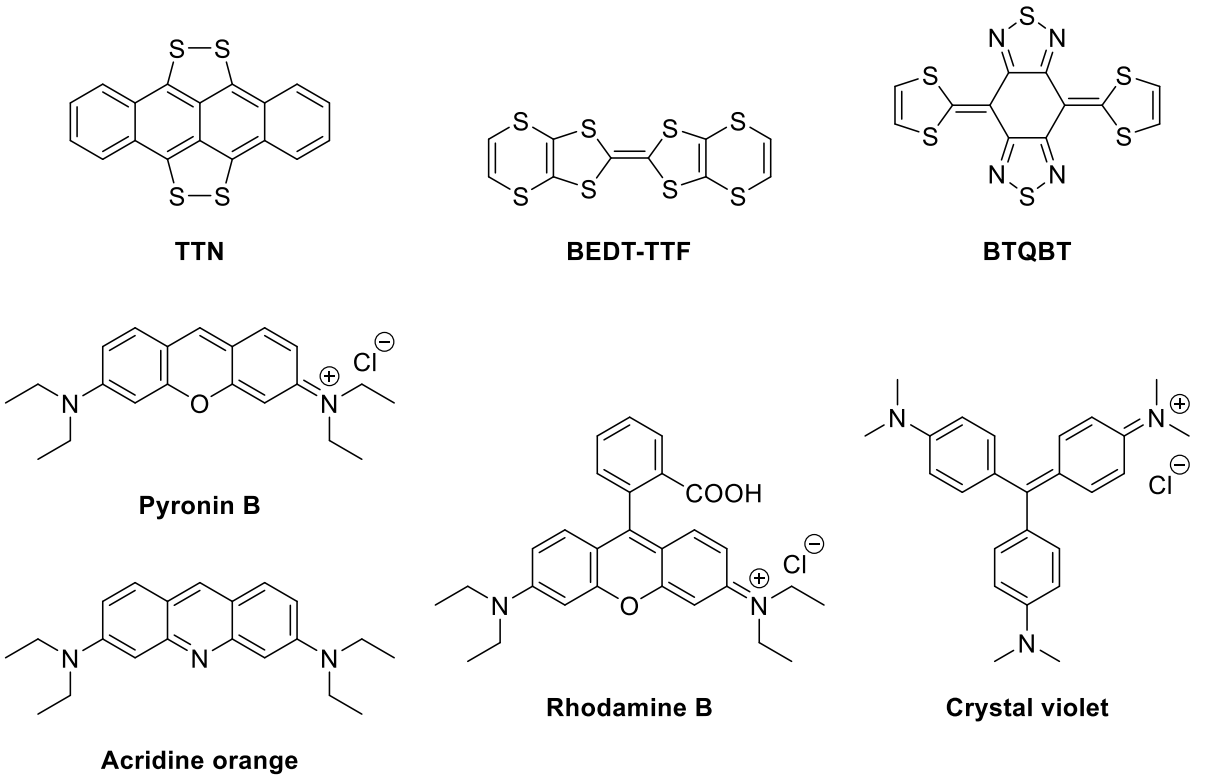

Figure 11: Structures of early n-type molecular dopants.

2.3.2.4. DMBI derivatives

One of the most commonly adapted designs for n-type molecular dopants derives from the DMBI molecule (Figure 12a). N-DMBI was first reported as a solution-processable, air-stable dopant for PCBM, with doping occurring via a thermally activated process involving hydride transfer.[187] The exact mechanism of this activation process has prompted much investigation as discussed in Section 2.2.2.[78,187–189] In brief, kinetic studies of the reaction between N-DMBI and PCBM suggest a hydride-transfer reaction to the fullerene, followed by electron transfer between the hydride-reduced PCBM and a neutral PCBM (Figure 12b).[188] Similar hydride-transfer pathways for the doping of other acceptor materials have also been proposed.[78,189] Although N-DMBI remains the most commonly employed molecular n-dopant, a multitude of related species has been synthesized in order to introduce or control various features of the dopant. Such species include halide salts and methoxy, alcohol, diphenylaniline substituted species, and dialkylaniline.[190–196] Glycol substituents have also been used to improve the dopant miscibility with glycol-containing fullerene-based semiconductors for thermoelectric applications.[197]

Fabiano and co-workers carried out a thorough study to investigate the correlation between the SOMO energy level of the active radical species and its doping efficiency.[198] By adding electron donating methyl and/or dimethylamine substituents to different positions of the DMBI core, they were able to finely tune the SOMO energy level. Subsequently, they were able to show a gradual increase in conductivity of a doped poly{[N,N'-bis(2-octyldodecyl)-naphthalene-1,4,5,8-bis(dicarboximide)-2,6-diyl]-alt-5,5'-(2,2'-bithiophene)} (P(NDI2OD-T2)) polymer as a result of the higher-lying SOMO energy of the dopant. They were able to increase the conductivity by an order of magnitude through a SOMO shift as small as 0.3 eV. One drawback of hydride precursors is the hydride transfer to the host semiconductor, potentially resulting in unwanted side-effects. To circumvent this issue, Marder, Bao and co-workers synthesized a set of air-stable DMBI dimers, in which two DMBI derivatives were directly linked to at the 2-position, inspired by the success of metallocene dimers as discussed below.[199] Like the hydride precursor, the reasonably air-stable dimers (stable over the course of several days or weeks) are thermally activated, and doping can proceed via two competing mechanisms: either via a rate limiting dimer cleavage, followed by electron transfer from each resulting radical species to the host semiconductor, or via a rate limiting electron transfer from the dimer to the host, followed by a bond cleavage, generating one ionic and one radical monomer species, prompting a second electron transfer of the radical species (Figure 12c).[200] An additional advantage of dimerized dopants is their suitability for both solution and vacuum processing. Additional modifications to the dimerized DMBI precursor have also been presented: Zhu and co-workers demonstrated how an introduction of methyl substituents to the DMBI core could improve the power factor of thermoelectric devices by raising the HOMO, compared to the reference DMBI dimer, and Pei and co-workers demonstrated a higher dopant efficiency of dimerized $(N\text{-}DMBI)_2$ compared to N-DMBI.[201,202] It is notable also that doping with $(N\text{-}DMBI)_2$ resulted in lesser impact on host morphology compared to doping with $(RuCp^*mes)_2$ (discussed below), due to its planar and less bulky structure.[202]

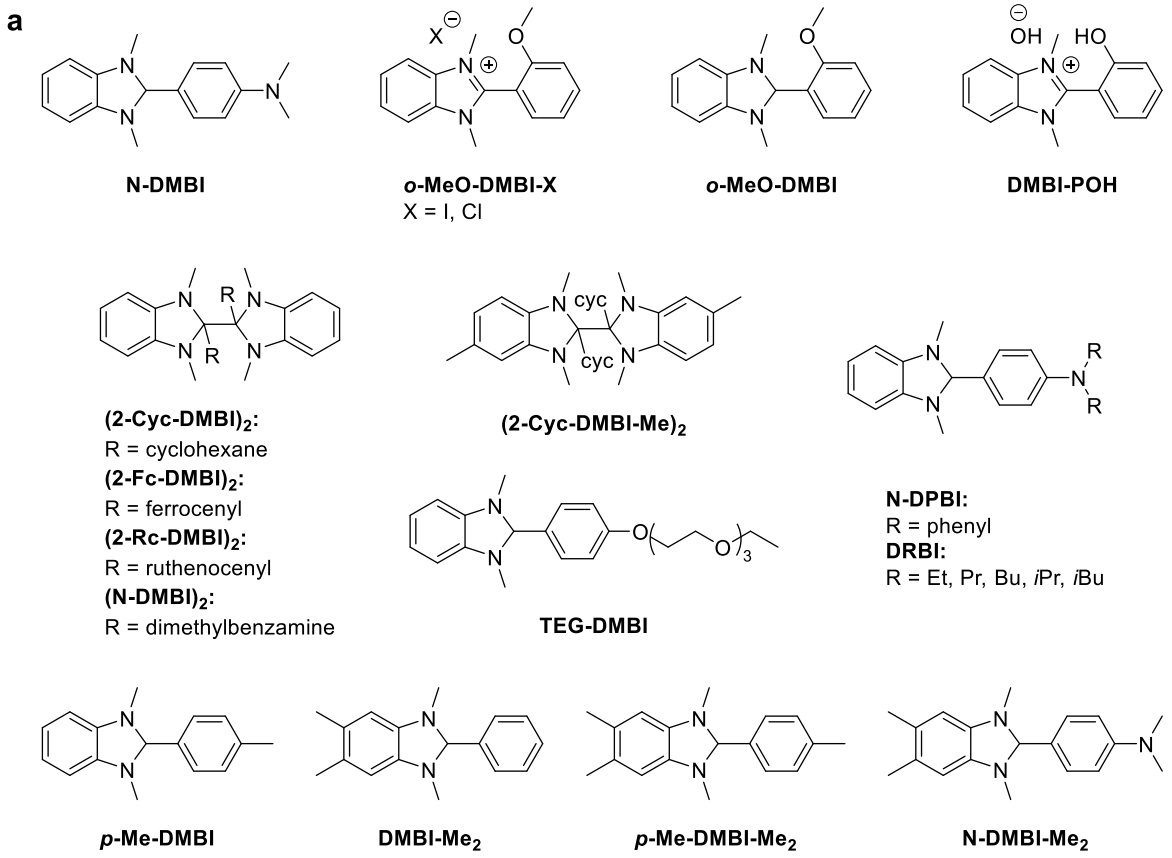

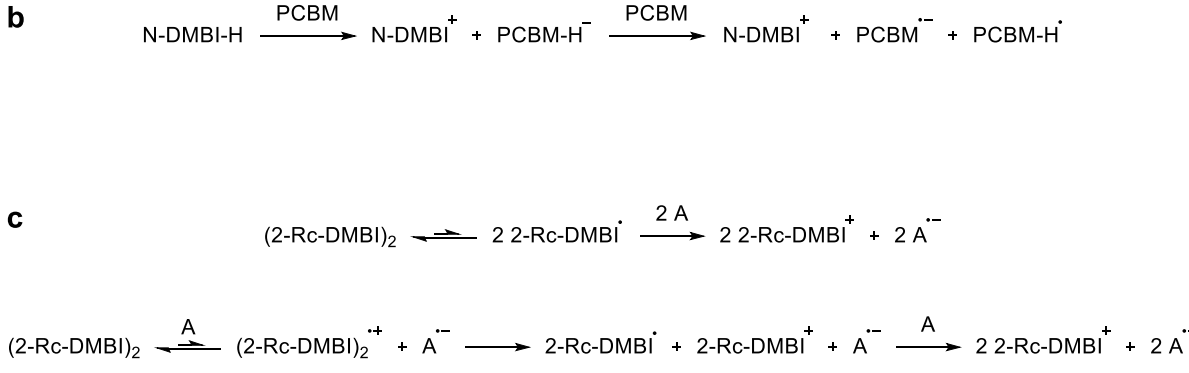

Figure 12: a) Structures of DMBI-based molecular dopants, b) hydride-transfer reaction steps between a fullerene derivative and N-DMBI, c) thermally activated doping mechanisms of DMBI dimers.

2.3.2.5. **Organometallics**

Organometallic dopants exist for both p- and n-type doping (Figure 13). $Mo(tfd)_3$ was introduced as a higher EA, less volatile, and less diffusive alternative to F_4-TCNQ.[203] $Mo(tfd\text{-}CO_2Me)_3$ and $Mo(tfd\text{-}COCF_3)_3$ followed as solution-processable alternatives, avoiding issues with precipitation sometimes occurring when doping with $Mo(tfd)_3$.[204,205] $Cr_2(hpp)_4$, $W_2(hpp)_4$, $Ru(terpy)_2$, and $Ru(t\text{-}but\text{-}terpy)_2$ have all been used for doping of n-type materials, but they all

suffer from high air-reactivity, somewhat limiting their impact as widely employed n-dopants.[57,206,207]

Sandwich compounds are another class of organometallic dopants that have been widely applied to n-type systems (Figure 13). The first example featured $CoCp_2$, followed by $CoCp^*_2$ in order to lower the IE and thereby increase the dopant strength.[208,209] A phenyl-substituted sandwich dopant, $Rh(C_5HPh_4)_2$ has also been reported, with the intention of reducing diffusivity as well as increasing the distance between the ionized host and the dopant counterion.[210] Although the dopant was rather insoluble with the P(NDI2OD-T2) polymeric host – which is thought to be the underlying reason for a rather low doping efficiency – dopant accumulation at the ITO electrodes led to a contact resistance reduction of a magnitude of five. Just like many other n-type dopants, sandwich compounds face challenges with air instability. To address this issue, a range of air-stable metal sandwich dimers were introduced as dopant precursors to be thermally activated, preceding the DMBI dimers previously discussed.[211–213] Once again, the mechanism may be initiated by either a dimer cleavage or an electron transfer, as previously outlined for DMBI dimers (Figure 12c). Which pathway is dominant seems to be dependent on the choice of both metal and ligand, which also impacts properties such as air stability. In the case of $(RuCp^*Mes)_2$, which has proven particularly useful for a variety of systems and host semiconductors, the dimer cleavage seems to be preceded by a reversible electron transfer, generating one cationic and one radical monomer, leading to a second electron transfer from the radical species.[214] A photo-activation mechanism has also been described for $(RuCp^*Mes)_2$, enabling the n-doping of materials with very high lying LUMO levels which are difficult to dope. The mechanism is proposed to involve either photoexcitation of the host material followed by an electron transfer from the ground state dimer, or direct excitation of the dimer leading to intermolecular charge transfer, both followed by dimer cleavage.[215,216]

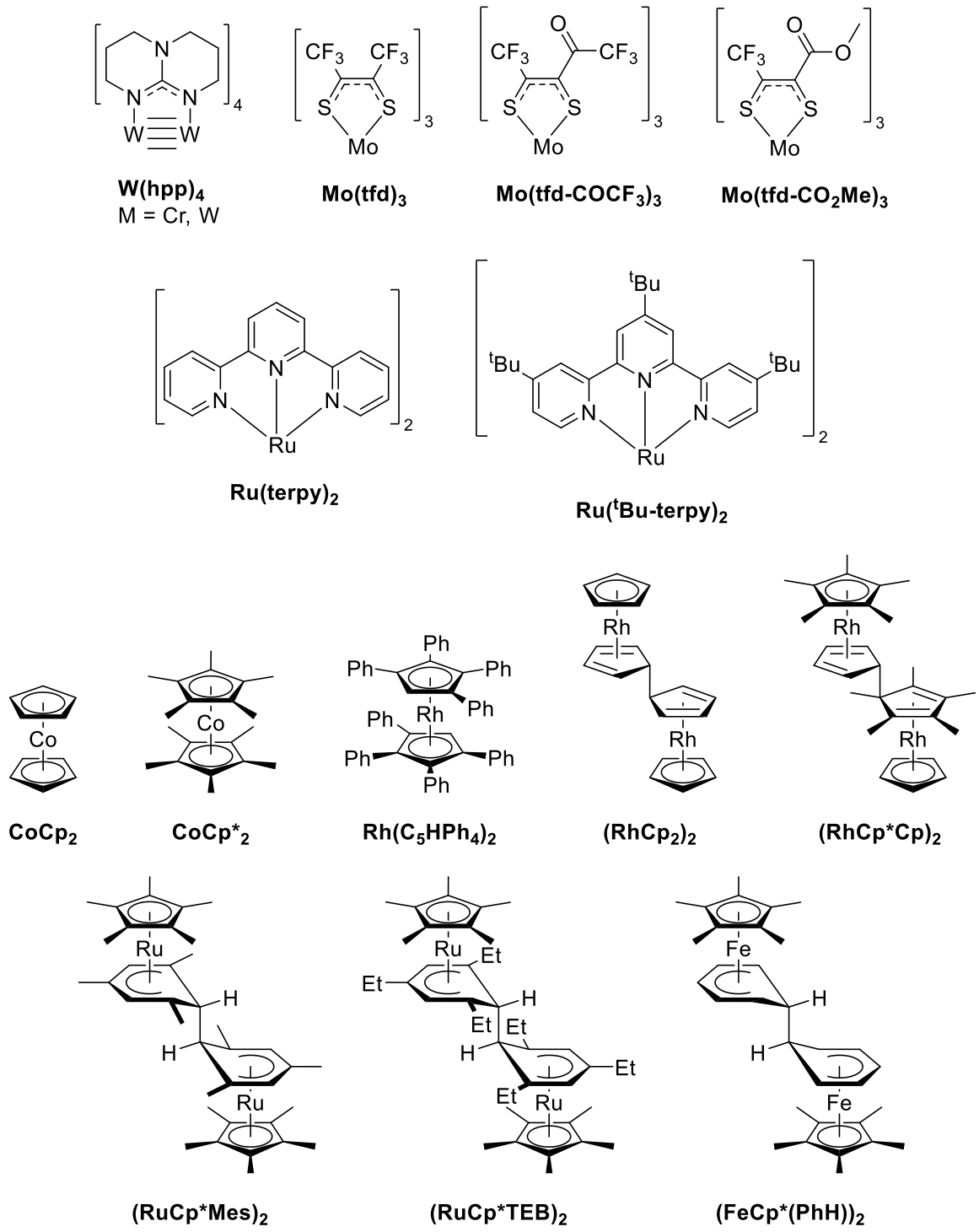

Figure 13: Structures of organometallic dopants.

2.3.3. Lewis acids and bases

Although Lewis acids have been extensively utilized as p-type dopants, traditionally these have been oxidizing Lewis acids such as $FeCl_3$ where doping occurs by electron transfer reactions. The development of non-oxidizing Lewis acids as dopants is one of the most significant

developments in the last decade. The first use of the non-oxidizing Lewis acid, boron trifluoride (BF_3), as a dopant was reported in 1995 by Utley et al who exposed a PPV polymer to an atmosphere saturated with BF_3.[79] The authors speculated that doping occurs via a polarized π-complex between the electron-rich alkene bonds of PPV and BF_3. One issue with BF_3 is its high chemical reactivity. For example, it readily reacts with water to give an adduct that can lose HF and ultimately afford fluoroboric and boric acid.[217] Such strong acids may have a detrimental effect on long-term device stability and are best avoided, although they may also play a role in the doping mechanism. The use of BCF, as discussed in previous sections, is an attractive alternative since it combines high Lewis acidity with improved tolerance for water and oxygen.[218] Welch *et al* investigated the influence of BCF on the optical properties of conjugated oligomers containing basic N atoms.[219] They found that BCF could form a complex with basic N atoms, resulting in a decrease of the intrinsic absorption of the oligomer and the formation of a new absorption band at lower energy. The extent of the shift could be modified by changing the strength of the Lewis acid, from weaker $AlMe_3$ to stronger BBr_3, suggesting that the optical changes are the result of a charge transfer complex.[220] Later, Zalar and co-workers used this phenomenon to tune the optoelectronic properties of polymer light-emitting diodes (PLEDs).[221] They used BCF in combination with a co-polymer containing a Lewis basic pyridyl group (F8Py), demonstrating that the photoluminescence (PL) not only shifted towards the higher wavelength but also increased its excited state lifetime and quantum yield.

BCF doping of another pyridyl co-polymer at low concentration (0.02 molar equivalent) was also found to be highly effective at increasing bulk mobility in diode devices, with a two order of magnitude improvement found for the optimized devices.[222] Again, the optical signature of charge transfer was clear, but there were no indications of polaron formation by NIR absorption or EPR, suggesting that doping via ICT was not occurring. Similar observations were found in other studies that reported non-oxidative doping by BCF of different donor-acceptor polymer systems could be precisely regulated by dopant concentrations.[223,224] Interestingly, Lewis Acids have been reported to lead to enhanced field-effect mobility in a variety of systems.[21,223,225] For instance, Han *et al*. observed a substantial improvement in the OTFT device performance of Lewis basic indenopyrazine containing polymers upon p-doping with BCF.[223] The device performance was found to be very sensitive to dopant concentration, with a substantial improvement at low dopant levels followed by a decrease in performance at higher concentrations, possibly due to structural disorder (see Section 4.2). The doping mechanism was suggested to occur via a Lewis Acid-Base interaction with the pyrazine lone pair, leading to the formation of 'pyrazinium' like cation, which induced

empty states into the band gap. Such a mechanism would be similar to the charge transfer complex doping reported by Mendaz *et al*,[66] except that rather than a molecular HOMO and LUMO interacting, it is specific to a Lewis acid/base pair, and as such may be easier to engineer into a system. There is also good evidence that the doping mechanism may occur via the interaction of BCF with water impurities present, generating a strong Bronsted acid, which leads to doping via protonation and subsequent electron transfer from a neutral polymer (see Section 2.1.2.3).[81] Whether such a mechanism operates in all reported examples is still an open question, and the possible doping mechanisms have recently been reviewed in detail by Baumgarten *et al*.[80]

Lewis acids have also been used for p-doping in hole transport layers (HTLs) and in active layers for solar cells due to their ability of interface refinement and energy level modification.[226–229] For example, BCF doping in the amorphous donor polymer poly(triaryl)amine (PTAA) was found to improve the hole mobility of the HTL along with the downshift of HOMO level resulting in the facilitation of hole extraction.[227–229] Again, even though consideration of the energy levels of the PTAA (HOMO ca. -5.2 eV) suggests that ICT to the BCF is unlikely, the formation of a frustrated Lewis pair (FLP) is suggested to facilitate the electron transfer from the PTAA.[227] BCF-doping of the solar cell blend PM6/IT-4F was shown to have a significant impact on device performance. Here, the authors suggest that different doping mechanisms occur with the donor and the acceptor, with the former undergoing a single electron transfer via the formation of an FLP between BCF and the PM6 (donor), whereas the latter forms a Lewis acid-base adduct with IT-4F (acceptor).[226]

Lewis Bases are a potentially attractive option for n-type doping, since they do not require the high lying HOMO required for ICT, potentially improving stability. A plausible mechanism would involve the interaction of a lone pair or anion with an electron-deficient conjugated system (sometimes called a π-acid). The extent of doping not only depends on the dopant strength but also on the π-acidity of the OSC. Hence, effective doping can only be found in electron-deficient semiconductors. In this context, perylene diimide (PDI) derivatives have been extensively studied with various Lewis bases such as hydroxide and halides. Russ *et al.* showed that a PDI containing an ammonium hydroxide based side chain can lead to self-doping affording a high-performance thermoelectric material with high conductivity and power factor compared to, at the time, other n-type thermoelectric materials.[220] A subsequent study by the same group established that the mechanism was based on a Hoffman type elimination of methanol during heating to afford a tethered dimethylamino side chain. The amine lone pair then acts as Lewis base for the subsequent doping mechanism.[230] The incorporation of

dimethylamino groups into the sidechains of electron deficient polymers and OSCs has also led to self-doping materials.[231–233]

The use of tetrabutyl ammonium fluorides (TBAF) and hydroxides (TBAOH) as dopants in an electron-deficient PDI containing conjugated polymer was reported by Kim *et al*.[234] This type of interaction was reported for a variety of anions including lithium benzoate,[235] acetates,[236] borates,[237] carboxylate,[160,238–242] and all types of tetrabutylammonium-halogen salts in OSCs used for transistors and solar cells.[243,244] In those cases, the increase in the conductivity and charge carrier concentration in OSCs due to n-doping played a key role in device performance improvement. More recently divalent anions, such as oxalate, have been shown to be much stronger electron donors and, unlike the monovalent Lewis anions, can even dope materials with low EA.[245] It should be noted that the mechanism of TBAF doping, in particular, has sparked some interest due to the high electron affinity of fluoride (see Sections 2.1.2.3 and 2.2.2).

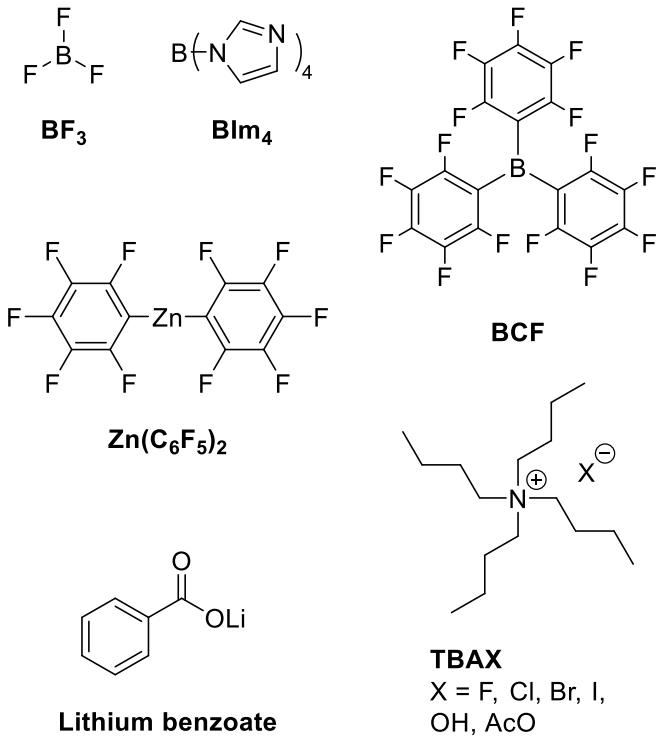

Figure 14: Structures of Lewis acids and bases.

2.3.4. **Radialene based dopants**

Radialenes are cyclic compounds containing cross-conjugated exocyclic double bonds. Whilst the parent unsubstituted system is rather unstable, those containing electron-withdrawing substituents can be readily synthesized and exhibit multielectron transfer due to the cross-conjugated π-system.[246] Recently, a radialene-based p-dopant, CN6-CP, has attracted much

attention due to its powerful doping abilities in OSCs. CN6-CP was first synthesized in 1976 by Fukunaga *et al.*,[247,248] but it was not reported as a dopant until 2016 when Karpov and co-workers studied its p-doping property in a donor-acceptor polymer poly[3,6-(dithiophene-2-yl)-2,5-di(6-dodecyloctadecyl)pyrrolo[3,4-c]pyrrole-1,4-dione-alt-thieno[3,2-b]thiophene] (PDPP(6-DO)$_2$TT).[249] The authors found that the dopant possesses a very high EA of 5.87 eV, which makes it an efficient p-dopant even for high-IE OSCs such as hole-transporting materials in OPVs and OLEDs.[250] The doping mechanism is believed to undergo a single-electron transfer process, which leads to the formation of an integer charge transfer complex (ICTC) where a host cation and dopant anion-radical (CN6-CP$^{\bullet-}$) is involved.[85,249–251] However, the low solubility of the dopant in common solvents limits its applicability for blend doping.

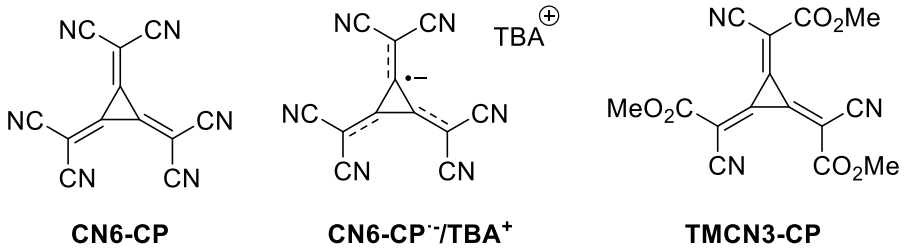

Figure 15: Structures of radialene-based dopants.

This solubility issue was addressed by replacing the neutral dopant with the salt of radical-anion (CN6-CP$^{\bullet-}$), which was readily prepared from commercially available tetrachloropropene in just two steps.[252] Depending on the cation, the solubility of the dopant varies from polar to non-polar solvents. Although the EA of the dopant is reduced to 5.1 eV compared to the neutral dopant, the organic soluble tetrabutylamine (TBA) salt was shown to be effective in p-doping P3HT to a high conductivity of 2.7 S cm^{-1}. Recently, Karpov *et al.* studied the doping performance of the radical-anion in two different approaches, conventional mixed solution, i.e. co-processing , where the dopant is mixed with P3HT in solution phase and sequential processing, where the bilayer of dopant and P3HT is fabricated using orthogonal solvents (see Section 3.1).[253] The study found that sequential processing is more efficient than co-processing in terms of conductivity improvement, which is due to the formation of sub-micrometer clusters in case of the former. Additionally, in case of co-processing, charge trapping was observed due to the formation of a higher number of ionized states which in turn suppress the conductivity.

Another approach to improving solubility is the synthesis of derivatives in which three of the nitrile groups are replaced by methyl esters. The resulting dopant, trimethyl 2,2′,2″-

(cyclopropane-1,2,3-triylidene)-tris(cyanoacetate) (TMCN3-CP), exhibits a reduced EA of 5.5 eV compared to CN6-CP but demonstrates significantly enhanced solubility in halogenated solvents. Effective doping of a range of p-type polymers such as P3HT and DPP co-polymers was demonstrated.[254]

2.3.5. Amine based n-dopants

Non-conjugated polymers containing aliphatic amine groups, such as polyethylenimine (PEI) have been demonstrated as universal surface modifiers, allowing the formation of air-stable low work function electrodes for efficient electron injection.[255] PEI has also been explored as a strong n-type dopant that can act as a polarity converter for certain ambipolar and p-type semiconductor into unipolar n-type transporting systems. The doping process is believed to result from electron transfer from the amine groups of PEI to the OSC, similar to that proposed for the dimethylamine functionalized semiconductors discussed earlier (Section 2.3.3). The complex structure of highly branched PEI with a variety of primary, secondary, and tertiary amine groups complicates the investigation of the mechanism. This is exemplified by the work of Fabiano *et al*. who found that a volatile component of PEI, identified as ethyleneimine oligomers, was effective at doping three different OSCs: poly(3,4-ethylenedioxythiophene) polystyrene sulfonate (PEDOT:PSS,), PCBM, and (P(NDI2OD-T2)).[256] Upon PEI vapor treatment, the p-type PEDOT:PSS film showed a visible color change from semitransparent light blue to dark blue indicating the reduction of $PEDOT^+$ to its neutral state, accompanied by a reduction of conductivity. A similar trend was observed in the case of PCBM and P(NDI2OD-T2) ambipolar OSCs, where the n-type conductivity increased by 2-4 orders of magnitude, reflecting the complete conversion of electrical polarity towards n-type behavior. The polarity conversion effect can also be seen upon blending of PEI in ambipolar and p-type polymers.[257] The electron-rich amine groups in PEI are believed to raise the Fermi level by filling electron traps in the semiconductors. Moreover, a significant improvement in electron mobility was found in PEI doped n-type OSCs.[258,259] Additionally, PEI can act as a trap site for holes that effectively suppress the p-type mobility and enforce the electrical polarity conversion.

Recently, Fabiano and co-workers also demonstrated an n-doped poly(benzoimidazobenzophenanthroline):PEI (BBL:PEI) polymer-polymer blend, deposited as an alcohol-based ink.[260] Owing to its intrinsically high conductivity (8 S cm^{-1}), thermal and ambient stability, resilience to organic solvents, and air-processability, it has the potential to

be used for n-type applications in an analogous fashion to the benchmark p-type material PEDOT:PSS.

For certain applications, the complex nature of PEI and related amine containing polymers, can become undesirable characteristics. Therefore, some work focused on developing molecular materials, which do not suffer the issues of traditional electron-rich, amine-containing dopants like tetrakis(dimethylamino)ethylene (TDAE), which is volatile and reacts with ambient oxygen. For example, the bulkier and non-volatile derivative (12a,18a)-5,6,12,12a,13,18,18a,19-octahydro-5,6-dimethyl-13,18[1′,2′]-benzenobisbenzimidazo[1,2-*b*:2′,1′-*d*]benzo[*i*][2.5]benzodiazocine (DMBI-BDZC), containing an electronrich enetetramine, was reported to be an effective n-dopant of both polymer and small molecule OSCs based OTFTs. The doping mechanism was proposed to follow the ICT process, as indicated by EPR and low-temperature charge transport measurements.[261] Slightly less electron-rich cyclic amines, such as amidines 1,8-diazabicyclo[5.4.0]undec-7-ene (DBU) and diazabicyclo(5.3.0)non-5-ene (DBN), have also been investigated. DBU was introduced in different organic semiconducting electron transporting layers (ETLs) for perovskite solar cells, where it was found to have a strong doping effect due to its electron-donating ability.[262] More recently several bicyclic guanidine-type structures, based on the super-base 1,5,7-triazabicyclo[4.4.0]dec-5-ene (TBD), have been reported as a readily prepared class of non-volatile dopants with high thermal stability, as demonstrated through the doping of PCBM-based ETLs in perovskite solar cells.[263]

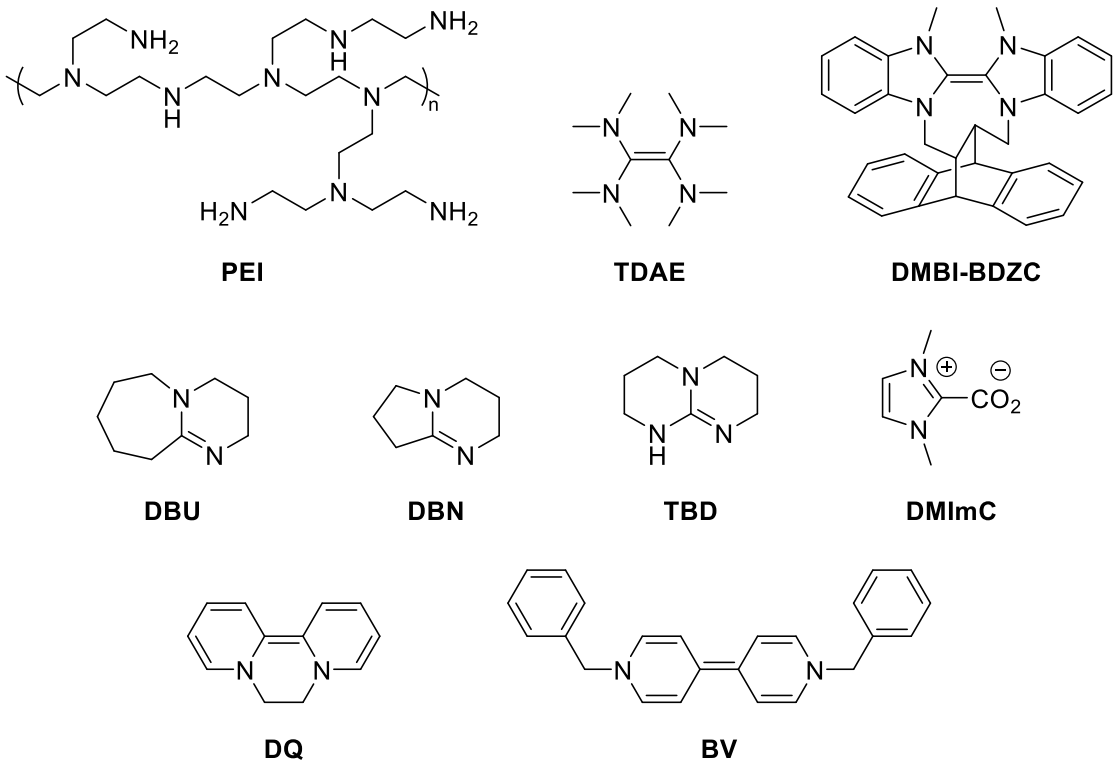

Figure 16: Structures of some amine-based dopants.

Furthermore, electron-rich amines based on diquat (DQ) and benzyl viologen (BV) have recently been investigated. DQ was found to be effective for doping in ternary blends for bulk heterojunction OPV applications, leading to an improvement in OPV device efficiency. [264] BV was proven to be a strong dopant in both OFET and thermoelectric devices, overcoming stability issues related to doping with TDAE, and contact resistance issues associated with DMBI and DPBI.[265] [266] Certain electron-rich enamines exist in equilibrium with their corresponding carbenes (the Wanzlick equilibria). Depending on their structures, the dimeric form may readily convert into the corresponding N-heterocyclic carbene (NHC). Such species are strong sigma-electron donors (Lewis bases) and nucleophiles. The formation of a such a NHC, from the thermal activation of a stable precursor, 1,3-dimethylimidazolium-2-carboxylate (DMImC), has been recently reported for sequential doping of n-type OSCs sequential processing.[267] The carbene was suggested to chemically react with the OSC to form a radical anion, as indicated by absorption and EPR measurements. Unlike the free carbene, the carbene precursor exhibited excellent air stability, and the doping species could be formed in situ with high doping efficiency, resulting in a substantial improvement in the OSC film conductivity.

2.3.6. Other new dopants

Several other examples of dopants have also been reported recently. For example, Sakai and coworkers have introduced a new class of p-dopants, based on a reactive mixture of dimethyl sulfoxide (DMSO) and hydrobromic acid (HBr).[268] Protonation of the DMSO is proposed to form an electron-accepting adduct, affording dimethyl sulfide and water upon doping of the OSC. Whilst diffusion of the bromide counterion caused issues in multi-layered devices at elevated temperatures, leading to de-doping, 10-camphorsulfonic acid (CSA) could be added to the DMSO-HBr mixture, with the larger size of camphorsulfonate resulting in reduced diffusivity. Another interesting example is the Mes_2B-TPFB salt, based on a strongly oxidizing doubly substituted borinium cation (Mes_2B^+) and a weakly coordinating tetrakis(pentafluorophenyl)borate (TPFB) anion. Wegner *et al*. used this organic salt as a p-dopant in P3HT and compared the doping mechanism and efficiency with that of BCF.[269] Interestingly, whilst optical absorption data showed that both dopants induce polaron formation, only the borinium salt showed an occurrence of a bipolaronic peak at higher dopant concentrations (≥10%), despite bipolarons usually being observed only in electrochemical doping or doping with oxidizing Lewis acids such as $FeCl_3$.[270–273]

The polaron (bipolaron) formation was proposed to occur via an (two) electron transfer from the polymer to a (two) Mes_2B^+ cation, leading to the formation of a (two) $Mes_2B^{\cdot}$ neutral radical, leaving the film as a volatile species, with TPFB as the charge balancing counterion. The resulting polaron (or bipolaron) is stabilized by the (two) TPFB anion to form an ion-pair complex. The bipolaron formation is energetically unfavorable for most dopants since it involves an electron transfer from a positively charged organic semiconductor to the dopant, but the high EA (5.9 eV) of the Mes_2B-TPFB salt facilitates the process in the case of P3HT.[274] Notably, the bulky TPFB counteranion forms a weaker ion-pair complex with low Coulombic binding energy compared to the conventional charge transfer dopants like F_4-TCNQ.[275] Hence, facilitated charge delocalization is observed, leading to pronounced charge transport. Hu *et al*. reported a similar approach with the organic salt trityl tetrakis(pentafluorophenyl) borate (TrTPFB), containing the TPFB anion with a trityl cation. It was shown to be an effective dopant for two p-type polymers in OFET devices.[275]

Another boron-containing bulky dopant, functionalized dodecaborane (DDB-F_{72}), was used by Aubry *et al*., for sequential p-doping of P3HT .[101] Dodecaborane (DDB) clusters are robust species with 3D aromaticity, and functionalization with 3,5-bis(trifluoromethyl)benzyloxy afforded a strong electron-accepting species (ca. 0.5 eV greater than F_4-TCNQ). The doping process is believed to result from a typical electron transfer to form the P3HT polaron. However, the extreme bulkiness of the dopant molecule prevents it

from the intercalation inside crystalline domains. Polaron delocalization is facilitated by the shielding of the anion within the DDB core. As such, no signature of polaron-counterion complex formation was observed, helping to explain the high conductivities observed (approximately one order of magnitude higher than for F_4-TCNQ doped P3HT). Follow-up work demonstrated how functionalization of the carborane with various benzyloxy groups could be used to tune the dopant electron affinity, with more electron-withdrawing substituents resulting in higher doping efficiency.[276]

Recently, a new type of hydride transfer dopant based on TAMs was introduced by Yang *et al*. in OSCs for thermoelectric applications.[277] The doping kinetics of the TAMs are slower than the conventional hydride transfer dopants like N-DMBI, but they are thermodynamically stable, with a substantial activation energy required for doping (thermally activated doping). Additionally, the high dopant-semiconductor miscibility and efficient doping performance make this class of dopants interesting. Hydride transfer n-dopants based on 1,4-dihydropyridine have also been reported.[278] Compared to traditional hydride transfer agents like N-DMBI, the 1,4-dihydropyridine framework is readily synthesized in four steps, which potentially facilitates tuning of the electronic and physical properties. Doping was shown to proceed for several electron-deficient polymers and PCBM via simple solution mixing, with no thermal or photochemical activation required.

An interesting approach was recently reported by Goel *et al*., based on the mixing of two p-type semiconductors, in which one of the OSCs is oxidized. In this case, chemically oxidized spiro-OMeTAD$(TFSI)_2$ with a partially filled HOMO.[70] Blending with a second, polymeric semiconductor based on DPP with a higher-lying HOMO than spiro-OMeTAD$(TFSI)_2$ resulted in hole transfer to the polymer. Since no new acceptor anions/or radical anions are formed as a result of doping, and the highly stable TFSI anion is already present, good thermal and air stability of the doped blends was observed. Recently, Kong *et al.* reported p-doping in spiro-OMeTAD:LiTFSI blend by bubbling the solution with CO_2 under UV light.[279] CO_2 acts as an oxidizing agent where electron transfer occurs from the photoexcited spiro-OMeTAD to CO_2 and subsequently, the charged gas reacts with Li-ion to form carbonates as a side product. The overall conductivity of the HTL increased substantially with the doping. A similar process occurs when p-doping polymers with the strong oxidant Magic Blue.[71,72]

Finally, a fascinating approach was recently reported by in which ground-state electron transfer was observed in an all-polymer system.[277] By utilizing small IP donor polymers based on electron-rich alkoxythiophenes in combination with the high-EA acceptor polymer BBL,

the simultaneous formation of p and n-polarons is observed by electron transfer at the interface. The resulting conducting interface has resistivity values five to six orders of magnitude lower than either individual polymer. Since no mobile dopants are present issues regarding dopant diffusion or phase segregation are avoided.

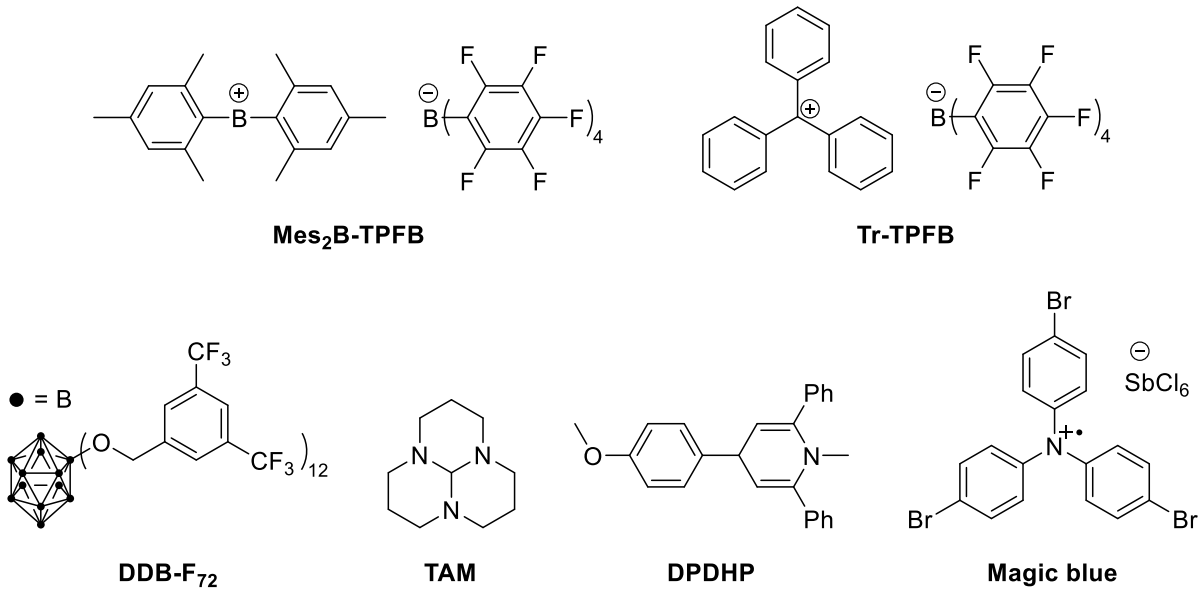

Figure 17: Structures of other novel dopants.

2.3.7. Self-doping species

Although the concept of self-doping in organic semiconductors – conjugated systems with side chains that can dope the backbone – has been around for a long time, interest in such materials has increased in recent years.[280–283] Such species avoid any issues with phase segregation of blends or diffusion of molecular dopants. Often, the side chains contain ionic groups to charge compensate the doped backbone, and as such they also tend to be soluble in water or highly polar organic solvents, facilitating multi-layer processing by orthogonal solvent processing. This combination of unusual properties makes such materials excellent candidates for charge extracting interfacial layers in organic semiconductor devices.

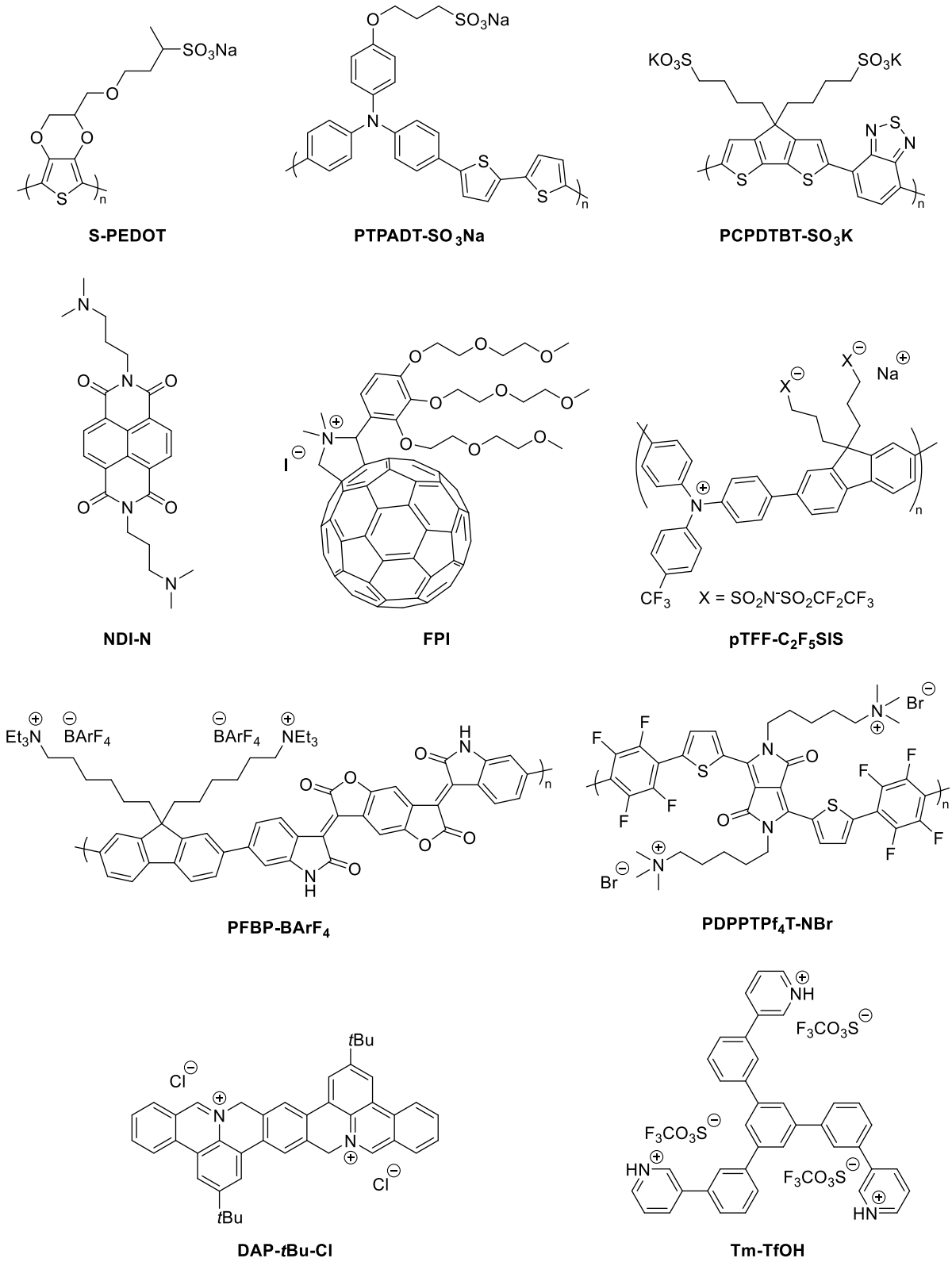

Figure 18: Structures of a selection of self-doping molecular species.

For the self-doping of p-type materials, a pendant sulfonate group is often attached to the backbone to charge compensate the doped backbone, similar to PEDOT:PSS.[284,285] Among

several examples, one self-doping PEDOT derivative (S-PEDOT, Figure 18) has recently been reported with conductivity values greater than 1000 S cm^{-1}, rivaling that of the commonly applied benchmark material PEDOT:PSS.[286,287] Similar examples of polythiophene derivatives also exist, analogous to the well-known polymer P3HT.[282,288] The use of self-doping polymers with pendant sulfonate groups as p-type interfacial materials has been demonstrated, with several materials, such as PTPADT-SO_3Na, outperforming the benchmark material PEDOT:PSS in perovskite or OPV devices, both in terms of power conversion efficiency and stability.[289–292] Several examples also exist of CPDT-BT derived polymers, for use in thermoelectric devices.[293] Mechanistic studies of the self-doping of CPDT-BT polymers suggested that the process is initiated by protonation of the polymer backbone, followed by intermolecular electron transfer from an adjacent polymer backbone, resulting in one protonated and one cationic radical species.[294] The choice of counter-ion has been shown to impact the properties of the polymer: polymers with Na^+ counter-ions showed higher conductivity than with K^+, whilst polymers with TBA^+ possessed too low values to be measured.[293] TBA^+, however, as a counter-ion with organic components, enables solubility in polar organic solvents, which is not possible with Na^+ or K^+.[295] Solubility in organic solvents was also achieved with a pendant neopentyl sulfonate group attached to 3-phenylthiophene and phenylacetylene polymers, acting as a precursor to the thermally activated self-doping polymers.[296] Interestingly, the use of cationic pyridyl groups instead of anionic sulfonate groups in CPDT-BT polymers, is shown to cause n-type self-doping instead of p-type, resulted in a shift in charge-carrier properties, from p-type to n-type.[297] This behavior was also subject to the choice of counter-ion.

Pendant ionic ammonium groups and Lewis basic tertiary amine groups are typically used in self-doping n-type materials, which are often based on the conjugated NDI or PDI core.[220,298] As discussed above, the self-doping is suggested to derive from *in situ* formation of the dimethyl amino group, which participates in the electron transfer.[230] However, recently reported polymers of both amine and ammonium functionalized analogues have shown various degrees of doping without any clear trends with regard to the choice of pendant group or counter-ion, calling for additional mechanistic studies of such materials.[232,299] Some trends have been identified with regards to the design of amine containing side chains, with self-doping being favored by sterically unencumbered amines, with increased steric hindrance having a detrimental effect on both polymer conductivity and its performance as an electron transporting interfacial layer in OPVs.[300,301] Using gradually longer alkyl chains between the core NDI molecule and its pendant ammonium group also resulted in gradual improvement of

conductivity and device performance – it is quite possible, however, that this is an effect of a favorable thin film structure, rather than higher doping efficiency.[220] The choice of polymer backbone units may also be important for n-type self-doping; Huang and Cao and co-workers showed that the incorporation of the open-shell diradical benzobisthiadiazo unit would promote self-doping, as well as enable photo-induced self-doping.[302]

Self-doping fullerene derivatives containing ammonium iodine salts have also been demonstrated, with application as interfacial layers.[303–305] Addition of self-doping fulleropyrrolidinium iodide (FPI) to a PCBM blend also resulted in enhanced conductivity, with the blend performing better than the pristine FPI.[306] Such intermolecular doping capabilities have also been found with self-doping NDI in various PDI blends.[233] Interestingly, changing from ammonium to the free amine suppressed the self-doping effect.[306]

Many self-doped materials have been successfully applied as electron transporting interfacial layers in OPV devices. As mentioned above, many of these materials are based on the NDI and PDI conjugate cores, often reaching excellent PCE and outperforming conventional materials.[220,231,232,298–300,307–309] Additional self-doping materials have been synthesized and tested for this purpose, for example: benzodifurandione-centered oligo(p-phenylene vinylene) (BDOPV)-fluorene polymers,[310] DPP-TP based polymers,[311] azaphenalene diradicaloids,[312] and 3,3′-(5′-(3-(pyridin-3-yl)phenyl)-[1,1′:3′,1″-terphenyl]-3,3″-diyl)dipyridine (TmPyPB) salts for OLED applications.[313]

A very promising route to highly doped materials was reported by Ho and co-workers, who presented a range of highly doped materials through a so-called self-compensating approach.[314] Rather than relying on the doping effect of the pendant acidic/ionic group, they oxidized/reduced the conjugated backbones with pendant ionic side chains using external dopants (Nitrosonium hexafluoroantimonate ($NOSbF_6$) and N-DMBI for p- and n-type polymers respectively), followed by internal ion exchange and removal of both the counter-ion and the dopant ion as a salt. This resulted in a charged polymer backbone, stabilized by the opposing charge of the pendant ionic group. Because excess ions are removed, and all remaining ions are covalently bonded, interlayer diffusion is suppressed, allowing for extremely high doping levels. This was demonstrated as a viable approach towards high-performing interfacial layers, with both p- and n-type materials outperforming conventional materials such as PEDOT:PSS and Ca, MoO_3, and Al, with successful applications in OPVs, OLEDs, and OFETs.[314–316]

2.4. Design of organic semiconductors for dopant/host interactions

It may seem obvious that the optimization of dopant/host compatibility is a two-sided challenge. It is therefore somewhat surprising that most research efforts have mainly looked into dopant design; it is only in recent years that studies have emerged which aim to understand what aspects of host design may improve doping efficiency - particularly within the scope of thermoelectric materials. Typical aspects of material optimization, such as dopant miscibility with the host material, film morphology of the doped mixture, favored dopant-host interactions, and minimized Coulombic interactions, all aim to improve the electronic performance of the doped material. In general, material design for this purpose can be split into two dominating categories: side chain and backbone engineering.

2.4.1. Side chain engineering

The choice of polymer side chains has a major impact on the eventual effect of added dopants. One of the most important discoveries has been the influence of polar glycol (also known as ethylene oxide) side chains, which have been found to improve dopant miscibility in the amorphous side chain regions of the host structure. This prevents dopant precipitation or aggregation and promotes dopant dispersity, generally leading to greatly improved doping efficiency and conductivity enhancement by up to several orders of magnitude (low doping regime), as well as allowing for higher dopant concentration.[97,317–322] Studies on random thiophene co-polymers containing partial incorporation of glycol side chains, have shown that there is not necessarily a beneficial impact on the electronic properties of the doped material, as F_4-TCNQ doped thiophene co-polymers with 5-30 % glycol monomers displayed a reduced degree of solid-state order and hence reduced charge-carrier mobility as compared to P3HT.[323] It is worth noting that the linking group attaching the glycol sidechain to the backbone is important as it can impact the energetics of the backbone, and therefore the driving force for doping. For example polythiophenes functionalised with triethylene glycol (TEG) either directly to the backbone, via an electron donating oxygen atom, or via a methylene ($-CH_2$) spacer behave very differently in terms of conductivity and thermal stability, with the former exhibiting higher performance.[324]

The beneficial effect of polar pendant groups has also been confirmed for PTEG-1 – a fullerene-based semiconductor with oligoethylene glycol pendant groups – where high miscibility of N-DMBI in the side chain region allowed for undisturbed π-π stacking of fullerene bodies.[325,326] The use of polar pendant groups also increased doping efficiency from a few percent to near 100 %, because of facilitated dissociation of formed CTCs.[322] When also

equipping the dopant, N-DMBI, with a polyethylene glycol (PEG) chain, the required dopant concentration to achieve equal performance was halved, from 40 to 20 mol%.[197] Even higher performance was achieved using Cs_2CO_3 as a dopant, compared to N-DMBI and TBAF, which was attributed to the small size of the dopant having a smaller effect on side chain spacing.[327] In a study conducted by Koster and co-workers, they compared the use of glycol side chains versus amphipathic side chains: glycol side chains with an aliphatic linker.[328] They showed that the use of amphipathic side chains in P(NDI-2Tz)-type polymers increased the Seebeck coefficient without impairing conductivity, implying that in addition to dopant/host miscibility, side chains can also play an important role in weakening the Coulombic interactions between the dopant/host ion pair (see Section 2.1.2.1).

Several recent studies have highlighted the increased thermal stability of doped systems as yet another benefit of the incorporation of glycol side chains, both under inert and ambient conditions.[317,324,326,329] This is of particular importance for thermoelectric devices, operating at elevated temperatures. A common rationale behind this phenomenon – predominantly based on studies on thiophene polymers doped with F_4-TCNQ – argues that the stabilization of the doped mixture stems from an energetically favorable environment for the dopant anion as provided by the polar side chains, reducing diffusion and sublimation of the dopant upon heating.[317,324,329] A recent study by Ratcliff, Pemberton and co-workers proposed an alternative mechanism based on side reactions between the dopant and polymer host.[330] They demonstrated the formation of protonated HF_4-$TCNQ^-$ upon heating in the presence of P3HT as a result of hydrogen abstraction from the aliphatic carbon adjacent to the polymer backbone. Replacing the methylene group with alkoxy linked glycol side chains completely suppressed this degradation pathway.

Regarding side chain length, studies on various types of side chains imply that length has a significant effect on electric performance of the doped species.[326,331,332] In the case of fullerene based OSCs with PEGs, there were large variations between PEG lengths and both electric performance and optimal dopant concentrations.[326] The resulting performance did not follow any obvious trends, making it difficult to predict the ideal chain length. Investigating alkyl side chain effect on the doping of PBTTT, Brinkmann and co-workers compared linear alkyl side chains consisting of 8, 12, 14, and 18 carbon atoms.[331] With increasing chain length, intercalation of the dopant into the lamellar region had a lesser effect on the polymer lattice. The polymer with a dodecyl (C_{12}) side chain turned out to perform better than the others. They hypothesized that this was due to the balance between a lamellar region that was either packed too tightly (C_{18}) or was too disordered (C_8) to effectively intercalate the dopant. In a similar

vein, reducing with sidechain density on a series PBTTT analogues was also found to promote doping efficiency.[333] The impact of alkyl branching has also been examined for polythiophene. In comparing branched 2-ethylhexyl sidechains with linear hexyl groups, the additional steric hindrance of the branched chains was found to force F_4-TCNQ dopants close to the conjugated backbone, where they formed a CTC with a moderate degree of charge transfer and low overall conductivity.[334] In contrast, in P3HT, the F_4-TCNQ dopant resides in alkyl region, and efficient ICT is found to occur.

2.4.2. Backbone engineering

Naturally, polymer backbone design is primarily associated with changes to the electronic properties of a material which fundamentally influence its ability to be doped. For example, the use of co-monomers which widen the gap between donor and host frontier molecular orbitals tends to result in higher doping efficiency.[335–338] Another important consideration when aiming to improve conductivity of the doped species is backbone planarization. This can be achieved by opting for co-monomers that result in a more planar configuration, or through the use of backbone linkers with low steric hindrance, e.g. through the coupling of NDI with bithiazole (Tz2) instead of bithiophene (T2).[339–341] Although generally attributed to inherent properties of the materials, such as morphology, some studies also highlight the important role of polaron delocalization in the doped species towards high conductivity.[335,339,342] Interestingly, many of these materials display higher conductivities in their doped states despite lower mobilities of the pristine materials.[339,340,343]

Backbone modifications may also lead to various degrees of dopant miscibility. For example, Sommer and Caironi and co-workers managed to improve dopant miscibility, and consequently doping efficiency, by introducing kinked co-monomers into the backbone of P(NDI2OD-T2) by the use of *meta* coupled benzene.[344] It should be mentioned, however, that in this particular case, negative effects on charge carrier mobility resulted in overall reduced performance. Furthermore, Pei and co-workers demonstrated that choosing co-monomers which cause a lower degree of lamellar order may be favorable towards dopant miscibility, resulting in higher structural tolerance to doping.[345] Finally, the use of monomer units with an ability to form large crystallite structures have been shown to reduce Coulombic dopant/host interactions by distancing the dopant molecules from the tightly packed polymer backbones, allowing for high doping efficiency and conductivity.[342]

Another aspect of backbone design is the choice of heteroatoms to be incorporated into the conjugated system. Comparing a series of poly(3-alkylchalcogenophene) polymers (P3RX, X

= T, Se, Te, R = 3,7-dimethyloctyl), Yee and co-workers showed that polymers based on heavier heteroatoms were more susceptible to doping, i.e. they required lower dopant concentrations to reach the same conductivity values.[346] They later showed that this stems from a higher degree of ICT, rather than CTC formation, as a result of more planar backbone packing, directing the dopant molecule towards the lamellar regions.[347] Schwartz and Tolbert and co-workers compared random co-polymers of thiophene and selenophene, and demonstrated a relationship, albeit unpredictable, between backbone composition and the ability of the polymer to accommodate dopant molecules.[348] Experimentation with various heteroatoms has also led to more stable polymers. Through the substitution of two oxygen atoms with sulfur in the otherwise air-sensitive doped P(NDI2OD-T2), the new polymer could be exposed to air in its doped state for several hours without detrimental effects on conductivity.[349] This modification also had a positive impact on doping efficiency. The incorporation of specific heteroatoms or functional groups has also been utilized to promote specific doping interactions. For example, the incorporation of Lewis basic pyridyl or pyrazine based co-monomers has been used to promote interactions with Lewis acid dopants like BCF.[130,222,223,350] Such approaches can facilitate doping when ICT is energetically unfavorable.

2.5. Experimental characterization

To unravel a comprehensive understanding of the physicochemical processes that underlie doping and the resulting material properties, a wide range of complementary experimental methods must be applied. In the following, we briefly discuss those that are either diagnostic tools for the doping process or can shine light on the most relevant charge transport properties that result upon doping of OSCs.

2.5.1. Diagnostic methods for doping

Organic semiconductors feature a pronounced excitonic nature. Therefore, changes of the local charge density distribution, *e.g.*, upon dopant or semiconductor ionization and polaron formation, result in a rearrangement of the nuclear coordinates, which goes in hand with intramolecular bond length alterations and electronic energy level reorganization. Consequently, vibrational and optical spectroscopies are powerful, yet widely available, methods to inspect whether notable ground state charge transfer occurs for a given material pair.

The energy of vibrational modes depends on the local charge density near the involved atoms. The latter changes due to ionization, and diagnostic softening or strengthening of characteristic modes of dopant and/or semiconductor molecules can thus be a clear indication of doping, obtained from *infrared absorption spectroscopy*. As an example for dopants, the C≡N stretch mode of the widely employed tetracyano-quinodimethane *p*-type dopants becomes significantly softened upon anion formation due to the increased electron density of this bond. For these compounds, the energy shift of the nitrile-vibrational bands can be used to quantify the amount of charge transfer.[68] In addition to evidencing integer electron transfer, also ground state charge transfer complex formation with fractional charge transfer can be identified.[66] Likewise, for molecular and polymer semiconductors many vibrational modes of the conjugated moieties exhibit characteristic shifts upon polaron formation.[122,351] Raman peak shifts and intensity ratios have been recently proposed as a tool to determine the local degree of doping.[352]

The vast majority of conjugated organic compounds exhibits very different optical transitions in their neutral and ionized state, which make *optical absorption spectroscopy* a prime tool to investigate doping. Typically, the lowest energy absorption of charged species is significantly red-shifted compared to that of the charge-neutral compound, so that corroborating the presence of ionized dopants and/or semiconductors is rather straightforward, particularly in solution as long as aggregate formation does not complicate the assignment.[353] Careful analysis of the shape of optical and IR absorption spectra can provide an estimate for the polaron density, i.e the oxidation level of the polymer[354] as well as information about the polaron-counterion distance and polaron delocalization.[355] Yet, it should be stressed that the energy of optical transitions can vary substantially with the nano- and micro-structure within solid state samples, and intermolecular coupling of excitations can make a clear-cut spectral assignment challenging. If dopants possess clear diagnostic absorption features in the ionic state, the absence of these features in doped samples can be a good indication of ground state charge transfer complex formation when yet low-energy transitions (not belonging to the respective ionic compounds) are observed.[66] As a rough estimate, features in the optical spectra can be resolved to doping concentrations of around 1 mol%, but this depends on many factors e.g. doping efficiency. For such cases, photothermal deflection spectroscopy can be used to detect sub-band gap states with low absorption coefficients.[86,123]

Since the Fermi level (E_F) position in the energy gap of a semiconductor is a function of type and density of charge carriers, a movement of E_F from its roughly mid-gap position for

an undoped materials towards the valence band / HOMO-manifold (conduction band / LUMO-manifold) can also be regarded as clear indication for *p*-type (*n*-type) doping. The experimental method to directly assess the E_F position with respect to the frontier energy levels is *ultraviolet photoelectron spectroscopy* (UPS). However, a careful choice of substrate and film thickness for undoped and doped semiconductor films is mandatory. As noted in Section 2.1.6, if the film thickness is below the depletion region width (w), the position of E_F measured by UPS at the sample surface is strongly influenced by the substrate work function, and not representative of its position in the bulk of the doped material. Furthermore, dopant diffusion towards the substrate and reaction with it can change the work function, and concomitantly shift E_F.[210,356] If this occurs, doping of the semiconductor can be just mimicked by the dopant-substrate interaction.

EPR measurements can be used to determine the number of ionized dopant and host molecules in both solution and thin film samples. The spectroscopic technique uses the Zeeman effect to study unpaired electronic spins. In the presence of an external magnetic field B_0, the magnetic moment of an unpaired electron will either align itself parallel ($m_s = -1/2$) or antiparallel ($m_s = +1/2$) to the field and each state has a specific energy. These energy differences can be probed using electromagnetic radiation, usually in the microwaves (MW) range. The resonance condition is fulfilled when a photon has an energy equal to the splitting caused by the Zeeman Effect. Under this condition, the photon is absorbed. Experimentally, the frequency of the microwave radiation is kept constant and the external magnetic field strength is varied. EPR is well-suited to studying doped organic semiconductors as two unpaired spins are generated after charge transfer in the doping process: one species on the host and the other on the dopant. As the technique is sensitive to magnetic interactions at the molecular level, these two spin-bearing species can often be resolved. Quantitative EPR analysis then proceeds by calculating the absolute number of each species in the sample and comparing it to a reference sample with a known number of spins. Therefore, if the dopant density in the sample is known, EPR allows for the determination of the ionization efficiency in the semiconductor.[269,357] In addition, the EPR signal can offer insight into polaron mobility, activation energy for charge transport, and an indication of dopant clustering through spin coupling effects.[123] Such EPR analysis is limited by anti-ferromagnetic coupling, at high doping concentrations, when the spin-bearing species are close to one another.[358]

The ionized dopant density can be determined electrically, by *capacitance-voltage measurements*. The differential capacitance, $C = \delta Q / \delta V$, is measured by the AC current response to a small applied AC voltage, whilst scanning over a range of DC voltage offsets V_{dc}.

Assuming the depletion approximation (see Section 2.1.6), the depletion width will vary as function of V_{dc}. Furthermore, with an abrupt end to the depletion region and a free-carrier relaxation time that is short compared to the applied AC signal frequency, the measured capacitance will follow that of the parallel-plate capacitor,

$$C = \varepsilon\varepsilon_0 A/W \tag{9}$$

where A is the device area and W is the width of the depletion region. Substituting equation (9) into equation (8), and rearranging for the number of ionized dopants N^-_{dopant}, gives

$$N^-_{dopant} = -\frac{2}{q\varepsilon\varepsilon_0 A^2}\left(\frac{d(C^{-2})}{dV_{dc}}\right)^{-1}. \tag{10}$$

Therefore, C-V measurements are usually presented with C^{-2} against V_{dc}, with the gradient of the straight-line fit used to extract N^-_{dopant}. Attention should be paid to the validity of the depletion approximation: the semiconducting layer should be thick, and/or the doping density should be high enough such that injected charges from the electrodes are negligible as compared to charges generated by doping.[359]

2.5.2. Mobility and charge-carrier density measurements

The mobility and charge-carrier density are closely linked through Ohm's law, and as such are usually determined in a complementary fashion. Beginning with mobility, experimental measurements can give different results depending on many factors, including the measurement technique[360], the device geometry[361], and the sample preparation conditions[362]. Moreover, physical models developed to derive the charge-carrier mobility need to be used with care, since their applicability can become questionable in presence of extrinsic factors, not related to the semiconductor itself.[363–366] The mobility may also depend on the charge-carrier density, and can vary between different techniques, typically yielding higher values in the high doping regime (see Section 3.3.1). Therefore, direct comparisons of mobility between experimental studies is difficult. Even similar measurements using the same samples have been found to depend on the lab they are measured in[367].

2.5.2.1. Field-effect mobility

The charge carrier mobility is an important parameter in OTFTs, dictating the performance of the devices. The electrical characterization of transistors involves measurements of the source-drain current I_{ds} under two sweep conditions: scans over source-drain voltage V_{ds}, resulting in

output curves and scans over the gate voltage V_g, called transfer curves, from which the mobility can be extracted, as we discuss in Section 4.2. These devices configuration assess the charge transport of devices at the interface with the dielectric, rather than in the bulk of the OSC, and at high charge carrier density, on the order of 10^{18}–10^{19} cm^{-3}.

2.5.2.2. SCLC mobility

In contrast to transistor mobility, in which the conducting channel is confined at the interface with a dielectric layer, space-charge limited current (SCLC) measurements evaluate the charge carrier mobility in the bulk. Moreover, the charge carrier density is lower (on the order of 10^{15}–10^{16} for undoped films), hence the charge transport remains highly affected by energetic disorder and traps, when compared to high charge density transistor measurements. As a consequence, SCLC mobilities are typically orders of magnitude lower than those measured in transistor configurations.[368–370] Since optoelectronic devices (*e.g.*, OPV, OLEDs) are usually fabricated in a sandwich stack geometry and operated at low charge densities, the SCLC mobility is most relevant. SCLC devices are single carrier devices, where the charge carrier density in the semiconducting layer is solely dictated by space charge. It follows that the drift current density J for a single carrier device can be described by the Mott-Gurney square law,

$$J = \frac{9}{8}\mu\varepsilon_0\varepsilon_r\frac{V^2}{L^3} \tag{11}$$

where V is the applied voltage and L is the thickness of the semiconducting layer. Therefore, mobility is extracted by fitting a quadratic to a J-V measurement of the SCLC device. When considering highly doped semiconductor layers, finding a region in the J-V curve where $J \propto V^2$ can become difficult. As the doping density increases, the current across the semiconducting layer shifts from being space-charge limited to Ohmic. Therefore, the SCLC mobility can only be reliably determined for a doped film up to a certain doping density, depending on the film thickness.[371] Furthermore, the assumption that the current is space-charge limited in the device prevents the use of Ohm's law to estimate charge carrier density from the SCLC mobility.[371] For example, in a 100 nm-thick layer, the Mott-Gurney law will be valid up to a dopant density of around 10^{16} cm^{-3}. Above this, Ohm's Law becomes applicable.

2.5.2.3. CELIV Technique

Carrier extraction by linearly increasing voltage (CELIV) allows for both measurements of mobility and charge carrier density. CELIV measurements on doped layers require a diode

structure similar to SCLC devices. A linearly increasing voltage is applied in reverse bias so that, for measurements on p-doped films, doping-induced holes are extracted whilst charge injection from the other electrode is avoided. The current transient out of the device peaks, with its timing corresponding to the mobility of the semiconductor[372], and its area proportional to the number of mobile carriers[373]. Sandberg *et al.* have extended the CELIV method to deal with doped organic semiconductor layers in the low doping regime, taking into account the effects of built-in voltage, diffusion and band bending.[373]

2.5.2.4. Hall voltage and Hall mobility

Charge carrier density can be determined through measurements of the Hall voltage V_H. The basic effect underlying Hall measurements is the Lorentz Force, i.e. the perpendicular force felt by a charge when it moves through a magnetic field $\boldsymbol{B}$. For a p-doped sample with a constant current I flowing perpendicular to $\boldsymbol{B}$, the magnetic field pushes positive charge to one side of the sample. The resulting potential difference across the sample is called the Hall voltage given as

$$V_H = \frac{I|\boldsymbol{B}|}{qpd} \tag{12}$$

where, p is the bulk charge carrier density and d is the sample thickness. In combination with a Van der Pauw measurement of sheet resistance R_s the Hall mobility is given by

$$\mu = \frac{|V_H|}{R_s I \boldsymbol{B}} \tag{13}$$

Hall mobility measurements have been reported on p-doped polymer films[101,374] and p-doped organic single crystals[375].

3. Processing and nanostructure of molecularly doped polymers

3.1. Doping methods: co-processing and sequential doping

There is a complex interplay between doping and the ensuing nano/micro-structure. For example, different polymorphs and the dopant position within the polymer matrix have been observed to promote different doping mechanisms (i.e., integer and partial charge transfer, see above).[94,334,376,377] Simultaneously, the amount of introduced dopant and its size can modify the nanostructure of the host semiconductor either due to space-filling, charge delocalization effects, or planarization of the polymer backbone.[378] Indeed, beneficial as well as detrimental

effects on charge transport have been reported. On the other hand, the doping method determines how much control over the nanostructure can be attained, as well as the amount of introduced dopant. As we will describe in this section, the two main families of doping methods can be classified as either co-processing or sequential processing techniques. The choice of a particular doping method primarily depends on the materials' chemical and physical properties and the intended application.

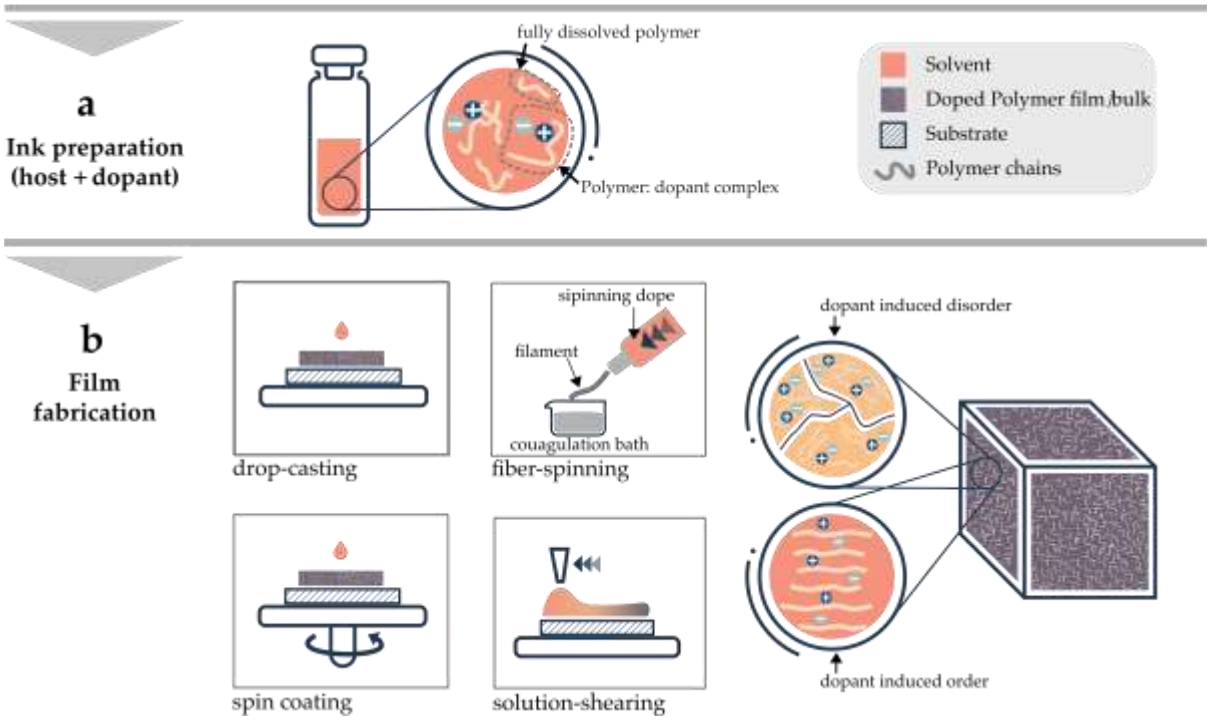

Figure 19: Typical routes for co-processing of semiconductor and dopant. (a) Preparation of a host + dopant solution (typically referred to as ink) followed by (b) the deposition of a film or casting of a freestanding material. The bottom right image shows two of the possible outcomes for the nanostructure of the resulting solid-state material.

3.1.1. **Co-processing**

Co-processing, or co-deposition, methods refer to the simultaneous deposition of the semiconductor host and the dopant. This can be done from solution by dissolving both compounds in a given solvent system and then solution processing this mixture (by e.g., spin coating, solution-shearing, fiber spinning, or drop-casting) as illustrated in Figure 19. Alternatively, both substances can be co-evaporated using vacuum deposition in order to fabricate the solid-state material, an approach that finds widespread use for the manufacture of OLEDs.[114] Attractive traits of the co-processing techniques are their simplicity and the fact that

the dopant concentration can be adjusted easily by regulating the relative amount of each material. On the other hand, it is difficult to predict the resulting film microstructure, which, as we will see, can strongly affect electronic transport. An exception is vapor deposition of organic semiconductors, which can result in the formation of highly stable glassy layers.[379]

For solution-based processes, the materials should be partially miscible with respect to each other as well as a given solvent system. As the energy levels of both materials are designed so that the dopant and semiconductor interact electronically (as discussed in previous sections), CTCs can already develop in the solution-state. This often leads to the formation of gels, bi-molecular crystals, and aggregates.[66,380,381] The latter has important implications for the processability of the systems, and it can significantly affect the achievable doping levels and, generally speaking, the resulting charge transport properties of the formed layer. For instance, films co-deposited from mixtures of F_4-TCNQ and polythiophene derivatives (such as PBTTT and P3HT) have fewer and less interconnected crystalline domains than their polymer-only counterparts,[380,381] which in turn can influence the charge transport properties.[382] Consequently, moderate electrical conductivities (< 2 S cm^{-1}) have been obtained for such systems using co-deposition methods (i.e. two orders of magnitude lower than what is achieved by sequential processing). Besides changing the way in which the semiconductor solidifies, the dopant can also change the ordered phase of the semiconductor. For example, F_4-TCNQ and 4T form bi-molecular crystals in the solid-state, which impacts the degree of intermolecular hybridization between the host and dopant and leads exclusively to the formation of charge-transfer complexes.[66] Many dopants are also incorporated into crystalline polymer domains and a common observation is that the $\pi - \pi$ stacking distance is reduced while the lamellar spacing increases, suggesting that the dopant is located between the side chains (cf. Section 3.3).[383–386] In the case of F_4-TCNQ and P3HT, the resulting host polymorph dictates if a CTC is formed or whether ICT occurs.[94] Another aspect is steric hindrance introduced by branched side chains such as those of P3EHT, which also forms a CTC with F_4-TCNQ.[334]

Besides pre-aggregation in solution, co-deposition can also result in phase separated domains due to other mechanisms, such as binodal or spinodal decomposition driven by poor miscibility. For instance, atomic force microscopy (AFM) images of co-deposited films of P3HT:F_4-TCNQ showed strongly phase separated domains, even at very low dopant contents.[381] Interestingly, there is also a possibility that dopants act as additives that modify the nanostructure of the host, which benefits the electrical and, in some cases, also the mechanical properties (cf. Section 3.3.2).[387] Paterson *et al*. suggested the former for a co-processed (NDI) and bithiophene copolymer mixed with the Lewis base ammonium salt TBAF

(section 3.3).[128] A different example lies in oriented spun fibers from carbon nanotube polyelectrolyte composites, where charge transfer in solution imparts a liquid crystal behavior that aids in orienting the fibers during the extrusion process.[388]

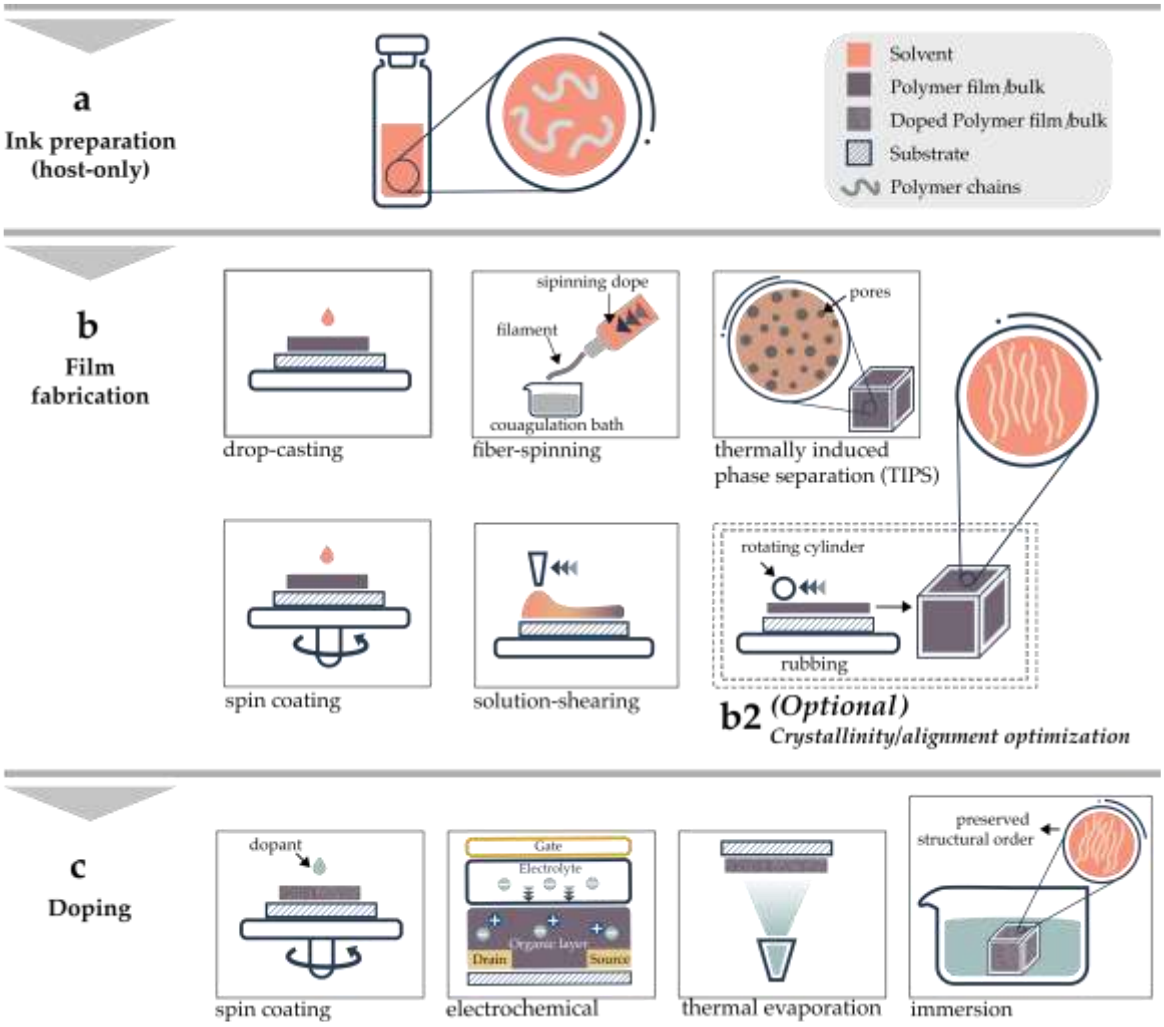

Figure 20: Typical routes for sequential processing of semiconductor and dopant. (a) Preparation of a host only ink followed by the deposition of a film or casting of a freestanding material. For example, a membrane or a sponge using thermally induced phase separation (TIPS). (b2) An extra step can be included (enclosed in dashed lines) to enhance the molecular orientation or crystallinity of the material. Depicted In the image is the polymer rubbing process. (c) Doping of the host material using common solution-based, electrochemical, or thermal evaporation methods.

3.1.2. Sequential doping

Sequential processing methods rely on adding the dopant into a preexisting host semiconductor film. First, the host is evaporated or solution-processed as a layer or cast as a free-standing material (e.g., a sponge or membrane, Figure 20).[389,390] In some cases, additional steps are

made to optimize the microstructure of the organic semiconductor to maximize electrical transport. These, for instance, include optimizing the degree of crystallinity (e.g., via thermal or vapor annealing)[391,392] or degree of molecular alignment (e.g., via stretching and rubbing).[386,393,394] The next step consists of doping itself, which is often achieved by using electrochemistry, or by depositing a molecular dopant from solution (e.g., by spin coating or immersion) or thermal evaporation. Note that for thermal evaporation-based technologies, it is also possible to reverse the order of deposition steps, depositing the dopant first and then the host material.[395]

For electrochemical oxidation/reduction, there exist two basic geometries. The first one uses multichannel electrochemical workstations, in which the electrochemical oxidation/reduction of the organic film is carried out in a three-electrode cell. The film deposited onto one conductor (e.g., ITO/glass) acts as the working electrode, a platinum grid as the typical counter-electrode, and then a reference electrode, such as Ag/AgCl electrode in a 0.1 M of $LiClO_4$ in acetonitrile solution.[396] Operando X-ray scattering has revealed that anions first infiltrate the amorphous regions, and then penetrate the crystalline regions during electrochemical oxidation of semicrystalline P3HT;[397] while holes first reside in the crystalline regions. A similar charge/counterion distribution picture was observed for sequential p-doping of conjugated polymers.[398] Selective incorporation of F_4-TCNQ into amorphous regions of regioregular P3HT enhances the conjugation of amorphous chains.[398,399] By systematically varying the crystallinity of the polymer, the charges become more delocalized.[398] Importantly, the electrochemical oxidation of the polymer such as regiorandom P3HT can be carried out followed by removal of the electrolyte and drying, which results in a fully solid polymer film with a conductivity of up to 224 S cm^{-1}.[400]

Alternatively, a transistor geometry can also be used. For this, the host layer is normally deposited on top of the source and drain electrodes and acts as the semiconductor/channel. This layer is separated from a third metal electrode (the gate) by a thin dielectric or by a polyelectrolyte. In traditional electrochemical processes, the voltage applied between the gate and the channel leads to field-effect oxidation/reduction of the host, but only near the dielectric interface. Instead, in permeable hosts, often referred to as organic electrochemical transistors (OECTs), ions are injected from the electrolyte into the host, accompanied by solvent molecules which swell the material, and oxidation/reduction occurs over the entire volume of the channel.[401,402]

Another common sequential doping approach is thermal evaporation of the dopants (often referred to as vapor doping) using a vacuum chamber or even using simpler setups when

dealing with small molecules like F_4-TCNQ or TDAE. In fact, exposure of polyacetylene to iodine vapor, which varied the conductivity of the polymer by more than 7 orders of magnitude,[403] gave birth to the field of conducting polymers and led to the 2000 Nobel prize in chemistry. Diffusion into the film is temperature-dependent, with the geometry and size of the dopant playing a significant role. For instance, F_4-TCNQ diffuses relatively well at room temperature in systems such as P3HT, while bulkier dopants like $C_{60}F_{36}$ may require thermal annealing steps to induce mixing.[395] One important aspect of thermal evaporation is the possibility of using a shadow mask to define regions of different degree of doping level, which can be beneficial for applications such as transistors, (see Section 4.2.3).[404,405] When using solution-based techniques, patterning of the doped region (or dopant) has thus far been less explored, although, recently, a few examples have been reported, including the work on local dedoping[406] or local diffusion through semipermeable membranes.[352]

For solution-based methods, a solution containing the dopant is spin-coated onto the host or used to immerse/dip the latter. Changing the dopant solution concentration or immersion time allows partial control over the doping level. A key element is that solvents containing the dopant must be orthogonal to the host (i.e., the solvent must not dissolve the semiconductor)[399] unless specific multilayer geometries are used.[352] Varying the solvent miscibility with respect to the host allows to selectively place the dopant in different regions of the semicrystalline matrix (i.e., amorphous regions vs. crystalline regions).[399,407]

Sequential processing methods are advantageous if the goal is to largely preserve the structural order (e.g., for highly ordered/oriented materials). Here, it is important to note that sequential doping can nevertheless alter the micro- and nanostructure of the polymer film, e.g., through dopant intercalation or an increase in the degree of order of the semiconductor. For instance, electrical conductivities as high as 600 S cm^{-1} have been obtained for PBTTT doped with F_4-TCNQ via vapor doping,[380] which has been attributed to the dopant intercalating preferentially between the solubilizing chains while simultaneously retaining a high level of nanostructural order.[380,408] In films of regioregular-P3HT mixed with regiorandom-P3HT as well as neat regionrandom-P3HT, vapor doping with F_4-TCNQ has even been shown to induce order and increase the long-range connectivity of the semiconductor compared to that of the neat state,[378,409] and was ascribed to charge delocalization along the polymer chain.[378] Like vapor doping, there have also been observations that doping using these methods can increase the conjugation length and the connectivity between domains, improving electrical conductivity at low doping levels in films of F_4-TCNQ -doped RR-P3HT.[399] As the structural order is largely retained during the doping process, high electrical conductivities (above 10^5 S

cm^{-1}) have been achieved in rubbed films of PBTTT doped with solutions containing $FeCl_3$.[386,410] This remarkable high electrical conductivity is associated to the high alignment of the samples, without which the reported values of conductivity for these materials systems are the order of 10^3 10^5 S cm^{-1}.[411,412]

A recent breakthrough by Yamashita *et al*. demonstrated that it is possible to achieve very high doping levels in PBTTT using a hybrid ion-exchange doping method. Here, the host semiconductor is immersed in a bath containing a molecular dopant and a polyelectrolyte. After an initial charge-transfer step, the dopant ion exchanges with the electrolyte anion, leading to a material identical to that obtained by electrochemical doping.[413] The method was then extended to various semicrystalline polymers like P3HT, IDTBT, and DPP-BTz, producing similar results while also revealing that trapping effects by anions are negligible at high doping levels.[411]

However, solution-based and vapor doping processes do not come without challenges. Dopant diffusion is thickness limited, and the ability to homogeneously dope the entire material depends on the host film thickness and porosity, as well as the diffusion coefficient of the dopant. In fact, some of the best electrically conductive materials have been achieved by doping films of around 50 nm.[380,408,410] The latter poses a significant drawback for applications such as thermoelectrics that require micrometer to millimeter thick materials that are able to maintain large thermal gradients.

3.2. Doping of bulk materials

Doped bulk materials are needed for a number of applications such as thermoelectrics and wearable electronics. For example, the optimal thickness of the legs of a thermoelectric generator is on the order of several 100 micrometers to a few millimeters,[414–416] which necessitates doping of considerably thicker structures than the typically 50 to 100 nm thin films discussed in Section 3.1. The low diffusion coefficient of dopant molecules, e.g. $D \approx 10^{-11}$ cm^2 s^{-1} of neutral F_4-TCNQ in P3HT at 25 ºC,[417] indicates that it will take $t = x^2/4D \approx 3$ days to dope a x = 100 µm thick slab of the polymer through sequential doping. One approach to circumvent the low diffusion rate of molecular dopants is to create porous structures, which ease infiltration. Thermally induced phase separation (TIPS) has been used to create millimeter thick foams of P3HT that feature both micrometer- as well as nanometer-sized pores (Figure 21).[389] Sequential doping of such foams with F_4-TCNQ in acetonitrile, which is able to ingress into the porous structure, allowed rapid doping, reaching a dopant concentration of 7 mol% in only 1 hour, compared to several days in the case of fully solid bulk samples.

Despite being a slow process, sequential doping of solid bulk materials is a suitable approach if the goal is to maintain the microstructure of the material. Stretch-aligned P3HT tapes with a thickness of 10 to 40 µm could be homogeneously doped without affecting the uniaxial orientation of the polymer by placing samples in a solution of $Mo(tfd\text{-}COCF_3)_3$ in acetonitrile for 3 days, reaching a relatively high dopant concentration of 9 mol% and conductivity of 13 S cm^{-1}.[418] Further, doping of stretched P3HT did not influence the glass transition temperature $T_g \approx 21$ ºC and only slightly reduced the Young's modulus, e.g. from 1.1 to 0.4 GPa along the direction of alignment, which indicates that mechanically robust doped polymers can be realized.[418] The size of the dopant is particularly important when sequential doping of bulk materials is attempted since larger dopants tend to diffuse more slowly.[395] While $Mo(tfd\text{-}COCF_3)_3$ likely diffuses slowly due to its large size, other dopants such as $FeCl_3$ and especially I_2 can more rapidly enter a solid material. On the other hand, small dopants such as I_2 with a high vapor pressure are also most likely to sublime from within the host material, resulting in poor long-term stability. Wet- and melt-spun fibers of P3HT could be strongly doped with $FeCl_3$ dissolved in nitromethane, reaching conductivities of 160 and 320 S cm^{-1}, respectively.[419,420] Other conducting polymer fibers have been sequentially doped with I_2 vapor, reaching a conductivity of 2000 S cm^{-1} in case of poly(2,5-thienylene vinylene) and 13'000 S cm^{-1} for polyaniline fibers, both with a Young's modulus of about 7 GPa.[420] Blend fibers of poly(3-octylthiophene) (P3OT) and ultra-high molecular-weight polyethylene (UHMWPE), again vapor doped with I_2, show an even higher Young's modulus of up to 20 GPa but lower conductivity of not more than 9 S cm^{-1} due to the presence of the insulating polymer.[421] Doped conjugated polymer fibers tend to show a correlation between the Young's modulus and electrical conductivity (Figure 22), since both the transmission of mechanical force as well as charge transport benefit from the alignment of polymer chains.[422,423]

Some polymer:dopant pairs are poorly soluble when co-processed from the same solution. P3HT and F_4-TCNQ, for example, tend to aggregate in solution, leading to a brittle solid. Solution blending of P3HT:F_4-TCNQ with a commodity polymer such as PEG (also known as poly(ethylene oxide), PEO) imparts some mechanical robustness and allows to prepare free-standing samples.[424] Instead of blending with PEG, the solubility of the polythiophene can be adjusted by replacing the alkyl side chains with oligoether ones. The resulting polymer poly(3,3'-bis(tetraethylene glycol methyl)-2,2'-dithiophene-thiophene) (p($g_4$2T-T)) remains soluble when mixed with F_4-TCNQ or various acids such as 1,3-propanedisulfonic acid and allows hot-pressing of free-standing doped films (Figure 21).[74]

One approach to mitigate the poor solubility of some doped polymers is the use of latent dopants that can be processed together with the polymer without occurrence of the doping reaction, followed by activation of the dopant in the solid state through, e.g., heating. The latent dopant is positioned in the bulk material, instead of having to diffuse into the solid structure, and can sequentially dope the polymer from within once activated. 4-ethylbenzenesulfonic acid (EBSA) capped with an *o*-nitrobenzyl capping moiety (EBSAc) can be solution co-processed with P3HT, PBTTT and p($g_4$2T-T), followed by thermal activation at 140 ºC, which releases 2-nitrosobenzaldehyde and frees the EBSA acid dopant leading to p-doping of the bulk sample (Figure 21).[267,425] We anticipate that latent n-dopants such as a recently reported N-heterocyclic carbene-based dopant, which is thermally activated at 160 ºC,[425] may ease bulk processing of n-type conductors.

Bulk materials can be prepared through co-processing if suitable counterions are selected that impart melt- and/or solution processability. Polyaniline doped with dodecylbenzenesulfonic acid (DBSA) or camphorsulfonic acid (CSA) can be dissolved in, e.g., chloroform and m-cresol, which facilitates solution blending with insulating polymers such as poly(methyl methacrylate) (PMMA).[426] More recently, a paste of polyaniline and DBSA has been used for direct ink writing of millimeter-sized 3D objects using a modified fused filament fabrication (FFF) printer.[427] Another widely used material is PEDOT:PSS, prepared through oxidative polymerization of 3,4-ethylenedioxythiophene (EDOT) in the presence of PSS, which serves as the counterion.[428] The resulting PEDOT:PSS complex can be processed as an aqueous dispersion, facilitated by an excess of PSS, which has been used for the preparation of free-standing films[429] as well as wet-spinning of highly conducting fibers (typical diameter 5 to 10 µm) with a conductivity of up to 4000 S cm^{-1} and Young's modulus of up to 22 GPa.[430–434] To reach a high conductivity it is necessary to remove excess PSS from the material, which is done through wet-spinning of the aqueous PEDOT:PSS dope into a sulfuric acid coagulation bath that selectively dissolves PSS but not the conducting polymer. The conductivity and Young's modulus of the fibers can be enhanced further by cold drawing, confirming the correlation of electrical and mechanical properties with the degree of alignment of the conducting polymer (Figure 22).[434,435]

Conducting objects with intricate shapes can also be prepared through the oxidative polymerization of monomers within 3D-printed scaffolds.[436] For example, polypyrrole has been grown in hydrogels 3D-printed by direct light processing[437,438] and PEDOT has been synthesized within anionic Nafion-based bulk templates prepared by melt-spinning or FFF type 3D printing.[439] The polymerization can be photochemically activated, which has been used to

define 3D patterns of PEDOT in 200 mm thick Nafion sheets by direct laser writing.[439] It can be anticipated that additive manufacturing with conducting polymers will open up intriguing possibilities for micro- and bioelectronics.

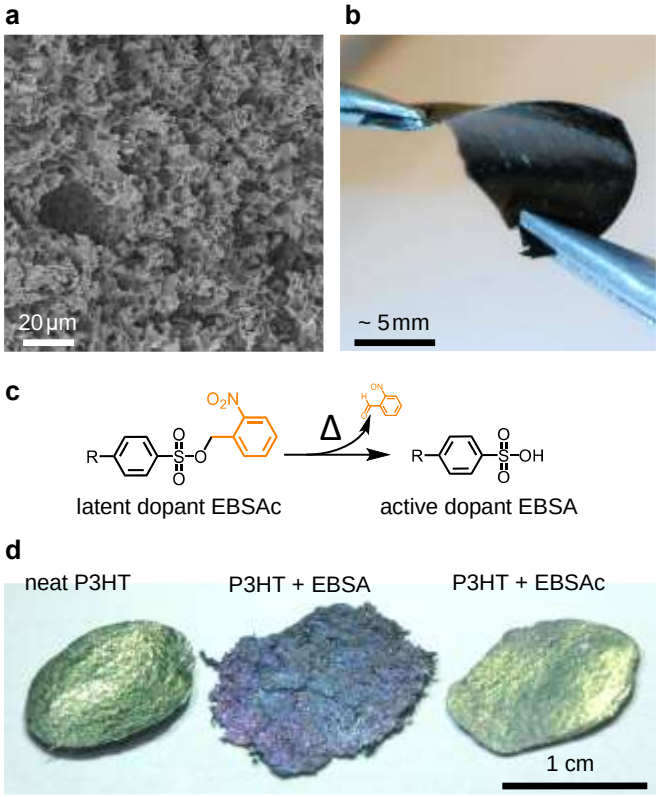

Figure 21: (a) P3HT foam (Adapted with permission from ref [389]. Copyright 2017 Kroon et al. under Creative Commons Attribution-NonCommercial License https://creativecommons.org/licenses/) (b) hot-pressed film of p($g_4$2T-T) doped with 1,3-propanedisulfonic acid (Reprinted with permission from ref [74]. Copyright 2018 Hofmann et al. under Creative Commons Attribution-NonCommercial 3.0 Unported Licence https://creativecommons.org/licenses/by-nc/3.0/. (c) thermal activation of the latent dopant EBSAc releases 2-nitrosobenzaldehyde and yields the active dopant 4-ethylbenzenesulfonic acid (EBSA; R = ethyl); (d) P3HT remains malleable when hot-pressed together with the latent dopant EBSAc while P3HT in combination with the active dopant EBSA is intractable (Reprinted with permission from ref [440]. Copyright 2019 American Chemical Society).

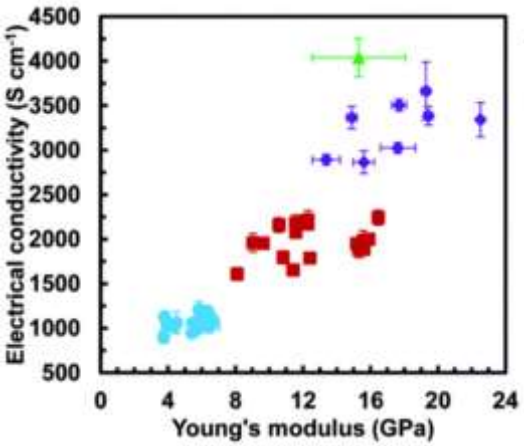

Figure 22: Electrical conductivity versus Young's modulus of PEDOT:PSS fibers prepared by wet-spinning into a sulfuric acid coagulation bath (blue), followed by drawing in a dimethyl sulfoxide (DMSO) or sulfuric acid bath (purple, green); Reprinted with permission from ref [434]. Copyright 2020, The Royal Society of Chemistry.

3.3. Interplay between doping and microstructure

As discussed in Section 3.1, there is a complex interplay between doping and microstructure in organic materials. In Section 3.3.1 we discuss how control of the processing-structure-property relationships plays a fundamental role, while Section 3.3.2 focuses in applications involving low dopant concentrations where unexpected microstructural changes emerge as a convenient tool for tuning the properties of organic semiconductors and their devices.

3.3.1. Highly conducting materials

For some applications such as thermoelectrics materials with a high electrical conductivity are required. Typically, a large amount of dopant of more than >10 mol% must be added to the organic semiconductor in order to reach a high electrical conductivity in the range of 10^0 to 10^5 S cm^{-1}. In case of thermoelectric materials, the thermoelectric power factor of both p- and n-doped organic semiconductors monotonically increases with the electrical conductivity,[441,442] meaning that it is desirable to achieve a high degree of doping (Figure 23).

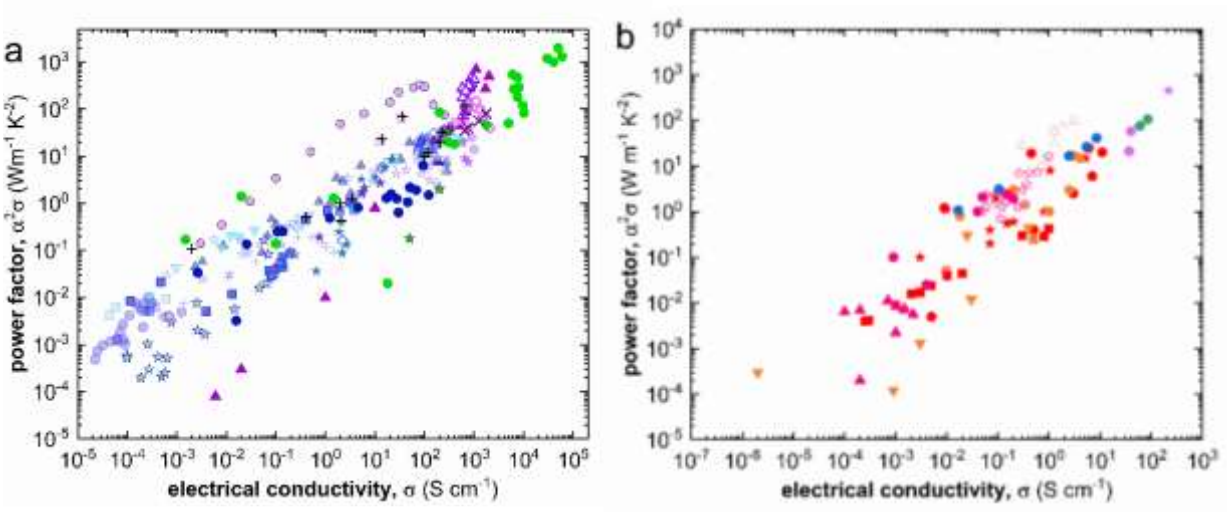

Figure 23: The thermoelectric power factor $\alpha^2\sigma$ of p-doped (left) and n-doped (right) organic semiconductors increases with σ (α = Seebeck coefficient; σ = electrical conductivity); Reproduced with permission from ref [441] and included the data from ref [345] and [442]. Copyright 2018 Elsevier B.V. Ref. [441] Ref. [345] Ref. [442]

Such large amounts of dopant can alter the nanostructure of the semiconductor and therefore, most highly conducting materials are prepared through sequential processing steps where the semiconductor is first solidified from solution or melt, followed by introduction of the dopant to the semiconductor host via a solution or vapor phase (Section 3.1). The majority of studies that aim to maximize the conductivity use polythiophenes such as P3HT and PBTTT in case of p-doping, and NDI based polymers or fullerenes in case of n-doping. In case of p-doped P3HT, for example, the charge-carrier mobility and hence conductivity strongly depends on the crystallinity of the polymer, which is affected by factors such as the regioregularity and molecular weight of the polymer as well as the processing solvent.[443] Doping of P3HT with F_4-TCNQ vapor has resulted in a charge density of up to 5×10^{20} cm^{-3} and conductivity of up to 48 S cm^{-1}, indicating a charge-carrier mobility of 0.6 cm^2 V^{-1} s^{-1}.[163] The conductivity of polythiophenes can be improved by replacing the alkyl side chains with thioalkyl or oligoether side chains, resulting in up to 350 S cm^{-1} in case of PQTS12 p-doped with the strong oxidant $NOBF_4$.[153]

The charge-carrier mobility and hence conductivity of P3HT can be enhanced in one direction through in-plane alignment, which can be achieved through high-temperature rubbing of thin films with a microfiber cloth[444] or epitaxial crystallization using crystallizable solvents such as 1,3,5-trichlorobenzene.[393] Both studies report a charge density of about $6\cdot10^{20}$ cm^{-3}, indicating that the orientation of the polymer does not improve the degree of doping. The conductivity displayed considerable anisotropy with 160 S cm^{-1} and 320 S cm^{-1} along the

alignment direction, which translates into a charge-carrier mobility of up to 2.5 cm^2 V^{-1} s^{-1}.[393,444] An even higher conductivity of up to 681 S cm^{-1} has been reported for rubbed P3HT films doped with Mo(tfd-$COCF_3$)$_3$, likely because the larger dopant allows a higher fraction of the 4×10^{20} cm^{-3} charges to contribute to transport (cf. Section 3.2).[445] The selection of a high-mobility polymer such as PBTTT gives rise to even higher conductivities of 670 S cm^{-1} when doped with F_4-TCNQ vapor.[380,408] The conductivity can be further enhanced to 1400 S cm^{-1} through sequential doping of rubbed PBTTT films with F_4-TCNQ dissolved in acetonitrile, and 2400 S cm^{-1} if F_6-TCNNQ is used.[446] A record value of 2.2×10^5 S cm^{-1} has been reported for rubbed PBTTT films p-doped with the strong oxidant $FeCl_3$,[410] which even exceeds the conductivity reported for I_2-doped polyacetylene.[447]

The degree of n-doping and hence the electrical conductivity that can be attained lag behind values reported for p-doped semiconductors. Thus, the current focus is on developing host materials that can be more readily n-doped.[26,448] In the pioneering work by Schlitz *et al*., co-processing of a copolymer with a naphthalenediimide-bithiophene backbone P(NDI2OD-T2); with N-DMBI generated a charge density of about 10^{17} cm^{-3}, leading to an electrical conductivity of more than 10^{-3} S cm^{-1}.[192,343] One widely explored strategy to increase the conductivity of n-doped polymers focuses on planarization of the conjugated backbone. For example, replacing the two thiophene rings that are part of the P(NDI2OD-T2) backbone with two thiazole (Tz) rings results in a more planar P(NDI-Tz2) backbone, which upon n-doping with N-DMBI displays a conductivity of about 10^{-1} S cm^{-1}.[340] In case of the ladder-type polymer BBL, which has a highly rigid and planar backbone, a conductivity as high as 1-2 S cm^{-1} is obtained upon doping with TDAE vapor or sequential doping with N-DMBI dissolved in chloroform, which has been rationalized with a high polaron delocalization length.[192,449] The highest conductivities for n-doped polymers have been reported for benzodifurandione-based copolymers co-processed with N-DMBI. For the copolymer FBDPPV, for instance, a conductivity of 14 S cm^{-1} has been reported when co-processed with N-DMBI,[450] and 21 S cm^{-1} when n-doped with a triaminomethane derivative.[277] Recently, a very high charge density above 10^{20} cm^{-3} and hence record electrical conductivity of 90 S cm^{-1} were achieved for the copolymer TBDPPV co-processed with N-DMBI.[345]

For a given dopant:semiconductor pair there will be a maximum amount of dopant that can be dissolved in the host matrix, resulting in aggregation at higher concentrations. Many dopant molecules are polar and hence tend to aggregate within most organic semiconductor matrices,[192] leading to a low doping efficiency at high dopant concentrations. In case of P3HT

p-doped with F_4-TCNQ, for instance, the choice of doping process, i.e. sequential doping *vs*. co-processing, strongly impacts the degree of dopant aggregation.[381] One strategy to improve the compatibly between dopant and host semiconductor is the use of more polar side chains instead of alkyl side chains (see Section 2.4.1). For example, the polythiophene p($g_4$2T-T) with tetraethylene glycol side chains displays good compatibility with, e.g., F_4-TCNQ as well as acid dopants, leading to a charge density of up to 2×10^{20} cm^{-3} and electrical conductivity as high as 100 S cm^{-1}.[74,317] The same strategy has also been widely explored for n-doped materials, where both fullerenes and polymers with oligoether side chains display enhanced compatibility with dopants such as N-DMBI.[97,319,325] In order to facilitate n-type conductors with a high conductivity, different strategies can be combined as exemplified by a copolymer with a planar P(NDI-Tz2) backbone but oligoether instead of alkyl side chains, which shows a charge-carrier density of about 10^{19} cm^{-3} and hence conductivity of up to 2 S cm^{-1} when co-processed with N-DMBI.[341] Instead of modifying the semiconductor, it is also possible to attach alkyl ester or oligoether pendant groups to the dopant molecule, which offers an alternative approach to tune the interaction between dopant and semiconductor.[167,197] Despite many promising reports the incorporation of polar side chains does not guarantee that the required compatibility with the semiconductor and is important to consider the specific dopant:semiconductor interactions in each case.[324]

3.3.2. Dopants as morphological modifiers additives

The addition of low amounts of additives such as nucleating agents –some of them originally developed for commodity polymers such as polypropylene–[451–453] to organic semiconductors is a powerful tool to control their crystallization process and thus their properties. For example, nucleating agents such as 1,3:2,4-bis(3,4-dimethylbenzylidene)sorbitol (DMDBS) allow to control the crystallization of semiconducting polymers and small molecules when co-processed at low loadings of 0.1–2 wt% in the context of OTFTs and solar cells.[454–456] Doping of the active layers of organic electronic devices is usually performed by adding similarly low and ultra-low amounts, *i.e.*, 0.1-3 wt%, of molecular dopants to the OSC solution, following a co-processing method, in order to adjust the relative amount of component. It is not a surprise then, if the addition of dopants is attracting an interest in terms of their ability to control the microstructure and morphology of the semiconductor's thin film, which ultimately play a crucial role in device optimization. Indeed, as we discussed in section 3.1, the two species may interact, resulting in charge transfer processes leading to effective doping of the semiconductor,

which tends to affect its solubility and the way it solidifies. Effectively, there has been a progressive transition from the classic concept according to which the introduction of a dopant would lead to disruption of the crystal order of the film, towards the exploitation of synergistic effects of dopants both in terms of electronic and structural properties.

Dopant-induced structural changes are diverse and can influence both the molecular arrangements at the nanoscale (Figure 24) as well as the texture of micrometer-size domains (Figure 25). For instance, dopants can improve molecular order (Figure 24c), change the stacking distance (Figure 24d), and alter the stacking orientation relative to the substrate (Figure 24a), compared to the pristine material. Moreover, the formation of new crystal structures can occur through the formation of dopant/semiconductor co-crystals (Figure 24b). At a micrometer length scale, dopants can have an impact on the domain size and connectivity. The magnitude of these dopant-induced changes depends on the particular system and on the processing conditions. Above a critical dopant concentration, the crystalline order can be subjected to strong disruption.

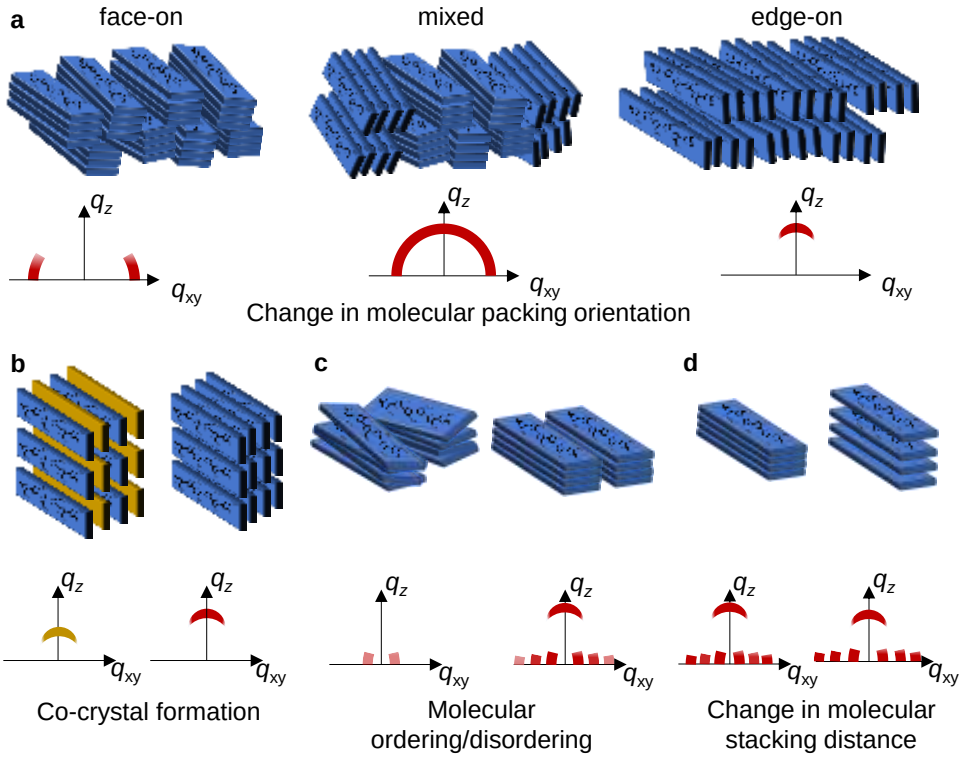

Figure 24: Illustration of how the texture in thin-films can be affected by the introduction of low fractions of dopants and corresponding 2D-GIWAXS patterns. a) change in molecular packing orientation (lamellar packing is shown). b) formation of co-crystals (dopant molecules in yellow), π-π stacking is shown. c) dopant-induced change in the degree of molecular order, d) change in stacking distance.

For instance, in the extensively studied P3HT:F_4-TCNQ model system, upon co-processing the two species in chlorobenzene solution, a threshold concentration of around 1.2 mol% has been identified below which the crystal structure of the films is not affected.[457] It is worth noticing that even at these low concentrations the dopant is ionized. Moreover, Ma *et al*. suggested that weak doping of P3HT films with 0.1 wt% (~ 0.06 mol%) F_4-TCNQ, co-processed from chloroform solutions, can improve the polymer edge-on orientation, while 0.6 wt% (~ 0.36 mol%) dopant reduced the degree of order.[458] F_4-TCNQ has also been reported to cause changes in the crystal structure of other OSCs, through formation of dopant-semiconductor co-crystals. For instance, doping of 4T with F_4-TCNQ, upon vacuum co-deposition, leads to the formation of a new crystal structure even at a concentration as low as 1.3 mol%.[66] Similarly, the high-mobility small molecule C_{10}-BTBT doped with F_4-TCNQ (co-processed in solution) forms a co-crystal motif at low doping concentrations, *e.g.* 2 mol%.[69] In this doping regime, the microstructure is still dominated by unaltered crystals of the OSCs.

Another useful model system to assess the impact of dopants on the nano- and microstructure of organic semiconductors is P(NDI2OD-T2), also known as N2200. A range of dopants (co-processed in solution with the polymer) such as TTF and TCNQ,[459] BV,[460] $CoCp_2$ and CsF, [461] as well as a DMBI potassium triflate adduct, DMBI-BDZC,[462] have been found to induce structural changes upon the addition of 0.1-3 mol% dopant. For example, Panidi *et al*. found that the addition of up to 1 mol % DMBI-BDZC progressively decreases the surface roughness and leads to a more densely packed film.[462] Similarly, Kang *et al*. studied how low concentrations of TTF and TCNQ, below 2 mol%, modify the nanostructure of the polymer despite negligible electrical doping, enhancing the coherence and orientation of fibrillar domains, which is accompanied by changes of molecular packing and orientation.[459] Moreover, differential scanning calorimetry (DSC) thermographs showed how molecular additives led to decreased melting and crystallization temperatures, suggesting a nucleation inhibition. Thus, the molecular additives can possibly favor chain motion, which in turn can lead to fibril ordering/elongation and changes in molecular packing.[459] Further, P(NDI2OD-T2) has also been blended with insulating polymers,[259,463] which do not cause any structural changes, and semiconducting polymers[464] such as up to 3% PDVT-8, which acts as a dopant as well as a morphological modifier. Generally, dopants affect the nano- and microstructure of P(NDI2OD-T2) films to a lesser extent when processing protocols are selected that per se result in highly ordered fibrils. The same holds for other highly ordered polymers, *e.g.*, DPPTTT, PCPDTPT.[275] In contrast, when processing conditions result in less ordered films, dopants may enhance crystallization and hence their impact on the final microstructure becomes more

noticeable. A similar behavior is observed in case of other organic semiconductors, such as TIPS-pentacene, a high-mobility solution processable small molecule. For instance, Naab *et al*. reported how *o*-MeO-DMBI doped TIPS-pentacene films (co-processed from toluene solution) could be produced with high crystallinity and with a ribbon-like microstructure, essentially retaining the same properties as reference undoped films.[191] In contrast, Wang *et al*. reported that the addition of tetrafluorophthalonitrile (TFP) and octafluoronaphthalene (OFN) significantly enhances the crystallinity of otherwise close to amorphous TIPS-pentacene films, co-processed from chloroform solutions.[465] More than 10 wt% of the dopant had to be added to strongly improve the crystallinity, similar to doping-induced ordering of amorphous regio-random P3HT.[378,409]

A useful feature that is often observed upon introduction of dopant molecular additives is their ability to regulate the orientation of the organic semiconductor with respect to the substrate. For example, doping can alter the edge-on/face-on orientation of crystallites in P3HT and P(NDI2OD-T2) thin films, as illustrated in Figure 24a.[458,459,464] This is particularly useful since charge transport in organic semiconductors is typically favored along certain packing directions. For instance, thiophene-based polymers are associated with an improved charge-carrier mobility along the π-π stacking direction of the conjugated backbone. Hence, these materials exhibit enhanced transport, in a transistor configuration, when the π–π staking is oriented parallel to the substrate plane, i.e. edge-on. Another example of such a dopant-induced change in orientation has been reported for the small molecule p-DTS(FBTTh$_2$)$_2$ doped with iodine (co-processing from solution), which shows a stronger edge-on orientation when compared to the mainly face-on orientation of the undoped molecule.[466] Similarly, the polymer FBDPPV displays an increase in face-on orientation upon doping with N-DMBI (co-processing from solution).[467]

Doping also tends to influence the nanostructure of semiconductor blends such as BHJ for solar cells and polymer:small molecule blends for high-mobility OTFTs, co-processed from solution. For instance, blade-coated films comprising a blend of C$_{16}$IDT-BT an C$_8$-BTBT exhibit a topography that features highly ordered terraces of the C$_8$-BTBT small molecule (Figure 25). These terraces show improved uniformity upon doping with C$_{60}$F$_{48}$, without affecting the crystal structure.[468] A similar improved nanostructure was observed in the same system doped with Lewis acids, Zn(C$_6$F$_5$)$_2$ and BCF.[21,225] BCF has also been found to modify the surface roughness and texture of other semiconductor such as TIPS-pentacene:PTAA and diF-TESADT:PTAA blends.[21] The latter displayed a dramatic change in microstructure upon doping from an uneven topography to the formation of large molecular terraces extending for

more than 10 µm accompanied by enhanced crystallinity and a reduced number of grain boundaries (Figure 25 a-b-c).[21] Thin films of the small molecule PTCDI-e feature a similar change in microstructure upon doping with TTF and TMTSF.[469]

In the case of BHJs for OPVs, Lin *et al.* observed that the addition of DQ to a PM6:Y6:$PC_{71}BM$ ternary blend results in a more even film topography as compared to undoped blends.[264] Changes in the BHJ nanostructure were also observed in, *e.g.*, BV doped PM6:IT-4F blends and F_4-TCNQ doped FTAZ:IT-M blends, confirming that the molecular additive-induced structural changes are a general trend.[118] Doped bulk heterojunction blends do not necessarily undergo a change in molecular packing. For example, Xiong *et al*. reported that the addition of F_4-TCNQ to FTAZ:IT-M films does not alter the crystal structure of the blend components, but enhances the purity of mixed domains.[470]

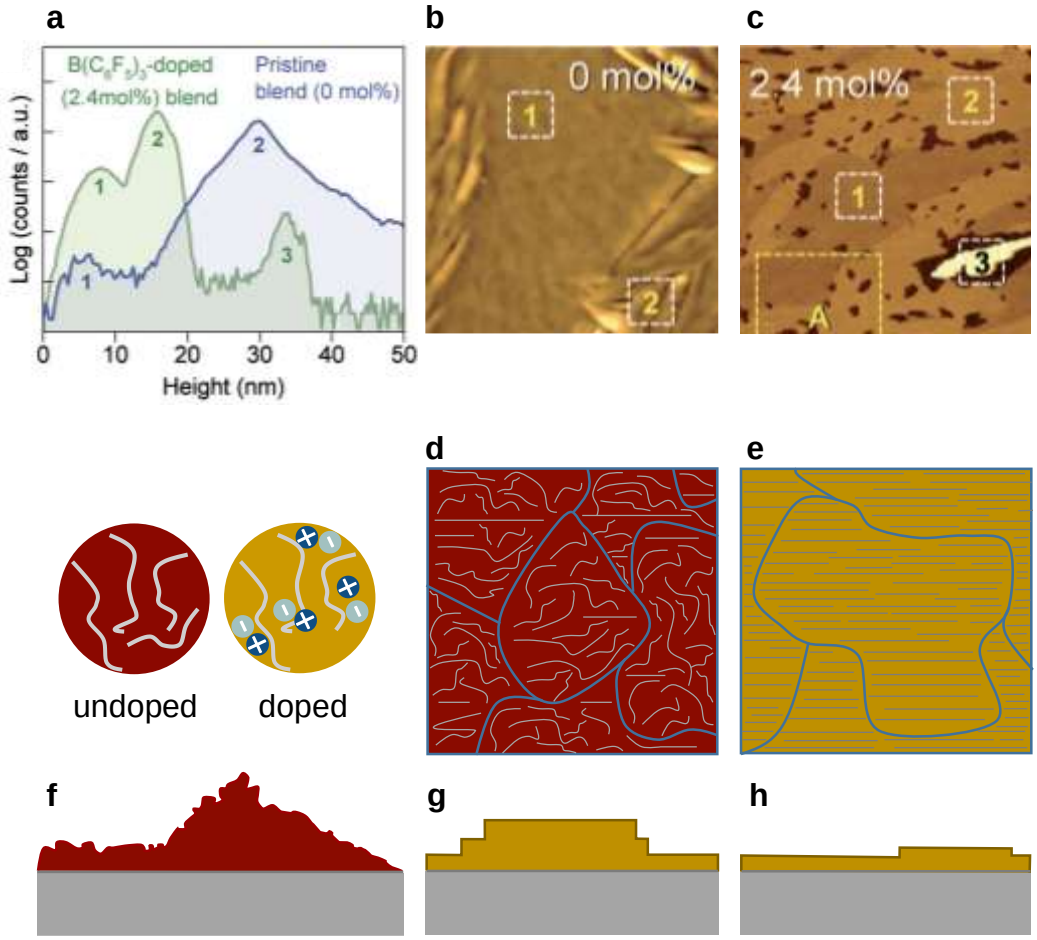

Figure 25: a) Height histograms and topographical AFM images of b) a pristine (0 mol%) and c) a BCF-doped (2.4 mol%) diF-TESADT:PTAA layer, Reprinted with permission from ref [21]. Copyright 2017 Panidi et al. under Creative Commons Attribution License https://creativecommons.org/licenses/. Illustration of the topography of a pristine disordered and dopant-induced ordered film, d) and e) respectively. Illustration of layer cross-sections of a f) pristine and g-h) doped layers that undergo the formation of ordering and densifying terraces.

A systematic understanding with regard to how a dopant modifies the nanostructure of organic semiconductors is still emerging. However, the structure-property relationships described in this section appear to be general and not specific to a particular class of molecules. Depending on the degree of charge transfer between the dopant and the OSC in solution, the solubility of the ionized dopant-semiconductor pair will be affected (likely, the solubility decreases except of the counterion-induced solubility discussed in Section 3.2), which can influence how the semiconductor solidifies. It may for instance lead to the formation of pre-aggregates in solution which drive structure formation, *e.g.,* through nucleation. Another possible mechanism is related to the change in chain conformation (stiffening of the backbone) occurring due to the formation of polarons on the polymer backbone, which could lead to increased π-stacking. Moreover, dopants can change the surface tension of the solution and in turn alter the orientation of the dissolved semiconductor molecules at the interface with the substrate, similar to solution-deposition on surfaces modified with a self-assembled monolayer. In case of weak or negligible doping, classical mechanisms that control crystal nucleation and growth likely govern at least some of the dopant-induced structural changes that have been discussed in this section. It has proven challenging to detect the often-subtle changes with standard experimental techniques, especially in case of multicomponent systems where the complexity of the microstructural landscape increases significantly and the induced change might be limited to a certain buried part of the film. Nevertheless, the ability of dopants to modify the solid-state nano- and microstructure of organic semiconductors represents an extremely versatile tool for the realization of high-efficiency devices.

4. Doping of electronic devices

The envisioned future of organic electronics comprises a large variety of devices and architectures that have been progressively engineered to achieve the required performance. For the vast majority of these applications the semiconductor is placed between two or more electrodes from where charges are injected/collected during operation. As was already discussed in Section 2.1.6, the efficiency of charge injection/extraction depends on the properties of the materials used as well as on their interfaces. Moreover, the low intrinsic conductivity of organic layers can impose significant restrictions on the transport of the charge carriers throughout the semiconductor part of the device. As a result, more complex device architectures that rely on complex fabrication routes, are usually needed to unlock the full potential of OSCs. The latter point is reflected in the pioneering work by Tang and VanSlyke,

who in 1987 demonstrated how the use of a carefully engineered bilayer device architecture can be exploited to produce efficient OLEDs.[471] Their multilayered device architecture paved the way to current state-of-the-art fabrication strategies often involving doped interlayers as a mean to further improve the overall device performance (e.g. efficiency and lifetime). The advances in doped layers in OLEDs have been extensively reviewed in recent years and is beyond the purpose of this work.[12,114,472] Instead, the focus of this section is placed on discussing how molecular doping can be exploited to tune the operation of different type of OSC-based devices including thermoelectrics (Section 4.3), as well as memory devices, bioelectronics, photodetectors, and diodes (section 4.4). Our discussion is limited to OSCs obtained via standard synthetic routes and processing schemes and does not cover high-purity single crystals and ultra-low dopant concentrations. We refer the interested reader to the recent comprehensive work by Hiramoto *et al*.[473]

4.1. Doping in OPV

The key characteristic of a solar cell is its ability to convert light into electricity, known as power conversion efficiency (PCE). The PCE of a solar cell can calculated using the formula PCE = $V_{OC}\,J_{SC}\,FF/P_{in,}$ where the P_{in} is the incident power of the sun. The numerator includes three important parameters of the solar cell: i) the open-circuit voltage (V_{OC}), ii) the short-circuit current density (J_{SC}), and iii) the fill-factor (FF). The V_{OC} is the voltage at which the applied electric field cancels out the built-in electric field, the J_{SC} is the photogenerated current of the cell measured at 0 V, and FF is the ratio of the actual power of the cell to its theoretical power assuming zero series resistance and an infinite shunt resistance.

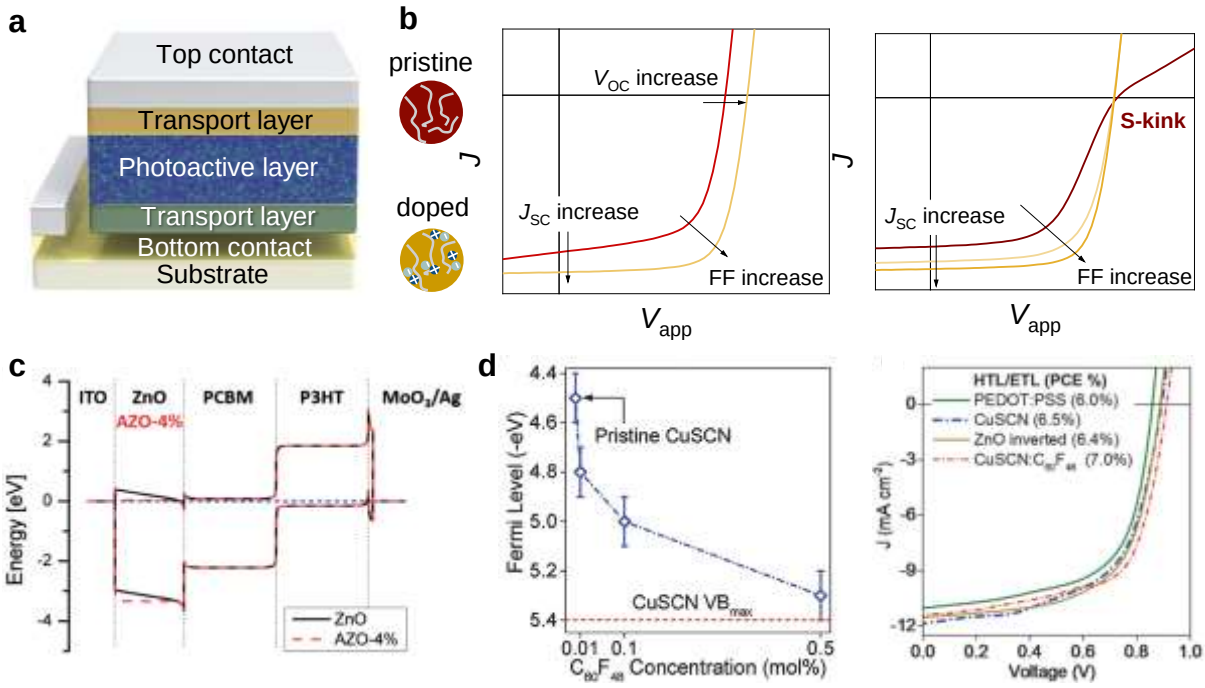

Figure 26: (a) Device architecture of a typical organic photovoltaic (OPVs) cell. (b) Schematic depiction of the impact of the transport layer's doping on J-V characteristics of the OPV. Left panel: doping improves the conductivity (σ) of the transport layer and reduce the energetic mismatch between the contact and the transport layer. This can lead to enhanced J_{SC} and fill-factor (FF). Right panel: doping decreases the energetic mismatch between the different layers and improves the ohmicity of the relevant contact which in turn leads to higher FF, V_{OC}, and J_{SC}. **(c)** The simulated band diagram of the inverted OPV devices using ZnO (black lines) and Al-doped ZnO (AZO) (red lines) with 4% Al electron transport layer. Reproduced with permission. Reprinted with permission from ref. [474] Copyright 2018 Jiang et al. under Creative Commons Attribution-NonCommercial 3.0 Unported Licence https://creativecommons.org/licenses/by-nc/3.0/. **(d)** Fermi level energy (E_F) and valence band maximum (VB_{max}) in CuSCN:$C_{60}F_{48}$ blend films spin-cast on ITO-coated glass and annealed at 100 °C for different concentrations of $C_{60}F_{48}$. J–V characteristics measured under AM1.5 illumination for OPV cells based on different HTLs, namely; PEDOT:PSS, CuSCN, and p-doped CuSCN:$C_{60}F_{48}$ (0.005 mol%). The J–V curve of an inverted cell based on ZnO electron-transport layer is also shown for comparison. Reprinted with permission from ref [475]. Copyright 2018 Wiley-VCH GmbH.

Organic photovoltaics (Figure 26a) represent a promising 3rd generation PV technology, with a maximum reported PCE of over 18%.[476–480] The J_{SC} of OPV is known to be affected by numerous parameters including, the absorption spectrum of the photoactive layer (i.e. BHJ), charge generation, carrier transport and extraction efficiency, whereas the V_{OC} is controlled by the energy levels of the photoactive materials, work functions of the anode/cathode electrodes, and charge recombination rates. Additionally, the FF of OPV is primarily influenced by the charge transport and recombination rates in the photoactive layer and on the charge extraction properties of the transport layers employed.[481] Therefore, the

development of new photoactive materials in tandem with new transport layers are two approaches often pursued to improve the OPV performance. To this end, the intentional doping of both the BHJ and interlayer(s) provides an extremely powerful tool that can be utilized to minimize associated power losses and as such further advance the performance of OPVs.

4.1.1. Doping of charge transport layers

The transport layers are a critical component of all state-of-the-art OPVs and are often added to one or both contacts to control, primarily, charge collection. To create an Ohmic contact for holes (electrons), the electrode work function (W_F) should match the ionization energy (electron affinity) of the organic semiconductor.[482] However, irrespective of the materials selection, a sizeable energy barrier exists at almost any real metal/semiconductor junctions. The use of doped charge transport interlayers could thus play an important role and provide a practical technological solution.[475,483–486, 487] The effect of doping the transport layers in a typical OPV is schematically depicted in Figure 26b (left panel). In the presence of contacts with large energy barriers, the ensuing cell typically exhibits lower V_{OC}, FF, and J_{SC}. Use of doped charge transport layers has been shown to be able to mitigate some of these effects and enhance the built-in electric field and as such the charge harvesting capabilities of the cell, ultimately leading to OPVs with increased V_{OC}, J_{SC}, and FF (see Figure 26b, left panel).[483,488] It is also worth mentioning that the presence of large contact barriers, or use of transport layer with low conductivity/carrier concentration, often manifests in S-shaped J-V curves (inflection point behavior seen in Figure 26, right panel). The latter has generally been attributed to enhanced recombination within the active layer and/or at BHJ/contact interface(s).[474,489–491] To this end, chemical doping has been shown to be able to mitigate this behaviour and lead to OPVs with improved performance.[474,489]. An example of the impact of intentionally doping the ZnO electron transport layer in an inverted OPV, is shown in the band diagram of Figure 26c.[474]

The pioneering work by Pfeiffer and co-workers in 2000 was the first to describe the incorporation of molecular dopant in the charge transport layer of an OPV in order to improve its performance.[484] They showed that the hole transport layers could be efficiently doped by co-evaporation with the strong electron acceptor F_4-TCNQ resulting to an enhanced photovoltage. Since then, F_4-TCNQ derivatives have been often used to improve the HTL's conductivity for use in OPVs. Furthermore, F_4-TCNQ doping was shown to optimize the energy level alignment, layer morphology, hole mobility, and work-function of PEDOT:PSS HTL, leading to a considerable reduction of the leakage current and recombination losses across the device.[486] $C_{60}F_{48}$ has also been used as an effective p-dopant for the wide bandgap

semiconductor copper(I) thiocyanate (CuSCN) (Figure 26d).[475] Incorporation of these $C_{60}F_{48}$-doped CuSCN HTLs in OPV yields devices with significantly enhanced device performance than control cells based on pristine CuSCN and PEDOT:PSS HTLs (Figure 26d). Furthermore, various metal oxides materials, such as MoO_3, ReO_3 and WO_3, have also been used as highly effective p-type dopants for different HTL systems due to their large EA, leading to very promising results.[144,492–494]

Doping is by no means limited to HTLs and the same idea has been extended to ETLs. In brief, Maennig *et al*. combined an F_4-TCNQ-doped HTL with Rhodamine B n-doped ETL to realize OPV cells where the Fermi level in both charge transport layers are controlled by molecular doping, essentially introducing the concept of the p-i-n OPV.[495] Another example is the use of $CoCP_2$ as the n-dopant for C_{60} ETL, which was shown to improve electron transport across the interlayer, reducing the Ohmic losses and ultimately resulting to OPVs with higher J_{SC}, FF, and PCE.[485] n-doping of a polymeric ETL with N-DMBI was also reported to substantially improved the PCE of OPVs from 0.7% to 3.4%.[496] Various salts [e.g. Cs_2CO_3 (Cs)] were also shown to n-dope TiO_2 and C_{60} ETLs resulting in better Ohmic contacts yielding OPVs with improved performance.[483,497] A similar n-doping approach has recently been used in tandem OPVs to improve the Ohmic nature of the recombination junction.[495,498,499] Timmreck *et al*. showed that use of highly-doped recombination layers enable subcell integration with minimal absorption or reflection as compared to conventional metal-based junctions (i.e. use of very thin metal interlayers).[499] To this end we note that molecularly doped recombination layers are rarely employed in tandem OPVs, with the vast majority of the relevant studies relying on undoped recombination junctions such as PEDOT:PSS/ZnO nanoparticles.[500–502]

4.1.2. Molecular doping of the BHJ layer

Recent work has highlighted the suitability of molecular dopants for incorporation directly into the BHJ of the OPV cells.[118,129,264] A summary of the empirical observations of the various effects induced upon doping the BHJ, are schematically depicted in Figure 27. Overall, doping of the BHJ with different molecular dopant has been found to increase the carrier concentration and enhance carrier transport, which in certain systems appears to be one of the limiting factors.[470,503,504] Optimal extrinsic doping was also shown to induce balanced carrier transport and improved charge extraction, ultimately leading to suppression of adverse processes such as space-charge effect and recombination losses, resulting in the enhanced J_{SC} and FF (Figure 27). To this end, recent work showed that addition of a tiny amount of dopant was enough to

enhance both the J_{SC} and FF (**Table 1**) by improving the carrier photogeneration efficiency and suppressing bimolecular recombination while simultaneously affecting the morphology of the BHJ. [118,129,508–517,226,518,244,264,470,503,505–507] Increasing the concentration of molecular dopants in the BHJ beyond the optimal value was shown to result in drastic performance deterioration, often leading to lower J_{SC}, V_{OC}, and FF (Figure 27).[381, 519,520]

Although the benefits associated with doped BHJs are now obvious, the success of the technology, especially in relation to high-performance OPVs, is limited due to the small selection of molecular dopants available. To this end, most of the reported doped OPVs are based on the p-type dopants such as the F_4-TCNQ, which has shown to result in increased charge transport, favorable formation of photogenerated carriers, and trap filling.[470,503,517,505,506,509,510,512,513,515,516] However, the LUMO of F_4-TCNQ is not deep enough to p-dope recently developed, high-performance donor polymers such as PM6 (-5.47 eV), PM7 (-5.51 eV), and D18 (-5.51 eV).[479,521] Furthermore, the limited solubility of F_4-TCNQ introduces additional processing issues. [398,522]

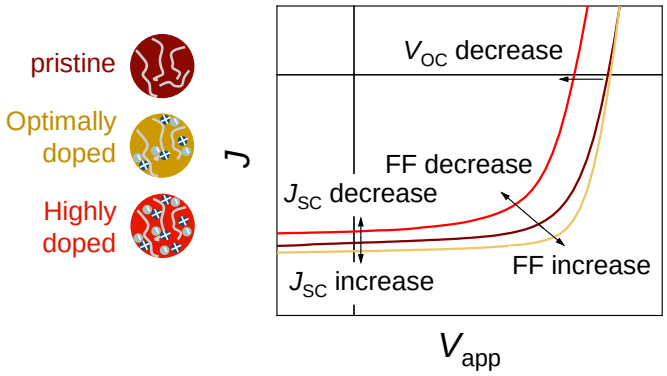

Figure 27: The effect of active-layer doping on J-V characteristics of OPV. Pristine (dark red), optimaly doped with small amount of dopant (yellow), and highly doped active layer (red).

Recently, an alternative dopant, namely tris(pentafluorophenyl)-borane (BCF), a Lewis acid, was successfully utilized to p-dope high IP Lewis basic donor polymers in OTFTs.[223] Unlike the conventional integer charge transfer model, doping mediated by the formation of Lewis acid-base adducts can overcome the issue of extreme energetics that conventional dopants rely on.[219,350] The approach has recently been extended to high-performance OPVs.[129,226,508,511,518] Doping with BCF was also found to exert unusual synergistic effects, simultaneously modifying the BHJ's electronic properties and its microstructure, resulting in increased carrier mobility, longer photocarrier lifetime and reduced nongeminate

recombination.[226,511] Resulting OPV cells exhibited increased J_{SC} and FF, leading to an impressive PCE of 16.0% for cells based on PM6:Y6 blends.[226]

When compared to p-doping of the BHJ of OPVs, the use of molecular n-dopants has been significantly less explored. It was only recently that the n-type dopant BV was utilized to significantly enhance the PCE of state-of-the-art OPVs.[523] To this end, most known n-type dopants could in principle be used to dope numerous high-performance non-fullerene acceptors including, IT-4F,[524] Y6,[525] and BTP-eC9, due to their favorable for doping deep LUMO energies (for full chemical names see *Supplementary Information* section).[477] An important attractive characteristics associated with the neutral BV is its high solubility in common non-polar organic solvents, including toluene and various chlorinated solvents, which makes it easier to use. Optimized BV-doped OPVs where found to exhibit remarkable PCEs in excess of 17%[118,514] due to the simultaneous enhancement of J_{SC} and FF. Just like in the case of p-doped OPVs using BCF, n-doping with BV was found to affect the cells' charge transport characteristics as well as the microstructure of the BHJ, ultimately resulting in enhanced π-π stacking, higher photoresponse and reduced carrier recombination losses.[118] More recently, DQ with HOMO levels of -3.53 eV and -3.95 eV, for the neutral DQ and $DQ^{\bullet+}$ states respectively, was isolated and studied as n-dopant in OPVs based on the state-of-the-art PM6:BTP-eC9:$PC_{71}BM$, blend.[264] Optimally doped cells exhibited a remarkable PCE of 18.3%, which is the highest values among all doped OPVs. The greatly improved performance was attributed to numerous synergistic effects, including; i) increased absorption of the doped BHJ, ii) microstructural changes observed within the BHJ, iii) increased and balanced hole/electron mobilities, iv) longer carrier lifetimes, and v) reduced bimolecular recombination losses. Despite the limited number of studies it is already clear that controlled molecular doping of the BHJ in OPVs can assist us towards achieving the ultimate performance that has recently been predicted to surpass 20% for single-junction OPVs.[25]

Table 1. Summary of performance parameters, current density, fill-factor, and power conversion efficiency (J_{SC}, FF, and PCE) (J_{SC}, FF, and PCE) of OPVs with different n-type and p-type dopants incorporated in the BHJ.

Type	Dopant	Dopant Amount	Active layer	J_{SC} [mA cm^{-2}]	FF [%]	PCE [%]	Reference
P-type	F_4-TCNQ	0.08 wt%	FTAZ:IT-M	18.2	70.4	12.2	[470]
	w/o	/		17.8	68.7	11.9	
	F_4-TCNQ	0.15 wt%	PBDB-T:PNDT-T:DCNBT-IDT	17.5	74.4	11.9	[515]
	w/o	/		16.7	71.1	10.7	
	F_4-TCNQ	0.1 wt %	PBDB-T:ITIC:$PC_{71}BM$	16.1	70.0	10.1	[509]
	w/o	/		15.1	67.0	8.9	

	F_4-TCNQ	0.01 wt %	PCE10:PC_{71} BM	17.4	61.8	8.6	512
	w/o	/		17.1	55.2	7.6	
	F_4-TCNQ	0.4 wt%	PCDTBT:PC_{71}BM	14.0	63.0	7.9	503
	w/o	/		11.0	67.0	6.4	
	F_4-TCNQ	0.1 wt%	P3HT:ICBA	9.9	68.0	5.8	513
	w/o	/		8.2	63.2	4.5	
	F_4-TCNQ	0.5 wt%	P3HT:PC_{60}BM	9.9	68.0	4.0	517
	w/o	/		9.0	63.0	3.5	
	F_4-TCNQ	$5x10^{-3}$ wt%	P3HT:PC_{60}BM	9.8	72.0	4.1	505
	w/o	/		9.4	70.0	3.7	
	F_4-TCNQ	1.0 wt%	P3HT:PC_{60}BM	9.4	67.0	4.2	516
	w/o	/		9.1	63.0	3.7	
	F_4-TCNQ	0.5 wt%	PCPDTBT:PC_{60}BM	10.3	56.0	3.6	510
	w/o	/		9.4	55.4	3.3	
	TCNQ	12 wt%	J52:IEICO	18.6	53.4	8.2	506
	w/o	/		13.2	55.2	6.3	
	BCF	0.01 wt%	PM6:Y6	26.0	73.5	16.0	226
	w/o	/		25.5	72.3	15.4	
	BCF	0.001mg/mL	PCE10:FOIC	22.8	65.5	10.9	508
	w/o	/		21.7	62.7	10.1	
	BCF	0.1 wt %	PBDB-T:ITIC	15.9	66.8	10.0	511
	w/o	/		15.41	64.5	9.5	
	BCF	0.05 wt%	PCE10:PC_{71}BM	17.5	68.6	9.6	129
	w/o	/		16.6	67.7	8.9	
	BCF	Solvent vapor doping	PCE10:PC_{71}BM	17.3	65.6	9.4	518
	w/o	/		16.4	69.0	8.6	
N-type	DQ	0.01 wt%	PM6:BTP-eC9 :PC_{71}BM	26.9	79.4	18.3	264
	w/o	/		26.2	75.7	17.4	
	BV	0.004 wt%	PM6:Y6:PC_{71}BM	26.3	77.0	17.1	118
	w/o	/		25.7	75.0	16.3	
	BV	0.04 wt%[a]	PM6:BTP-CO-4Cl	26.1	77.7	17.3	514
	BV	0.04 wt%		25.8	76.5	16.8	
	w/o	/		25.2	73.2	15.6	
	N-DMBI	0.01 wt%	PCE10:FOIC	22.6	59.8	10.0	508
	w/o	/		22.3	60.8	10.0	
	TBAI	0.04 wt %	PBDB-T: P(NDI2OD-T2)	12.5	65.3	7.00	244
	w/o	/		11.5	58.4	5.81	
	N-DMBI	0.3 wt %	PCE-10: P(NDI2OD-T2)	10.4	52.3	4.4	507
	w/o	/		9.4	46.5	3.5	

[a]Using a halogen-free solvent toluene.

4.2. Doping in OTFTs

OTFTs have attracted strong interest during the past few decades owing to their numerous attractive attributes that are particularly relevant for emerging applications in the area of consumer electronics. This strong interest is clearly reflected in the huge number of studies manifested in the large volume of the relevant scientific literature (Figure 28a). The standard approach for fabricating an OTFT relies on the use of an intrinsic (*i.e.,* non-doped) organic semiconductor that is deposited onto a substrate containing two pre-patterned electrodes

(source/drain, S/D), followed by the deposition of a dielectric layer and a gate electrode (Figure 27b). The formed device is the so-called top-gate, bottom-contact (TG-BC) configuration, although numerous other architectures can be adopted depending the specific needs and materials' properties (see Section 4.2.3). The use of dopants, either as part of an injection layer or embedded within the semiconductor channel, has been relatively limited despite the increasing interest in doped OTFTs (see Figure 28a).

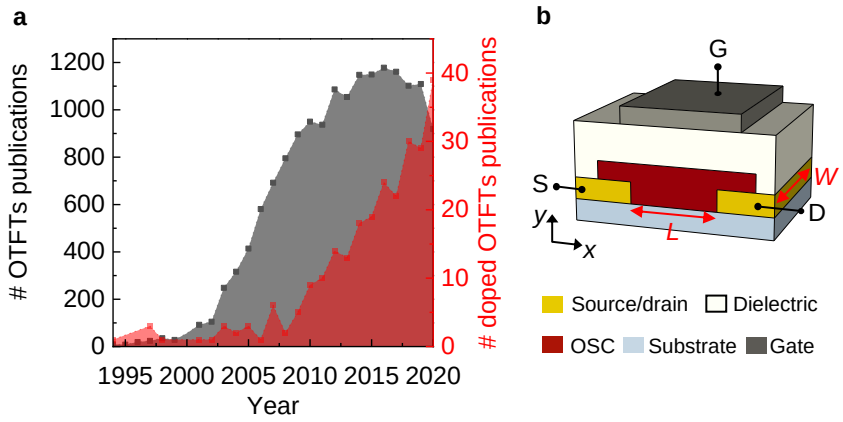

Figure 28: a) Research development in OTFTs and the relative quota for doping. The plot indicates the number of publications per year (from ISI Web of Science) involving OTFTs (grey) and how many of them encompassed the doping approach (red). b) Schematic illustration of a top-gate, bottom-contact (TG-BC) transistor architecture.

The reasons behind the scarce employment of dopants in OTFTs relate to the geometry and working principle of these devices. In a typical OTFT the organic semiconductor bridges the source and drain electrodes to form the semiconducting channel the conductivity of which is modulated by the external gate field (V_G). The vast majority of OTFTs operate in "accumulation mode", which means that upon application of a suitable V_G, the resulting polarization of the dielectric causes the injected charges to accumulate at the semiconductor/dielectric interface forming the so-called "channel". The potential difference between source and drain terminals leads to an electric current flowing across the channel, which increases proportionally with increasing $|V_G|$. The low charge carrier density in the semiconductor prior to gate biasing guarantees a low intrinsic channel conductivity, and hence a low off current (I_{off}), while the gate-induced field-effect leads to a channel current modulation of several orders of magnitude. As a consequence, the introduction of dopants poses some major challenges, since an increase in the semiconductor's bulk conductivity could result in an unintentional increase of I_{off}, ultimately compromising the device operation. Moreover, since

the source and drain electrodes lie in the same plane with the semiconductor, it is challenging to spatially separate a conducting layer from the channel of the device, as it is typically done in other staggered device geometries, such as OLEDs and OPV using HTLs and ETLs. The approach becomes even more complicated when taking into account the lack of stability displayed by many dopants upon incorporation into an organic matrix, rendering a localized doping pattern particularly problematic.

Despite these complications, however, dopants continue to play an increasingly important role towards OTFTs with higher carrier mobility and improved operational stability. The recent developments of improved OSCs and their integration in state-of-the-art OTFTs and integrated circuits have yielded new challenges related to charge injection and transport both of which could in principle be addressed by doping. Next we discuss the impact of doping on the operating characteristics of transistors and highlight how the technology could lead to devices with improved performance. Emphasis is placed on the two main doping approaches often adopted for OTFTs, namely channel doping and contact doping.

4.2.1. Controlling charge transport in OTFT with doping

The current-voltage characteristics of conventional OTFTs can be described by the gradual channel approximation model. The main assumption here is that the variation of the electric field across the channel is much larger than that along it, $\partial E_y/\partial y \gg \partial E_x/\partial x$, hence E_x is essentially constant. Moreover, the current in the channel is modeled to be dominated by drift and not by diffusion, no mobile charges are assumed in the dielectric layer, nor to flow across it (*i.e.,* zero leakage current) and the carrier mobility is assumed to be independent of the applied bias.[526] The operating regimes, as a function of the biasing conditions, predicted by this model are the linear, nonlinear, and saturation regimes. For simplicity, we discuss here the current-voltage relationship in saturation regime, which can be expressed as

$$I_D = \frac{WC}{2L}\mu(V_G - V_T)^2 \tag{14}$$

Here, W and L are width and length of the channel, C is the capacitance of the dielectric layer per unit area, μ is the charge carrier mobility, V_G is the gate voltage and V_T is the threshold voltage. Saturation is achieved for $V_D \geq V_G - V_T$, where V_D is the drain voltage. From the equation above, the charge carrier mobility can then be expressed as

$$\mu = \frac{2L}{WC}\left(\frac{\partial\sqrt{|I_D|}}{\partial V_G}\right)^2 \tag{15}$$

Figure 29a shows a representative transfer characteristic calculated from this model using an arbitrary set of device and material parameters. The threshold voltage should in principle be zero and at higher voltages the slope of the curve should be constant; conditions rarely encountered in real OTFTs. These deviations from ideality are related to the energetic disorder often encountered in organics that leads to charge localization and to a Gaussian distribution of DOS (discussed in Section 2.1.1). Moreover, other causes include the presence of structural defects in the films (e.g. grain boundaries), the non-optimal charge injection from the contacts, and the interfacial electronic disorder at the dielectric/semiconductor interface. This behavior is in stark contrast with the Ohmic injection and delocalization of charges over large lattice distances typical of ordered, crystalline inorganic semiconductors such as silicon. This deviation from the ideal current-voltage characteristics poses some limitations to the use of Eq. (14) to extract key figures of merit (FOM) and to assess the intrinsic properties of OSCs.

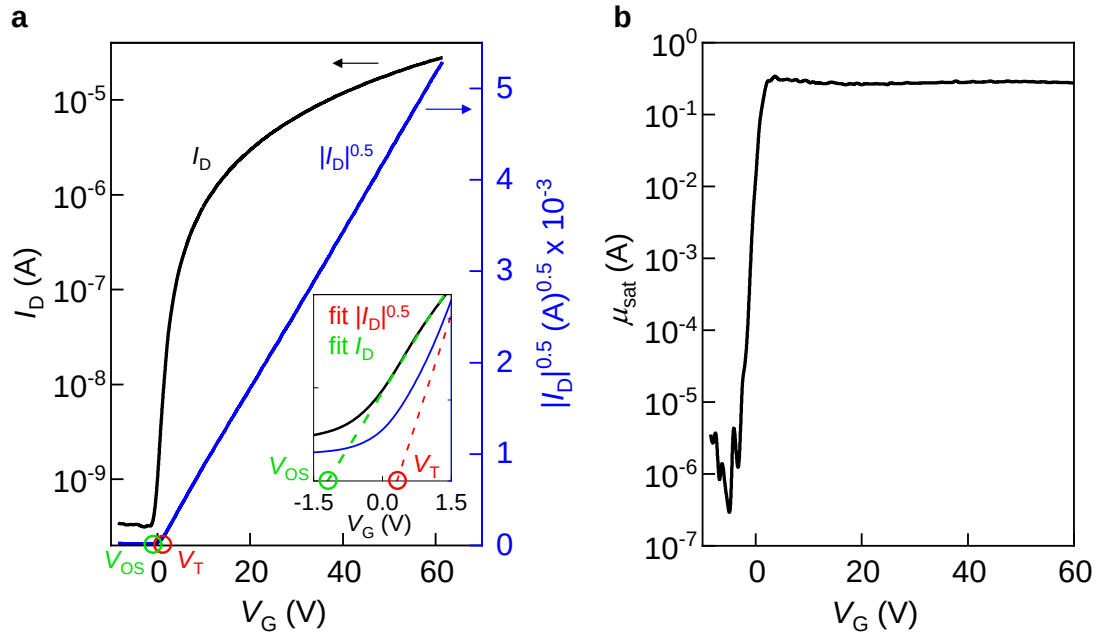

Figure 29: Schematic illustration of a unipolar, n-type OTFT in saturation regime. a) Transfer curve (black) and the corresponding plot of $|I_D|^{0.5}$ as a function of V_G (blue). V_T and switch-on voltage (V_{SO}) are shown with a red and green circle respectively, the inset shows the fits and intercepts for their extraction. b) Corresponding field-effect mobility as a function of applied V_G.

For instance, the charge carrier mobility for an ideal OTFT should be constant and independent of V_G (Figure 29b). In reality, however, the value extracted is a fit parameter and is usually referred to as apparent mobility (μ_{app}). The latter provides information about the specific device, rather than to the intrinsic mobility of the semiconductor (μ_{intr}) employed. Moreover, the threshold voltage in OTFTs is also a fit parameter as it is extracted from the intercept of $|I_D|^{0.5}$ with the V_G axis, and does not hold the same physical definition encountered

in inorganic transistors; *i.e.,* the onset of strong inversion. Nevertheless, V_T provides an indication of the gate voltage at which the transistor switches on.[527,528] A similar parameter, the switch-on voltage (V_{SO}), has been proposed to model the *I*-*V* characteristics of disordered OTFTs and is defined as the voltage below which the variation of the channel current with the gate voltage is zero.[527] It should be noted that at $V_T \geq V_{SO}$ and at low V_G, a deviation from the straight line in the $|I_D|^{0.5}$ (V_G) plot occurs. The voltage range below V_T and above V_{SO} voltage defines the so-called subthreshold regime, whose slope indicates how sharply the device turns on.

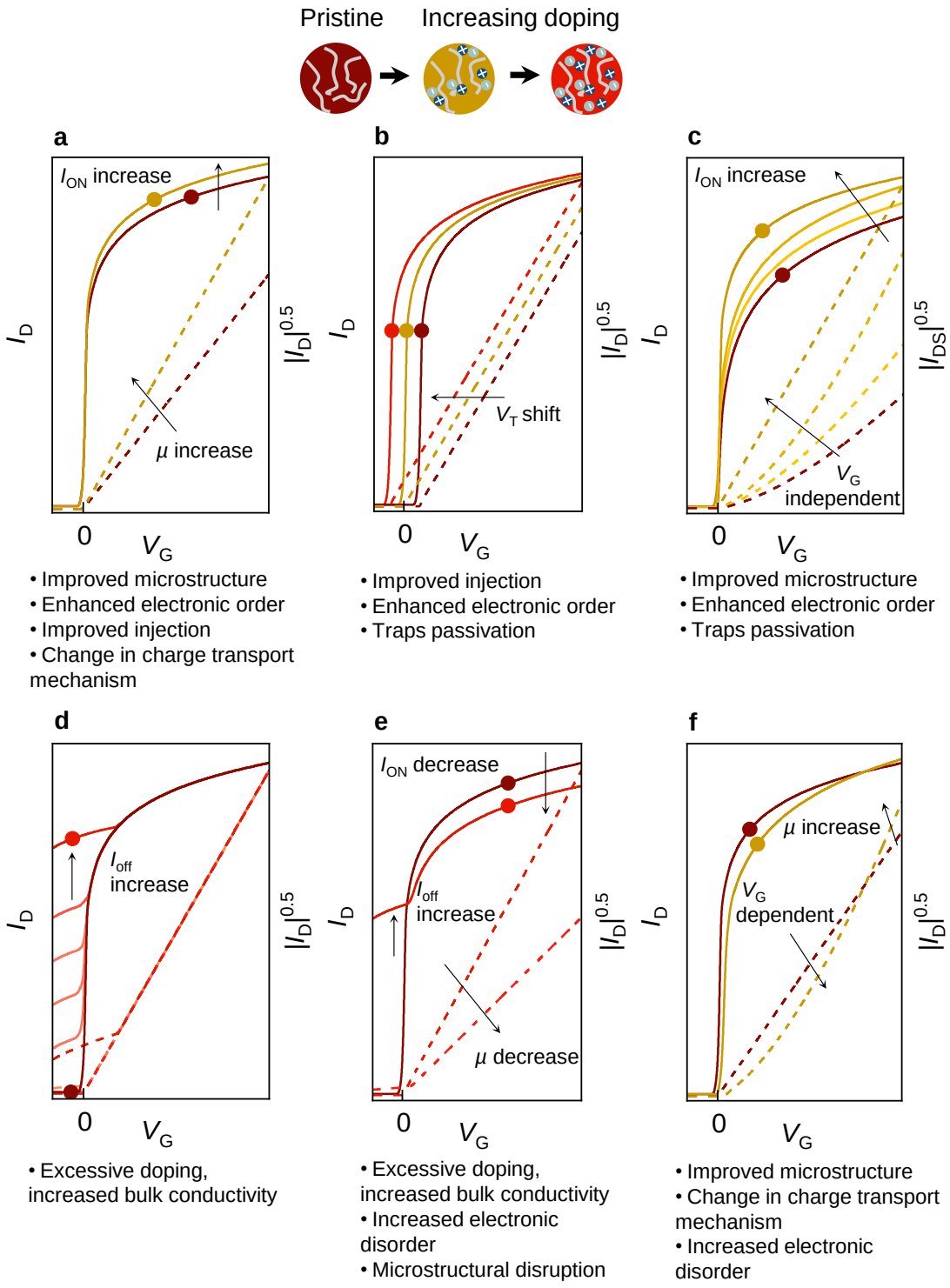

Figure 30: Doping effect on the OTFT transfer curve. In the top panel, a schematic representation shows the pristine (dark red) and doped OSC (dopant concentration increasing from yellow to red), which serves as a color scale for the I_D-V_G curves. In the bottom panel, the variation upon doping of transfer characteristics (solid lines) and $|I_D|^{0.5}$ as a function of V_G (dashed lines) is shown for different conditions (a-f). The affected figures of merit upon doping are indicated in each panel, while the reasons leading to those changes are listed below the panel. Yellow curves depict doped transistors at low concentrations that show improved device performance, while red curves show highly doped devices exhibiting reduced performance. The direction of the arrow and the color gradient in c) and d) indicate an increase in doping concentration.

Addition of dopants, either in the bulk of the OSC or in proximity to the injecting contacts, can affect the current-voltage characteristics of the OTFT. Figure 30 summarizes the various changes often observed in the operating characteristics of OTFTs. For instance, a transistor parameter that is highly sensitive to doping is the V_T. In the presence of Ohmic contacts and considering a trap-free regime, V_T should be zero. In reality, however, V_T is often non-zero due to a number of extrinsic effects such as charge injection limitations and the presence of traps. In the case of Ohmic contacts, the applied gate bias would first fill the trap states at the interface with the dielectric, and only after trap-filling, mobile charge carriers would start being accumulated in the channel. Thus, V_T can be approximated as the voltage required to fill the trap states before accumulation. As a consequence an increased number of traps causes a progressive shift in the V_T.[44] Simultaneously, the current in the subthreshold region is also affected since it is dominated by charge diffusion and inevitably by the carrier concentration. Thus, the presence of trap states tends to reduce the so-called subthreshold slope (S_{SS}) of the device, ultimately rendering it more difficult to turn-on. Such trap-dominated devices exhibit I_D-V_G curves that are non-linear accompanied by an apparent V_G-dependence of μ.

Molecular doping could affect the energetic landscape of the semiconductor and hence the overall transistor characteristics. Use of low doping concentrations has been shown to be able to fill trap states.[529] Interestingly, OSCs with trap concentrations in the range of 10^{16}-10^{19} cm^{-3} undergo trap filling upon dopant incorporation at molar concentrations $<10^{-3}$. However, at higher concentrations, dopants can increase the trap density even though the energetic disorder reduces. The latter occurs in systems showing an intrinsic high density of trap states, for which the electrostatic disorder associated to charge formation is compensated by deep traps filling, with a mechanism denominated "disorder compensation".[529] In the case of OTFTs the deactivation of trap states leads to a shift in V_T towards zero (Figure 30b) and to a lower S_{SS}, accompanied by an increased linearity in the $I_D^{0.5}$ *vs*. V_G plot (Figure 30c). On the other hand, if the dopant concentration is too high it may create excess charges in the bulk of the semiconductor, ultimately increasing the channel current even at $V_G = 0$ V. As a consequence, a reverse bias has to be applied to deplete the excess charges and turn-off the device.

The reduced energetic disorder and deactivation of trap states upon doping of the channel may affect the overall carrier transport across the device and lead to mobility enhancement (Figure 30a).[45,107,137,530] However, this is not necessarily valid for extremely ordered molecular semiconductors that exhibit band-like charge transport. In such systems, the low intrinsic energetic disorder can be increased upon doping, besides detrimental structural

effects, and reduce the mobility. To this end, a number of organic systems exist where charge transport shows moderate temperature activation,[46,531–533] temperature-independent behaviour,[534] or both.[468,535,536] In these systems, doping may overcome the thermal activation barrier and not only increase the charge carrier mobility, but also broaden the temperature regime associated with band-like transport.[468,537] In contrast, high dopant loadings can lead to DOS broadening of the host OSC, regardless of its intrinsic energetic disorder, with detrimental consequences on OTFT operation that include; a shift in V_T towards higher potentials, reduced S_{SS}, a decreased current-voltage linearity, and ultimately lower μ. Furthermore, under such doping conditions the conductivity of the channel may increase, which can in turn compromise the on/off ratio of the transistor, among other important parameters (see Figure 30d-e).

To add to the complexity, the microstructure of the OSC is also critical for the energetic landscape and hence charge transport. Equally, the structural properties of the semiconductor are sensitive to the presence of dopants (see Section 3.3), which in turn introduces a complex energetics-doping-microstructure interrelationship. Dopant-induced structural ordering is often accompanied by a reduced trap density, while structural disruption of the host semiconductor due to doping leads to increased disorder. As such, doping-induced structural changes can induce major variations in the charge transport of OSCs, even at small dopant concentrations. Dopants may, for instance, promote the formation of large crystallites with differently geometries and lead to better performing OTFTs (Figure 30a). Ultimately, microstructural effects could dominate over the intended electronic doping of the host OSC.

The relationship between doping and transistor performance is more complex and it is also strongly coupled to charge injection and as such contact resistance (R_C). The latter relates to the mismatch between the contact work function (Φ_m) and the energetics of the OSC (see Section 2.1.6). Often R_C is modeled as a resistance connected in series to the transistor channel (R_{CH}). The former becomes increasingly relevant as the mobility in state-of-the-art OSCs increases and correspondingly R_{CH} reduces. Despite best efforts, R_C can indeed remain high enough to dominate the operation of the OTFT, ultimately undermining the validity of the gradual channel approximation model [Eq. (14)]. In relation to this, we refer the interested reader to the comprehensive review by Bittle *et al*.[538] Even when $R_C \ll R_{CH}$, a non-negligible voltage drop still occurs at the contacts, with the effective applied voltage (V_{app}) between the source-drain electrodes becoming

$$V_{app} = \Delta V_S + \Delta V_{ch} + \Delta V_D = I_D(R_S + R_{ch} + R_D) \tag{16}$$

Here ΔV_S and ΔV_D are the voltage drops at the source and drain electrodes, respectively, ΔV_{ch} is the voltage drop across the channel, and R_S & R_D are the contact resistances at the source and drain electrodes. R_C can strongly affect the current-voltage characteristics, with some of the most commonly observed effects summarized Figure 31. For example, the existence of a high R_C can lead to the formation of local current hypes (Figure 31e-f-h) that lead to the extraction of erroneous mobility values (Figure 31h-i),[363–365, 366] and can limit the maximum operating frequency of the OTFT.[539] These adverse effects are more pronounced in coplanar than staggered transistor geometries.[540] Contact limitations become even more apparent in short channel devices since R_C remains identical, while the channel resistance (R_{CH}) decreases linearly upon reducing the channel length.

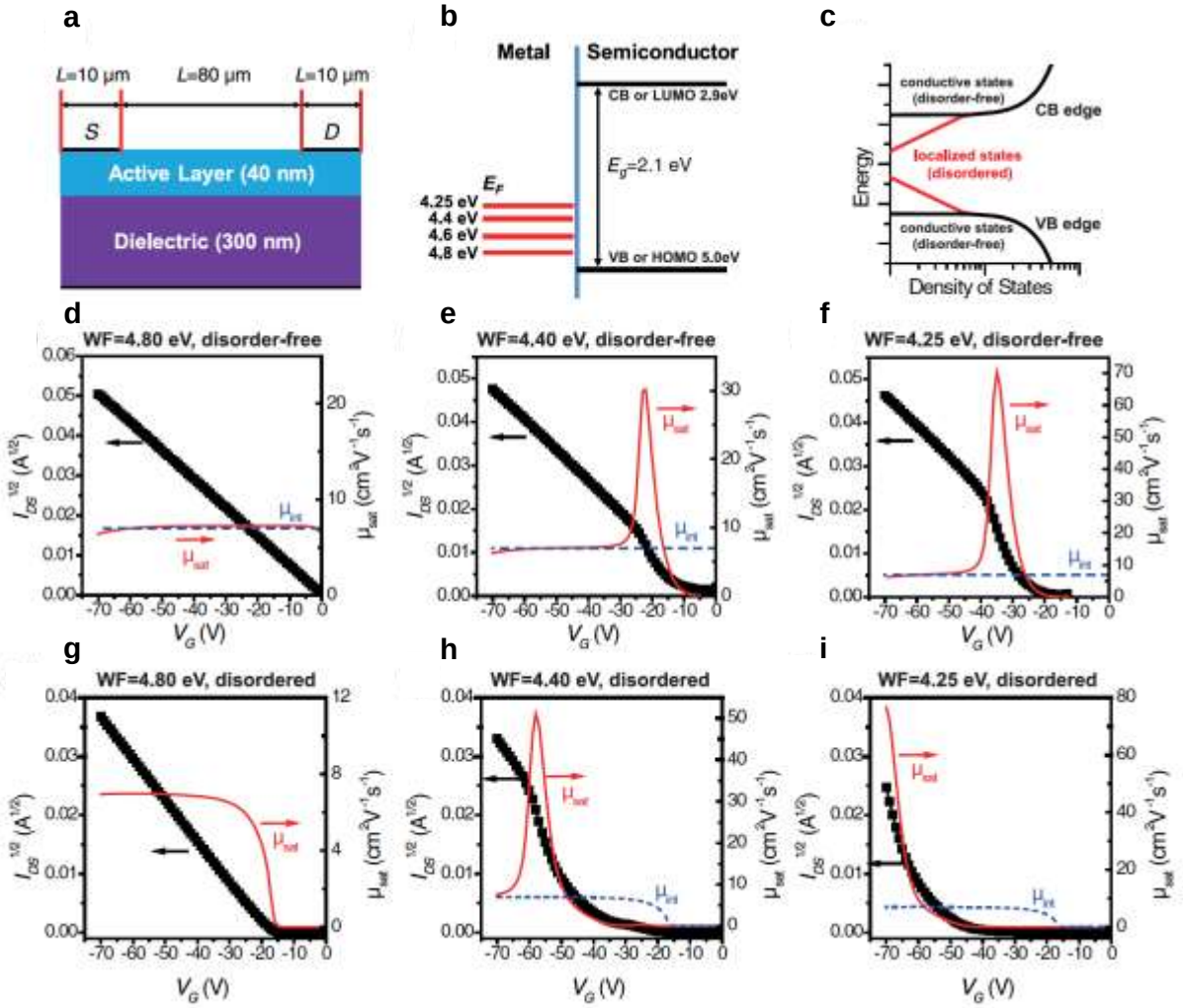

Figure 31: Effect of injection barrier on the I_D-V_G curves and field-effect mobility in the saturated regime. Schematic of a) device structure and b) energy levels at the contact. c) Semiconductor density of states of a disorder-free semiconductor (black), and for a disordered semiconductor (red), exhibiting localized, tails states. $|I_D|^{0.5}$ (black) and field-effect mobility (red) as a function of V_G for contacts with a metal workfunction (as indicated) with increasing injection barrier for a disorder-free d) –

f) and disordered g) – i) OSC. The set mobility measured for an Ohmic contact is shown in blue dashes. Reprinted with permission from ref [366]. Copyright 2017 American Physical Society.

Some of the adverse effects associated with presence of large R_C can be partially mitigated by increasing the carrier concentration within the OSC via doping. As already discussed in Section 2.1.6, higher carrier concentration can narrow the depletion region width at the metal/semiconductor junction, leading to improved charge injection and smaller R_C. In some instances, controlling the injection and carrier transport through doping may also be exploited to control the polarity of an OTFT, and even the operation of logic circuits. A good example are diketopyrrolopyrrole-containing polymers[541] which are known to exhibit (under certain conditions) balanced ambipolar transport. Addition of a suitable dopant may aid the transport of one type of carrier (majority carrier) while suppressing the other (minority carrier), hence enabling complete control over charge transport through appropriate doping schemes.[542,543] These capabilities enabled by doping are unique and have already started having an impact in the field of organic electronics.

An additional important requirement for any OTFT technology is stability, both towards atmospheric elements (shelf life) and continuous operational (bias-stress). The former is mainly determined by the air-stability of the organic semiconductor,[544] while the latter is attributed primarily to carrier trapping in the bulk of the semiconductor and/or at the OSC/dielectric interface, and/or at the source-drain contacts.[545] Both effects often manifest as shifts in V_T and may also affect the subthreshold slope and the charge carrier mobility of the device.[546] Another mechanism that has been argued to contribute to the bias-stress behaviour of OTFTs is the presence of water molecules in the semiconductor.[547,548] In relation to these effects, use of molecular additives provides an additional tool that can be used to overcome such extrinsic instabilities although the origin for the observed improvements is still the subject of heated debate.

4.2.2. Channel doping in OTFTs

The idea of incorporating a dopant directly into an organic semiconductor has been explored since the early days of OTFTs. The pioneering work by Jarret *et al*. in 1995 showed how the charge carrier mobility of the amorphous poly(β'-dodecyloxy-α,α',-α,α''terthienyl (polyDOT$_3$) was increasing upon doping with 2,3-dichloro-5,6-dicyano-1,4-benzoquinone (DDQ), and reported a linear dependence between mobility and the conductivity of the ensuing polymer:dopant blend.[549] Additional studies at that time explored the use of dopants as a mean

to tune the operation of OTFTs and highlighted how the improvements in charge transport came at the expense of bulk resistivity and hence current on/off ratio.[550–553] The latter effect represents the main reason why the direct doping of the semiconducting channel was, for long time, considered inferior to other strategies towards the development of state-of-the-art OTFTs. Some critical discoveries were made in 2000s which highlighted the untapped potential of dopants for OTFTs. Wei *et al*. reported on n-doping of PCBM with N-DMBI and described how extrinsic doping improved the stability of electron transport in the air owing to passivation of O_2 induced trap (Figure 32).[554] Soon after the charge carrier mobility and V_T of n-channel OTFTs were shown to be controlled by doping as well, paving the way to further developments.[469,555]

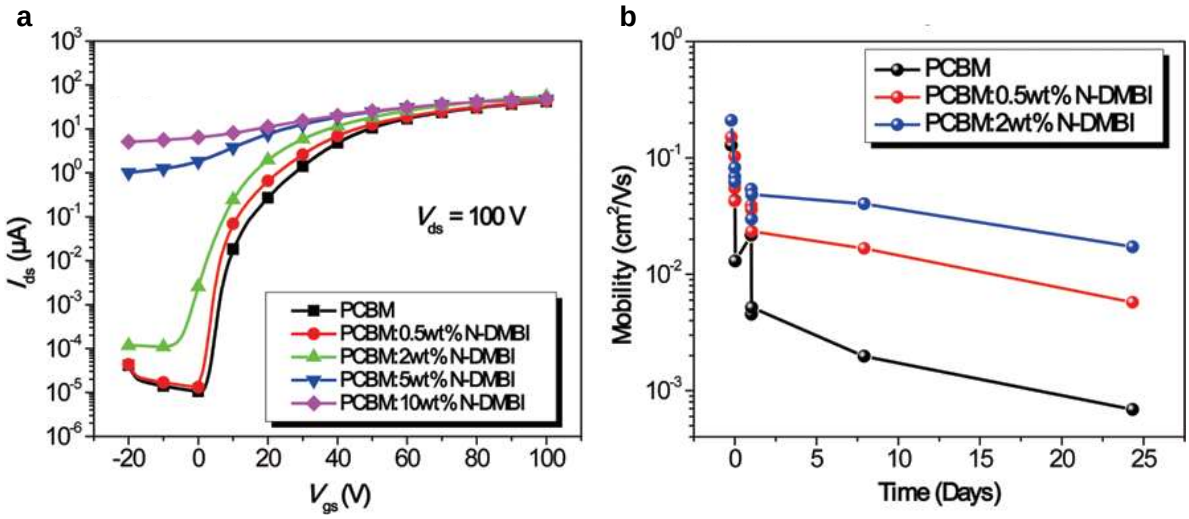

Figure 32: a) Transfer characteristics of PCBM and N-DMBI doped (as indicated) OTFTs measured in the glovebox. b) Evolution of field-effect mobilities for devices measured in the air as a function of time for pristine and N-DMBI-doped (0.5 and 2 wt %) PCBM OTFTs. Reprinted with permission from ref [554]. Copyright 2017 American Chemical Society.

The ability to tune charge injection and to modulate the concentration of traps have also enabled researchers to study electron conduction in OSCs that are typically associated with hole transport, *e.g.*, TIPS-Pentacene doped with *o*-MeO-DMBI.[191] Doping, mostly using F_4-TCNQ, of p-type OTFTs was also shown to control the device operation, exhibiting stable V_T close to zero, improved device ideality, and enhanced mobility.[458,556–560] A combination of p- and n-type doping was also reported to give rise to transistors operating in inversion and depletion regimes, rather than the standard accumulation regime.[91] The effect of unintentional O_2 doping on p-type devices was also extensively studied and was found to be responsible for the high off currents in polythiophene-based OTFTs.[137,561] This feature was exploited in

P3HT:polystyrene blends, where the dilution of the semiconductor with the insulator led to enhanced devices with low bulk currents, upon oxygen exposure.[562] These early studies provided strong evidence that optimized doping could be explored to improve transistor performance significantly.

The deposition of a thin dopant layer directly onto the OSC or co-evaporation of the two materials, are two alternative doping approaches described in the literature.[563–565] An analytic model that describes the operation of such OTFTs has also been recently proposed.[566] Similarly, spin coating the dopant onto the OSC film using orthogonal solvents was also investigated.[567,568] The researchers spin coated a layer of F_4-TCNQ and PEI onto the semi-crystalline polymer DPP-BTz and studied the effect of the crystal orientation of the polymer on the doping process and on device performance (Figure 33). They showed how doping the polymer on a face-on orientation was leading to a fivefold increase of μ, while in the case of edge-on orientation, only a slight increase was observed. The stark differences were related to the different doping efficiencies for the two polymer configurations and the associated trap densities.[568] An important aspect of these sequential doping methods is their ability to preserve the microstructure of the neat OSC beneath (see relevant discussion in Section 3.1.2).

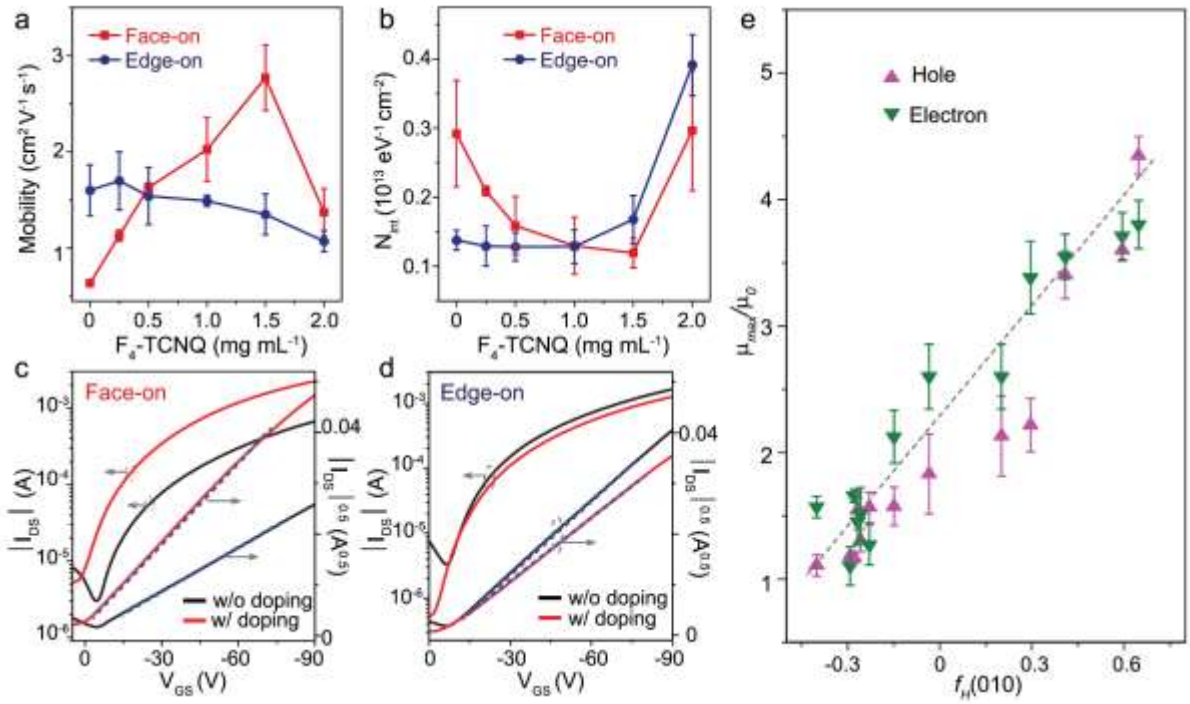

Figure 33: Effect of OSC orientation on the mobility enhancement. a) Field-effect mobilities and b) interfacial trap state density of DPP-BTz devices doped with F_4-TCNQ. Transfer characteristics of face-on (c) and edge-on (d) pristine and doped devices, F_4-TCNQ solution concentration of 1.5 mg mL^{-1}. e) F_4-TCNQ and PEI doping-induced mobility enhancements as a function

of Herman's orientation factor. An $f_H(010)$ value of 1 corresponds to a perfect face-on π–π stacking and a value of −0.5 represents a perfect edge-on orientation. Reprinted with permission from ref [568]. Copyright 2020 Wiley-VCH GmbH.

To date, co-processing the semiconductor:dopant blend from solution is the most commonly employed processing route. It has been applied to a large number of systems including: F_4-TCNQ:DPP-BTz,[568] pyronin B:DPPTTT,[181] TFP and OFN blended with P3HT and TIPS-Pentacene,[465] FTCS:TIPS-Pentacene,[569] o-BnO-DMBI and o-AzBnO-DMBI to compensate oxygen doping in P3HT,[570] BCF with various polymers, various small-molecules as well as polymer:small molecules blends.[21,223] It combines simplicity with the potential benefits associated with the various electronic and structural effects induced upon doping. For instance, Panidi *et al*. showed how BCF leads to remarkable improvements for a range of semiconductor systems, where the microstructure and morphology play a crucial role on OTFT operation.[21] Another interesting doping approach relies on the use of a dopant (F_4-TCNQ)/semiconductor (C_{12}-BTBT)/electret (polystyrene) trilayer architecture, which results in charge modulation, *i.e.*, device modulation by both doping and electret.[571]

Following the pioneering work by Wei *et al.*,[554] doping proved extremely successful in realizing n-type OTFTs.[125,234,572–576,243,257,259,262,275,461,462,565] This is primarily due to the intrinsically poor environmental stability of n-type OSCs due to their sensitivity toward atmospheric oxidants, as compared to their p-type counterparts. Significant effort focused on P(NDI2OD-T2), DPP based polymers and fullerene derivatives, using a wide range of dopants [e.g. PEI,[257,259,568] BV,[573] TBAX (X = F, OH, Br),[234,243,275,576] amino-functionalized silanes (TMA, TEDA),[575] $CoCp_2$,[461] CsF,[461,542] N-DMBI,[554,572] DMBI-BDZC,[462] DBU].[262] In these systems, the impact of dopants on the device performance was often found to be remarkable. For instance, P(NDI2OD-T2) is known to undergo reversible and irreversible degradation processes in presence of oxygen and water, respectively. As a consequence, thermal annealing under an inert atmosphere is usually required to improve the OTFT stability, even though the device remains intrinsically unstable towards the same atmospheric species.[142,143] Doping-induced trap passivation works in a similarly manner and allows stabilization of the device. In the latter case however the OTFTs can remain stable upon re-exposure to air. Stability improvements to bias-stress upon channel doping have also been reported for both p- and n-channel OTFTs.[461,563,565,572]. Furthermore, different groups showed how the ambipolarity of OTFTs can be controlled through channel doping leading to purely unipolar operation or even alter the polarity of the majority carrier in the channel.[181,191,234,257,542,573] Khim *et al*. showed,

for instance, how p- and n-dopants, could be patterned by inkjet printing onto PCBM layer, demonstrating the possibility to fabricate organic complementary circuits based on a single semiconductor that has been spatially doped (Figure 34b, e).[542]

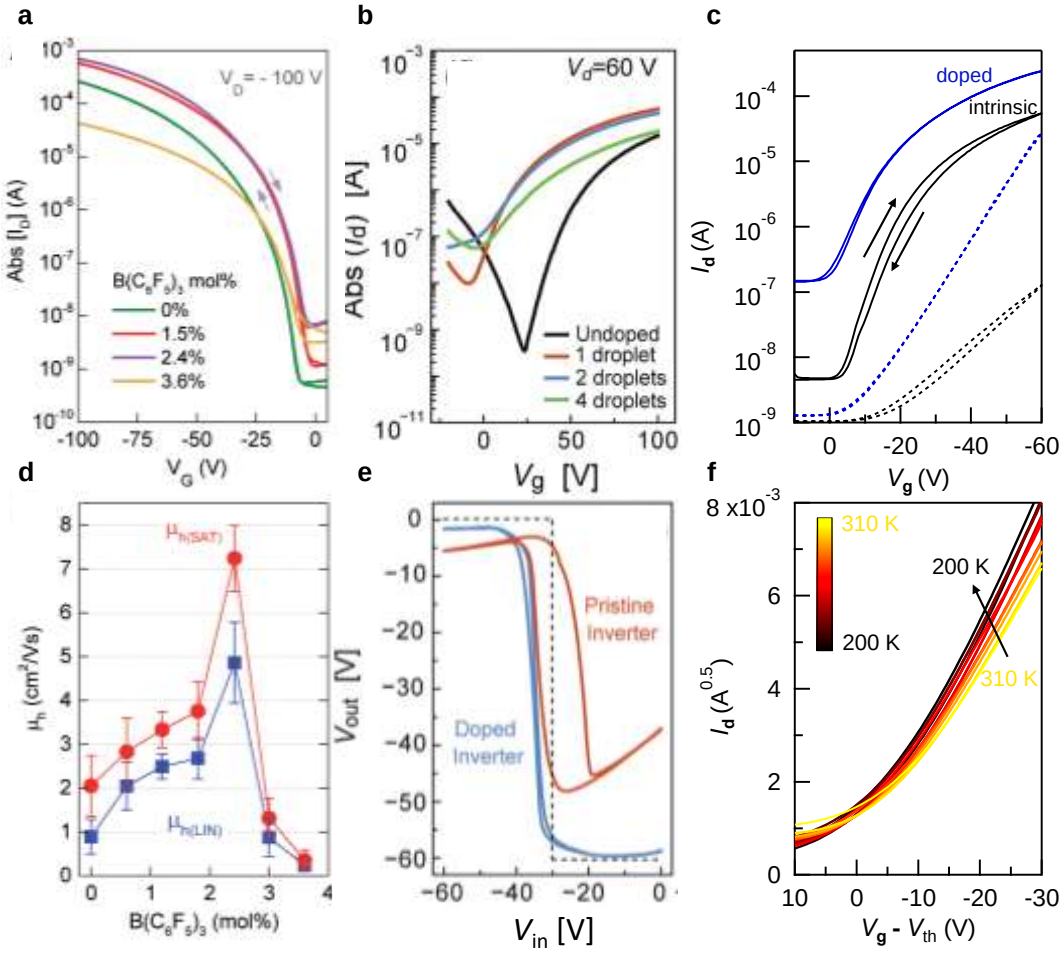

Figure 34: a) Transfer characteristics and corresponding d) field-effect mobility evolution, upon doping diF-TESADT:PTAA with BCF in the range 0–3.6 mol%. Reprinted with permission from ref [21]. Copyright 2017 Panidi et al. under Creative Commons Attribution License https://creativecommons.org/licenses/. b) PCBM OTFTs doped by CsF. The dopant solution is inkjet-printed onto the PCBM channel and the transfer characteristics are reported as a function of the jetting number. Each droplet by inkjet printing has an average diameter of ≈30 μm. e) Voltage transfer characteristics (VTCs) of inverters based on two identical PCBM OTFTs (orange solid line), inkjet-printed n- and p-doped PCBM OTFTs (blue solid line), and ideal inverter (black dashed line) at V_{dd} = –60 V. Reprinted with permission from ref [542]. Copyright 2014 Wiley-VCH GmbH. c) C_{16}IDTBT:C_8-BTBT blend doped with $C_{60}F_{48}$. OTFTs transfer characteristics of pristine (black line) and doped (blue line) and corresponding $|I_D|^{0.5}$ as a function of V_G (dashed line). V_D = −60 V. f) Temperature dependence of C_{16}IDTBT:C_8-BTBT, $C_{60}F_{48}$ doped OTFTs. The different temperatures are indicated with a color gradient shown in the inset, ranging from 310 to 200 K with a 10 K step. $|I_D|^{0.5}$ is plotted as a function of $V_G - V_T$, V_D = −60 V. Reprinted with permission from ref [537]. Copyright 2020 Wiley-VCH GmbH.

There is a class of OSC systems in which doping can dramatically affect the OTFT performance. This is the family of OSC blends comprising a semiconducting polymer and a

small molecule. In these blends, the polymer often acts both a binder, assisting the film formation, and as a charge transport medium, improving the interconnection between the high mobility small molecule crystallites that form spontaneously upon spin coting. Furthermore, the specific materials and processing conditions are selected so that the high mobility small molecule preferentially segregates on the surface of the blend layer and hence creates a high-mobility transport pathway in top-gate bottom-contact devices. One of the best examples known to date is the semiconducting blend comprised of the polymer C_{16}-IDTBT and small molecule C_8-BTBT. Record high mobilities are however only achieved upon addition of a molecular dopant, *e.g.*, $C_{60}F_{48}$,[15,468,537,546,577] ZnCF,[17] BCF.[21] These dopants have been shown to aid the charge transport across the channel due to their ability to deactivate traps present in the grain boundaries, allowing an efficient charge transfer between polymer and small molecule that if not, would lead to charge localization on the polymer, and in some cases by improving the morphology of the small-molecule phase.[537,546] Importantly, the enhancement in hole mobility was accompanied by the appearance of a band-like transport regime (Figure 34c, f).[468,537] These polymer:small-molecule:dopant systems are amongst the best performing OTFTs reported to date.

4.2.3. Contact doping in OTFTs

With the advent of high mobility OSCs, improving carrier injection, *i.e.*, reducing R_C, has become a key necessity for the development of high-performance OTFTs. Different approaches have been suggested to improve the charge injection at the metal-OSC contact, including:

(i) Selection of appropriate electrode materials to minimize the mismatch between the metal workfunction and semiconductor energy levels

(ii) Introduction of self-assembled monolayer and metal oxides at the metal-OSC interface to tune the metal workfunction and injection characteristics[578–584]

(iii) Adjustment of device topology (co-planar and staggered) to control the injection area of the electrodes[538,585–587]

(iv) Modification of the OSC microstructure to increase ordering[588]

(v) Optimization of the metal deposition to control the workfunction[589]

(vi) Employment of high capacitance dielectrics in coplanar devices[590,591]

(vii) Contact doping[363,538,592–594]

A few comprehensive reviews on the impact of contact on charge injection and its effect on OFET operation already exists,[538,592–594] and our focus here will be on reviewing the strategies that have been adopted over the years to improve the R_C through contact doping. The

fabrication of doped contacts in OTFTs was first suggested by Horowizt *et al*. who showed how a thin layer of TCNQ, evaporated between an oligomeric semiconductor (4T) and gold electrodes, in a bottom-gate top-contact configuration, was leading to enhanced charge injection.[595] Soon after other researchers explored similar approaches for different OSC systems[596–599]. As already discussed, doping helps to improve the charge injection from metal to OSC by manipulating the width of the depletion region at the metal-OSC interface (see section 2.1.6). Besides the interface energetics, doping increases the semiconductor bulk conductivity in proximity to the contacts, reducing the OSC's bulk resistance (R_{bulk}), which plays a considerable role, especially in staggered device configurations.

The advantage of contact doping, when compared to bulk/channel doping, is that the dopant is confined close to the contacts and as a consequence, the channel remains unaffected. Hence, the doping concentration can be optimized solely based on the ability to improve charge injection, often involving considerable amounts of dopant. Doped contacts can be fabricated either by vapor or solution deposition methods or through the employment of SAMs (see Section 3.1.2). The fabrication strategy depends strongly on the device architecture (Figure 35). For instance, in case of coplanar geometries, *e.g.*, bottom-gate bottom-contact (BGBC) (Figure 35a), the contacts lie in the same plane of the semiconductor/dielectric interface, hence the dopant layer is typically patterned in close proximity to the source and drain to spatially separate it from the channel. The patterning is typically achieved through evaporation via shadow mask or other patterning methods. Staggered devices, *e.g.*, bottom-gate top-contact (TGBC) (Figure 35e), are characterized by a spatial separation between contact/semiconductor and semiconductor/dielectric interface. As a consequence, patterning is not strictly necessary and a thin doping layer can be uniformly deposited onto the semiconductor prior to the contact deposition. On the other hand, bottom-contact configurations are compatible with SAM formation, while the same does not hold for top-contact geometries.

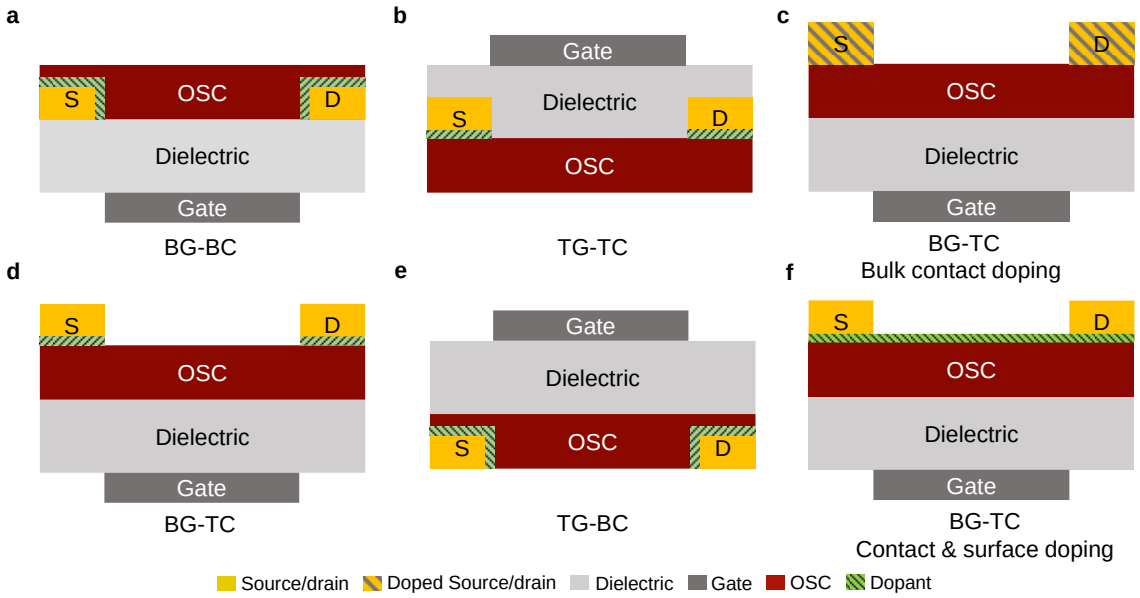

Figure 35: Schematic representation of doped contacts fabrication strategies. a, b, d, e) Conventional contact doping in different OFET device architectures, a) BG-BC, b) TG-TC, d) BG-TC, e) TG-BC. c) Bulk contact doping by mixing the dopant with the metal ink used for printing the contact, and f) simultaneous doping of contact and surface for BGTC device.

Doping can change the typical perception according to which staggered devices lead to better injection when compared to coplanar architecture, similarly to what is observed for devices with thin dielectrics.[590,591] Indeed, charge injection in coplanar devices occurs at the edge of the source contact, parallel to the channel, in a limited region dictated by the lateral area of the electrode. On the other hand, in staggered devices, the entire electrode is in contact with the semiconductor and as such larger areas of it can be involved in the carrier injection process that occurs perpendicularly to the channel. The effective area participating to the injection process depends on the relative values of R_C and R_{CH}, leading to the so-called current crowding effect. Hence, from a geometrical point of view, injection is favored in staggered devices, despite the increased R_{bulk}. However, when an optimal doping protocol is employed in coplanar devices, the energetics at the semiconductor/metal junction can lead to efficient charge injection, which together with the negligible R_{bulk} can reduce the contact resistance outperforming staggered devices.[543,585]

Many traditional p-dopants such as $FeCl_3$,[585,588,597,598,600] F_4-TCNQ,[586,601–603] F_6-TCNNQ,[405] NDP-9,[604,605] $Mo(tfd)_3$,[579,606] $C_{60}F_{36}$,[607] $C_{60}F_{48}$,[173] as well as n-dopants such as Pyronin B,[555] Rhodocene dimer,[404] lithium benzoate,[235] $W_2(hpp)_4$,[235] and bathocuproine (BCP),[608] have been used for contact engineering via vapor deposition. Solution processing

techniques are generally adopted for doping pre-patterned bottom electrodes using SAMs[255,609] and polyelectrolytes.[610] In all the cases the substantial R_C reduction is observed along with the improvement of other figures of merit such as mobility enhancement,[255,404,585,600,604,609–612] V_T control,[255,314,610,405,555,579,585,597,600,606,608] S_{SS} steepening,[604] environmental and operational stability enhancement,[173,555,605] and on/off ratio increase.[585,604,610] However, in some cases contact doping was found to decrease the on/off ratio of the device due to dopant diffusion from the contact to the bulk (unintentional channel doping).[613] The latter led to increased off current and reduced device stability. To address this issue, Kim *et al*. used argon plasma etching to treat OFETs doped with F_4-TCNQ to decrease the dopant diffusion from the contact to the bulk.[612] Further they extend their study to the incorporation of a less diffusive and electrically inert molecule as a 'dopant-blockade molecule' between the source and drain to limit the diffusion of the contact dopants into the bulk of the OSC channel (Figure 36b).[611] In the latter work, TCNQ was used as a dopant-blockade molecule, which provides a similar molecular structure as F_4-TCNQ and higher LUMO level compared to the HOMO level of OSC used (Figure 36a), hence it diminishes any possible charge transfer interaction in the bulk. The presence of TCNQ effectively suppressed the diffusion of F_4-TCNQ into the bulk, which in turn improved the overall device stability.

An unconventional doping approach was demonstrated by Tang *et al.* and Seah *et al.* for suppressing dopant migration, where they incorporated the dopants ion into a polyelectrolyte SAM modified metal surface via ion exchange.[314,614] In this case, the doping of the OSC was done by the dopant ion where the polyelectrolyte provides the counterion. This counterion, unlike conventional dopant-derived counterion, cannot diffuse into the bulk of the OSC hence suppressing dopant migration. A few other alternative doping strategies have also been explored for contact doping. For example, Schaur *et al*. used the electrochemical process for the deposition of tetrabutylammonium hexafluorophosphate ($TBAPF_6$) dopant at the gold-pentacene interface which helps to reduce the contact resistance by more than 60%.[615] Recently, Zhang *et al.* developed an interesting method where they used inject-printing of S/D electrode using F_4-TCNQ doped Ag nanoparticle ink to improve the charge injection (Figure 36b).[616]

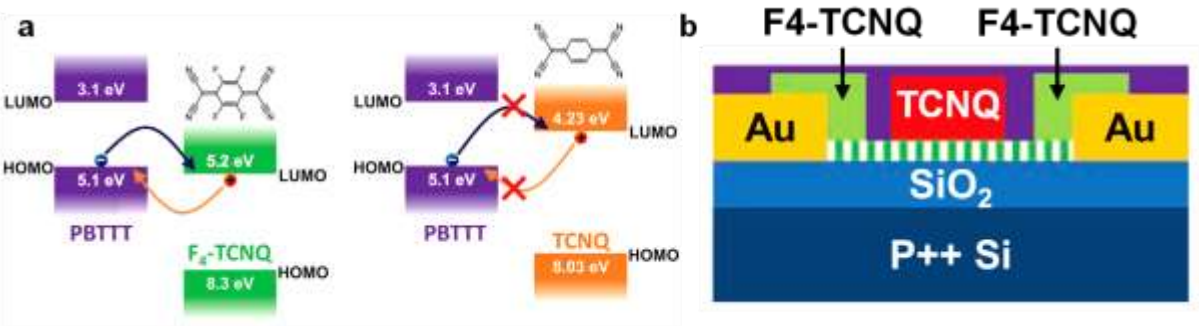

Figure 36: (a) HOMO and LUMO levels of the OSC and F_4-TCNQ and TCNQ. (b) Device architecture of the OFET fabricated using dopant blockade method. Striped region denotes the OTS SAM and purple region represents the OSC. Reprinted with permission from ref [611]. Copyright 2020 WILEY-VCH Verlag GmbH & Co. KGaA, Weinheim.

4.3. Doping in Organic Thermoelectrics

A thermoelectric generator (TEG) is a device able to convert heat directly into electricity. When a temperature gradient is applied across a thermoelectric material, charge carriers −electrons for n-type and holes for p-type (semi)conductors− diffuse from the hot side to the cold side of the material, as schematically shown in Figure 37a. This charge diffusion generates an electrical potential across the sample, a phenomenon commonly known as Seebeck effect. The Seebeck coefficient (S) of the material is defined as the generated voltage (ΔV) divided by the temperature gradient (ΔT), thus $S = -\Delta V/\Delta T$.

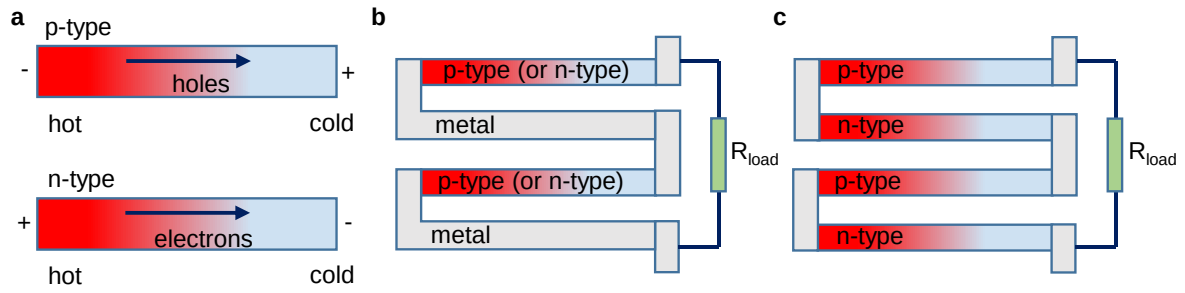

Figure 37: Schematic of (a) Seebeck effect in p- and n-type materials, (b) p-type (or n-type) leg TEG, (c) p-n leg TEG.

In general, a TEG can be constructed in two types of architectures, namely vertical and planar. The former architecture is commonly employed in inorganic semiconductors, where the temperature gradient is applied between the bottom and top sides of the materials. To do so, a semiconductor pellet with a thickness on the micrometer/millimeter scale is required to maintain the temperature gradient within the material. A handful of studies have also reported the fabrication of micrometer-thick organic semiconductor structures in a vertical

configuration.[416,617–620] However, since organic semiconductors are usually processed from solution, a planar architecture is the most commonly used, where the temperature gradient is applied laterally. As depicted in Figure 37, organic thermoelectrics (OTE) can be fabricated by connecting p-type (or n-type) materials, the so-called legs, in series with metal electrodes. These in-plane devices can then be folded to create out-of-plane architecutres.[415] To further improve the output voltage and the power generated by the TEG, both p- and n-type materials are employed in the same device, by connecting them in arrays where legs are connected electrically in series and thermally in parallel, sharing a common heat source and a common heat sink, as illustrated in Figure 37c. The total voltage generated in the TEG is proportional to the number of p-n legs and hence, the array dimension is increased in order to maximize ΔV. Besides these geometrical considerations, the efficiency of a TEG strictly depends on the thermoelectric properties of the materials employed. The latter are characterized by a dimensionless figure-of-merit, *ZT,* that is directly proportional to the electrical conductivity (σ) and Seebeck coefficient (S), and inversely proportional to the thermal conductivity (κ), and is given by

$$ZT = \frac{\sigma S^2}{\kappa} T \tag{17}$$

where T denotes the absolute temperature. ZT strongly determines the conversion efficiency (η)

$$\eta = \left(1 - \frac{T_c}{T_h}\right)\left(\frac{\sqrt{1+ZT}-1}{\sqrt{1+ZT}+\frac{T_c}{T_h}}\right) \tag{18}$$

$$T = \frac{T_c + T_h}{2} \tag{19}$$

Here, T_c and T_h are the temperatures of cold and hot sides of a thermoelectric material. Therefore, as a rule of thumb, a thermoelectric material should exhibit high electric conductivity and Seebeck coefficient, typically expressed by the power factor, $PF=\sigma S^2$ (Figure 23), while retaining a low thermal conductivity. Accordingly, organic semiconductors offer some advantages in comparison to their inorganic counterparts. Indeed, molecular interactions in organic semiconductors are governed by weak Van der Waals forces, which are responsible for their low thermal conductivity, while a relatively high electrical conductivity can be achieved, while maintaining a reasonably high Seebeck coefficient. A material fulfilling these conditions is referred to as phonon-glass electron-crystal (PGEC), since it possesses the

electronic properties of semiconductor single crystals while having thermal properties of amorphous materials. Effectively, these properties can be found in organic semiconductors under optimized conditions, rendering them promising TEG building blocks with a high ZT near room temperature (RT). Despite promising results, improving the thermoelectric power factor of OTEs still remains an open challenge. This is mainly due to a trade-off between the electrical conductivity and the Seebeck coefficient. As previously explained, an increase of the carrier density leads to an enhancement of the electrical conductivity (see Section 3.4). On the other hand, the Seebeck coefficient decreases with charge-carrier density and is given by

$$S = \frac{8\pi^2 k_B^2}{3eh^2} m^* T \left(\frac{\pi}{3p}\right)^{2/3} \quad (20)$$

where k_B, m^*, and h denote Boltzmann constant, effective mass, and Planck constant. Hence, controlling carrier density p, for instance by doping, is critical to enhance the power factor, thus the overall ZT of OTEs. Therefore, a great effort in the field of OTE has been devoted to the study of doping in organic semiconductors for the optimization of ZT, while only limited reports are available on the effect of doping on the performance of the TEG itself.

One strategy to increase the Seebeck coefficient is that of controlling the density of states (DOS) of the thermoelectric material. In a unipolar material, the Seebeck coefficient is related to the offset between the E_F and transport level (E_{trans}) as follows

$$S = \frac{k_B}{e}\left[\left(\frac{E_F - E_{trans}}{k_B T}\right) - A\right] \quad (21)$$

where A is the heat transport. In the high doping regime $E_F \approx E_{trans,}$ which results in the Mott relationship,[621,622]

$$S \approx A \approx \frac{\pi^2 k_B^2 T}{3e}\left(\frac{d(ln\sigma)}{dE}\right)_{E_F} = \frac{\pi^2 k_B^2 T}{3e}\left(\frac{1}{N}\frac{dg(E)}{dE} + \frac{1}{\mu}\frac{d\mu(E)}{dE}\right)_{E_F} \quad (22)$$

where $g(E)$, $\mu(E)$, and N are DOS, charge carrier mobility, and total number of charge carrier, respectively. Therefore, the Seebeck coefficient can be enhanced by having a sudden change in the DOS. This manipulation of DOS in thermoelectric materials can be achieved by using a

hybrid approach, for instance by blending organic semiconductors with inorganic materials.[623–625]

PEDOT:PSS is one of the most studied systems in OTE because of its easy processing and tunable electronic properties, ranging from moderate electrical conductivity (σ < 1 S cm^{-1}), due to the presence of the insulating PSS chains, to high conductivity (σ > 2000 S cm^{-1}) when particular processing methods are employed, *e.g.*, solvent treatment for PSS removal. Wang *et al*. reported a high electrical conductivity of 1995 S cm^{-1} in PEDOT:PSS films upon treatment with benzenesulfonic acid (BSA).[39] The acid treatment allows the removal of some PSS moieties in PEDOT:PSS films, as shown by X-ray photoelectron spectroscopy (XPS) measurement, where the intensity ratio of PSS/PEDOT decreases after treatment with acid. Upon BSA treatment, the carrier density increases by three orders of magnitude from 2 × 10^{18} to 2 × 10^{21} cm^{-3}, while the Hall mobility is enhanced by a factor of five. The acid-treated PEDOT:PSS films show a Seebeck coefficient of 17.5 µV K^{-1} and a power factor of 61 µW m^{-1} K^{-2}. A TEG with 16 legs of p-type acid-treated PEDOT:PSS films was fabricated, demonstrating an output voltage of 4.6 mV when applying a temperature gradient of 8 ^{o}C. In another report, Xu *et al.* studied the improvement of the thermoelectric power factor in PEDOT:PSS films by using several post-treatment protocols, including PSS removal with formamide/ -H_2SO_4 and de-doping with $NaBH_4$.[627] The formamide-H_2SO_4 treated PEDOT:PSS films show an electrical conductivity as high as 2974 S cm^{-1} with a Seebeck coefficient of 13 µV K^{-1}. To control the carrier density, PEDOT:PSS films were treated with $NaBH_4$, which results in a reduced electrical conductivity of 1786 S cm^{-1}. Despite the lower electrical conductivity, formamide-H_2SO_4-$NaBH_4$ treated PEDOT:PSS films exhibit an improvement of the Seebeck coefficient by a factor of two, leading to a power factor as high as 141 µW m^{-1} K^{-2} at RT. A 14 leg TEG constructed from formamide-H_2SO_4-$NaBH_4$ treated PEDOT:PSS films generated an output voltage of 2.9 mV and an output power density of 1 µW cm^{-2} with a temperature gradient of 18 ^{o}C.

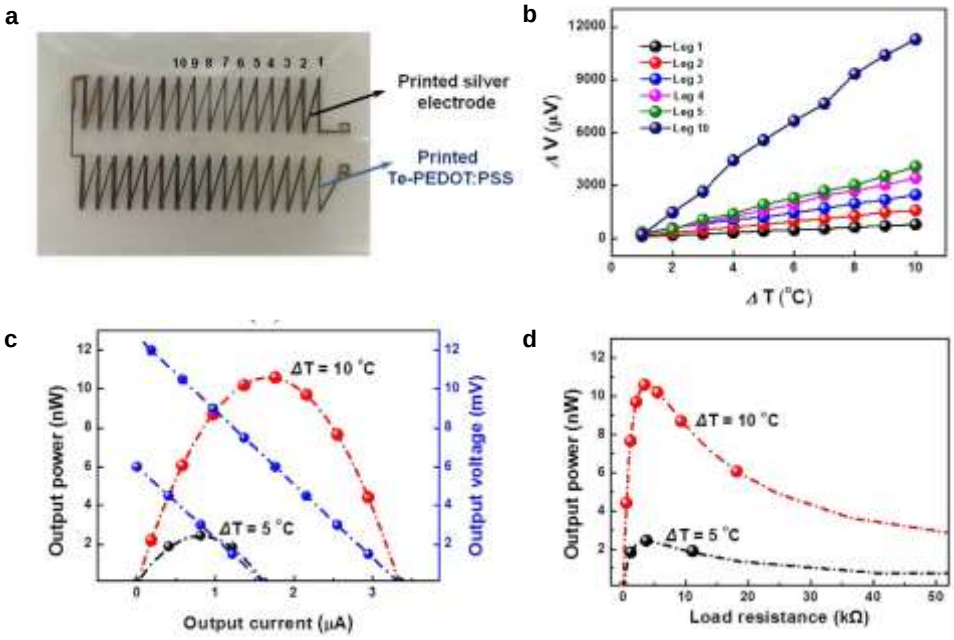

Figure 38: (a) 32 legs TEG made of printed Te-PEDOT:PSS. (b) Open circuit voltage in TEG as a function of the number of TE leg. (c) Output power and voltage at different temperature gradients. (d) Output power at different temperature gradients with respect to the load resistance. Reprinted with permission from ref [628]. Copyright 2016 Bae et al. under a Creative Commons Attribution 4.0 International License http://creativecommons.org/licenses/by/4.0/.

Acid treatment has been also reported to improve the thermoelectric properties of hybrid organic/inorganic materials. Bae *et al.* reported a study on the effect of H_2SO_4 treatment on the thermoelectric properties of PEDOT:PSS and tellurium (Te)-PEDOT:PSS films. With the aid of H_2SO_4 treatment, PEDOT:PSS films show a high electrical conductivity of 4839 S cm^{-1}, while Te-PEDOT:PSS films possess a lower electrical conductivity of 214 S cm^{-1}.[628] Despite the lower electrical conductivity, acid-treated Te-PEDOT:PSS films show a significantly higher Seebeck coefficient of 115 μV K^{-1} than that in acid-treated PEDOT:PSS films, which is attributed to the engineering of the DOS in the Te-based system. Furthermore, this enhanced Seebeck coefficient results in a thermoelectric power factor of 284 μW m^{-1} K^{-2}, leading to a high ZT value up to 0.39. Based on these excellent properties, a flexible p-type TEG with 32 TE legs was printed (Figure 38a). The TEG made of H_2SO_4-treated Te-PEDOT:PSS films demonstrates an output thermal voltage of 12.5 mV and output power of 10.6 nW by applying a temperature gradient of 10 °C.

Another extensively studied conjugated polymer for thermoelectric applications is P3HT, because of its established synthetic route, the broad knowledge about all aspects of the material and the relatively high hole mobility. Upon F_4-TCNQ doping, the electrical conductivity of P3HT films can vary from 1 to 48 S cm^{-1}, with a power factor up to 27 μW m^{-}

^{1} K^{-2}, depending on doping processing.[163,457,629] Hwang *et al*. fabricated a vertical TEG structure constructed from 48 pairs of P3HT layers, as schematically shown in Figure 39.[630] The P3HT layer was deposited by drop casting, which results in a layer thickness of 100 µm. Upon doping with F_4-TCNQ, P3HT layers exhibit a poor electrical conductivity of <1 S cm^{-1}. On the other hand, doping P3HT with Fe^{3+}-$Tos_3 \cdot 6H_2O$ was found to result in an electrical conductivity as high as 55 S cm^{-1} and a power factor of 30 µW m^{-1} K^{-2}. By controlling the concentration of the dopant, the 48-leg p-type TEG is able to generate an output voltage nearly 100 mV and a maximum power output of up to 2.5 µW at a temperature gradient of 40 °C.

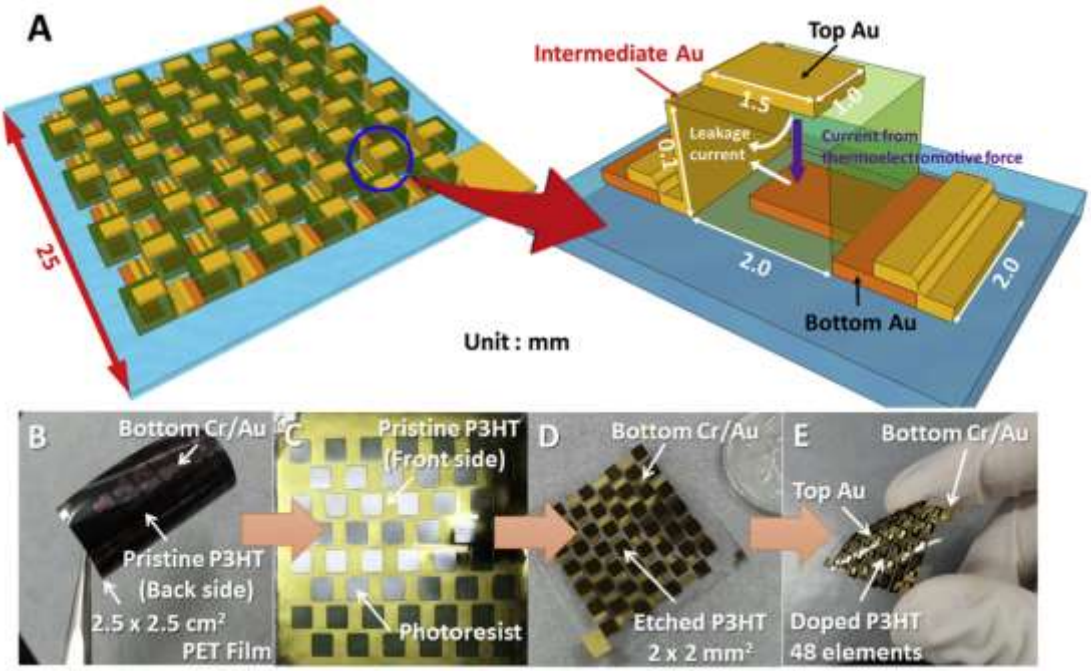

Figure 39: (a) Schematic of vertical 48-leg TEG constructed from drop-casted P3HT layer. (b-e) schematic of the fabrication process of the TEG. Reprinted with permission from ref [630]. Copyright 2016 Elsevier B.V.

Fabrication of TEGs has so far focused on p- or (n-type) only legs, while only limited reports are available on TEGs with both p- and n-type legs. In 2011, Bubnova and co-workers demonstrated the fabrication of p-n leg TEG.[619] As a p-type component, they employed PEDOT:Tos which was deposited using inkjet printing methods while the organic conducting salt tetrathiafulvalene-tetracyanoquinodimethane (TTF-TCNQ) was used as the n-type leg. To control the doping and oxidation level in the PEDOT:Tos legs, the sample was exposed to TDAE vapor. By varying the TDAE exposure time, the electrical conductivity decreased from 300 to 6 × 10^{-4} S cm^{-1}. At the same time, the Seebeck coefficient of the PEDOT:Tos dramatically increased from 40 to 780 µV K^{-1}. At an intermediate oxidation level a power factor as high as 324 µW m^{-1} K^{-2} was obtained. The thermal conductivity of PEDOT:Tos was

measured by the 3ω technique, which yielded a thermal conductivity of 0.37 W m^{-1} K^{-1} and hence a ZT value as high as 0.25 at room temperature. For the n-type leg, TTF-TCNQ was blended with polyvinylchloride (PVC), which forms a black paste with a sheet resistivity of about 11 kΩ cm^{-1} and a Seebeck coefficient of −48 μV K^{-1}. With the remarkable properties of the PEDOT:Tos, the p-n TEG demonstrates a notable power output density as high as 0.128 μW at a temperature gradient of only 10 ºC. TTF-TCNQ has also been used for the fabrication of n-type legs in combination with different p-type materials. Pudzs *et al.* reported a p-n leg TEG employing TTF-TCNQ as the n-type leg and TTF-doped with iodine vapor as the p-type leg.[631] Upon doping with iodine vapor, the electrical conductivity of the p-type TTF film increases from 1×10^{-3} to 1.3 S cm^{-1}, achieving a power factor of 0.52 μW m^{-1} K^{-2}. On the other hand, the n-type TTF-TCNQ possesses an electrical conductivity of 0.057 S cm^{-1} and Seebeck coefficient of -75 μV K^{-1}, resulting in a power factor of 0.33 μW m^{-1} K^{-2}. They further fabricated a planar p-n leg TEG that shows an output thermal voltage of 0.9 mV and a power output of 5.5 pW at a temperature gradient of 10 ºC.

Further efforts to employ n-type organic semiconductors in p-n leg TEG has been reported by Kluge *et al.*[632] In the TEG, P(NDI2OD-T2) was used as the n-type leg, while PEDOT:PSS treated with ethylene glycol was employed as the p-type leg. To improve the electrical conductivity of the n-type film, the P(NDI2OD-T2) polymer was doped with N-DPBI at different concentrations. Upon N-DPBI doping, the electrical conductivity of the n-type films increased to 0.33 S cm^{-1}. The doping also resulted in a Seebeck coefficient of -100 μV K^{-1} and a power factor of 2.4 μW m^{-1} K^{-2}. The fabricated p-n leg TEG demonstrated an output voltage of 1.1 mV and a power output of 0.24 pW at a temperature gradient of 1 ºC.

As already mentioned, progress with regard to the fabrication of TEGs has been mostly achieved using p- or n-type leg only devices, with only limited work on p-n leg TEGs. This is primarily been determined by the poor thermoelectric properties of n-doped organic semiconductors as compared to their p-type counterpart, which leads to considerable current and power losses in p-n TEGs. Hence, even though p-n leg TEG promise increased output power density, in reality, their performance lies behind those of p-type only TEGs. This major limitation has driven recent research efforts towards the improvement of the thermoelectric properties of n-doped organic semiconductors, both by investigating novel dopant and organic semiconductors. For instance, Yuan *et al*. synthesized different types of DMBI derivatives which include 2-Cyc-DMBI-H, $(2\text{-Cyc-DMBI})_2$, and $(2\text{-Cyc-DMBI-Me})_2$ (cyc: cyclohexyl).[201] By using $(2\text{-Cyc-DMBI-Me})_2$ dopant, they reported an excellent thermoelectric power factor of 33 μW m^{-1} K^{-2} in n-type 2DQTTo-OD small molecules. Liu *et al.* also reported the use of

fullerene derivatives as promising n-type organic thermoelectrics.[633] C_{60} has been studied to show a promisingly ultralow thermal conductivity of ~0.1 W m^{-1} K^{-1} because the lattice vibrations are localized within each molecule,[634] while its solution processable derivatives retain a low thermal conductivity because of a mismatch in the vibrational density of states between the buckyball and the alkyl side chain groups.[635,636] For instance, using a fullerene derivative, namely PTEG-2, Liu *et al*. reported an ultralow in-plane thermal conductivity up to 0.064 W m^{-1} K^{-1}.[633] With the aid of N-DMBI doping, the PTEG-2 films demonstrate an electrical conductivity of 12.9 S cm^{-1} and a power factor of 80 μW m^{-1} K^{-2}, while maintaining the low in-plane thermal conductivity. These remarkable values resulted in a record ZT value for n-type OTE up to 0.34 near room temperature. Despite the progress on n-type OTE, however, no reports are available so far on the use of the high-performance n-type OTE on p-n leg TEGs. Therefore, employing such n-type materials, combined with high-performance p-type materials is expected to result in highly efficient p-n leg TEGs.

4.4. Doping in other organic device technologies

Device performance tuning via molecular doping has been reported for various other technologies over the years. Nonvolatile memory devices are among them, where doping was found to improve critical device parameters like storage capacity,[637,638] on/off ratio,[639–642] memory window,[638,639,642,643] trapping density,[639–642,644] to name but a few. Doping of OFET-based memory has been reported either by adding an n-type dopant (*o*-MeO-DMBI)[637] to a p-type semiconductor or an ionic dopant (TBAP) in an ambipolar semiconductor.[638] In both cases doping occurred through CTC formation which was argued to enhance the charge storage while broadening the memory window. For n-doped p-channel devices, introduction of charge storage facilitates the bistable (ON and OFF state) switching upon the application of a gate bias. Additionally, the enhanced electron transport helped to improve the memory behavior in the semiconductor.

The electret-based OFET memories are a comparatively new class of nonvolatile memory devices.[645–649] Here doping can be implemented by incorporating the dopant molecules in the semiconductor layer[641] or in the electret layer.[639,642–644] Both approaches have shown to improve the carrier trapping density which in turn helped to enhance the storage capabilities by widening the memory window. In addition to 3-terminal OFET memories, numerous studies have also reported the development of two-terminal devices using fluorescent dye[640] and ionic conductors[650] as dopants. Moreover, molecular dopants such as F_4-TCNQ,[651,652] F_6-TCNNQ,[63,652,653] and $C_{60}F_{36}$,[63,653] have been used in unipolar and Schottky

diodes to increase the charge carrier density and device performance, while enabling new fundamental studies. Recently, Wang *et al.*[654] extended the use of a range of molecular dopants (both n- and p-type), including BV, BCF and N-DMBI, to organic photodetectors (OPDs). The ensuing devices exhibited increased photocurrents without compromising (i.e. increasing) the OPD's dark current. The environmental stability of the OPDs was also found to improve upon n-doping, exhibiting improved performance over undoped and p-doped devices.

Recently, n-type doping of organic electrochemical transistors (OECTs) was reported by Paterson and co-workers.[128] The conjugated polymer, P-90, was n-doped using TBAF in solution phase before being spin-coated. The transconductance of the ensuing OECTs was found to improve due to the synergistic effect of molecular n-doping and morphological changes. The doping in this particular materials system was attributed to the presence of F^- ions which was argued generate unpaired/delocalized electrons in the polymer backbone. The n-doping not only helped to increase the carrier mobility, conductivity, and capacitance of the device, but it also improved the electrochemical doping efficiency of the polymer. The presence of TBAF in P-90 was shown to improve the surface roughness of the polymer layer but without disturbing its molecular ordering. Importantly, optimally doped OECTs exhibited improve operational and shelf-life stability when operated under physiological relevant environment, clearly highlighting the potential of molecular doping for use in bioelectronics.

5. Conclusions and future perspectives

Doping of organic semiconductors represents an emerging technology of fundamental importance for the development of efficient and reliable organic electronics of the future. The increasing use of molecular dopants and the progress towards new materials and innovative doping techniques are the results of continuously improved understanding of the key electronic processes involved in combination with the emergence of new promising applications. Similarly, the establishment of key processing-structure-property relationships has facilitated a better control over the doping efficiency, which has in turn enabled the practical implementation of the technology in a wider range of functional devices. As highlighted in numerous recent studies, molecular doping has the potential to play the role of an enabling agent capable to further advance the functionality of OSC-based technologies owing to a multitude of synergetic effects.

In this review we attempted to capture most of these developments including experimental but also theoretical work. For instance, we used selected examples to highlight the most

prominent doping mechanisms and how they have been addressed by atomistic studies in different cases. All these examples have added valuable new information on the respective host-dopant systems either by corroborating previous suggestions or by proposing novel routes for electronic doping. Nevertheless, further studies are needed in order to establish their range of applicability and the conditions under which they are preferred over competing processes. For instance, Lewis acids (e.g. BCF) have been shown to affect the electronic and transport properties of OSCs in different ways, but at this point it is unclear which is the prevalent mechanism and what one can expect a priori for a certain host-dopant system. Similar considerations apply to other classes of dopants as well. To add to the complexity, the experimental data are often a fragmented patchwork, with extensive studies performed for some dopants (e.g. F_4-TCNQ) and extremely limited for others, making a rationale on their performance and novel designs remarkably challenging. Moreover, the specific dopant-host interactions make an absolute model system virtually impossible but highlight the importance of the design and synthesis of both new OSCs as well as tailor-made dopants for specific applications. Whilst most OSCs of today have been developed following design principles made for undoped OFET, OPV, and OLED applications, recent research shows that additional principles apply to doped materials. Important discoveries thus far include the impact of using various polymer side chains, for example the use of more polar oligoether side chains, but overall this is still a research topic in its infancy. Important questions that are yet to be answered include further mechanistic explanations to some of the effects of side-chain variations and grafting density, and the interplay between polymer backbone design and doping efficiency and susceptibility.

An aid may come from computational studies, which have so far been limited. Indeed, as computational power increases, it becomes easier to carry out not just calculations targeting individual host-dopant pairs, but a large number of concurrent investigations in so-called high-throughput calculations. This option has been recognized as a new powerful tool in modelling and in-silico synthesis of materials, including organic electronic materials with enhanced functionalities.[655] A recent atomistic study[277] has demonstrated the potential of this approach also in the identification of novel hydride n-dopants with good stability and efficiency. In particular, computational screening of a group of triaminomethane (TAM) derivatives employed first DFT to obtain key parameters, such as the reaction energy of hydride transfer, the energy of the SOMO of the resulting dopant radical and the charge (or NMR chemical shift) at the pertinent hydrogen site, as evaluation factors for doping performance. In a second stage, MD simulations probed the interactions between screened TAM dopants and polymers with

side chains, in order to fulfill the goal of high dopant miscibility and suppression of dopant clustering. The most promising TAM was then synthesized and its doping efficiency was confirmed experimentally. This synergistic effort of theory and experiment is really a representative example of what large-scale atomistic studies can achieve in the future also in the field of molecular doping of OSCs using computer-assisted screening of materials and high-throughput calculations. As our knowledge of the relevant doping mechanisms improves and the library of dopant/semiconductor materials continues to expand, it is very likely that doped OSCs will continue to provide solutions to major technological challenges for a plethora of incumbent as well as emerging applications.

One example is the burgeoning field of organic thermoelectrics where the exploration of new dopant/semiconductor pairs is likely to result in a further increase in the attainable figure of merit, in particular for n-type materials. Experimental as well as theoretical work that elucidates the impact of doping not only on charge transport, and hence the electrical conductivity, but also on the Seebeck coefficient and thermal conductivity is needed to facilitate the rational design of high-performance organic thermoelectric materials. Since thermoelectric devices expose the doped material to temperature gradients over prolonged periods of time, it will be important to develop materials with a high degree of not only ambient but also thermal stability. Here, all-polymer based conductors are particularly intriguing since they do not contain small-molecular dopants that are prone to diffusion, and in some cases sublimation. Such materials can be realized through the combination of a p- or n-type conjugated polymer with a polymeric counterion or dopant (e.g. PEDOT:PSS and its recently reported n-type equivalent BBL:PEI[260] but also bulk-heterojunctions of a p- and n-type polymer that undergo ground-state electron transfer.[656]

Furthermore, the application of doped layers has been spreading towards novel functions that seemed inconceivable until very recently, such as their use as active layers in transistors and solar cells. These complex multicomponent systems are expected to become the platform paving the way to organic devices with record high efficiency and stability, which single component systems fail to deliver. We envision the spread of the same approach in the multifaceted field of organic bioelectronics, where doping could play a major role in achieving the touted maturity required for translational biomedical applications. This process has already started, as we showed discussing the increased stability and transconductance of n-type OECTs upon addition of molecular dopants.[128] In general, organic semiconductors have been employed in a wide number of applications where they serve as bio-interfaces for electrical/optical probing and stimulating living cells and tissues.[657] Here, the employment of highly conducting

materials plays already a crucial role, as conducting polymers ─ PEDOT:PSS being the ubiquitous example─ have been pioneering the field of organic bioelectronics as coatings for metallic electrodes.[658] The facile optoelectronic and structural modulation of organic semiconductors provided by doping can offer the platform to create engineered bio-interfaces to widen both the understanding of biological processes and the development of novel clinical opportunities. In addition, organic conductors displaying enhanced and stable electrical conductivity may improve the performance of existing implant technologies.

Finally, research efforts in the field of organic electronics have been mainly focused on matters related to performance, cost and process scalability. Nevertheless, with the foreseen widespread use of organic electronic devices for a growing number of applications, the environmental impact of this technology needs to be taken under serious consideration. To do so, the synthesis and processing of each component and the end-of-life of the device need to take the direction towards a green and circular vision. Doping will not be an exception, and accordingly, there will be the need of "green dopants" that can be prepared through low-energy, benign synthetic routes and are non-toxic when they come in contact with the environment or the user in case of wearable applications or bioelectronics. Moreover, doping could represent a viable strategy to compensate the likely loss of performance associated with an environmental friendly synthesis and processing of organic semiconductors, in the same way in which, for instance, doping is showing the capability to stabilize the n-type properties of these materials.

Acknowledgements

This work was from King Abdullah University of Science and Technology (KAUST) Office of Sponsored Research (OSR) under Award No: OSR-2018-CARF/CCF-3079, and No: OSR-2019-CRG8-4095.3. F.A. acknowledges the support from The Wilkinson Charitable Foundation.

Supporting Information

Full name of the materials mentioned in this Review. Figure S1: Chemical structures of organic semiconductors discussed in this Review.

References

(1) Someya, T.; Bauer, S.; Kaltenbrunner, M. Imperceptible Organic Electronics. *MRS Bull.* **2017**, *42*, 124–130. https://doi.org/10.1557/mrs.2017.1.

(2) Malliaras, G. G. Organic Bioelectronics: A New Era for Organic Electronics. *Biochim. Biophys. Acta* **2013**, *1830*, 4286–4287. https://doi.org/10.1016/j.bbagen.2012.10.007.

(3) Chang, J. S.; Member, S.; Facchetti, A. F.; Reuss, R. A Circuits and Systems Perspective of Organic / Printed Electronics : Review , Challenges , and Contemporary and Emerging Design Approaches. **2017**, *7*, 7–26. https://doi.org/10.1109/jetcas.2017.2673863.

(4) Liao, C.; Zhang, M.; Yao, M. Y.; Hua, T.; Li, L.; Yan, F. Flexible Organic Electronics in Biology: Materials and Devices. *Adv. Mater.* **2015**, *27*, 7493–7527. https://doi.org/10.1002/adma.201402625.

(5) Forrest, S. R.; Thompson, M. E. Introduction: Organic Electronics and Optoelectronics. *Chem. Rev.* **2007**, *107*, 923–925. https://doi.org/10.1021/cr0501590.

(6) Shaw, J. M.; Seidler, P. F. Organic Electronics: Introduction. *IBM J. Res. Dev.* **2001**, *45*, 3–9. https://doi.org/10.1147/rd.451.0003.

(7) Głowacki, E. D.; Voss, G.; Sariciftci, N. S. 25th Anniversary Article: Progress in Chemistry and Applications of Functional Indigos for Organic Electronics. *Adv. Mater.* **2013**, *25*, 6783–6800. https://doi.org/10.1002/adma.201302652.

(8) He, Z.; Zhang, Z.; Bi, S. Nanoparticles for Organic Electronics Applications. *Mater. Res. Express* **2020**, *7*, 012004. https://doi.org/10.1088/2053-1591/ab636f.

(9) Geffroy, B.; le Roy, P.; Prat, C. Organic Light-Emitting Diode (OLED) Technology: Materials, Devices and Display Technologies. *Polym. Int.* **2006**, *55*, 572–582. https://doi.org/10.1002/pi.1974.

(10) Thejo Kalyani, N.; Dhoble, S. J. Organic Light Emitting Diodes: Energy Saving Lighting Technology—A Review. *Renew. Sustain. Energy Rev.* **2012**, *16*, 2696–2723. https://doi.org/10.1016/j.rser.2012.02.021.

(11) Chen, H. W.; Lee, J. H.; Lin, B. Y.; Chen, S.; Wu, S. T. Liquid Crystal Display and Organic Light-Emitting Diode Display: Present Status and Future Perspectives. *Light: Science and Applications*. **2018**, *7*, 17168. https://doi.org/10.1038/lsa.2017.168.

(12) Pfeiffer, M.; Leo, K.; Zhou, X.; Huang, J. S.; Hofmann, M.; Werner, A.; Blochwitz-Nimoth, J. Doped Organic Semiconductors: Physics and Application in Light Emitting Diodes. *Org. Electron.* **2003**, *4*, 89–103. https://doi.org/10.1016/j.orgel.2003.08.004.

(13) Walzer, K.; Männig, B.; Pfeiffer, M.; Leo, K. Highly Efficient Organic Devices Based on Electrically Doped Transport Layers. *Chemical Reviews*. **2007**, *107*, 1233–1271. https://doi.org/10.1021/cr050156n.

(14) Xu, L.; Chen, X.; Jin, J.; Liu, W.; Dong, B.; Bai, X.; Song, H.; Reiss, P. Inverted Perovskite Solar Cells Employing Doped NiO Hole Transport Layers: A Review. *Nano Energy*. **2019**, *63*, 103860. https://doi.org/10.1016/j.nanoen.2019.103860.

(15) Paterson, A. F.; Treat, N. D.; Zhang, W.; Fei, Z.; Wyatt-Moon, G.; Faber, H.; Vourlias, G.; Patsalas, P. A.; Solomeshch, O.; Tessler, N.; et al. Small Molecule/Polymer Blend Organic Transistors with Hole Mobility Exceeding 13 Cm2 V−1 S−1. *Adv. Mater.* **2016**, *28*, 7791–7798. https://doi.org/10.1002/adma.201601075.

(16) Hunter, S.; Mottram, A. D.; Anthopoulos, T. D. Temperature and Composition-Dependent Density of States in Organic Small-Molecule/Polymer Blend Transistors. *J. Appl. Phys.* **2016**, *120*. 025502, https://doi.org/10.1063/1.4955282.

(17) Paterson, A. F.; Tsetseris, L.; Li, R.; Basu, A.; Faber, H.; Emwas, A.-H.; Panidi, J.; Fei, Z.; Niazi, M. R.; Anjum, D. H.; et al. Addition of the Lewis Acid Zn(C6F5)2 Enables Organic Transistors with a Maximum Hole Mobility in Excess of 20 Cm2 V−1 S−1. *Adv. Mater.* **2019**, *31*, 1900871. https://doi.org/10.1002/adma.201900871.

(18) Smith, J.; Zhang, W.; Sougrat, R.; Zhao, K.; Li, R.; Cha, D.; Amassian, A.; Heeney, M.; McCulloch, I.; Anthopoulos, T. D. Solution-Processed Small Molecule-Polymer Blend Organic Thin-Film Transistors with Hole Mobility Greater than 5 Cm2/Vs. *Adv. Mater.* **2012**, *24*, 2441–2446. https://doi.org/10.1002/adma.201200088.

(19) Hamilton, R.; Smith, J.; Ogier, S.; Heeney, M.; Anthony, J. E.; McCulloch, I.; Veres, J.; Bradley, D. D. C.; Anthopoulos, T. D. High-Performance Polymer-Small Molecule Blend Organic Transistors. *Adv. Mater.* **2009**, *21*, 1166–1171. https://doi.org/10.1002/adma.200801725.

(20) Smith, J.; Hamilton, R.; Qi, Y.; Kahn, A.; Bradley, D. D. C.; Heeney, M.; McCulloch, I.; Anthopoulos, T. D. The Influence of Film Morphology in High-Mobility Small-Molecule:Polymer Blend Organic Transistors. *Adv. Funct. Mater.* **2010**, *20*, 2330–2337. https://doi.org/10.1002/adfm.201000427.

(21) Panidi, J.; Paterson, A. F.; Khim, D.; Fei, Z.; Han, Y.; Tsetseris, L.; Vourlias, G.; Patsalas, P. A.; Heeney, M.; Anthopoulos, T. D. Remarkable Enhancement of the Hole Mobility in Several Organic Small-Molecules, Polymers, and Small-Molecule:Polymer Blend Transistors by Simple Admixing of the Lewis Acid p-Dopant B(C6F5)3. *Adv. Sci.* **2018**, *5*, 1700290. https://doi.org/10.1002/advs.201700290.

(22) Yu, J.; Zheng, Y.; Huang, J. Towards High Performance Organic Photovoltaic Cells: A Review of Recent Development in Organic Photovoltaics. *Polymers (Basel).* **2014**, *6*, 2473–2509. https://doi.org/10.3390/polym6092473.

(23) Le, T. P.; Shang, Z.; Wang, L.; Li, N.; Vajjala Kesava, S.; O'Connor, J. W.; Chang, Y.; Bae, C.; Zhu, C.; Hexemer, A.; et al. Miscibility and Acid Strength Govern Contact Doping of Organic Photovoltaics with Strong Polyelectrolytes. *Macromolecules* **2015**, *48*, 5162–5171. https://doi.org/10.1021/acs.macromol.5b00724.

(24) Kippelen, B.; Brédas, J.-L. Organic Photovoltaics. *Energy Environ. Sci.* **2009**, *2*, 251. https://doi.org/10.1039/b812502n.

(25) Firdaus, Y.; Le Corre, V. M.; Khan, J. I.; Kan, Z.; Laquai, F.; Beaujuge, P. M.; Anthopoulos, T. D. Key Parameters Requirements for Non-Fullerene-Based Organic Solar Cells with Power Conversion Efficiency >20%. *Adv. Sci.* **2019**, *6*, 1802028. https://doi.org/10.1002/advs.201802028.

(26) Zhao, W.; Ding, J.; Zou, Y.; Di, C.; Zhu, D. Chemical Doping of Organic Semiconductors for Thermoelectric Applications. *Chem. Soc. Rev.* **2020**, *49*, 7210–7228. https://doi.org/10.1039/D0CS00204F.

(27) Kim, G. H.; Shao, L.; Zhang, K.; Pipe, K. P. Engineered Doping of Organic Semiconductors for Enhanced Thermoelectric Efficiency. *Nat. Mater.* **2013**, *12*, 719–723. https://doi.org/10.1038/nmat3635.

(28) Koopmans, T. Über Die Zuordnung von Wellenfunktionen Und Eigenwerten Zu Den Einzelnen Elektronen Eines Atoms. *Physica* **1934**, *1*, 104–113. https://doi.org/10.1016/S0031-8914(34)90011-2.

(29) Bredas, J.-L. L. Mind the Gap! *Mater. Horizons* **2014**, *1*, 17–19. https://doi.org/10.1039/c3mh00098b.

(30) Wegner, B.; Grubert, L.; Dennis, C.; Opitz, A.; Röttger, A.; Zhang, Y.; Barlow, S.; Marder, S. R.; Hecht, S.; Müllen, K.; et al. Predicting the Yield of Ion Pair Formation in Molecular Electrical Doping: Redox-Potentials: Versus Ionization Energy/Electron Affinity. *J. Mater. Chem. C* **2019**, *7*, 13839–13848. https://doi.org/10.1039/c9tc04500g.

(31) Wang, C.; Ouyang, L.; Xu, X.; Braun, S.; Liu, X.; Fahlman, M. Relationship of Ionization Potential and Oxidation Potential of Organic Semiconductor Films Used in Photovoltaics. *Sol. RRL* **2018**, *2*, 1800122. https://doi.org/10.1002/solr.201800122.

(32) Sato, N.; Seki, K.; Inokuchi, H. Polarization Energies of Organic Solids Determined by Ultraviolet Photoelectron Spectroscopy. *J. Chem. Soc. Faraday Trans. 2* **1981**, *77*, 1621. https://doi.org/10.1039/f29817701621.

(33) Okutsu, S.; Onikubo, T.; Tamano, M.; Enokida, T. Molecular Design of Hole Transport Material with Various Ionization Potential for Organic Light-Emitting Diode Applications. *IEEE Trans. Electron Devices* **1997**, *44*, 1302–1306. https://doi.org/10.1109/16.605472.

(34) Chen, W.; Huang, H.; Chen, S.; Huang, Y. L.; Gao, X. Y.; Wee, A. T. S. Molecular Orientation-Dependent Ionization Potential of Organic Thin Films. *Chem. Mater.* **2008**, *20*, 7017–7021. https://doi.org/10.1021/cm8016352.

(35) Duhm, S.; Heimel, G.; Salzmann, I.; Glowatzki, H.; Johnson, R. L.; Vollmer, A.; Rabe, J. P.; Koch, N. Orientation-Dependent Ionization Energies and Interface Dipoles in Ordered Molecular Assemblies. *Nat. Mater.* **2008**, *7*, 326–332. https://doi.org/10.1038/nmat2119.

(36) Bounds, P. J.; Munn, R. W. Polarization Energy of a Localized Charge in a Molecular Crystal.III Submolecule Treatment. *Chem. Phys.* **1981**, *59*, 47–53. https://doi.org/10.1016/0301-0104(81)80084-5.

(37) Hug, G.; Berry, R. S. Interaction of Electrons and Holes in a Molecular Crystal. *J. Chem. Phys.* **1971**, *55*, 2516–2521. https://doi.org/10.1063/1.1676441.

(38) Yoshida, H.; Yamada, K.; Tsutsumi, J.; Sato, N. Complete Description of Ionization Energy and Electron Affinity in Organic Solids: Determining Contributions from Electronic Polarization, Energy Band Dispersion, and Molecular Orientation. *Phys. Rev. B* **2015**, *92*, 075145. https://doi.org/10.1103/PhysRevB.92.075145.

(39) Heimel, G.; Salzmann, I.; Duhm, S.; Koch, N. Design of Organic Semiconductors from Molecular Electrostatics. *Chem. Mater.* **2011**, *23*, 359–377. https://doi.org/10.1021/cm1021257.

(40) Schwarze, M.; Tress, W.; Beyer, B.; Gao, F.; Scholz, R.; Poelking, C.; Ortstein, K.; Günther, A. A.; Kasemann, D.; Andrienko, D.; et al. Band Structure Engineering in Organic Semiconductors. *Science.* **2016**, *352*, 1446–1449. https://doi.org/10.1126/science.aaf0590.

(41) D'Avino, G.; Muccioli, L.; Castet, F.; Poelking, C.; Andrienko, D.; Soos, Z. G.; Cornil, J.; Beljonne, D. Electrostatic Phenomena in Organic Semiconductors: Fundamentals and Implications for Photovoltaics. *J. Phys. Condens. Matter* **2016**, *28*, 433002. https://doi.org/10.1088/0953-8984/28/43/433002.

(42) Nakayama, Y.; Kera, S.; Ueno, N. Photoelectron Spectroscopy on Single Crystals of Organic Semiconductors: Experimental Electronic Band Structure for Optoelectronic Properties. *J. Mater. Chem. C* **2020**, *8*, 9090–9132.

https://doi.org/10.1039/D0TC00891E.

(43) Ortmann, F.; Bechstedt, F.; Hannewald, K. Charge Transport in Organic Crystals: Theory and Modelling. *Phys. status solidi* **2011**, *248*, 511–525. https://doi.org/10.1002/pssb.201046278.

(44) Haneef, H. F.; Zeidell, A. M.; Jurchescu, O. D. Charge Carrier Traps in Organic Semiconductors: A Review on the Underlying Physics and Impact on Electronic Devices. *J. Mater. Chem. C* **2020**, *8*, 759–787. https://doi.org/10.1039/c9tc05695e.

(45) Arkhipov, V. I.; Heremans, P.; Emelianova, E. V.; Bässler, H. Effect of Doping on the Density-of-States Distribution and Carrier Hopping in Disordered Organic Semiconductors. *Phys. Rev. B - Condens. Matter Mater. Phys.* **2005**, *71*, 045214. https://doi.org/10.1103/PhysRevB.71.045214.

(46) Noriega, R.; Rivnay, J.; Vandewal, K.; Koch, F. P. V; Stingelin, N.; Smith, P.; Toney, M. F.; Salleo, A. A General Relationship between Disorder, Aggregation and Charge Transport in Conjugated Polymers. *Nat. Mater.* **2013**, *12*, 1038–1044. https://doi.org/10.1038/nmat3722.

(47) Tummala, N. R.; Zheng, Z.; Aziz, S. G.; Coropceanu, V.; Brédas, J. L. Static and Dynamic Energetic Disorders in the C60, PC61BM, C70, and PC71BM Fullerenes. *J. Phys. Chem. Lett.* **2015**, *6*, 3657–3662. https://doi.org/10.1021/acs.jpclett.5b01709.

(48) Salzmann, I.; Heimel, G.; Oehzelt, M.; Winkler, S.; Koch, N. Molecular Electrical Doping of Organic Semiconductors: Fundamental Mechanisms and Emerging Dopant Design Rules. *Acc. Chem. Res.* **2016**, *49*, 370–378. https://doi.org/10.1021/acs.accounts.5b00438.

(49) Lüssem, B.; Keum, C.-M. M.; Kasemann, D.; Naab, B.; Bao, Z.; Leo, K. Doped Organic Transistors. *Chem. Rev.* **2016**, *116*, 13714–13751. https://doi.org/10.1021/acs.chemrev.6b00329.

(50) Jacobs, I. E.; Moulé, A. J. Controlling Molecular Doping in Organic Semiconductors. *Adv. Mater.* **2017**, *29*, 1703063. https://doi.org/10.1002/adma.201703063.

(51) Salzmann, I.; Heimel, G. Toward a Comprehensive Understanding of Molecular Doping Organic Semiconductors (Review). *J. Electron Spectros. Relat. Phenomena* **2015**, *204*, 208–222. https://doi.org/10.1016/j.elspec.2015.05.001.

(52) Mityashin, A.; Olivier, Y.; Van Regemorter, T.; Rolin, C.; Verlaak, S.; Martinelli, N. G.; Beljonne, D.; Cornil, J.; Genoe, J.; Heremans, P. Unraveling the Mechanism of Molecular Doping in Organic Semiconductors. *Adv. Mater.* **2012**, *24*, 1535–1539. https://doi.org/10.1002/adma.201104269.

(53) Gao, W.; Kahn, A. Controlled p Doping of the Hole-Transport Molecular Material N,N′-Diphenyl-N,N′-Bis(1-Naphthyl)-1,1′-Biphenyl-4,4′-Di Amine with Tetrafluorotetracyanoquinodimethane. *J. Appl. Phys.* **2003**, *94*, 359–366. https://doi.org/10.1063/1.1577400.

(54) Pfeiffer, M.; Beyer, A.; Fritz, T.; Leo, K. Controlled Doping of Phthalocyanine Layers by Cosublimation with Acceptor Molecules: A Systematic Seebeck and Conductivity Study. *Appl. Phys. Lett.* **1998**, *73*, 3202–3204. https://doi.org/10.1063/1.122718.

(55) Glaser, T.; Beck, S.; Lunkenheimer, B.; Donhauser, D.; Köhn, A.; Kröger, M.; Pucci, A. Infrared Study of the MoO3 Doping Efficiency in 4,4′-Bis(N-Carbazolyl)-1,1′-Biphenyl (CBP). *Org. Electron.* **2013**, *14*, 575–583. https://doi.org/10.1016/j.orgel.2012.11.031.

(56) Maennig, B.; Pfeiffer, M.; Nollau, A.; Zhou, X.; Leo, K.; Simon, P. Controlled P-Type Doping of Polycrystalline and Amorphous Organic Layers: Self-Consistent Description of Conductivity and Field-Effect Mobility by a Microscopic Percolation Model. *Phys. Rev. B* **2001**, *64*, 195208. https://doi.org/10.1103/PhysRevB.64.195208.

(57) Harada, K.; Riede, M.; Leo, K.; Hild, O. R.; Elliott, C. M. Pentacene Homojunctions: Electron and Hole Transport Properties and Related Photovoltaic Responses. *Phys. Rev. B - Condens. Matter Mater. Phys.* **2008**, *77*, 195212. https://doi.org/10.1103/PhysRevB.77.195212.

(58) Ghani, F.; Opitz, A.; Pingel, P.; Heimel, G.; Salzmann, I.; Frisch, J.; Neher, D.; Tsami, A.; Scherf, U.; Koch, N. Charge Transfer in and Conductivity of Molecularly Doped Thiophene-Based Copolymers. *J. Polym. Sci. Part B Polym. Phys.* **2015**, *53*, 58–63. https://doi.org/10.1002/polb.23631.

(59) Devreese, J. T. Polarons. *Encycl. Appl. Phys.* **1996**, *14*, 383–409.

(60) Bredas, J. L.; Street, G. B. Polarons, Bipolarons, and Solitons in Conducting Polymers. *Acc. Chem. Res.* **1985**, *18*, 309–315. https://doi.org/10.1021/ar00118a005.

(61) Knupfer, M. Exciton Binding Energies in Organic Semiconductors. *Appl. Phys. A* **2003**, *77*, 623–626. https://doi.org/10.1007/s00339-003-2182-9.

(62) Hughes, M. P.; Rosenthal, K. D.; Ran, N. A.; Seifrid, M.; Bazan, G. C.; Nguyen, T.-Q. Determining the Dielectric Constants of Organic Photovoltaic Materials Using Impedance Spectroscopy. *Adv. Funct. Mater.* **2018**, *28*, 1801542. https://doi.org/10.1002/adfm.201801542.

(63) Tietze, M. L.; Benduhn, J.; Pahner, P.; Nell, B.; Schwarze, M.; Kleemann, H.; Krammer, M.; Zojer, K.; Vandewal, K.; Leo, K. Elementary Steps in Electrical Doping of Organic

Semiconductors. *Nat. Commun.* **2018**, *9*, 1–8. https://doi.org/10.1038/s41467-018-03302-z.

(64) Hood, S. N.; Kassal, I. Entropy and Disorder Enable Charge Separation in Organic Solar Cells. *J. Phys. Chem. Lett.* **2016**, *7*, 4495–4500. https://doi.org/10.1021/acs.jpclett.6b02178.

(65) Pingel, P.; Neher, D. Comprehensive Picture of P-Type Doping of P3HT with the Molecular Acceptor F4TCNQ. *Phys. Rev. B - Condens. Matter Mater. Phys.* **2013**, *87*, 115209. https://doi.org/10.1103/PhysRevB.87.115209.

(66) Méndez, H.; Heimel, G.; Winkler, S.; Frisch, J.; Opitz, A.; Sauer, K.; Wegner, B.; Oehzelt, M.; Röthel, C.; Duhm, S.; et al. Charge-Transfer Crystallites as Molecular Electrical Dopants. *Nat. Commun.* **2015**, *6*, 8560. https://doi.org/10.1038/ncomms9560.

(67) Meneghettim, M.; Pecile, C. Charge-Transfer Organic Crystals: Molecular Vibrations and Spectroscopic Effects of Electron-Molecular Vibration Coupling of the Strong Electron Acceptor TCNQF4. *J. Chem. Phys.* **1986**, *84*, 4149–4162. https://doi.org/10.1063/1.450086.

(68) Chappell, J. S.; Bryden, W. A.; Maxfield, M.; Cowan, D. O.; Bloch, A. N.; Poehler, T. O. Degree of Charge Transfer in Organic Conductors by Infrared Absorption Spectroscopy. *J. Am. Chem. Soc.* **1981**, *103*, 2442–2443. https://doi.org/10.1021/ja00399a066.

(69) Méndez, H.; Heimel, G.; Opitz, A.; Sauer, K.; Barkowski, P.; Oehzelt, M.; Soeda, J.; Okamoto, T.; Takeya, J.; Arlin, J. B.; et al. Doping of Organic Semiconductors: Impact of Dopant Strength and Electronic Coupling. *Angew. Chemie - Int. Ed.* **2013**, *52*, 7751–7755. https://doi.org/10.1002/anie.201302396.

(70) Goel, M.; Siegert, M.; Krauss, G.; Mohanraj, J.; Hochgesang, A.; Heinrich, D. C.; Fried, M.; Pflaum, J.; Thelakkat, M. HOMO–HOMO Electron Transfer: An Elegant Strategy for P-Type Doping of Polymer Semiconductors toward Thermoelectric Applications. *Adv. Mater.* **2020**, *32*, 2003596. https://doi.org/10.1002/adma.202003596.

(71) Pittelli, S. L.; Gregory, S. A.; Ponder, J. F.; Yee, S. K.; Reynolds, J. R. Inducing Planarity in Redox-Active Conjugated Polymers with Solubilizing 3,6-Dialkoxy-Thieno[3,2-b]Thiophenes (DOTTs) for Redox and Solid-State Conductivity Applications. *J. Mater. Chem. C* **2020**, *8*, 7463–7475. https://doi.org/10.1039/D0TC00914H.

(72) Hofmann, A. I.; Kroon, R.; Zokaei, S.; Järsvall, E.; Malacrida, C.; Ludwigs, S.; Biskup, T.; Müller, C. Chemical Doping of Conjugated Polymers with the Strong Oxidant Magic

Blue. *Adv. Electron. Mater.* **2020**, *6*, 2000249. https://doi.org/10.1002/aelm.202000249.

(73) Patel, S. N.; Glaudell, A. M.; Kiefer, D.; Chabinyc, M. L. Increasing the Thermoelectric Power Factor of a Semiconducting Polymer by Doping from the Vapor Phase. *ACS Macro Lett.* **2016**, *5*, 268–272. https://doi.org/10.1021/acsmacrolett.5b00887.

(74) Hofmann, A. I.; Kroon, R.; Yu, L.; Müller, C. Highly Stable Doping of a Polar Polythiophene through Co-Processing with Sulfonic Acids and Bistriflimide. *J. Mater. Chem. C* **2018**, *6*, 6905–6910. https://doi.org/10.1039/C8TC01593G.

(75) Patolsky, F.; Timko, B. P.; Yu, G.; Fang, Y.; Greytak, A. B.; Zheng, G.; Lieber, C. M. Detection, Stimulation, and Inhibition of Neuronal Signals with High-Density Nanowire Transistor Arrays. *Science.* **2006**, *313*, 1100–1104. https://doi.org/10.1126/science.1128640.

(76) Han, C. C.; Elsenbaumer, R. L. Protonic Acids: Generally Applicable Dopants for Conducting Polymers. *Synth. Met.* **1989**, *30*, 123–131. https://doi.org/10.1016/0379-6779(89)90648-6.

(77) Naab, B. D.; Guo, S.; Olthof, S.; Evans, E. G. B.; Wei, P.; Millhauser, G. L.; Kahn, A.; Barlow, S.; Marder, S. R.; Bao, Z. Mechanistic Study on the Solution-Phase n-Doping of 1,3-Dimethyl-2-Aryl-2,3-Dihydro-1H-Benzoimidazole Derivatives. *J. Am. Chem. Soc.* **2013**, *135*, 15018–15025. https://doi.org/10.1021/ja403906d.

(78) Zeng, Y.; Zheng, W.; Guo, Y.; Han, G.; Yi, Y. Doping Mechanisms of N-DMBI-H for Organic Thermoelectrics: Hydrogen Removal vs. Hydride Transfer. *J. Mater. Chem. A* **2020**, *8*, 8323–8328. https://doi.org/10.1039/D0TA01087A.

(79) Utley, J. H. P.; Gao, Y.; Gruber, J.; Zhang, Y.; Munoz-Escalona, A. An Electrochemical Route to Poly(p-Phenylenevinylene) Polymers (PPVs) and Copolymers via Cathodically Generated Quinodimethanes: Preparative and Structural Aspects. *J. Mater. Chem.* **1995**, *5*, 1837–1845. https://doi.org/10.1039/jm9950501837.

(80) Bridges, C. R.; Baumgartner, T. Lewis Acids and Bases as Molecular Dopants for Organic Semiconductors. *J. Phys. Org. Chem.* **2020**, *33*, 1–17. https://doi.org/10.1002/poc.4077.

(81) Yurash, B.; Cao, D. X.; Brus, V. V.; Leifert, D.; Wang, M.; Dixon, A.; Seifrid, M.; Mansour, A. E.; Lungwitz, D.; Liu, T.; et al. Towards Understanding the Doping Mechanism of Organic Semiconductors by Lewis Acids. *Nat. Mater.* **2019**, *18*, 1327–1334. https://doi.org/10.1038/s41563-019-0479-0.

(82) Guha, S.; Goodson, F. S.; Corson, L. J.; Saha, S. Boundaries of Anion/Naphthalenediimide Interactions: From Anion-π Interactions to Anion-Induced

Charge-Transfer and Electron-Transfer Phenomena. *J. Am. Chem. Soc.* **2012**, *134*, 13679–13691. https://doi.org/10.1021/ja303173n.

(83) Li, C.-Z. Z.; Chueh, C.-C. C.; Ding, F.; Yip, H.-L. L.; Liang, P.-W. W.; Li, X.; Jen, A. K.-Y. K. Y. Doping of Fullerenes via Anion-Induced Electron Transfer and Its Implication for Surfactant Facilitated High Performance Polymer Solar Cells. *Adv. Mater.* **2013**, *25*, 4425–4430. https://doi.org/10.1002/adma.201300580.

(84) Weber, C. D.; Bradley, C.; Lonergan, M. C. Solution Phase N-Doping of C60 and PCBM Using Tetrabutylammonium Fluoride. *J. Mater. Chem. A* **2014**, *2*, 303–307. https://doi.org/10.1039/C3TA14132B.

(85) Li, J.; Duchemin, I.; Roscioni, O. M.; Friederich, P.; Anderson, M.; Da Como, E.; Kociok-Köhn, G.; Wenzel, W.; Zannoni, C.; Beljonne, D.; et al. Host Dependence of the Electron Affinity of Molecular Dopants. *Mater. Horizons* **2019**, *6*, 107–114. https://doi.org/10.1039/C8MH00921J.

(86) Warren, R.; Privitera, A.; Kaienburg, P.; Lauritzen, A. E.; Thimm, O.; Nelson, J.; Riede, M. K. Controlling Energy Levels and Fermi Level En Route to Fully Tailored Energetics in Organic Semiconductors. *Nat. Commun.* **2019**, *10*, 5538. https://doi.org/10.1038/s41467-019-13563-x.

(87) Hubbard, J. Electron Correlations in Narrow Energy Bands. *Proc. R. Soc. London, Ser. A* **1963**, *276*, 238–257. https://doi.org/10.1098/rspa.1963.0204.

(88) Schwedhelm, R.; Kipp, L.; Dallmeyer, A.; Skibowski, M. Experimental Band Gap and Core-Hole Electron Interaction in Epitaxial Films. *Phys. Rev. B* **1998**, *58*, 13176–13180. https://doi.org/10.1103/PhysRevB.58.13176.

(89) Winkler, S.; Amsalem, P.; Frisch, J.; Oehzelt, M.; Heimel, G.; Koch, N. Probing the Energy Levels in Hole-Doped Molecular Semiconductors. *Mater. Horizons* **2015**, *2*, 427–433. https://doi.org/10.1039/c5mh00023h.

(90) Marcus, R. A. Electron Transfer Reactions in Chemistry. Theory and Experiment. *Rev. Mod. Phys.* **1993**, *65*, 599–610. https://doi.org/10.1103/RevModPhys.65.599.

(91) Lüssem, B.; Tietze, M. L.; Kleemann, H.; Hoßbach, C.; Bartha, J. W.; Zakhidov, A.; Leo, K. Doped Organic Transistors Operating in the Inversion and Depletion Regime. *Nat. Commun.* **2013**, *4*, 2775. https://doi.org/10.1038/ncomms3775.

(92) Tietze, M. L.; Pahner, P.; Schmidt, K.; Leo, K.; Lüssem, B. Doped Organic Semiconductors: Trap-Filling, Impurity Saturation, and Reserve Regimes. *Adv. Funct. Mater.* **2015**, *25*, 2701–2707. https://doi.org/10.1002/adfm.201404549.

(93) Neelamraju, B.; Watts, K. E.; Pemberton, J. E.; Ratcliff, E. L. Correlation of Coexistent

Charge Transfer States in F 4 TCNQ-Doped P3HT with Microstructure. *J. Phys. Chem. Lett.* **2018**, *9*, 6871–6877. https://doi.org/10.1021/acs.jpclett.8b03104.

(94) Jacobs, I. E.; Cendra, C.; Harrelson, T. F.; Bedolla Valdez, Z. I.; Faller, R.; Salleo, A.; Moulé, A. J. Polymorphism Controls the Degree of Charge Transfer in a Molecularly Doped Semiconducting Polymer. *Mater. Horizons* **2018**, *5*, 655–660. https://doi.org/10.1039/c8mh00223a.

(95) Zapata-Arteaga, O.; Dörling, B.; Perevedentsev, A.; Martín, J.; Reparaz, J. S.; Campoy-Quiles, M. Closing the Stability-Performance Gap in Organic Thermoelectrics by Adjusting the Partial to Integer Charge Transfer Ratio. *Macromolecules* **2020**, *53*, 609–620. https://doi.org/10.1021/acs.macromol.9b02263.

(96) Kiefer, D.; Kroon, R.; Hofmann, A. I.; Sun, H.; Liu, X.; Giovannitti, A.; Stegerer, D.; Cano, A.; Hynynen, J.; Yu, L.; et al. Double Doping of Conjugated Polymers with Monomer Molecular Dopants. *Nat. Mater.* **2019**, *18*, 149–155. https://doi.org/10.1038/s41563-018-0263-6.

(97) Liu, J.; Qiu, L.; Alessandri, R.; Qiu, X.; Portale, G.; Dong, J.; Talsma, W.; Ye, G.; Sengrian, A. A.; Souza, P. C. T.; et al. Enhancing Molecular N-Type Doping of Donor-Acceptor Copolymers by Tailoring Side Chains. *Adv. Mater.* **2018**, *30*, 1704630. https://doi.org/10.1002/adma.201704630.

(98) Ghosh, R.; Chew, A. R.; Onorato, J.; Pakhnyuk, V.; Luscombe, C. K.; Salleo, A.; Spano, F. C. Spectral Signatures and Spatial Coherence of Bound and Unbound Polarons in P3HT Films: Theory Versus Experiment. *J. Phys. Chem. C* **2018**, *122*, 18048–18060. https://doi.org/10.1021/acs.jpcc.8b03873.

(99) Liang, Z.; Zhang, Y. Y.; Souri, M.; Luo, X.; Boehm, A. M.; Li, R.; Zhang, Y. Y.; Wang, T.; Kim, D. Y.; Mei, J.; et al. Influence of Dopant Size and Electron Affinity on the Electrical Conductivity and Thermoelectric Properties of a Series of Conjugated Polymers. *J. Mater. Chem. A* **2018**, *6*, 16495–16505. https://doi.org/10.1039/c8ta05922e.

(100) Untilova, V.; Hynynen, J.; Hofmann, A. I.; Scheunemann, D.; Zhang, Y.; Barlow, S.; Kemerink, M.; Marder, S. R.; Biniek, L.; Müller, C.; et al. High Thermoelectric Power Factor of Poly(3-Hexylthiophene) through In-Plane Alignment and Doping with a Molybdenum Dithiolene Complex. *Macromolecules* **2020**, *53*, 6314–6321. https://doi.org/10.1021/acs.macromol.0c01223.

(101) Aubry, T. J.; Axtell, J. C.; Basile, V. M.; Winchell, K. J.; Lindemuth, J. R.; Porter, T. M.; Liu, J. Y.; Alexandrova, A. N.; Kubiak, C. P.; Tolbert, S. H.; et al. Dodecaborane-

Based Dopants Designed to Shield Anion Electrostatics Lead to Increased Carrier Mobility in a Doped Conjugated Polymer. *Adv. Mater.* **2019**, *31*, 1–8. https://doi.org/10.1002/adma.201805647.

(102) Pingel, P.; Zhu, L.; Park, K. S.; Vogel, J. O.; Janietz, S.; Kim, E. G.; Rabe, J. P.; Brédas, J. L.; Koch, N. Charge-Transfer Localization in Molecularly Doped Thiophene-Based Donor Polymers. *J. Phys. Chem. Lett.* **2010**, *1*, 2037–2041. https://doi.org/10.1021/jz100492c.

(103) Karl, N.; Kraft, K.-H.; Marktanner, J.; Münch, M.; Schatz, F.; Stehle, R.; Uhde, H.-M. Fast Electronic Transport in Organic Molecular Solids? *J. Vac. Sci. Technol. A Vacuum, Surfaces, Film.* **1999**, *17*, 2318–2328. https://doi.org/10.1116/1.581767.

(104) Karl, N. Charge Carrier Transport in Organic Semiconductors. *Synthetic Metals* **2003**, 133–134, 649–657. https://doi.org/10.1016/S0379-6779(02)00398-3.

(105) Lluch, J. M. Perspective on "on the Theory of Oxidation-Reduction Reactions Involving Electron Transfer. I." *Theor. Chem. Accounts Theory, Comput. Model. (Theoretica Chim. Acta)* **2000**, *103*, 231–233. https://doi.org/10.1007/s002149900016.

(106) Gelinck, G.; Heremans, P.; Nomoto, K.; Anthopoulos, T. D. Organic Transistors in Optical Displays and Microelectronic Applications. *Adv. Mater.* **2010**, *22*, 3778–3798. https://doi.org/10.1002/adma.200903559.

(107) Olthof, S.; Mehraeen, S.; Mohapatra, S. K.; Barlow, S.; Coropceanu, V.; Brédas, J. L.; Marder, S. R.; Kahn, A. Ultralow Doping in Organic Semiconductors: Evidence of Trap Filling. *Phys. Rev. Lett.* **2012**, *109*, 1–5. https://doi.org/10.1103/PhysRevLett.109.176601.

(108) Koopmans, M.; Leiviskä, M. A. T.; Liu, J.; Dong, J.; Qiu, L.; Hummelen, J. C.; Portale, G.; Heiber, M. C.; Koster, L. J. A. Electrical Conductivity of Doped Organic Semiconductors Limited by Carrier–Carrier Interactions. *ACS Appl. Mater. Interfaces* **2020**, *12*, 56222–56230. https://doi.org/10.1021/acsami.0c15490.

(109) Wegner, B.; Lungwitz, D.; Mansour, A. E.; Tait, C. E.; Tanaka, N.; Zhai, T.; Duhm, S.; Forster, M.; Behrends, J.; Shoji, Y.; et al. An Organic Borate Salt with Superior P-doping Capability for Organic Semiconductors. *Adv. Sci.* **2020**, 2001322. https://doi.org/10.1002/advs.202001322.

(110) Futscher, M. H.; Schultz, T.; Frisch, J.; Ralaiarisoa, M.; Metwalli, E.; Nardi, M. V; Müller-Buschbaum, P.; Koch, N. Electronic Properties of Hybrid Organic/Inorganic Semiconductor Pn-Junctions. *J. Phys. Condens. Matter* **2019**, *31*, 064002. https://doi.org/10.1088/1361-648X/aaf310.

(111) Ishii, H.; Hayashi, N.; Ito, E.; Washizu, Y.; Sugi, K.; Kimura, Y.; Niwano, M.; Ouchi, Y.; Seki, K. Kelvin Probe Study of Band Bending at Organic Semiconductor/Metal Interfaces: Examination of Fermi Level Alignment. *Phys. status solidi* **2004**, *201*, 1075–1094. https://doi.org/10.1002/pssa.200404346.

(112) Futscher, M. H.; Schultz, T.; Frisch, J.; Ralaiarisoa, M.; Metwalli, E.; Nardi, M. V; Müller-Buschbaum, P.; Koch, N. Electronic Properties of Hybrid Organic/Inorganic Semiconductor Pn-Junctions. *J. Phys. Condens. Matter* **2019**, *31*, 064002. https://doi.org/10.1088/1361-648X/aaf310.

(113) Bussolotti, F.; Kera, S.; Kudo, K.; Kahn, A.; Ueno, N. Gap States in Pentacene Thin Film Induced by Inert Gas Exposure. *Phys. Rev. Lett.* **2013**, *110*, 267602. https://doi.org/10.1103/PhysRevLett.110.267602.

(114) Lüssem, B.; Riede, M.; Leo, K. Doping of Organic Semiconductors. *Phys. status solidi* **2013**, *210*, 9–43. https://doi.org/10.1002/pssa.201228310.

(115) Zhang, G.; Musgrave, C. B. Comparison of DFT Methods for Molecular Orbital Eigenvalue Calculations. *J. Phys. Chem. A* **2007**, *111*, 1554–1561. https://doi.org/10.1021/jp061633o.

(116) Becke, A. D. Density-Functional Thermochemistry. III. The Role of Exact Exchange. *J. Chem. Phys.* **1993**, *98*, 5648–5652. https://doi.org/10.1063/1.464913.

(117) Stephens, P. J.; Devlin, F. J.; Chabalowski, C. F.; Frisch, M. J. Ab Initio Calculation of Vibrational Absorption and Circular Dichroism Spectra Using Density Functional Force Fields. *J. Phys. Chem.* **1994**, *98*, 11623–11627. https://doi.org/10.1021/j100096a001.

(118) Lin, Y.; Firdaus, Y.; Nugraha, M. I.; Liu, F.; Karuthedath, S.; Emwas, A.-H.; Zhang, W.; Seitkhan, A.; Neophytou, M.; Faber, H.; et al. 17.1% Efficient Single-Junction Organic Solar Cells Enabled by n-Type Doping of the Bulk-Heterojunction. *Adv. Sci.* **2020**, *7*, 1903419. https://doi.org/10.1002/advs.201903419.

(119) Li, J.; D'Avino, G.; Pershin, A.; Jacquemin, D.; Duchemin, I.; Beljonne, D.; Blase, X. Correlated Electron-Hole Mechanism for Molecular Doping in Organic Semiconductors. *Phys. Rev. Mater.* **2017**, *1*, 25602. https://doi.org/10.1103/PhysRevMaterials.1.025602.

(120) Salzmann, I.; Heimel, G.; Duhm, S.; Oehzelt, M.; Pingel, P.; George, B. M.; Schnegg, A.; Lips, K.; Blum, R. P.; Vollmer, A.; et al. Intermolecular Hybridization Governs Molecular Electrical Doping. *Phys. Rev. Lett.* **2012**, *108*, 1–5. https://doi.org/10.1103/PhysRevLett.108.035502.

(121) Karpov, Y.; Erdmann, T.; Stamm, M.; Lappan, U.; Guskova, O.; Malanin, M.; Raguzin,

I.; Beryozkina, T.; Bakulev, V.; Günther, F.; et al. Molecular Doping of a High Mobility Diketopyrrolopyrrole-Dithienylthieno[3,2-b]Thiophene Donor-Acceptor Copolymer with F6TCNNQ. *Macromolecules* **2017**, *50*, 914–926. https://doi.org/10.1021/acs.macromol.6b02452.

(122) Di Nuzzo, D.; Fontanesi, C.; Jones, R.; Allard, S.; Dumsch, I.; Scherf, U.; Von Hauff, E.; Schumacher, S.; Da Como, E. How Intermolecular Geometrical Disorder Affects the Molecular Doping of Donor-Acceptor Copolymers. *Nat. Commun.* **2015**, *6*, 1–8. https://doi.org/10.1038/ncomms7460.

(123) Privitera, A.; Warren, R.; Londi, G.; Kaienburg, P.; Liu, J.; Sperlich, A.; Lauritzen, A. E.; Thimm, O.; Ardavan, A.; Beljonne, D.; et al. Electron Spin as Fingerprint for Charge Generation and Transport in Doped Organic Semiconductors. *J. Mater. Chem. C* **2021**, *9*, 2944–2954. https://doi.org/10.1039/d0tc06097f.

(124) Ryno, S. M.; Ravva, M. K.; Chen, X.; Li, H.; Brédas, J. L. Molecular Understanding of Fullerene – Electron Donor Interactions in Organic Solar Cells. *Advanced Energy Materials*. **2017**, *7*, 1601370. https://doi.org/10.1002/aenm.201601370.

(125) Paterson, A. F.; Li, R.; Markina, A.; Tsetseris, L.; MacPhee, S.; Faber, H.; Emwas, A.-H.; Panidi, J.; Bristow, H.; Wadsworth, A.; et al. N-Doping Improves Charge Transport and Morphology in the Organic Non-Fullerene Acceptor O-IDTBR. *J. Mater. Chem. C* **2021**, *9*, 4486–4495. https://doi.org/10.1039/D0TC05861K.

(126) Denti, I.; Cimò, S.; Brambilla, L.; Milani, A.; Bertarelli, C.; Tommasini, M.; Castiglioni, C. Polaron Confinement in N-Doped P(NDI2OD-T2) Unveiled by Vibrational Spectroscopy. *Chem. Mater.* **2019**, *31*, 6726–6739. https://doi.org/10.1021/acs.chemmater.9b01218.

(127) Zhao, X.; Madan, D.; Cheng, Y.; Zhou, J.; Li, H.; Thon, S. M.; Bragg, A. E.; DeCoster, M. E.; Hopkins, P. E.; Katz, H. E. High Conductivity and Electron-Transfer Validation in an n-Type Fluoride-Anion-Doped Polymer for Thermoelectrics in Air. *Adv. Mater.* **2017**, *29*, 1–7. https://doi.org/10.1002/adma.201606928.

(128) Paterson, A. F.; Savva, A.; Wustoni, S.; Tsetseris, L.; Paulsen, B. D.; Faber, H.; Emwas, A. H.; Chen, X.; Nikiforidis, G.; Hidalgo, T. C.; et al. Water Stable Molecular N-Doping Produces Organic Electrochemical Transistors with High Transconductance and Record Stability. *Nat. Commun.* **2020**, *11*, 3004. https://doi.org/10.1038/s41467-020-16648-0.

(129) Yan, H.; Chen, J.; Zhou, K.; Tang, Y.; Meng, X.; Xu, X.; Ma, W. Lewis Acid Doping Induced Synergistic Effects on Electronic and Morphological Structure for Donor and Acceptor in Polymer Solar Cells. *Adv. Energy Mater.* **2018**, *8*, 1–7.

https://doi.org/10.1002/aenm.201703672.

(130) Yurash, B.; Leifert, D.; Reddy, G. N. M.; Cao, D. X.; Biberger, S.; Brus, V. V; Seifrid, M.; Santiago, P. J.; Köhler, A.; Chmelka, B. F.; et al. Atomic-Level Insight into the Postsynthesis Band Gap Engineering of a Lewis Base Polymer Using Lewis Acid Tris(Pentafluorophenyl)Borane. *Chem. Mater.* **2019**, *31*, 6715–6725. https://doi.org/10.1021/acs.chemmater.9b01224.

(131) Quinn, J. T. E. E.; Zhu, J.; Li, X.; Wang, J.; Li, Y. Recent Progress in the Development of N-Type Organic Semiconductors for Organic Field Effect Transistors. *J. Mater. Chem. C* **2017**, *5*, 8654–8681. https://doi.org/10.1039/C7TC01680H.

(132) Chiang, C. K.; Fincher, C. R.; Park, Y. W.; Heeger, A. J.; Shirakawa, H.; Louis, E. J.; Gau, S. C.; Macdiarmid, A. G.; Chiang, C. K.; Fincher, C. R.; et al. Electrical Conductivity in Doped Polyacetylene. *Phys. Rev. Lett.* **1977**, *39*, 1098–1101. https://doi.org/10.1103/PhysRevLett.39.1098.

(133) Minakata, T.; Nagoya, I.; Ozaki, M. Highly Ordered and Conducting Thin Film of Pentacene Doped with Iodine Vapor. *J. Appl. Phys.* **1991**, *69*, 7354–7356. https://doi.org/10.1063/1.347594.

(134) Coppo, P.; Schroeder, R.; Grell, M.; Turner, M. L. Investigation of Solution Processed Poly(4,4-Dioctylcyclopentadithiophene) Thin Films as Transparent Conductors. *Synth. Met.* **2004**, *143*, 203–206. https://doi.org/10.1016/j.synthmet.2003.12.001.

(135) Jakabovič, J.; Vincze, A.; Kováč, J.; Srnánek, R.; Kováč Jr, J.; Dobročka, E.; Donoval, D.; Heinemeyer, U.; Schreiber, F.; Machovič, V.; et al. Surface and Interface Analysis of Iodine-Doped Pentacene Structures for OTFTs. *Surf. Interface Anal.* **2011**, *43*, 518–521. https://doi.org/10.1002/sia.3420.

(136) Matsuo, Y.; Sasaki, A.; Yoshida, Y.; Ikehata, S. New Stage Structure of Iodine Doped Pentacene Film (II). *Mol. Cryst. Liq. Cryst. Sci. Technol. Sect. A. Mol. Cryst. Liq. Cryst.* **2000**, *340*, 223–228. https://doi.org/10.1080/10587250008025470.

(137) Meijer, E. J.; Detcheverry, C.; Baesjou, P. J.; Van Veenendaal, E.; De Leeuw, D. M.; Klapwijk, T. M. Dopant Density Determination in Disordered Organic Field-Effect Transistors. *J. Appl. Phys.* **2003**, *93*, 4831–4835. https://doi.org/10.1063/1.1559933.

(138) Schafferhans, J.; Baumann, A.; Wagenpfahl, A.; Deibel, C.; Dyakonov, V. Oxygen Doping of P3HT:PCBM Blends: Influence on Trap States, Charge Carrier Mobility and Solar Cell Performance. *Org. Electron.* **2010**, *11*, 1693–1700. https://doi.org/10.1016/j.orgel.2010.07.016.

(139) Sperlich, A.; Kraus, H.; Deibel, C.; Blok, H.; Schmidt, J.; Dyakonov, V. Reversible and

Irreversible Interactions of Poly(3-Hexylthiophene) with Oxygen Studied by Spin-Sensitive Methods. *J. Phys. Chem. B* **2011**, *115*, 13513–13518. https://doi.org/10.1021/jp2077215.

(140) Lu, C.-K.; Meng, H.-F. Hole Doping by Molecular Oxygen in Organic Semiconductors: Band-Structure Calculations. *Phys. Rev. B* **2007**, *75*, 235206. https://doi.org/10.1103/PhysRevB.75.235206.

(141) Liao, H. H.; Yang, C. M.; Liu, C. C.; Horng, S. F.; Meng, H. F.; Shy, J. T. Dynamics and Reversibility of Oxygen Doping and De-Doping for Conjugated Polymer. *J. Appl. Phys.* **2008**, *103*. https://doi.org/10.1063/1.2917419.

(142) Di Pietro, R.; Sirringhaus, H. High Resolution Optical Spectroscopy of Air-Induced Electrical Instabilities in n-Type Polymer Semiconductors. *Adv. Mater.* **2012**, *24*, 3367–3372. https://doi.org/10.1002/adma.201200829.

(143) Di Pietro, R.; Fazzi, D.; Kehoe, T. B.; Sirringhaus, H. Spectroscopic Investigation of Oxygen- and Water-Induced Electron Trapping and Charge Transport Instabilities in n-Type Polymer Semiconductors. *J. Am. Chem. Soc.* **2012**, *134*, 14877–14889. https://doi.org/10.1021/ja304198e.

(144) Meyer, J.; Hamwi, S.; Kröger, M.; Kowalsky, W.; Riedl, T.; Kahn, A. Transition Metal Oxides for Organic Electronics: Energetics, Device Physics and Applications. *Adv. Mater.* **2012**, *24*, 5408–5427. https://doi.org/10.1002/adma.201201630.

(145) Meyer, J.; Hamwi, S.; Schmale, S.; Winkler, T.; Johannes, H.-H.; Riedl, T.; Kowalsky, W. A Strategy towards P-Type Doping of Organic Materials with HOMO Levels beyond 6 EV Using Tungsten Oxide. *J. Mater. Chem.* **2009**, *19*, 702–705. https://doi.org/10.1039/B819485H.

(146) Sakanoue, T.; Sirringhaus, H. Band-like Temperature Dependence of Mobility in a Solution-Processed Organic Semiconductor. *Nat. Mater.* **2010**, *9*, 736–740. https://doi.org/10.1038/nmat2825.

(147) Ivory, D. M.; Miller, G. G.; Sowa, J. M.; Shacklette, L. W.; Chance, R. R.; Baughman, R. H. Highly Conducting Charge-transfer Complexes of Poly(p -phenylene). *J. Chem. Phys.* **1979**, *71*, 1506–1507. https://doi.org/10.1063/1.438420.

(148) Earmme, T.; Jenekhe, S. A. Solution-Processed, Alkali Metal-Salt-Doped, Electron-Transport Layers for High-Performance Phosphorescent Organic Light-Emitting Diodes. *Adv. Funct. Mater.* **2012**, *22*, 5126–5136. https://doi.org/10.1002/adfm.201201366.

(149) Mort, J.; Grammatica, S.; Sandman, D. J.; Troup, A. Chemical Control of Conductivity

in a Molecularly-Doped Polymer. *J. Electron. Mater.* **1980**, *9*, 411–418. https://doi.org/10.1007/BF02670857.

(150) Jenekhe, S. A.; Wellinghoff, S. T.; Deng, Z. Electrically Conducting Complexes of Poly(3,6-N-Methylcarbazolyl Methylene. *Synth. Met.* **1985**, *10*, 281–292. https://doi.org/10.1016/0379-6779(85)90034-7.

(151) Yoon, S. E.; Park, J.; Kwon, J. E.; Lee, S. Y.; Han, J. M.; Go, C. Y.; Choi, S.; Kim, K. C.; Seo, H.; Kim, J. H.; et al. Improvement of Electrical Conductivity in Conjugated Polymers through Cascade Doping with Small-Molecular Dopants. *Adv. Mater.* **2020**, *32*, 2005129. https://doi.org/10.1002/adma.202005129.

(152) Fan, B.; de Castro, F. A.; Heier, J.; Hany, R.; Nüesch, F. High Performing Doped Cyanine Bilayer Solar Cell. *Org. Electron.* **2010**, *11*, 583–588. https://doi.org/10.1016/j.orgel.2009.12.017.

(153) Li, H.; DeCoster, M. E.; Ireland, R. M.; Song, J.; Hopkins, P. E.; Katz, H. E. Modification of the Poly(Bisdodecylquaterthiophene) Structure for High and Predominantly Nonionic Conductivity with Matched Dopants. *J. Am. Chem. Soc.* **2017**, *139*, 11149–11157. https://doi.org/10.1021/jacs.7b05300.

(154) Kido, J.; Matsumoto, T. Bright Organic Electroluminescent Devices Having a Metal-Doped Electron-Injecting Layer. *Appl. Phys. Lett.* **1998**, *73*, 2866–2868. https://doi.org/10.1063/1.122612.

(155) Ali Benamara, A.; Galtier, M.; Montaner, A. N Doping of Polyacetylene. *Synth. Met.* **1991**, *41*, 45–48. https://doi.org/10.1016/0379-6779(91)90993-F.

(156) Parthasarathy, G.; Shen, C.; Kahn, A.; Forrest, S. R. Lithium Doping of Semiconducting Organic Charge Transport Materials. *J. Appl. Phys.* **2001**, *89*, 4986–4992. https://doi.org/10.1063/1.1359161.

(157) Yook, K. S.; Jeon, S. O.; Joo, C. W.; Lee, J. Y.; Lee, T.-W.; Noh, T.; Yang, H.-J.; Kang, S.-K. Air Stable and Low Temperature Evaporable Li3N as a n Type Dopant in Organic Light-Emitting Diodes. *Synth. Met.* **2009**, *159*, 1664–1666. https://doi.org/10.1016/j.synthmet.2009.05.006.

(158) Cai, Y.; Wei, H. X.; Li, J.; Bao, Q. Y.; Zhao, X.; Lee, S. T.; Li, Y. Q.; Tang, J. X. Mechanism of Cs2CO3 as an N-Type Dopant in Organic Electron-Transport Film. *Appl. Phys. Lett.* **2011**, *98*, 113304. https://doi.org/10.1063/1.3567526.

(159) Lee, J.; Lee, H.; Jeon, P.; Jeong, K.; Gun Kim, T.; Won Kim, J.; Yi, Y. Direct Evidence of N-Type Doping in Organic Light-Emitting Devices: N Free Cs Doping from CsN3. *Appl. Phys. Lett.* **2012**, *100*, 203301. https://doi.org/10.1063/1.4718017.

(160) Kao, P.-C.; Wang, J.-Y.; Lin, J.-H.; Yang, C.-H. Effects of the Na2CO3 Dopant on Electron Injection and Transport in Organic Light Emitting Devices. *Thin Solid Films* **2013**, *527*, 338–343. https://doi.org/10.1016/j.tsf.2012.11.038.

(161) Maitrot, M.; Guillaud, G.; Boudjema, B.; André, J. J.; Simon, J. Molecular Material-based Junctions: Formation of a Schottky Contact with Metallophthalocyanine Thin Films Doped by the Cosublimation Method. *J. Appl. Phys.* **1986**, *60*, 2396–2400. https://doi.org/10.1063/1.337151.

(162) El-Khatib, N.; Boudjema, B.; Guillaud, G.; Maitrot, M.; Chermette, H. Theoretical and Experimental Doping of Molecular Materials: P and N Doping of Zinc Phthalocyanine. *J. Less Common Met.* **1988**, *143*, 101–112. https://doi.org/10.1016/0022-5088(88)90035-5.

(163) Lim, E.; Peterson, K. A.; Su, G. M.; Chabinyc, M. L. Thermoelectric Properties of Poly(3-Hexylthiophene) (P3HT) Doped with 2,3,5,6-Tetrafluoro-7,7,8,8-Tetracyanoquinodimethane (F4TCNQ) by Vapor-Phase Infiltration. *Chem. Mater.* **2018**, *30*, 998–1010. https://doi.org/10.1021/acs.chemmater.7b04849.

(164) Kang, K.; Schott, S.; Venkateshvaran, D.; Broch, K.; Schweicher, G.; Harkin, D.; Jellett, C.; Nielsen, C. B.; McCulloch, I.; Sirringhaus, H. Investigation of the Thermoelectric Response in Conducting Polymers Doped by Solid-State Diffusion. *Mater. Today Phys.* **2019**, *8*, 112–122. https://doi.org/10.1016/j.mtphys.2019.02.004.

(165) Koech, P. K.; Padmaperuma, A. B.; Wang, L.; Swensen, J. S.; Polikarpov, E.; Darsell, J. T.; Rainbolt, J. E.; Gaspar, D. J. Synthesis and Application of 1,3,4,5,7,8-Hexafluorotetracyanonaphthoquinodimethane (F6-TNAP): A Conductivity Dopant for Organic Light-Emitting Devices. *Chem. Mater.* **2010**, *22*, 3926–3932. https://doi.org/10.1021/cm1002737.

(166) Rainbolt, J. E.; Koech, P. K.; Polikarpov, E.; Swensen, J. S.; Cosimbescu, L.; Von Ruden, A.; Wang, L.; Sapochak, L. S.; Padmaperuma, A. B.; Gaspar, D. J. V. Synthesis and Characterization of P-Type Conductivity Dopant 2-(3-(Adamantan-1-Yl)Propyl)-3,5,6-Trifluoro-7,7,8,8-Tetracyanoquinodimethane. *J. Mater. Chem. C* **2013**, *1*, 1876-1884. https://doi.org/10.1039/c3tc00068k.

(167) Li, J.; Zhang, G.; Holm, D. M.; Jacobs, I. E.; Yin, B.; Stroeve, P.; Mascal, M.; Moulé, A. J. Introducing Solubility Control for Improved Organic P-Type Dopants. *Chem. Mater.* **2015**, *27*, 5765–5774. https://doi.org/10.1021/acs.chemmater.5b02340.

(168) Gao, Z. Q.; Mi, B. X.; Xu, G. Z.; Wan, Y. Q.; Gong, M. L.; Cheah, K. W.; Chen, C. H. An Organic P-Type Dopant with High Thermal Stability for an Organic Semiconductor.

Chem. Commun. **2008**, 117–119. https://doi.org/10.1039/B713566A.

(169) Solomeshch, O.; Yu, Y. J.; Goryunkov, A. A.; Sidorov, L. N.; Tuktarov, R. F.; Choi, D. H.; Jin, J.-I.; Tessler, N. Ground-State Interaction and Electrical Doping of Fluorinated C60 in Conjugated Polymers. *Adv. Mater.* **2009**, *21*, 4456–4460. https://doi.org/10.1002/adma.200900798.

(170) Smets, Y.; Stark, C. B.; Schmitt, F.; Edmonds, M. T.; Lach, S.; Wright, C. A.; Langley, D. P.; Rietwyk, K. J.; Schenk, A.; Tadich, A.; et al. Doping Efficiency and Energy-Level Scheme in $C_{60}F_{48}$-Doped Zinc–Tetraphenylporphyrin Films. *Org. Electron.* **2013**, *14*, 169–174. https://doi.org/10.1016/j.orgel.2012.11.007.

(171) Meerheim, R.; Olthof, S.; Hermenau, M.; Scholz, S.; Petrich, A.; Tessler, N.; Solomeshch, O.; Lssem, B.; Riede, M.; Leo, K. Investigation of $C_{60}F_{36}$ as Low-Volatility p-Dopant in Organic Optoelectronic Devices. *J. Appl. Phys.* 2011, 109, 103102. https://doi.org/10.1063/1.3590142.

(172) Nell, B.; Ortstein, K.; Boltalina, O. V.; Vandewal, K. Influence of Dopant–Host Energy Level Offset on Thermoelectric Properties of Doped Organic Semiconductors. *J. Phys. Chem. C* **2018**, *122*, 11730–11735. https://doi.org/10.1021/acs.jpcc.8b03804.

(173) Babuji, A.; Temiño, I.; Pérez-Rodríguez, A.; Solomeshch, O.; Tessler, N.; Vila, M.; Li, J.; Mas-Torrent, M.; Ocal, C.; Barrena, E. Double Beneficial Role of Fluorinated Fullerene Dopants on Organic Thin-Film Transistors: Structural Stability and Improved Performance. *ACS Appl. Mater. Interfaces* **2020**, *12*, 28416–28425. https://doi.org/10.1021/acsami.0c06418.

(174) Nollau, A.; Pfeiffer, M.; Fritz, T.; Leo, K. Controlled N-Type Doping of a Molecular Organic Semiconductor: Naphthalenetetracarboxylic Dianhydride (NTCDA) Doped with Bis(Ethylenedithio)-Tetrathiafulvalene (BEDT-TTF). *J. Appl. Phys.* **2000**, *87*, 4340–4343. https://doi.org/10.1063/1.373413.

(175) Tanaka, S.; Kanai, K.; Kawabe, E.; Iwahashi, T.; Nishi, T.; Ouchi, Y.; Seki, K. Doping Effect of Tetrathianaphthacene Molecule in Organic Semiconductors on Their Interfacial Electronic Structures Studied by UV Photoemission Spectroscopy. *Japanese J. Appl. Phys.* **2005**, *44*, 3760–3763. https://doi.org/10.1143/JJAP.44.3760.

(176) Xue, J.; Forrest, S. R. Bipolar Doping between a Molecular Organic Donor-Acceptor Couple. *Phys. Rev. B* **2004**, *69*, 245322. https://doi.org/10.1103/PhysRevB.69.245322.

(177) Li, F.; Werner, A.; Pfeiffer, M.; Leo, K.; Liu, X. Leuco Crystal Violet as a Dopant for N-Doping of Organic Thin Films of Fullerene C60. *J. Phys. Chem. B* **2004**, *108*, 17076–17082. https://doi.org/10.1021/jp0478615.

(178) Li, F.; Pfeiffer, M.; Werner, A.; Harada, K.; Leo, K.; Hayashi, N.; Seki, K.; Liu, X.; Dang, X. D. Acridine Orange Base as a Dopant for n Doping of C60 Thin Films. *J. Appl. Phys.* **2006**, *100,* 023716. https://doi.org/10.1063/1.2219374.

(179) Werner, A. G.; Li, F.; Harada, K.; Pfeiffer, M.; Fritz, T.; Leo, K. Pyronin B as a Donor for n-Type Doping of Organic Thin Films. *Appl. Phys. Lett.* **2003**, *82*, 4495–4497. https://doi.org/10.1063/1.1583872.

(180) Huseynova, G.; Lee, S.-H.; Joo, C. W.; Lee, Y.-S.; Lim, Y.-J.; Park, J.; Yoo, J.-M.; Cho, N. S.; Kim, Y. H.; Lee, J.; et al. Dye-Doped Poly(3,4-Ethylenedioxythiophene)-Poly(Styrenesulfonate) Electrodes for the Application in Organic Light-Emitting Diodes. *Thin Solid Films* **2020**, *707*, 138078. https://doi.org/10.1016/j.tsf.2020.138078.

(181) Huseynova, G.; Xu, Y.; Nketia Yawson, B.; Shin, E.-Y.; Lee, M. J.; Noh, Y.-Y. P-Type Doped Ambipolar Polymer Transistors by Direct Charge Transfer from a Cationic Organic Dye Pyronin B Ferric Chloride. *Org. Electron.* **2016**, *39*, 229–235. https://doi.org/10.1016/j.orgel.2016.10.012.

(182) Sapurina, I.; Li, Y.; Alekseeva, E.; Bober, P.; Trchová, M.; Morávková, Z.; Stejskal, J. Polypyrrole Nanotubes: The Tuning of Morphology and Conductivity. *Polymer.* **2017**, *113*, 247–258. https://doi.org/10.1016/j.polymer.2017.02.064.

(183) Minisy, I. M.; Bober, P.; Acharya, U.; Trchová, M.; Hromádková, J.; Pfleger, J.; Stejskal, J. Cationic Dyes as Morphology-Guiding Agents for One-Dimensional Polypyrrole with Improved Conductivity. *Polymer.* **2019**, *174*, 11–17. https://doi.org/10.1016/j.polymer.2019.04.045.

(184) Minisy, I. M.; Bober, P.; Šeděnková, I.; Stejskal, J. Methyl Red Dye in the Tuning of Polypyrrole Conductivity. *Polymer.* **2020**, *207*, 122854. https://doi.org/10.1016/j.polymer.2020.122854.

(185) Bober, P.; Li, Y.; Acharya, U.; Panthi, Y.; Pfleger, J.; Humpolíček, P.; Trchová, M.; Stejskal, J. Acid Blue Dyes in Polypyrrole Synthesis: The Control of Polymer Morphology at Nanoscale in the Promotion of High Conductivity and the Reduction of Cytotoxicity. *Synth. Met.* **2018**, *237*, 40–49. https://doi.org/10.1016/j.synthmet.2018.01.010.

(186) Li, Y.; Bober, P.; Trchová, M.; Stejskal, J. Polypyrrole Prepared in the Presence of Methyl Orange and Ethyl Orange: Nanotubes versus Globules in Conductivity Enhancement. *J. Mater. Chem. C* **2017**, *5*, 4236–4245. https://doi.org/10.1039/C7TC00206H.

(187) Wei, P.; Oh, J. H.; Dong, G.; Bao, Z. Use of a 1 H -Benzoimidazole Derivative as an n

-Type Dopant and to Enable Air-Stable Solution-Processed n -Channel Organic Thin-Film Transistors. *J. Am. Chem. Soc.* **2010**, *132*, 8852–8853. https://doi.org/10.1021/ja103173m.

(188) Naab, B. D.; Guo, S.; Olthof, S.; Evans, E. G. B.; Wei, P.; Millhauser, G. L.; Kahn, A.; Barlow, S.; Marder, S. R.; Bao, Z. Mechanistic Study on the Solution-Phase n-Doping of 1,3-Dimethyl-2-Aryl-2,3-Dihydro-1 H -Benzoimidazole Derivatives. *J. Am. Chem. Soc.* **2013**, *135*, 15018–15025. https://doi.org/10.1021/ja403906d.

(189) Jhulki, S.; Un, H.-I.; Ding, Y.-F.; Risko, C.; Mohapatra, S. K.; Pei, J.; Barlow, S.; Marder, S. R. Reactivity of an Air-Stable Dihydrobenzoimidazole n-Dopant with Organic Semiconductor Molecules. *Chem* **2021**, *7*, 1050–1065. https://doi.org/10.1016/j.chempr.2021.01.020.

(190) Wei, P.; Menke, T.; Naab, B. D.; Leo, K.; Riede, M.; Bao, Z. 2-(2-Methoxyphenyl)-1,3-Dimethyl-1H-Benzoimidazol-3-Ium Iodide as a New Air-Stable n-Type Dopant for Vacuum-Processed Organic Semiconductor Thin Films. *J. Am. Chem. Soc.* **2012**, *134*, 3999–4002. https://doi.org/10.1021/ja211382x.

(191) Naab, B. D.; Himmelberger, S.; Diao, Y.; Vandewal, K.; Wei, P.; Lussem, B.; Salleo, A.; Bao, Z. High Mobility N-Type Transistors Based on Solution-Sheared Doped 6,13-Bis(Triisopropylsilylethynyl)Pentacene Thin Films. *Adv. Mater.* **2013**, *25*, 4663–4667. https://doi.org/10.1002/adma.201205098.

(192) Schlitz, R. A.; Brunetti, F. G.; Glaudell, A. M.; Miller, P. L.; Brady, M. A.; Takacs, C. J.; Hawker, C. J.; Chabinyc, M. L. Solubility-Limited Extrinsic n-Type Doping of a High Electron Mobility Polymer for Thermoelectric Applications. *Adv. Mater.* **2014**, *26*, 2825–2830. https://doi.org/10.1002/adma.201304866.

(193) Zuo, G.; Li, Z.; Wang, E.; Kemerink, M. High Seebeck Coefficient and Power Factor in N-Type Organic Thermoelectrics. *Adv. Electron. Mater.* **2018**, *4*, 1700501. https://doi.org/10.1002/aelm.201700501.

(194) Menke, T.; Wei, P.; Ray, D.; Kleemann, H.; Naab, B. D.; Bao, Z.; Leo, K.; Riede, M. A Comparison of Two Air-Stable Molecular n-Dopants for C60. *Org. Electron.* **2012**, *13*, 3319–3325. https://doi.org/10.1016/j.orgel.2012.09.024.

(195) Schwarze, M.; Naab, B. D.; Tietze, M. L.; Scholz, R.; Pahner, P.; Bussolotti, F.; Kera, S.; Kasemann, D.; Bao, Z.; Leo, K. Analyzing the N-Doping Mechanism of an Air-Stable Small-Molecule Precursor. *ACS Appl. Mater. Interfaces* **2018**, *10*, 1340–1346. https://doi.org/10.1021/acsami.7b14034.

(196) Saglio, B.; Mura, M.; Massetti, M.; Scuratti, F.; Beretta, D.; Jiao, X.; McNeill, C. R.;

Sommer, M.; Famulari, A.; Lanzani, G.; et al. N-Alkyl Substituted 1H-Benzimidazoles as Improved n-Type Dopants for a Naphthalene-Diimide Based Copolymer. *J. Mater. Chem. A* **2018**, *6*, 15294–15302. https://doi.org/10.1039/C8TA04901G.

(197) Qiu, L.; Liu, J.; Alessandri, R.; Qiu, X.; Koopmans, M.; Havenith, R. W. A.; Marrink, S. J.; Chiechi, R. C.; Anton Koster, L. J.; Hummelen, J. C. Enhancing Doping Efficiency by Improving Host-Dopant Miscibility for Fullerene-Based n-Type Thermoelectrics. *J. Mater. Chem. A* **2017**, *5*, 21234–21241. https://doi.org/10.1039/C7TA06609K.

(198) Riera-Galindo, S.; Orbelli Biroli, A.; Forni, A.; Puttisong, Y.; Tessore, F.; Pizzotti, M.; Pavlopoulou, E.; Solano, E.; Wang, S.; Wang, G.; et al. Impact of Singly Occupied Molecular Orbital Energy on the N-Doping Efficiency of Benzimidazole Derivatives. *ACS Appl. Mater. Interfaces* **2019**, *11*, 37981–37990. https://doi.org/10.1021/acsami.9b12441.

(199) Naab, B. D.; Zhang, S.; Vandewal, K.; Salleo, A.; Barlow, S.; Marder, S. R.; Bao, Z. Effective Solution- and Vacuum-Processed n-Doping by Dimers of Benzimidazoline Radicals. *Adv. Mater.* **2014**, *26*, 4268–4272. https://doi.org/10.1002/adma.201400668.

(200) Zhang, S.; Naab, B. D.; Jucov, E. V.; Parkin, S.; Evans, E. G. B.; Millhauser, G. L.; Timofeeva, T. V.; Risko, C.; Brédas, J. L.; Bao, Z.; et al. N-Dopants Based on Dimers of Benzimidazoline Radicals: Structures and Mechanism of Redox Reactions. *Chem. Eur. J.* **2015**, *21*, 10878–10885. https://doi.org/10.1002/chem.201500611.

(201) Yuan, D.; Huang, D.; Zhang, C.; Zou, Y.; Di, C. A.; Zhu, X.; Zhu, D. Efficient Solution-Processed n-Type Small-Molecule Thermoelectric Materials Achieved by Precisely Regulating Energy Level of Organic Dopants. *ACS Appl. Mater. Interfaces* **2017**, *9*, 28795–28801. https://doi.org/10.1021/acsami.7b07282.

(202) Un, H.; Gregory, S. A.; Mohapatra, S. K.; Xiong, M.; Longhi, E.; Lu, Y.; Rigin, S.; Jhulki, S.; Yang, C.; Timofeeva, T. V.; et al. Understanding the Effects of Molecular Dopant on N-Type Organic Thermoelectric Properties. *Adv. Energy Mater.* **2019**, *9*, 1900817. https://doi.org/10.1002/aenm.201900817.

(203) Qi, Y.; Sajoto, T.; Barlow, S.; Kim, E.-G.; Brédas, J.-L.; Marder, S. R.; Kahn, A. Use of a High Electron-Affinity Molybdenum Dithiolene Complex to p-Dope Hole-Transport Layers. *J. Am. Chem. Soc.* **2009**, *131*, 12530–12531. https://doi.org/10.1021/ja904939g.

(204) Dai, A.; Zhou, Y.; Shu, A. L.; Mohapatra, S. K.; Wang, H.; Fuentes-Hernandez, C.; Zhang, Y.; Barlow, S.; Loo, Y. L.; Marder, S. R.; et al. Enhanced Charge-Carrier Injection and Collection via Lamination of Doped Polymer Layers p-Doped with a

Solution-Processible Molybdenum Complex. *Adv. Funct. Mater.* **2014**, *24*, 2197–2204. https://doi.org/10.1002/adfm.201303232.

(205) Paniagua, S. A.; Baltazar, J.; Sojoudi, H.; Mohapatra, S. K.; Zhang, S.; Henderson, C. L.; Graham, S.; Barlow, S.; Marder, S. R. Production of Heavily N- and p-Doped CVD Graphene with Solution-Processed Redox-Active Metal-Organic Species. *Mater. Horizons* **2014**, *1*, 111–115. https://doi.org/10.1039/c3mh00035d.

(206) Harada, K.; Werner, A. G.; Pfeiffer, M.; Bloom, C. J.; Elliott, C. M.; Leo, K. Organic Homojunction Diodes with a High Built-in Potential: Interpretation of the Current-Voltage Characteristics by a Generalized Einstein Relation. *Phys. Rev. Lett.* **2005**, *94*, 036601. https://doi.org/10.1103/PhysRevLett.94.036601.

(207) Menke, T.; Ray, D.; Meiss, J.; Leo, K.; Riede, M. In-Situ Conductivity and Seebeck Measurements of Highly Efficient n-Dopants in Fullerene C60. *Appl. Phys. Lett.* **2012**, *100*, 093304. https://doi.org/10.1063/1.3689778.

(208) Chan, C. K.; Amy, F.; Zhang, Q.; Barlow, S.; Marder, S.; Kahn, A. N-Type Doping of an Electron-Transport Material by Controlled Gas-Phase Incorporation of Cobaltocene. *Chem. Phys. Lett.* **2006**, *431*, 67–71. https://doi.org/10.1016/j.cplett.2006.09.034.

(209) Chan, C. K.; Kahn, A. N-Doping of Pentacene by Decamethylcobaltocene. *Appl. Phys. A* **2009**, *95*, 7–13. https://doi.org/10.1007/s00339-008-4997-x.

(210) Lungwitz, D.; Schultz, T.; Tait, C. E.; Behrends, J.; Mohapatra, S. K.; Barlow, S.; Marder, S. R.; Opitz, A.; Koch, N. Disentangling Bulk and Interface Phenomena in a Molecularly Doped Polymer Semiconductor. *Adv. Opt. Mater.* **2021, 9, 2002039**. https://doi.org/10.1002/adom.202002039.

(211) Guo, S.; Kim, S. B.; Mohapatra, S. K.; Qi, Y.; Sajoto, T.; Kahn, A.; Marder, S. R.; Barlow, S. N-Doping of Organic Electronic Materials Using Air-Stable Organometallics. *Adv. Mater.* **2012**, *24*, 699–703. https://doi.org/10.1002/adma.201103238.

(212) Mohapatra, S. K.; Fonari, A.; Risko, C.; Yesudas, K.; Moudgil, K.; Delcamp, J. H.; Timofeeva, T. V.; Brédas, J.-L.; Marder, S. R.; Barlow, S. Dimers of Nineteen-Electron Sandwich Compounds: Crystal and Electronic Structures, and Comparison of Reducing Strengths. *Chem. Eur. J.* **2014**, *20*, 15385–15394. https://doi.org/10.1002/chem.201404007.

(213) Higgins, A.; Mohapatra, S. K.; Barlow, S.; Marder, S. R.; Kahn, A. Dopant Controlled Trap-Filling and Conductivity Enhancement in an Electron-Transport Polymer. *Appl. Phys. Lett.* **2015**, *106*, 163301. https://doi.org/10.1063/1.4918627.

(214) Perry, E. E.; Chiu, C.-Y.; Moudgil, K.; Schlitz, R. A.; Takacs, C. J.; O'Hara, K. A.; Labram, J. G.; Glaudell, A. M.; Sherman, J. B.; Barlow, S.; et al. High Conductivity in a Nonplanar n -Doped Ambipolar Semiconducting Polymer. *Chem. Mater.* **2017**, *29*, 9742–9750. https://doi.org/10.1021/acs.chemmater.7b03516.

(215) Lin, X.; Wegner, B.; Lee, K. M.; Fusella, M. A.; Zhang, F.; Moudgil, K.; Rand, B. P.; Barlow, S.; Marder, S. R.; Koch, N.; et al. Beating the Thermodynamic Limit with Photo-Activation of n-Doping in Organic Semiconductors. *Nat. Mater.* **2017**, *16*, 1209–1215. https://doi.org/10.1038/nmat5027.

(216) Smith, H. L.; Dull, J. T.; Longhi, E.; Barlow, S.; Rand, B. P.; Marder, S. R.; Kahn, A. N-Doping of a Low-Electron-Affinity Polymer Used as an Electron-Transport Layer in Organic Light-Emitting Diodes. *Adv. Funct. Mater.* **2020**, *30*, 2000328. https://doi.org/10.1002/adfm.202000328.

(217) Wamser, C. A. Equilibria in the System Boron Trifluoride—Water at 25°. *J. Am. Chem. Soc.* **1951**, *73*, 409–416. https://doi.org/10.1021/ja01145a134.

(218) Körte, L. A.; Schwabedissen, J.; Soffner, M.; Blomeyer, S.; Reuter, C. G.; Vishnevskiy, Y. V.; Neumann, B.; Stammler, H.-G.; Mitzel, N. W. Tris(Perfluorotolyl)Borane-A Boron Lewis Superacid. *Angew. Chem. Int. Ed.* **2017**, *56*, 8578–8582. https://doi.org/10.1002/anie.201704097.

(219) Welch, G. C.; Coffin, R.; Peet, J.; Bazan, G. C. Band Gap Control in Conjugated Oligomers via Lewis Acids. *J. Am. Chem. Soc.* **2009**, *131*, 10802–10803. https://doi.org/10.1021/ja902789w.

(220) Russ, B.; Robb, M. J.; Brunetti, F. G.; Miller, P. L.; Perry, E. E.; Patel, S. N.; Ho, V.; Chang, W. B.; Urban, J. J.; Chabinyc, M. L.; et al. Power Factor Enhancement in Solution-Processed Organic n-Type Thermoelectrics through Molecular Design. *Adv. Mater.* **2014**, *26*, 3473–3477. https://doi.org/10.1002/adma.201306116.

(221) Zalar, P.; Henson, Z. B.; Welch, G. C.; Bazan, G. C.; Nguyen, T. Q. Color Tuning in Polymer Light-Emitting Diodes with Lewis Acids. *Angew. Chem. Int. Ed.* **2012**, *51*, 7495–7498. https://doi.org/10.1002/anie.201202570.

(222) Zalar, P.; Kuik, M.; Henson, Z. B.; Woellner, C.; Zhang, Y.; Sharenko, A.; Bazan, G. C.; Nguyen, T. Q. Increased Mobility Induced by Addition of a Lewis Acid to a Lewis Basic Conjugated Polymer. *Adv. Mater.* **2014**, *26*, 724–727. https://doi.org/10.1002/adma.201303357.

(223) Han, Y.; Barnes, G.; Lin, Y.-H.; Martin, J.; Al-Hashimi, M.; AlQaradawi, S. Y.; Anthopoulos, T. D.; Heeney, M. Doping of Large Ionization Potential Indenopyrazine

Polymers via Lewis Acid Complexation with Tris(Pentafluorophenyl)Borane: A Simple Method for Improving the Performance of Organic Thin-Film Transistors. *Chem. Mater.* **2016**, *28*, 8016–8024. https://doi.org/10.1021/acs.chemmater.6b03761.

(224) Poverenov, E.; Zamoshchik, N.; Patra, A.; Ridelman, Y.; Bendikov, M. Unusual Doping of Donor–Acceptor-Type Conjugated Polymers Using Lewis Acids. *J. Am. Chem. Soc.* **2014**, *136*, 5138–5149. https://doi.org/10.1021/ja501024n.

(225) Paterson, A. F.; Tsetseris, L.; Li, R.; Basu, A.; Faber, H.; Emwas, A. H.; Panidi, J.; Fei, Z.; Niazi, M. R.; Anjum, D. H.; et al. Addition of the Lewis Acid $Zn(C_6F_5)_2$ Enables Organic Transistors with a Maximum Hole Mobility in Excess of 20 $Cm^2 V^{-1} s^{-1}$. *Adv. Mater.* **2019**, 31, *1900871*. https://doi.org/10.1002/adma.201900871.

(226) Zhang, D.; Li, Q.; Zhang, J.; Wang, J.; Zhang, X.; Wang, R.; Zhou, J.; Wei, Z.; Zhang, C.; Zhou, H.; et al. Control of Nanomorphology in Fullerene-Free Organic Solar Cells by Lewis Acid Doping with Enhanced Photovoltaic Efficiency. *ACS Appl. Mater. Interfaces* **2020**, *12*, 667–677. https://doi.org/10.1021/acsami.9b17238.

(227) Ye, T.; Chen, W.; Jin, S.; Hao, S.; Zhang, X.; Liu, H.; He, D. Enhanced Efficiency of Planar Heterojunction Perovskite Solar Cells by a Light Soaking Treatment on Tris(Pentafluorophenyl)Borane-Doped Poly(Triarylamine) Solution. *ACS Appl. Mater. Interfaces* **2019**, *11*, 14004–14010. https://doi.org/10.1021/acsami.8b18663.

(228) Luo, J.; Xia, J.; Yang, H.; Chen, L.; Wan, Z.; Han, F.; Malik, H. A.; Zhu, X.; Jia, C. Toward High-Efficiency, Hysteresis-Less, Stable Perovskite Solar Cells: Unusual Doping of a Hole-Transporting Material Using a Fluorine-Containing Hydrophobic Lewis Acid. *Energy Environ. Sci.* **2018**, *11*, 2035–2045. https://doi.org/10.1039/c8ee00036k.

(229) Luo, J.; Xia, J.; Yang, H.; Malik, H. A.; Han, F.; Shu, H.; Yao, X.; Wan, Z.; Jia, C. Novel Approach toward Hole-Transporting Layer Doped by Hydrophobic Lewis Acid through Infiltrated Diffusion Doping for Perovskite Solar Cells. *Nano Energy* **2020**, *70*, 104509. https://doi.org/10.1016/j.nanoen.2020.104509.

(230) Russ, B.; Robb, M. J.; Popere, B. C.; Perry, E. E.; Mai, C.-K.; Fronk, S. L.; Patel, S. N.; Mates, T. E.; Bazan, G. C.; Urban, J. J.; et al. Tethered Tertiary Amines as Solid-State n-Type Dopants for Solution-Processable Organic Semiconductors. *Chem. Sci.* **2016**, *7*, 1914–1919. https://doi.org/10.1039/C5SC04217H.

(231) Jia, J.; Fan, B.; Xiao, M.; Jia, T.; Jin, Y.; Li, Y.; Huang, F.; Cao, Y. N-Type Self-Doped Water/Alcohol-Soluble Conjugated Polymers with Tailored Energy Levels for High-Performance Polymer Solar Cells. *Macromolecules* **2018**, *51*, 2195–2202.

https://doi.org/10.1021/acs.macromol.8b00126.

(232) Hu, Z.; Chen, Z.; Zhang, K.; Zheng, N.; Xie, R.; Liu, X.; Yang, X.; Huang, F.; Cao, Y. Self-Doped N-Type Water/Alcohol Soluble-Conjugated Polymers with Tailored Backbones and Polar Groups for Highly Efficient Polymer Solar Cells. *Sol. RRL* **2017**, *1*, 1700055. https://doi.org/10.1002/solr.201700055.

(233) Schmidt, S. B.; Biskup, T.; Jiao, X.; McNeill, C. R.; Sommer, M. Controlling Intermolecular Redox-Doping of Naphthalene Diimides. *J. Mater. Chem. C* **2019**, *7*, 4466–4474. https://doi.org/10.1039/c9tc00721k.

(234) Kim, J.; Khim, D.; Baeg, K.-J. J.; Park, W.-T. T.; Lee, S.-H. H.; Kang, M.; Noh, Y.-Y. Y.; Kim, D.-Y. Y. Systematic Study of Widely Applicable N-Doping Strategy for High-Performance Solution-Processed Field-Effect Transistors. *Adv. Funct. Mater.* **2016**, *26*, 7886–7894. https://doi.org/10.1002/adfm.201602610.

(235) Huseynova, G.; Shin, E. Y.; Park, W. T.; Noh, Y. Y. Lithium Benzoate Doped High Performance N-Type Diketopyrrolopyrrole Based Organic Thin-Film Transistors. *Dyes Pigm.* **2019**, *162*, 243–248. https://doi.org/10.1016/j.dyepig.2018.10.032.

(236) Wang, R.; Zhang, D.; Xie, S.; Wang, J.; Zheng, Z.; Wei, D.; Sun, X.; Zhou, H.; Zhang, Y. High Efficiency Non-Fullerene Organic Solar Cells without Electron Transporting Layers Enabled by Lewis Base Anion Doping. *Nano Energy* **2018**, *51*, 736–744. https://doi.org/10.1016/j.nanoen.2018.07.022.

(237) Mai, C.-K.; Russ, B.; Fronk, S. L.; Hu, N.; Chan-Park, M. B.; Urban, J. J.; Segalman, R. A.; Chabinyc, M. L.; Bazan, G. C. Varying the Ionic Functionalities of Conjugated Polyelectrolytes Leads to Both P- and N-Type Carbon Nanotube Composites for Flexible Thermoelectrics. *Energy Environ. Sci.* **2015**, *8*, 2341–2346. https://doi.org/10.1039/C5EE00938C.

(238) Schmid, G.; Wemken, J. H.; Maltenberger, A.; Diez, C.; Jaeger, A.; Dobbertin, T.; Hietsoi, O.; Dubceac, C.; Petrukhina, M. A. Fluorinated Copper(I) Carboxylates as Advanced Tunable p-Dopants for Organic Light-Emitting Diodes. *Adv. Mater.* **2014**, *26*, 878–885. https://doi.org/10.1002/adma.201303252.

(239) Wemken, J. H.; Krause, R.; Mikolajick, T.; Schmid, G. Low-Cost Caesium Phosphate as n-Dopant for Organic Light-Emitting Diodes. *J. Appl. Phys*. **2012**, *111*, 074502.. https://doi.org/10.1063/1.3699008.

(240) Leem, D. S.; Kim, S. Y.; Kim, J. J.; Chen, M. H.; Wu, C. I. Rubidium-Carbonate-Doped 4,7-Diphenyl-1,10-Phenanthroline Electron Transporting Layer for High-Efficiency p-i-n Organic Light Emitting Diodes. *Electrochem. Solid-State Lett.* **2008**, *12*, J8-J10.

https://doi.org/10.1149/1.3007239.

(241) Kao, P. C.; Lin, J. H.; Wang, J. Y.; Yang, C. H.; Chen, S. H. Li2CO3 as an N-Type Dopant on Alq3-Based Organic Light Emitting Devices. *J. Appl. Phys.* **2011**, *109*, 094505. https://doi.org/10.1063/1.3585767.

(242) Kao, P. C.; Chang, C. C.; Lin, S. Y. Role of K2CO3 as an N-Type Dopant in Enhancing the Electron Injection and Transport of Organic Light-Emitting Devices. *Surf. Coatings Technol.* **2013**, *231*, 135–139. https://doi.org/10.1016/j.surfcoat.2012.01.066.

(243) Han, Y.; Fei, Z.; Lin, Y.-H. H.; Martin, J.; Tuna, F.; Anthopoulos, T. D.; Heeney, M. Anion-Induced N-Doping of Naphthalenediimide Polymer Semiconductor in Organic Thin-Film Transistors. *npj Flex. Electron.* **2018**, *2*, 11. https://doi.org/10.1038/s41528-018-0024-2.

(244) Xu, Y.; Yuan, J.; Sun, J.; Zhang, Y.; Ling, X.; Wu, H.; Zhang, G.; Chen, J.; Wang, Y.; Ma, W. Widely Applicable N-Type Molecular Doping for Enhanced Photovoltaic Performance of All-Polymer Solar Cells. *ACS Appl. Mater. Interfaces* **2018**, *10*, 2776–2784. https://doi.org/10.1021/acsami.7b15000.

(245) Tang, C. G.; Syafiqah, M. N.; Koh, Q.-M.; Zhao, C.; Zaini, J.; Seah, Q.-J.; Cass, M. J.; Humphries, M. J.; Grizzi, I.; Burroughes, J. H.; et al. Multivalent Anions as Universal Latent Electron Donors. *Nature* **2019**, *573*, 519–525. https://doi.org/10.1038/s41586-019-1575-7.

(246) Hopf, H.; Maas, G. Preparation and Properties, Reactions, and Applications of Radialenes. *Angew. Chem. Int. Ed. Engl.* **1992**, *31*, 931–954. https://doi.org/10.1002/anie.199209313.

(247) Fukunaga, T. Negatively Substituted Trimethylenecyclopropane Dianions. *J. Am. Chem. Soc.* **1976**, *98*, 610–611. https://doi.org/10.1021/ja00418a050.

(248) Fukunaga, T.; Gordon, M. D.; Krusic, P. J. Negatively Substituted Trimethylenecyclopropanes and Their Radical Anions. *J. Am. Chem. Soc.* **1976**, *98*, 611–613. https://doi.org/10.1021/ja00418a051.

(249) Karpov, Y.; Erdmann, T.; Raguzin, I.; Al-Hussein, M.; Binner, M.; Lappan, U.; Stamm, M.; Gerasimov, K. L.; Beryozkina, T.; Bakulev, V.; et al. High Conductivity in Molecularly P-Doped Diketopyrrolopyrrole-Based Polymer: The Impact of a High Dopant Strength and Good Structural Order. *Adv. Mater.* **2016**, *28*, 6003–6010. https://doi.org/10.1002/adma.201506295.

(250) Liu, Y.; Nell, B.; Ortstein, K.; Wu, Z.; Karpov, Y.; Beryozkina, T.; Lenk, S.; Kiriy, A.; Leo, K.; Reineke, S. High Electron Affinity Molecular Dopant CN6-CP for Efficient

Organic Light-Emitting Diodes. *ACS Appl. Mater. Interfaces* **2019**, *11*, 11660–11666. https://doi.org/10.1021/acsami.8b21865.

(251) Dong, C.; Schumacher, S. Molecular Doping in Few-Molecule Polymer-Dopant Complexes Shows Reduced Coulomb Binding. *J. Mater. Chem. C* **2020**, *8*, 11929–11935. https://doi.org/10.1039/D0TC02185G.

(252) Karpov, Y.; Kiriy, N.; Al-Hussein, M.; Hambsch, M.; Beryozkina, T.; Bakulev, V.; Mannsfeld, S. C. B.; Voit, B.; Kiriy, A. Hexacyano-[3]-Radialene Anion-Radical Salts: A Promising Family of Highly Soluble p-Dopants. *Chem. Commun.* **2018**, *54*, 307–310. https://doi.org/10.1039/C7CC08671G.

(253) Karpov, Y.; Kiriy, N.; Formanek, P.; Hoffmann, C.; Beryozkina, T.; Hambsch, M.; Al-Hussein, M.; Mannsfeld, S. C. B.; Büchner, B.; Debnath, B.; et al. Sequentially Processed P3HT/CN6-CP $^{\bullet-}$ NBu $^{4+}$ Films: Interfacial or Bulk Doping?. *Adv. Electron. Mater.* **2020**, *6*, 1901346. https://doi.org/10.1002/aelm.201901346.

(254) Saska, J.; Gonel, G.; Bedolla-Valdez, Z. I.; Aronow, S. D.; Shevchenko, N. E.; Dudnik, A. S.; Moulé, A. J.; Mascal, M. A Freely Soluble, High Electron Affinity Molecular Dopant for Solution Processing of Organic Semiconductors. *Chem. Mater.* **2019**, *31*, 1500–1506. https://doi.org/10.1021/acs.chemmater.8b04150.

(255) Zhou, Y.; Fuentes-Hernandez, C.; Shim, J.; Meyer, J.; Giordano, A. J.; Li, H.; Winget, P.; Papadopoulos, T.; Cheun, H.; Kim, J.; et al. A Universal Method to Produce Low-Work Function Electrodes for Organic Electronics. *Science* **2012**, *336*, 327–332. https://doi.org/10.1126/science.1218829.

(256) Fabiano, S.; Braun, S.; Liu, X.; Weverberghs, E.; Gerbaux, P.; Fahlman, M.; Berggren, M.; Crispin, X. Poly(Ethylene Imine) Impurities Induce n-Doping Reaction in Organic (Semi)Conductors. *Adv. Mater.* **2014**, *26*, 6000–6006. https://doi.org/10.1002/adma.201401986.

(257) Sun, B.; Hong, W.; Thibau, E. S.; Aziz, H.; Lu, Z.-H.; Li, Y. Polyethylenimine (PEI) As an Effective Dopant To Conveniently Convert Ambipolar and p-Type Polymers into Unipolar n-Type Polymers. *ACS Appl. Mater. Interfaces* **2015**, *7*, 18662–18671. https://doi.org/10.1021/acsami.5b05097.

(258) Long, D. X.; Karakawa, M.; Noh, Y.-Y. An Improvement of Performance in N-Channel Organic Field Effect Transistors with N-Phenyl[60]Fulleropyrrolidines by Molecular Doping. *Phys. Chem. Chem. Phys.* **2016**, *18*, 23904–23909. https://doi.org/10.1039/C6CP02940J.

(259) Long, D. X.; Choi, E.-Y.; Noh, Y.-Y. High Performance and Stable Naphthalene

Diimide Based N-Channel Organic Field-Effect Transistors by Polyethylenimine Doping. *Dye. Pigment.* **2017**, *142*, 323–329. https://doi.org/10.1016/j.dyepig.2017.03.053.

(260) Yang, C.-Y.; Stoeckel, M.-A.; Ruoko, T.-P.; Wu, H.-Y.; Liu, X.; Kolhe, N. B.; Wu, Z.; Puttisong, Y.; Musumeci, C.; Massetti, M.; et al. A High-Conductivity n-Type Polymeric Ink for Printed Electronics. *Nat. Commun.* **2021**, *12*, 2354. https://doi.org/10.1038/s41467-021-22528-y.

(261) Panidi, J.; Kainth, J.; Paterson, A. F.; Wang, S.; Tsetseris, L.; Emwas, A.; McLachlan, M. A.; Heeney, M.; Anthopoulos, T. D. Introducing a Nonvolatile N-Type Dopant Drastically Improves Electron Transport in Polymer and Small-Molecule Organic Transistors. *Adv. Funct. Mater.* **2019**, *29*, 1902784. https://doi.org/10.1002/adfm.201902784.

(262) Hu, L.; Liu, T.; Duan, J.; Ma, X.; Ge, C.; Jiang, Y.; Qin, F.; Xiong, S.; Jiang, F.; Hu, B.; et al. An Amidine-Type n-Dopant for Solution-Processed Field-Effect Transistors and Perovskite Solar Cells. *Adv. Funct. Mater.* **2017**, *27*, 1703254. https://doi.org/10.1002/adfm.201703254.

(263) Nakayama, H.; Schneider, J. A.; Faust, M.; Wang, H.; Read de Alaniz, J.; Chabinyc, M. L. A New Family of Liquid and Solid Guanidine-Based n-Type Dopants for Solution-Processed Perovskite Solar Cells. *Mater. Chem. Front.* **2020**, *4*, 3616–3622. https://doi.org/10.1039/D0QM00437E.

(264) Lin, Y.; Nugraha, M. I.; Firdaus, Y.; Scaccabarozzi, A. D.; Aniés, F.; Emwas, A.-H.; Yengel, E.; Zheng, X.; Liu, J.; Wahyudi, W.; et al. A Simple N-Dopant Derived from Diquat Boosts the Efficiency of Organic Solar Cells to 18.3%. *ACS Energy Lett.* **2020**, 3663–3671. https://doi.org/10.1021/acsenergylett.0c01949.

(265) Huseynova, G.; Shrestha, N. K.; Xu, Y.; Shin, E.-Y.; Park, W.-T.; Ji, D.; Noh, Y.-Y. Benzyl Viologen as an N-Type Dopant for Organic Semiconductors. *Org. Electron.* **2018**, *62*, 572–580. https://doi.org/10.1016/j.orgel.2018.06.033.

(266) Dexter Tam, T. L.; Lin, T. T.; Omer, M. I.; Wang, X.; Xu, J. The Benzyl Viologen Radical Cation: An Effective n-Dopant for Poly(Naphthalenediimide-Bithiophene). *J. Mater. Chem. A* **2020**, *8*, 18916–18924. https://doi.org/10.1039/D0TA06315K.

(267) Ding, Y.; Yang, C.; Huang, C.; Lu, Y.; Yao, Z.; Pan, C.; Wang, J.; Pei, J. Thermally Activated N-Doping of Organic Semiconductors Achieved by N-Heterocyclic Carbene Based Dopant. *Angew. Chem. Int. Ed.* **2021**, *60*, 5816–5820. https://doi.org/10.1002/anie.202011537.

(268) Sakai, N.; Warren, R.; Zhang, F.; Nayak, S.; Liu, J.; Kesava, S. V.; Lin, Y.-H.; Biswal, H. S.; Lin, X.; Grovenor, C.; et al. Adduct-Based p-Doping of Organic Semiconductors. *Nat. Mater.* **2021**, *20*, 1248-1254. https://doi.org/10.1038/s41563-021-00980-x.

(269) Wegner, B.; Lungwitz, D.; Mansour, A. E.; Tait, C. E.; Tanaka, N.; Zhai, T.; Duhm, S.; Forster, M.; Behrends, J.; Shoji, Y.; et al. An Organic Borate Salt with Superior p - Doping Capability for Organic Semiconductors. *Adv. Sci.* **2020**, *7*, 2001322. https://doi.org/10.1002/advs.202001322.

(270) Enengl, C.; Enengl, S.; Pluczyk, S.; Havlicek, M.; Lapkowski, M.; Neugebauer, H.; Ehrenfreund, E. Doping-Induced Absorption Bands in P3HT: Polarons and Bipolarons. *ChemPhysChem* **2016**, *17*, 3830-3830. https://doi.org/10.1002/cphc.201601221.

(271) Yamamoto, J.; Furukawa, Y. Electronic and Vibrational Spectra of Positive Polarons and Bipolarons in Regioregular Poly(3-Hexylthiophene) Doped with Ferric Chloride. *J. Phys. Chem. B* **2015**, *119*, 4788–4794. https://doi.org/10.1021/jp512654b.

(272) Ratcliff, E. L.; Lee, P. A.; Armstrong, N. R. Work Function Control of Hole-Selective Polymer/ITO Anode Contacts: An Electrochemical Doping Study. *J. Mater. Chem.* **2010**, *20*, 2672–2679. https://doi.org/10.1039/B923201J.

(273) Ratcliff, E. L.; Jenkins, J. L.; Nebesny, K.; Armstrong, N. R. Electrodeposited, "Textured" Poly(3-Hexyl-Thiophene) (e-P3HT) Films for Photovoltaic Applications. *Chem. Mater.* **2008**, *20*, 5796–5806. https://doi.org/10.1021/cm8008122.

(274) Tsokkou, D.; Peterhans, L.; Cao, D. X.; Mai, C.; Bazan, G. C.; Nguyen, T.; Banerji, N. Excited State Dynamics of a Self-Doped Conjugated Polyelectrolyte. *Adv. Funct. Mater.* **2020**, *30*, 1906148. https://doi.org/10.1002/adfm.201906148.

(275) Hu, Y.; Rengert, Z. D.; McDowell, C.; Ford, M. J.; Wang, M.; Karki, A.; Lill, A. T.; Bazan, G. C.; Nguyen, T. Q. Doping Polymer Semiconductors by Organic Salts: Toward High-Performance Solution-Processed Organic Field-Effect Transistors. *ACS Nano* **2018**, *12*, 3938–3946. https://doi.org/10.1021/acsnano.8b01460.

(276) Aubry, T. J.; Winchell, K. J.; Salamat, C. Z.; Basile, V. M.; Lindemuth, J. R.; Stauber, J. M.; Axtell, J. C.; Kubena, R. M.; Phan, M. D.; Bird, M. J.; et al. Tunable Dopants with Intrinsic Counterion Separation Reveal the Effects of Electron Affinity on Dopant Intercalation and Free Carrier Production in Sequentially Doped Conjugated Polymer Films. *Adv. Funct. Mater.* **2020**, *30*, 2001800. https://doi.org/10.1002/adfm.202001800.

(277) Yang, C. Y.; Ding, Y. F.; Huang, D.; Wang, J.; Yao, Z. F.; Huang, C. X.; Lu, Y.; Un, H. I.; Zhuang, F. D.; Dou, J. H.; et al. A Thermally Activated and Highly Miscible Dopant for N-Type Organic Thermoelectrics. *Nat. Commun.* **2020**, *11*, 1–10.

https://doi.org/10.1038/s41467-020-17063-1.

(278) Shi, K.; Lu, Z.-Y.; Yu, Z.-D.; Liu, H.-Y.; Zou, Y.; Yang, C.-Y.; Dai, Y.-Z.; Lu, Y.; Wang, J.-Y.; Pei, J. A Novel Solution-Processable n-Dopant Based on 1,4-Dihydropyridine Motif for High Electrical Conductivity of Organic Semiconductors. *Adv. Electron. Mater.* **2017**, *3*, 1700164. https://doi.org/10.1002/aelm.201700164.

(279) Kong, J.; Shin, Y.; Röhr, J. A.; Wang, H.; Meng, J.; Wu, Y.; Katzenberg, A.; Kim, G.; Kim, D. Y.; Li, T.-D.; et al. CO2 Doping of Organic Interlayers for Perovskite Solar Cells. *Nature* **2021**, *594*, 51–56. https://doi.org/10.1038/s41586-021-03518-y.

(280) Gregg, B. A.; Chen, S.-G.; Branz, H. M. On the Superlinear Increase in Conductivity with Dopant Concentration in Excitonic Semiconductors. *Appl. Phys. Lett.* **2004**, *84*, 1707–1709. https://doi.org/10.1063/1.1668326.

(281) Chayer, M.; Faïd, K.; Leclerc, M. Highly Conducting Water-Soluble Polythiophene Derivatives. *Chem. Mater.* **1997**, *9*, 2902–2905. https://doi.org/10.1021/cm970238v.

(282) Patil, A. O.; Ikenoue, Y.; Basescu, N.; Colaneri, N.; Chen, J.; Wudl, F.; Heeger, A. J. Self-Doped Conducting Polymers. *Synth. Met.* **1987**, *20*, 151–159. https://doi.org/10.1016/0379-6779(87)90554-6.

(283) Stéphan, O.; Schottland, P.; Le Gall, P.-Y.; Chevrot, C.; Mariet, C.; Carrier, M. Electrochemical Behaviour of 3, 4-Ethylenedioxythiophene Functionalized by a Sulphonate Group. Application to the Preparation of Poly(3, 4-Ethylenedioxythiophene) Having Permanent Cation-Exchange Properties. *J. Electroanal. Chem.* **1998**, *443*, 217–226. https://doi.org/10.1016/S0022-0728(97)00548-2.

(284) Mousavi, Z.; Alaviuhkola, T.; Bobacka, J.; Latonen, R.-M.; Pursiainen, J.; Ivaska, A. Electrochemical Characterization of Poly(3,4-Ethylenedioxythiophene) (PEDOT) Doped with Sulfonated Thiophenes. *Electrochim. Acta* **2008**, *53*, 3755–3762. https://doi.org/10.1016/j.electacta.2007.09.010.

(285) Karlsson, R. H.; Herland, A.; Hamedi, M.; Wigenius, J. A.; Åslund, A.; Liu, X.; Fahlman, M.; Inganäs, O.; Konradsson, P. Iron-Catalyzed Polymerization of Alkoxysulfonate-Functionalized 3,4-Ethylenedioxythiophene Gives Water-Soluble Poly(3,4-Ethylenedioxythiophene) of High Conductivity. *Chem. Mater.* **2009**, *21*, 1815–1821. https://doi.org/10.1021/cm801512r.

(286) Yano, H.; Kudo, K.; Marumo, K.; Okuzaki, H. Fully Soluble Self-Doped Poly(3,4-Ethylenedioxythiophene) with an Electrical Conductivity Greater than 1000 S Cm $^{-1}$. *Sci. Adv.* **2019**, *5*, eaav9492. https://doi.org/10.1126/sciadv.aav9492.

(287) Beaumont, C.; Turgeon, J.; Idir, M.; Neusser, D.; Lapointe, R.; Caron, S.; Dupont, W.;

D'Astous, D.; Shamsuddin, S.; Hamza, S.; et al. Water-Processable Self-Doped Conducting Polymers via Direct (Hetero)Arylation Polymerization. *Macromolecules* **2021**, *54*, 5464–5472. https://doi.org/10.1021/acs.macromol.1c00847.

(288) Zeglio, E.; Vagin, M.; Musumeci, C.; Ajjan, F. N.; Gabrielsson, R.; Trinh, X. T.; Son, N. T.; Maziz, A.; Solin, N.; Inganäs, O. Conjugated Polyelectrolyte Blends for Electrochromic and Electrochemical Transistor Devices. *Chem. Mater.* **2015**, *27*, 6385–6393. https://doi.org/10.1021/acs.chemmater.5b02501.

(289) Li, S.; Wan, L.; Chen, L.; Deng, C.; Tao, L.; Lu, Z.; Zhang, W.; Fang, J.; Song, W. Self-Doping a Hole-Transporting Layer Based on a Conjugated Polyelectrolyte Enables Efficient and Stable Inverted Perovskite Solar Cells. *ACS Appl. Energy Mater.* **2020**, *3*, 11724–11731. https://doi.org/10.1021/acsaem.0c01827.

(290) Zhou, H.; Zhang, Y.; Mai, C.-K.; Seifter, J.; Nguyen, T.-Q.; Bazan, G. C.; Heeger, A. J. Solution-Processed PH-Neutral Conjugated Polyelectrolyte Improves Interfacial Contact in Organic Solar Cells. *ACS Nano* **2015**, *9*, 371–377. https://doi.org/10.1021/nn505378m.

(291) Jo, J. W.; Jung, J. W.; Bae, S.; Ko, M. J.; Kim, H.; Jo, W. H.; Jen, A. K.-Y.; Son, H. J. Development of Self-Doped Conjugated Polyelectrolytes with Controlled Work Functions and Application to Hole Transport Layer Materials for High-Performance Organic Solar Cells. *Adv. Mater. Interfaces* **2016**, *3*, 1500703. https://doi.org/10.1002/admi.201500703.

(292) Xu, H.; Zou, H.; Zhou, D.; Zeng, G.; Chen, L.; Liao, X.; Chen, Y. Printable Hole Transport Layer for 1.0 Cm2 Organic Solar Cells. *ACS Appl. Mater. Interfaces* **2020**, *12*, 52028–52037. https://doi.org/10.1021/acsami.0c16124.

(293) Mai, C.; Schlitz, R. A.; Su, G. M.; Spitzer, D.; Wang, X.; Fronk, S. L.; Cahill, D. G.; Chabinyc, M. L.; Bazan, G. C. Side-Chain Effects on the Conductivity, Morphology, and Thermoelectric Properties of Self-Doped Narrow-Band-Gap Conjugated Polyelectrolytes. *J. Am. Chem. Soc.* **2014**, *136*, 13478–13481. https://doi.org/10.1021/ja504284r.

(294) Cao, D. X.; Leifert, D.; Brus, V. V.; Wong, M. S.; Phan, H.; Yurash, B.; Koch, N.; Bazan, G. C.; Nguyen, T.-Q. The Importance of Sulfonate to the Self-Doping Mechanism of the Water-Soluble Conjugated Polyelectrolyte PCPDTBT-SO_3K. *Mater. Chem. Front.* **2020**, *4*, 3556–3566. https://doi.org/10.1039/D0QM00073F.

(295) Mai, C.-K.; Zhou, H.; Zhang, Y.; Henson, Z. B.; Nguyen, T.-Q.; Heeger, A. J.; Bazan, G. C. Facile Doping of Anionic Narrow-Band-Gap Conjugated Polyelectrolytes During

Dialysis. *Angew. Chem. Int. Ed.* **2013**, *52*, 12874–12878. https://doi.org/10.1002/anie.201307667.

(296) Mori, A.; Kubota, C.; Fujita, K.; Hayashi, M.; Ogura, T.; Suzuki, T.; Okano, K.; Funahashi, M.; Horie, M. Thermally Induced Self-Doping of π-Conjugated Polymers Bearing a Pendant Neopentyl Sulfonate Group. *Macromolecules* **2020**, *53*, 1171–1179. https://doi.org/10.1021/acs.macromol.9b02554.

(297) Henson, Z. B.; Zhang, Y.; Nguyen, T.-Q.; Seo, J. H.; Bazan, G. C. Synthesis and Properties of Two Cationic Narrow Band Gap Conjugated Polyelectrolytes. *J. Am. Chem. Soc.* **2013**, *135*, 4163–4166. https://doi.org/10.1021/ja400140d.

(298) Reilly, T. H.; Hains, A. W.; Chen, H. Y.; Gregg, B. A. A Self-Doping, O2-Stable, n-Type Interfacial Layer for Organic Electronics. *Adv. Energy Mater.* **2012**, *2*, 455–460. https://doi.org/10.1002/aenm.201100446.

(299) Wang, Z.; Zheng, N.; Zhang, W.; Yan, H.; Xie, Z.; Ma, Y.; Huang, F.; Cao, Y. Self-Doped, n-Type Perylene Diimide Derivatives as Electron Transporting Layers for High-Efficiency Polymer Solar Cells. *Adv. Energy Mater.* **2017**, *7*, 1700232. https://doi.org/10.1002/aenm.201700232.

(300) Jia, T.; Sun, C.; Xu, R.; Chen, Z.; Yin, Q.; Jin, Y.; Yip, H.-L.; Huang, F.; Cao, Y. Naphthalene Diimide Based N-Type Conjugated Polymers as Efficient Cathode Interfacial Materials for Polymer and Perovskite Solar Cells. *ACS Appl. Mater. Interfaces* **2017**, *9*, 36070–36081. https://doi.org/10.1021/acsami.7b10365.

(301) Powell, D.; Campbell, E. V.; Flannery, L.; Ogle, J.; Soss, S. E.; Whittaker-Brooks, L. Steric Hindrance Dependence on the Spin and Morphology Properties of Highly Oriented Self-Doped Organic Small Molecule Thin Films. *Mater. Adv.* **2021**, *2*, 356–365. https://doi.org/10.1039/D0MA00822B.

(302) Tang, H.; Liu, Z.; Tang, Y.; Du, Z.; Liang, Y.; Hu, Z.; Zhang, K.; Huang, F.; Cao, Y. Organic Diradicals Enabled N-Type Self-Doped Conjugated Polyelectrolyte with High Transparency and Enhanced Conductivity. *Giant* **2021**, *6*, 100053. https://doi.org/10.1016/j.giant.2021.100053.

(303) Li, C.-Z.; Chueh, C.-C.; Yip, H.-L.; O'Malley, K. M.; Chen, W.-C.; Jen, A. K. Y. Effective Interfacial Layer to Enhance Efficiency of Polymer Solar Cells via Solution-Processed Fullerene-Surfactants. *J. Mater. Chem.* **2012**, *22*, 8574. https://doi.org/10.1039/c2jm30755c.

(304) O'Malley, K. M.; Li, C.-Z.; Yip, H.-L.; Jen, A. K. Y. Enhanced Open-Circuit Voltage in High Performance Polymer/Fullerene Bulk-Heterojunction Solar Cells by Cathode

Modification with a C60 Surfactant. *Adv. Energy Mater.* **2012**, *2*, 82–86. https://doi.org/10.1002/aenm.201100522.

(305) Liu, Y.; Sheri, M.; Cole, M. D.; Yu, D. M.; Emrick, T.; Russell, T. P. Transforming Ionene Polymers into Efficient Cathode Interlayers with Pendent Fullerenes. *Angew. Chem. Int. Ed.* **2019**, *58*, 5677–5681. https://doi.org/10.1002/anie.201901536.

(306) Li, C. Z.; Chueh, C. C.; Yip, H. L.; Ding, F.; Li, X.; Jen, A. K. Y. Solution-Processible Highly Conducting Fullerenes. *Adv. Mater.* **2013**, *25*, 2457–2461. https://doi.org/10.1002/adma.201204543.

(307) Liu, J.; Zheng, N.; Hu, Z.; Wang, Z.; Yang, X.; Huang, F.; Cao, Y. Self-Doped n-Type Small Molecular Electron Transport Materials for High-Performance Organic Solar Cells. *Sci. China Chem.* **2017**, *60*, 1136–1144. https://doi.org/10.1007/s11426-017-9057-1.

(308) Kang, Q.; Ye, L.; Xu, B.; An, C.; Stuard, S. J.; Zhang, S.; Yao, H.; Ade, H.; Hou, J. A Printable Organic Cathode Interlayer Enables over 13% Efficiency for 1-Cm^2 Organic Solar Cells. *Joule* **2019**, *3*, 227–239. https://doi.org/10.1016/j.joule.2018.10.024.

(309) Liu, Y.; Cole, M. D.; Jiang, Y.; Kim, P. Y.; Nordlund, D.; Emrick, T.; Russell, T. P. Chemical and Morphological Control of Interfacial Self-Doping for Efficient Organic Electronics. *Adv. Mater.* **2018**, *30*, 1705976. https://doi.org/10.1002/adma.201705976.

(310) Tian, L.; Jing, J.; Tang, H.; Liang, Y.; Hu, Z.; Rafiq, M.; Huang, F.; Cao, Y. Aldol Condensation-Polymerized n -Doped Conjugated Polyelectrolytes for High-Performance Nonfullerene Polymer Solar Cells. *Sol. RRL* **2021**, *5*, 2000523. https://doi.org/10.1002/solr.202000523.

(311) Jin, X.; Wang, Y.; Cheng, X.; Zhou, H.; Hu, L.; Zhou, Y.; Chen, L.; Chen, Y. Fluorine-Induced Self-Doping and Spatial Conformation in Alcohol-Soluble Interlayers for Highly-Efficient Polymer Solar Cells. *J. Mater. Chem. A* **2018**, *6*, 423–433. https://doi.org/10.1039/C7TA08669E.

(312) Yin, X.; Liu, X.; Peng, Y.; Zeng, W.; Zhong, C.; Xie, G.; Wang, L.; Fang, J.; Yang, C. Multichannel Strategies to Produce Stabilized Azaphenalene Diradicals: A Predictable Model to Generate Self-Doped Cathode Interfacial Layers for Organic Photovoltaics. *Adv. Funct. Mater.* **2019**, *29*, 1806125. https://doi.org/10.1002/adfm.201806125.

(313) Yin, X.; Xie, G.; Peng, Y.; Wang, B.; Chen, T.; Li, S.; Zhang, W.; Wang, L.; Yang, C. Self-Doping Cathode Interfacial Material Simultaneously Enabling High Electron Mobility and Powerful Work Function Tunability for High-Efficiency All-Solution-Processed Polymer Light-Emitting Diodes. *Adv. Funct. Mater.* **2017**, *27*, 1700695.

https://doi.org/10.1002/adfm.201700695.

(314) Tang, C. G.; Ang, M. C. Y.; Choo, K. K.; Keerthi, V.; Tan, J. K.; Syafiqah, M. N.; Kugler, T.; Burroughes, J. H.; Png, R. Q.; Chua, L. L.; et al. Doped Polymer Semiconductors with Ultrahigh and Ultralow Work Functions for Ohmic Contacts. *Nature* **2016**, *539*, 536–540. https://doi.org/10.1038/nature20133.

(315) Ricciardulli, A. G.; van der Zee, B.; Philipps, K.; Wetzelaer, G. A. H.; Png, R.-Q.; Ho, P. K. H.; Chua, L.-L.; Blom, P. W. M. Polymer–Perovskite Blend Light-Emitting Diodes Using a Self-Compensated Heavily Doped Polymeric Anode. *APL Mater.* **2020**, *8*, 021101. https://doi.org/10.1063/1.5140519.

(316) Zhao, C.; Tang, C. G.; Seah, Z.-L.; Koh, Q.-M.; Chua, L.-L.; Png, R.-Q.; Ho, P. K. H. Improving Organic Photovoltaic Cells by Forcing Electrode Work Function Well beyond Onset of Ohmic Transition. *Nat. Commun.* **2021**, *12*, 2250. https://doi.org/10.1038/s41467-021-22358-y.

(317) Kroon, R.; Kiefer, D.; Stegerer, D.; Yu, L.; Sommer, M.; Müller, C. Polar Side Chains Enhance Processability, Electrical Conductivity, and Thermal Stability of a Molecularly p-Doped Polythiophene. *Adv. Mater.* **2017**, *29*, 1700930. https://doi.org/10.1002/adma.201700930.

(318) Tripathi, A.; Ko, Y.; Kim, M.; Lee, Y.; Lee, S.; Park, J.; Kwon, Y. W.; Kwak, J.; Woo, H. Y. Optimization of Thermoelectric Properties of Polymers by Incorporating Oligoethylene Glycol Side Chains and Sequential Solution Doping with Preannealing Treatment. *Macromolecules* **2020**, *53*, 7063–7072. https://doi.org/10.1021/acs.macromol.0c01025.

(319) Kiefer, D.; Giovannitti, A.; Sun, H.; Biskup, T.; Hofmann, A.; Koopmans, M.; Cendra, C.; Weber, S.; Anton Koster, L. J.; Olsson, E.; et al. Enhanced N-Doping Efficiency of a Naphthalenediimide-Based Copolymer through Polar Side Chains for Organic Thermoelectrics. *ACS Energy Lett.* **2018**, *3*, 278–285. https://doi.org/10.1021/acsenergylett.7b01146.

(320) Mazaheripour, A.; Thomas, E. M.; Segalman, R. A.; Chabinyc, M. L. Nonaggregating Doped Polymers Based on Poly(3,4-Propylenedioxythiophene). *Macromolecules* **2019**, *52*, 2203–2213. https://doi.org/10.1021/acs.macromol.8b02389.

(321) Ye, G.; Liu, J.; Qiu, X.; Stäter, S.; Qiu, L.; Liu, Y.; Yang, X.; Hildner, R.; Koster, L. J. A.; Chiechi, R. C. Controlling N-Type Molecular Doping via Regiochemistry and Polarity of Pendant Groups on Low Band Gap Donor–Acceptor Copolymers. *Macromolecules* **2021**, *54*, 3886–3896. https://doi.org/10.1021/acs.macromol.1c00317.

(322) Liu, J.; Maity, S.; Roosloot, N.; Qiu, X.; Qiu, L.; Chiechi, R. C.; Hummelen, J. C.; Hauff, E.; Koster, L. J. A. The Effect of Electrostatic Interaction on N-Type Doping Efficiency of Fullerene Derivatives. *Adv. Electron. Mater.* **2019**, *5*, 1800959. https://doi.org/10.1002/aelm.201800959.

(323) Finn, P. A.; Jacobs, I. E.; Armitage, J.; Wu, R.; Paulsen, B. D.; Freeley, M.; Palma, M.; Rivnay, J.; Sirringhaus, H.; Nielsen, C. B. Effect of Polar Side Chains on Neutral and P-Doped Polythiophene. *J. Mater. Chem. C* **2020**, *8*, 16216–16223. https://doi.org/10.1039/D0TC04290K.

(324) Dong, B. X.; Nowak, C.; Onorato, J. W.; Ma, T.; Niklas, J.; Poluektov, O. G.; Grocke, G.; DiTusa, M. F.; Escobedo, F. A.; Luscombe, C. K.; et al. Complex Relationship between Side-Chain Polarity, Conductivity, and Thermal Stability in Molecularly Doped Conjugated Polymers. *Chem. Mater.* **2021**, *33*, 741–753. https://doi.org/10.1021/acs.chemmater.0c04153.

(325) Liu, J.; Qiu, L.; Portale, G.; Koopmans, M.; ten Brink, G.; Hummelen, J. C.; Koster, L. J. A. N-Type Organic Thermoelectrics: Improved Power Factor by Tailoring Host-Dopant Miscibility. *Adv. Mater.* **2017**, *29*, 1701641. https://doi.org/10.1002/adma.201701641.

(326) Liu, J.; Qiu, L.; Portale, G.; Torabi, S.; Stuart, M. C. A.; Qiu, X.; Koopmans, M.; Chiechi, R. C.; Hummelen, J. C.; Anton Koster, L. J. Side-Chain Effects on N-Type Organic Thermoelectrics: A Case Study of Fullerene Derivatives. *Nano Energy* **2018**, *52*, 183–191. https://doi.org/10.1016/j.nanoen.2018.07.056.

(327) Liu, J.; Garman, M. P.; Dong, J.; van der Zee, B.; Qiu, L.; Portale, G.; Hummelen, J. C.; Koster, L. J. A. Doping Engineering Enables Highly Conductive and Thermally Stable N-Type Organic Thermoelectrics with High Power Factor. *ACS Appl. Energy Mater.* **2019**, *2*, 6664–6671. https://doi.org/10.1021/acsaem.9b01179.

(328) Liu, J.; Ye, G.; Potgieser, H. G. O.; Koopmans, M.; Sami, S.; Nugraha, M. I.; Villalva, D. R.; Sun, H.; Dong, J.; Yang, X.; et al. Amphipathic Side Chain of a Conjugated Polymer Optimizes Dopant Location toward Efficient N-Type Organic Thermoelectrics. *Adv. Mater.* **2021**, *33*, 2006694. https://doi.org/10.1002/adma.202006694.

(329) Li, J.; Rochester, C. W.; Jacobs, I. E.; Aasen, E. W.; Friedrich, S.; Stroeve, P.; Moulé, A. J. The Effect of Thermal Annealing on Dopant Site Choice in Conjugated Polymers. *Org. Electron.* **2016**, *33*, 23–31. https://doi.org/10.1016/j.orgel.2016.02.029.

(330) Watts, K. E.; Neelamraju, B.; Moser, M.; McCulloch, I.; Ratcliff, E. L.; Pemberton, J. E. Thermally Induced Formation of HF4TCNQ^{-} in F4TCNQ-Doped Regioregular

P3HT. *J. Phys. Chem. Lett.* **2020**, *11*, 6586–6592. https://doi.org/10.1021/acs.jpclett.0c01673.

(331) Vijayakumar, V.; Zaborova, E.; Biniek, L.; Zeng, H.; Herrmann, L.; Carvalho, A.; Boyron, O.; Leclerc, N.; Brinkmann, M. Effect of Alkyl Side Chain Length on Doping Kinetics, Thermopower, and Charge Transport Properties in Highly Oriented F_4TCNQ-Doped PBTTT Films. *ACS Appl. Mater. Interfaces* **2019**, *11*, 4942–4953. https://doi.org/10.1021/acsami.8b17594.

(332) Li, B.; Li, X.; Yang, F.; Chen, Y.; Mao, X.; Wan, S.; Xin, H.; Yan, S.; Wang, M.; Gao, C.; et al. Enhanced Thermoelectric Performance of a Donor–Acceptor-Based Two-Dimensional Conjugated Polymer with High Crystallinity. *ACS Appl. Energy Mater.* **2021**, *4*, 4662–4671. https://doi.org/10.1021/acsaem.1c00274.

(333) Li, H.; DeCoster, M. E.; Ming, C.; Wang, M.; Chen, Y.; Hopkins, P. E.; Chen, L.; Katz, H. E. Enhanced Molecular Doping for High Conductivity in Polymers with Volume Freed for Dopants. *Macromolecules* **2019**, *52*, 9804–9812. https://doi.org/10.1021/acs.macromol.9b02048.

(334) Thomas, E. M.; Davidson, E. C.; Katsumata, R.; Segalman, R. A.; Chabinyc, M. L. Branched Side Chains Govern Counterion Position and Doping Mechanism in Conjugated Polythiophenes. *ACS Macro Lett.* **2018**, *7*, 1492–1497. https://doi.org/10.1021/acsmacrolett.8b00778.

(335) Dexter Tam, T. L.; Ng, C. K.; Lim, S. L.; Yildirim, E.; Ko, J.; Leong, W. L.; Yang, S.-W.; Xu, J. Proquinoidal-Conjugated Polymer as an Effective Strategy for the Enhancement of Electrical Conductivity and Thermoelectric Properties. *Chem. Mater.* **2019**, *31*, 8543–8550. https://doi.org/10.1021/acs.chemmater.9b03684.

(336) Cassinelli, M.; Cimò, S.; Biskup, T.; Jiao, X.; Luzio, A.; McNeill, C. R.; Noh, Y.; Kim, Y.; Bertarelli, C.; Caironi, M. Enhanced N-Type Doping of a Naphthalene Diimide Based Copolymer by Modification of the Donor Unit. *Adv. Electron. Mater.* **2021**, 2100407. https://doi.org/10.1002/aelm.202100407.

(337) Li, H.; Song, J.; Xiao, J.; Wu, L.; Katz, H. E.; Chen, L. Synergistically Improved Molecular Doping and Carrier Mobility by Copolymerization of Donor–Acceptor and Donor–Donor Building Blocks for Thermoelectric Application. *Adv. Funct. Mater.* **2020**, *30*, 2004378. https://doi.org/10.1002/adfm.202004378.

(338) Dong, C.; Meng, B.; Liu, J.; Wang, L. B ← N Unit Enables N-Doping of Conjugated Polymers for Thermoelectric Application. *ACS Appl. Mater. Interfaces* **2020**, *12*, 10428–10433. https://doi.org/10.1021/acsami.9b21527.

(339) Naab, B. D.; Gu, X.; Kurosawa, T.; To, J. W. F.; Salleo, A.; Bao, Z. Role of Polymer Structure on the Conductivity of N-Doped Polymers. *Adv. Electron. Mater.* **2016**, *2*, 1600004. https://doi.org/10.1002/aelm.201600004.

(340) Wang, S.; Sun, H.; Erdmann, T.; Wang, G.; Fazzi, D.; Lappan, U.; Puttisong, Y.; Chen, Z.; Berggren, M.; Crispin, X.; et al. A Chemically Doped Naphthalenediimide-Bithiazole Polymer for n-Type Organic Thermoelectrics. *Adv. Mater.* **2018**, *30*, 1801898. https://doi.org/10.1002/adma.201801898.

(341) Liu, J.; Ye, G.; Zee, B. van der; Dong, J.; Qiu, X.; Liu, Y.; Portale, G.; Chiechi, R. C.; Koster, L. J. A. N-Type Organic Thermoelectrics of Donor-Acceptor Copolymers: Improved Power Factor by Molecular Tailoring of the Density of States. *Adv. Mater.* **2018**, *30*, 1804290. https://doi.org/10.1002/adma.201804290.

(342) Liu, J.; Shi, Y.; Dong, J.; Nugraha, M. I.; Qiu, X.; Su, M.; Chiechi, R. C.; Baran, D.; Portale, G.; Guo, X.; et al. Overcoming Coulomb Interaction Improves Free-Charge Generation and Thermoelectric Properties for n-Doped Conjugated Polymers. *ACS Energy Lett.* **2019**, *4*, 1556–1564. https://doi.org/10.1021/acsenergylett.9b00977.

(343) Wang, S.; Fazzi, D.; Puttisong, Y.; Jafari, M. J.; Chen, Z.; Ederth, T.; Andreasen, J. W.; Chen, W. M.; Facchetti, A.; Fabiano, S. Effect of Backbone Regiochemistry on Conductivity, Charge Density, and Polaron Structure of n-Doped Donor–Acceptor Polymers. *Chem. Mater.* **2019**, *31*, 3395–3406. https://doi.org/10.1021/acs.chemmater.9b00558.

(344) Shin, Y.; Massetti, M.; Komber, H.; Biskup, T.; Nava, D.; Lanzani, G.; Caironi, M.; Sommer, M. Improving Miscibility of a Naphthalene Diimide-Bithiophene Copolymer with n-Type Dopants through the Incorporation of "Kinked" Monomers. *Adv. Electron. Mater.* **2018**, *4*, 1700581. https://doi.org/10.1002/aelm.201700581.

(345) Lu, Y.; Yu, Z.; Un, H.; Yao, Z.; You, H.; Jin, W.; Li, L.; Wang, Z.; Dong, B.; Barlow, S.; et al. Persistent Conjugated Backbone and Disordered Lamellar Packing Impart Polymers with Efficient N-Doping and High Conductivities. *Adv. Mater.* **2021**, *33*, 2005946. https://doi.org/10.1002/adma.202005946.

(346) Gregory, S. A.; Menon, A. K.; Ye, S.; Seferos, D. S.; Reynolds, J. R.; Yee, S. K. Effect of Heteroatom and Doping on the Thermoelectric Properties of Poly(3-alkylchalcogenophenes). *Adv. Energy Mater.* **2018**, *8*, 1802419. https://doi.org/10.1002/aenm.201802419.

(347) Gordon, M. P.; Gregory, S. A.; Wooding, J. P.; Ye, S.; Su, G. M.; Seferos, D. S.; Losego, M. D.; Urban, J. J.; Yee, S. K.; Menon, A. K. Microstructure and Heteroatom Dictate

the Doping Mechanism and Thermoelectric Properties of Poly(Alkyl-Chalcogenophenes). *Appl. Phys. Lett.* **2021**, *118*, 233301. https://doi.org/10.1063/5.0052604.

(348) Scholes, D. T.; Yee, P. Y.; McKeown, G. R.; Li, S.; Kang, H.; Lindemuth, J. R.; Xia, X.; King, S. C.; Seferos, D. S.; Tolbert, S. H.; et al. Designing Conjugated Polymers for Molecular Doping: The Roles of Crystallinity, Swelling, and Conductivity in Sequentially-Doped Selenophene-Based Copolymers. *Chem. Mater.* **2019**, *31*, 73–82. https://doi.org/10.1021/acs.chemmater.8b02648.

(349) Nava, D.; Shin, Y.; Massetti, M.; Jiao, X.; Biskup, T.; Jagadeesh, M. S.; Calloni, A.; Duò, L.; Lanzani, G.; McNeill, C. R.; et al. Drastic Improvement of Air Stability in an N-Type Doped Naphthalene-Diimide Polymer by Thionation. *ACS Appl. Energy Mater.* **2018**, *1*, 4626–4634. https://doi.org/10.1021/acsaem.8b00777.

(350) Welch, G. C.; Bazan, G. C. Lewis Acid Adducts of Narrow Band Gap Conjugated Polymers. *J. Am. Chem. Soc.* **2011**, *133*, 4632–4644. https://doi.org/10.1021/ja110968m.

(351) Kaake, L. G.; Zou, Y.; Panzer, M. J.; Frisbie, C. D.; Zhu, X. Y. Vibrational Spectroscopy Reveals Electrostatic and Electrochemical Doping in Organic Thin Film Transistors Gated with a Polymer Electrolyte Dielectric. *J. Am. Chem. Soc.* **2007**, *129*, 7824–7830. https://doi.org/10.1021/ja070615x.

(352) Perevedentsev, A.; Campoy-Quiles, M. Rapid and High-Resolution Patterning of Microstructure and Composition in Organic Semiconductors Using 'Molecular Gates.' *Nat. Commun.* **2020**, *11*, 3610. https://doi.org/10.1038/s41467-020-17361-8.

(353) Mansour, A. E.; Lungwitz, D.; Schultz, T.; Arvind, M.; Valencia, A. M.; Cocchi, C.; Opitz, A.; Neher, D.; Koch, N. The Optical Signatures of Molecular-Doping Induced Polarons in Poly(3-Hexylthiophene-2,5-Diyl): Individual Polymer Chains: Versus Aggregates. *J. Mater. Chem. C* **2020**, *8*, 2870–2879. https://doi.org/10.1039/c9tc06509a.

(354) Murrey, T. L.; Riley, M. A.; Gonel, G.; Antonio, D. D.; Filardi, L.; Shevchenko, N.; Mascal, M.; Moulé, A. J. Anion Exchange Doping: Tuning Equilibrium to Increase Doping Efficiency in Semiconducting Polymers. *J. Phys. Chem. Lett.* **2021**, *12*, 1284–1289. https://doi.org/10.1021/acs.jpclett.0c03620.

(355) Sahalianov, I.; Hynynen, J.; Barlow, S.; Marder, S. R.; Müller, C.; Zozoulenko, I. UV-to-IR Absorption of Molecularly p-Doped Polythiophenes with Alkyl and Oligoether Side Chains: Experiment and Interpretation Based on Density Functional Theory. *J.*

Phys. Chem. B **2020**, *124*, 11280–11293. https://doi.org/10.1021/acs.jpcb.0c08757.

(356) Amsalem, P.; Wilke, A.; Frisch, J.; Niederhausen, J.; Vollmer, A.; Rieger, R.; Müllen, K.; Rabe, J. P.; Koch, N. Interlayer Molecular Diffusion and Thermodynamic Equilibrium in Organic Heterostructures on a Metal Electrode. *J. Appl. Phys.* **2011**, *110*, 113709. https://doi.org/10.1063/1.3662878.

(357) Biskup, T. Structure–Function Relationship of Organic Semiconductors: Detailed Insights From Time-Resolved EPR Spectroscopy. *Front. Chem*. **2019**, *7*, 10. https://doi.org/10.3389/fchem.2019.00010.

(358) Tsutsui, Y.; Okamoto, H.; Sakamaki, D.; Sugiyasu, K.; Takeuchi, M.; Seki, S. Landscape of Charge Carrier Transport in Doped Poly(3-Hexylthiophene): Noncontact Approach Using Ternary Combined Dielectric, Paramagnetic, and Optical Spectroscopies. *J. Phys. Chem. Lett.* **2018**, *9*, 3639–3645. https://doi.org/10.1021/acs.jpclett.8b01465.

(359) Kirchartz, T.; Gong, W.; Hawks, S. A.; Agostinelli, T.; MacKenzie, R. C. I.; Yang, Y.; Nelson, J. Sensitivity of the Mott-Schottky Analysis in Organic Solar Cells. *J. Phys. Chem. C* **2012**, *116*, 7672–7680. https://doi.org/10.1021/jp300397f.

(360) Kokil, A.; Yang, K.; Kumar, J. Techniques for Characterization of Charge Carrier Mobility in Organic Semiconductors. *J. Polym. Sci.* **2012**, *50*, 1130– 1144. https://doi.org/10.1002/polb.23103.

(361) Tiwari, S.; Greenham, N. C. Charge Mobility Measurement Techniques in Organic Semiconductors. *Opt Quant Electron*. **2009**, *41*, 69–89. https://doi.org/10.1007/s11082-009-9323-0.

(362) Bao, Z.; Lovinger, A. J.; Dodabalapur, A. Organic Field-effect Transistors with High Mobility Based on Copper Phthalocyanine. *Appl. Phys. Lett.* **1996**, *69*, 3066–3068. https://doi.org/10.1063/1.116841.

(363) Paterson, A. F.; Singh, S.; Fallon, K. J.; Hodsden, T.; Han, Y.; Schroeder, B. C.; Bronstein, H.; Heeney, M.; McCulloch, I.; Anthopoulos, T. D. Recent Progress in High-Mobility Organic Transistors: A Reality Check. *Adv. Mater.* **2018**, *30*, 1801079. https://doi.org/doi:10.1002/adma.201801079.

(364) Choi, H. H.; Cho, K.; Frisbie, C. D.; Sirringhaus, H.; Podzorov, V. Critical Assessment of Charge Mobility Extraction in FETs. *Nat. Mater.* **2017**, *17*, 2-7. https://doi.org/10.1038/nmat5035.

(365) Bittle, E. G.; Basham, J. I.; Jackson, T. N.; Jurchescu, O. D.; Gundlach, D. J. Mobility Overestimation Due to Gated Contacts in Organic Field-Effect Transistors. *Nat.*

Commun. **2016**, *7*, 10908. https://doi.org/10.1038/ncomms10908.

(366) Liu, C.; Li, G.; Di Pietro, R.; Huang, J.; Noh, Y.-Y.; Liu, X.; Minari, T. Device Physics of Contact Issues for the Overestimation and Underestimation of Carrier Mobility in Field-Effect Transistors. *Phys. Rev. Appl.* **2017**, *8*, 34020. https://doi.org/10.1103/PhysRevApplied.8.034020.

(367) Blakesley, J. C.; Castro, F. A.; Kylberg, W.; Dibb, G. F. A.; Arantes, C.; Valaski, R.; Cremona, M.; Kim, J. S.; Kim, J.-S. Towards Reliable Charge-Mobility Benchmark Measurements for Organic Semiconductors. *Org. Electron.* **2014**, *15*, 1263–1272. https://doi.org/10.1016/j.orgel.2014.02.008.

(368) Tanase, C.; Meijer, E. J.; Blom, P. W. M.; de Leeuw, D. M. Unification of the Hole Transport in Polymeric Field-Effect Transistors and Light-Emitting Diodes. *Phys. Rev. Lett.* **2003**, *91*, 216601. https://doi.org/10.1103/PhysRevLett.91.216601.

(369) Deledalle, F.; Shakya Tuladhar, P.; Nelson, J.; Durrant, J. R.; Kirchartz, T. Understanding the Apparent Charge Density Dependence of Mobility and Lifetime in Organic Bulk Heterojunction Solar Cells. *J. Phys. Chem. C* **2014**, *118*, 8837–8842. https://doi.org/10.1021/jp502948y.

(370) Pasveer, W. F.; Cottaar, J.; Tanase, C.; Coehoorn, R.; Bobbert, P. A.; Blom, P. W. M.; de Leeuw, D. M.; Michels, M. A. J. Unified Description of Charge-Carrier Mobilities in Disordered Semiconducting Polymers. *Phys. Rev. Lett.* **2005**, *94*, 206601. https://doi.org/10.1103/PhysRevLett.94.206601.

(371) Röhr, J. A.; Kirchartz, T.; Nelson, J. On the Correct Interpretation of the Low Voltage Regime in Intrinsic Single-Carrier Devices. *J. Phys. Condens. Matter* **2017**, *29*. https://doi.org/10.1088/1361-648X/aa66cc.

(372) Juška, G.; Arlauskas, K.; Viliunas, M.; Kočka, J. Extraction Current Transients: New Method of Study of Charge Transport in Microcrystalline Silicon. *Phys. Rev. Lett.* **2000**, *84*, 4946. https://doi.org/10.1103/PhysRevLett.84.4946.

(373) Sandberg, O. J.; Nyman, M.; Österbacka, R. Direct Determination of Doping Concentration and Built-in Voltage from Extraction Current Transients. *Org. Electron.* **2014**, *15*, 3413–3420. https://doi.org/10.1016/j.orgel.2014.09.027.

(374) Fujimoto, R.; Yamashita, Y.; Kumagai, S.; Tsurumi, J.; Hinderhofer, A.; Broch, K.; Schreiber, F.; Watanabe, S.; Takeya, J. Molecular Doping in Organic Semiconductors: Fully Solution-Processed, Vacuum-Free Doping with Metal-Organic Complexes in an Orthogonal Solvent. *J. Mater. Chem. C* **2017**, *5*, 12023–12030. https://doi.org/10.1039/c7tc03905k.

(375) Ohashi, C.; Izawa, S.; Shinmura, Y.; Kikuchi, M.; Watase, S.; Izaki, M.; Naito, H.; Hiramoto, M. Hall Effect in Bulk-Doped Organic Single Crystals. *Adv. Mater.* **2017**, *29*. https://doi.org/10.1002/adma.201605619.

(376) Zapata-Arteaga, O.; Dörling, B.; Perevedentsev, A.; Martín, J.; Reparaz, J. S.; Campoy-Quiles, M. Closing the Stability–Performance Gap in Organic Thermoelectrics by Adjusting the Partial to Integer Charge Transfer Ratio. *Macromolecules* **2020**, *53*, 609–620. https://doi.org/10.1021/acs.macromol.9b02263.

(377) Neelamraju, B.; Watts, K. E.; Pemberton, J. E.; Ratcliff, E. L. Correlation of Coexistent Charge Transfer States in F4TCNQ-Doped P3HT with Microstructure. *J. Phys. Chem. Lett.* **2018**, *9*, 6871–6877. https://doi.org/10.1021/acs.jpclett.8b03104.

(378) Yee, P. Y.; Scholes, D. T.; Schwartz, B. J.; Tolbert, S. H. Dopant-Induced Ordering of Amorphous Regions in Regiorandom P3HT. *J. Phys. Chem. Lett.* **2019**, *10*, 4929–4934. https://doi.org/10.1021/acs.jpclett.9b02070.

(379) Bagchi, K.; Ediger, M. D. Controlling Structure and Properties of Vapor-Deposited Glasses of Organic Semiconductors: Recent Advances and Challenges. *J. Phys. Chem. Lett.* **2020**, *11*, 6935–6945. https://doi.org/10.1021/acs.jpclett.0c01682.

(380) Patel, S. N.; Glaudell, A. M.; Peterson, K. A.; Thomas, E. M.; O'Hara, K. A.; Lim, E.; Chabinyc, M. L. Morphology Controls the Thermoelectric Power Factor of a Doped Semiconducting Polymer. *Sci. Adv.* **2017**, *3*, 24–26. https://doi.org/10.1126/sciadv.1700434.

(381) Jacobs, I. E.; Aasen, E. W.; Oliveira, J. L.; Fonseca, T. N.; Roehling, J. D.; Li, J.; Zhang, G.; Augustine, M. P.; Mascal, M.; Moulé, A. J. Comparison of Solution-Mixed and Sequentially Processed P3HT:F4TCNQ Films: Effect of Doping-Induced Aggregation on Film Morphology. *J. Mater. Chem. C* **2016**, *4*, 3454–3466. https://doi.org/10.1039/c5tc04207k.

(382) Patel, S. N.; Chabinyc, M. L. Anisotropies and the Thermoelectric Properties of Semiconducting Polymers. *J. Appl. Polym. Sci.* **2017**, *134*, 44403. https://doi.org/10.1002/app.44403.

(383) Glaudell, A. M.; Cochran, J. E.; Patel, S. N.; Chabinyc, M. L. Impact of the Doping Method on Conductivity and Thermopower in Semiconducting Polythiophenes. *Adv. Energy Mater.* **2015**, *5*, 1401072. https://doi.org/10.1002/aenm.201401072.

(384) Cochran, J. E.; Junk, M. J. N.; Glaudell, A. M.; Miller, P. L.; Cowart, J. S.; Toney, M. F.; Hawker, C. J.; Chmelka, B. F.; Chabinyc, M. L. Molecular Interactions and Ordering in Electrically Doped Polymers: Blends of PBTTT and F4TCNQ. *Macromolecules*

2014, *47*, 6836–6846. https://doi.org/10.1021/ma501547h.

(385) Hase, H.; O'Neill, K.; Frisch, J.; Opitz, A.; Koch, N.; Salzmann, I. Unraveling the Microstructure of Molecularly Doped Poly(3-Hexylthiophene) by Thermally Induced Dedoping. *J. Phys. Chem. C* **2018**, *122*, 25893–25899. https://doi.org/10.1021/acs.jpcc.8b08591.

(386) Hamidi-Sakr, A.; Biniek, L.; Bantignies, J. L.; Maurin, D.; Herrmann, L.; Leclerc, N.; Lévêque, P.; Vijayakumar, V.; Zimmermann, N.; Brinkmann, M. A Versatile Method to Fabricate Highly In-Plane Aligned Conducting Polymer Films with Anisotropic Charge Transport and Thermoelectric Properties: The Key Role of Alkyl Side Chain Layers on the Doping Mechanism. *Adv. Funct. Mater.* **2017**, *27*, 1700173. https://doi.org/10.1002/adfm.201700173.

(387) Mun, J.; Kang, J.; Zheng, Y.; Luo, S.; Wu, Y.; Gong, H.; Lai, J.-C.; Wu, H.-C.; Xue, G.; Tok, J. B.-H.; et al. F4-TCNQ as an Additive to Impart Stretchable Semiconductors with High Mobility and Stability. *Adv. Electron. Mater.* **2020**, *6*, 2000251. https://doi.org/10.1002/aelm.202000251.

(388) Jiang, C.; Saha, A.; Young, C. C.; Hashim, D. P.; Ramirez, C. E.; Ajayan, P. M.; Pasquali, M.; Martí, A. A. Macroscopic Nanotube Fibers Spun from Single-Walled Carbon Nanotube Polyelectrolytes. *ACS Nano* **2014**, *8*, 9107–9112. https://doi.org/10.1021/nn502552q.

(389) Kroon, R.; Ryan, J. D.; Kiefer, D.; Yu, L.; Hynynen, J.; Olsson, E.; Müller, C. Bulk Doping of Millimeter-Thick Conjugated Polymer Foams for Plastic Thermoelectrics. *Adv. Funct. Mater.* **2017**, *27*, 1704183. https://doi.org/10.1002/adfm.201704183.

(390) Abdallah, F.; Ciammaruchi, L.; Jiménez-Arguijo, A.; Duraia, E.-S. M.; Ragab, H. S.; Dörling, B.; Campoy-Quiles, M. Investigating Thermoelectric Stability under Encapsulation Using PEI-Doped CNT Films as a Model System. *Adv. Mater. Technol.* **2020**, *5*, 2000256. https://doi.org/10.1002/admt.202000256.

(391) DeLongchamp, D. M.; Kline, R. J.; Jung, Y.; Lin, E. K.; Fischer, D. A.; Gundlach, D. J.; Cotts, S. K.; Moad, A. J.; Richter, L. J.; Toney, M. F.; et al. Molecular Basis of Mesophase Ordering in a Thiophene-Based Copolymer. *Macromolecules* **2008**, *41*, 5709–5715. https://doi.org/10.1021/ma800440f.

(392) Verploegen, E.; Miller, C. E.; Schmidt, K.; Bao, Z.; Toney, M. F. Manipulating the Morphology of P3HT–PCBM Bulk Heterojunction Blends with Solvent Vapor Annealing. *Chem. Mater.* **2012**, *24*, 3923–3931. https://doi.org/10.1021/cm302312a.

(393) Qu, S.; Yao, Q.; Wang, L.; Chen, Z.; Xu, K.; Zeng, H.; Shi, W.; Zhang, T.; Uher, C.;

Chen, L. Highly Anisotropic P3HT Films with Enhanced Thermoelectric Performance via Organic Small Molecule Epitaxy. *NPG Asia Mater.* **2016**, *8*, e292–e292. https://doi.org/10.1038/am.2016.97.

(394) Hynynen, J.; Kiefer, D.; Müller, C. Influence of Crystallinity on the Thermoelectric Power Factor of P3HT Vapour-Doped with F4TCNQ. *RSC Adv.* **2018**, *8*, 1593–1599. https://doi.org/10.1039/C7RA11912G.

(395) Li, J.; Rochester, C. W.; Jacobs, I. E.; Friedrich, S.; Stroeve, P.; Riede, M.; Moulé, A. J. Measurement of Small Molecular Dopant F4TCNQ and C60F36 Diffusion in Organic Bilayer Architectures. *ACS Appl. Mater. Interfaces* **2015**, *7*, 28420–28428. https://doi.org/10.1021/acsami.5b09216.

(396) Culebras, M.; Uriol, B.; Gómez, C. M.; Cantarero, A. Controlling the Thermoelectric Properties of Polymers: Application to PEDOT and Polypyrrole. *Phys. Chem. Chem. Phys.* **2015**, *17*, 15140–15145. https://doi.org/10.1039/C5CP01940K.

(397) Thomas, E. M.; Brady, M. A.; Nakayama, H.; Popere, B. C.; Segalman, R. A.; Chabinyc, M. L. X-Ray Scattering Reveals Ion-Induced Microstructural Changes During Electrochemical Gating of Poly(3-Hexylthiophene). *Adv. Funct. Mater.* **2018**, *28*, 1803687. https://doi.org/10.1002/adfm.201803687.

(398) Scholes, D. T.; Yee, P. Y.; Lindemuth, J. R.; Kang, H.; Onorato, J.; Ghosh, R.; Luscombe, C. K.; Spano, F. C.; Tolbert, S. H.; Schwartz, B. J. The Effects of Crystallinity on Charge Transport and the Structure of Sequentially Processed F4TCNQ-Doped Conjugated Polymer Films. *Adv. Funct. Mater.* **2017**, *27*, 1702654. https://doi.org/10.1002/adfm.201702654.

(399) Chew, A. R.; Ghosh, R.; Shang, Z.; Spano, F. C.; Salleo, A. Sequential Doping Reveals the Importance of Amorphous Chain Rigidity in Charge Transport of Semi-Crystalline Polymers. *J. Phys. Chem. Lett.* **2017**, *8*, 4974–4980. https://doi.org/10.1021/acs.jpclett.7b01989.

(400) Neusser, D.; Malacrida, C.; Kern, M.; Gross, Y. M.; van Slageren, J.; Ludwigs, S. High Conductivities of Disordered P3HT Films by an Electrochemical Doping Strategy. *Chem. Mater.* **2020**, *32*, 6003–6013. https://doi.org/10.1021/acs.chemmater.0c01293.

(401) Kaloni, T. P.; Giesbrecht, P. K.; Schreckenbach, G.; Freund, M. S. Polythiophene: From Fundamental Perspectives to Applications. *Chem. Mater.* **2017**, *29*, 10248–10283. https://doi.org/10.1021/acs.chemmater.7b03035.

(402) Rivnay, J.; Inal, S.; Salleo, A.; Owens, R. M.; Berggren, M.; Malliaras, G. G. Organic Electrochemical Transistors. *Nat. Rev. Mater.* **2018**, *3*, 17086.

https://doi.org/10.1038/natrevmats.2017.86.

(403) Shirakawa, H.; Louis, E. J.; MacDiarmid, A. G.; Chiang, C. K.; Heeger, A. J. Synthesis of Electrically Conducting Organic Polymers: Halogen Derivatives of Polyacetylene, (CH). *J. Chem. Soc. Chem. Commun.* **1977**, *16*, 578–580. https://doi.org/10.1039/C39770000578.

(404) Singh, S.; Mohapatra, S. K.; Sharma, A.; Fuentes-Hernandez, C.; Barlow, S.; Marder, S. R.; Kippelen, B. Reduction of Contact Resistance by Selective Contact Doping in Fullerene N-Channel Organic Field-Effect Transistors. *Appl. Phys. Lett.* **2013**, *102*, 153303. https://doi.org/10.1063/1.4802237.

(405) Hou, J. L.; Kasemann, D.; Widmer, J.; Günther, A. A.; Lüssem, B.; Leo, K. Reduced Contact Resistance in Top-Contact Organic Field-Effect Transistors by Interface Contact Doping. *Appl. Phys. Lett.* **2016**, *108*, 103303. https://doi.org/10.1063/1.4943646.

(406) Jacobs, I. E.; Aasen, E. W.; Nowak, D.; Li, J.; Morrison, W.; Roehling, J. D.; Augustine, M. P.; Moulé, A. J. Direct-Write Optical Patterning of P3HT Films Beyond the Diffraction Limit. *Adv. Mater.* **2017**, *29*, 1603221. https://doi.org/10.1002/adma.201603221.

(407) Jacobs, I. E.; Wang, F.; Hafezi, N.; Medina-Plaza, C.; Harrelson, T. F.; Li, J.; Augustine, M. P.; Mascal, M.; Moulé, A. J. Quantitative Dedoping of Conductive Polymers. *Chem. Mater.* **2017**, *29*, 832–841. https://doi.org/10.1021/acs.chemmater.6b04880.

(408) Kang, K.; Watanabe, S.; Broch, K.; Sepe, A.; Brown, A.; Nasrallah, I.; Nikolka, M.; Fei, Z.; Heeney, M.; Matsumoto, D.; et al. 2D Coherent Charge Transport in Highly Ordered Conducting Polymers Doped by Solid State Diffusion. *Nat. Mater.* **2016**, *15*, 896-902. https://doi.org/10.1038/nmat4634.

(409) Lim, E.; Glaudell, A. M.; Miller, R.; Chabinyc, M. L. The Role of Ordering on the Thermoelectric Properties of Blends of Regioregular and Regiorandom Poly(3-Hexylthiophene). *Adv. Electron. Mater.* **2019**, *5*, 1800915. https://doi.org/10.1002/aelm.201800915.

(410) Vijayakumar, V.; Zhong, Y.; Untilova, V.; Bahri, M.; Herrmann, L.; Biniek, L.; Leclerc, N.; Brinkmann, M. Bringing Conducting Polymers to High Order: Toward Conductivities beyond 10^5 S cm^{-1} and Thermoelectric Power Factors of 2 mW m^{-1} K^{-2}. *Adv. Energy Mater.* **2019**, *9*, 1900266. https://doi.org/10.1002/aenm.201900266.

(411) Jacobs, I. E.; D'Avino, G.; Lin, Y.; Lemaur, V.; Huang, Y.; Ren, X.; Simatos, D.; Wood, W.; Chen, C.; Harrelson, T.; et al. Ion-Exchange Doped Polymers at the Degenerate

Limit: What Limits Conductivity at 100% Doping Efficiency? arXiv:2101.01714. arXiv.org e-Print archive, Jan 5, 2021. https://arxiv.org/abs/2101.01714 (accessed Oct 22, 2021).

(412) Dörling, B.; Zapata-Arteaga, O.; Campoy-Quiles, M. A Setup to Measure the Seebeck Coefficient and Electrical Conductivity of Anisotropic Thin-Films on a Single Sample. *Rev. Sci. Instrum.* **2020**, *91*, 105111. https://doi.org/10.1063/5.0021715.

(413) Yamashita, Y.; Tsurumi, J.; Ohno, M.; Fujimoto, R.; Kumagai, S.; Kurosawa, T.; Okamoto, T.; Takeya, J.; Watanabe, S. Efficient Molecular Doping of Polymeric Semiconductors Driven by Anion Exchange. *Nature* **2019**, *572*, 634–638. https://doi.org/10.1038/s41586-019-1504-9.

(414) Kroon, R.; Mengistie, D. A.; Kiefer, D.; Hynynen, J.; Ryan, J. D.; Yu, L.; Müller, C. Thermoelectric Plastics: From Design to Synthesis, Processing and Structure–Property Relationships. *Chem. Soc. Rev.* **2016**. *45*, 6147. https://doi.org/10.1039/C6CS00149A.

(415) Russ, B.; Glaudell, A.; Urban, J. J.; Chabinyc, M. L.; Segalman, R. A. Organic Thermoelectric Materials for Energy Harvesting and Temperature Control. *Nat. Rev. Mater.* **2016**, *1*, 16050. https://doi.org/10.1038/natrevmats.2016.50.

(416) Lund, A.; Tian, Y.; Darabi, S.; Müller, C. A Polymer-Based Textile Thermoelectric Generator for Wearable Energy Harvesting. *J. Power Sources* **2020**, *480*, 228836. https://doi.org/10.1016/j.jpowsour.2020.228836.

(417) Li, J.; Koshnick, C.; Diallo, S. O.; Ackling, S.; Huang, D. M.; Jacobs, I. E.; Harrelson, T. F.; Hong, K.; Zhang, G.; Beckett, J.; et al. Quantitative Measurements of the Temperature-Dependent Microscopic and Macroscopic Dynamics of a Molecular Dopant in a Conjugated Polymer. *Macromolecules* **2017**, *50*, 5476–5489. https://doi.org/10.1021/acs.macromol.7b00672.

(418) Hynynen, J.; Järsvall, E.; Kroon, R.; Zhang, Y.; Barlow, S.; Marder, S. R.; Kemerink, M.; Lund, A.; Müller, C. Enhanced Thermoelectric Power Factor of Tensile Drawn Poly(3-Hexylthiophene). *ACS Macro Lett.* **2019**, *8*, 70–76. https://doi.org/10.1021/acsmacrolett.8b00820.

(419) Moulton, J.; Smith, P. Electrical and Mechanical Properties of Oriented Poly(3-Alkylthiophenes): 2. Effect of Side-Chain Length. *Polymer.* **1992**, *33*, 2340–2347. https://doi.org/10.1016/0032-3861(92)90525-2.

(420) Fanous, J.; Schweizer, M.; Schawaller, D.; Buchmeiser, M. R. Crystalline and Conductive Poly(3-Hexylthiophene) Fibers. *Macromol. Mater. Eng.* **2012**, *297*, 123–127. https://doi.org/10.1002/mame.201100092.

(421) Moulton, J.; Smith, P. Gel Processing of Electrically Conductive Blends of Poly(3-Octylthiophene) and Ultrahigh Molecular Weight Polyethylene. *J. Polym. Sci.* **1992**, *30*, 871–878. https://doi.org/10.1002/polb.1992.090300809.

(422) Xie, R.; Colby, R. H.; Gomez, E. D. Connecting the Mechanical and Conductive Properties of Conjugated Polymers. *Adv. Electron. Mater.* **2018**, *4*, 1700356. https://doi.org/10.1002/aelm.201700356.

(423) Lund, A.; van der Velden, N. M.; Persson, N.-K.; Hamedi, M. M.; Müller, C. Electrically Conducting Fibres for E-Textiles: An Open Playground for Conjugated Polymers and Carbon Nanomaterials. *Mater. Sci. Eng.* **2018**, *126*, 1–29. https://doi.org/10.1016/j.mser.2018.03.001.

(424) Kiefer, D.; Yu, L.; Fransson, E.; Gómez, A.; Primetzhofer, D.; Amassian, A.; Campoy-Quiles, M.; Müller, C. A Solution-Doped Polymer Semiconductor:Insulator Blend for Thermoelectrics. *Adv. Sci.* **2017**, *4*, 1600203. https://doi.org/10.1002/advs.201600203.

(425) Kroon, R.; Hofmann, A. I.; Yu, L.; Lund, A.; Müller, C. Thermally Activated in Situ Doping Enables Solid-State Processing of Conducting Polymers. *Chem. Mater.* **2019**, *31*, 2770–2777. https://doi.org/10.1021/acs.chemmater.8b04895.

(426) Cao, Y.; Smith, P.; Heeger, A. J. Counter-Ion Induced Processibility of Conducting Polyaniline and of Conducting Polyblends of Polyaniline in Bulk Polymers. *Synth. Met.* **1992**, *48*, 91–97. https://doi.org/10.1016/0379-6779(92)90053-L.

(427) Holness, F. B.; Price, A. D. Direct Ink Writing of 3D Conductive Polyaniline Structures and Rheological Modelling. *Smart Mater. Struct.* **2017**, *27*, 15006. https://doi.org/10.1088/1361-665x/aa981c.

(428) Elschner, A.; Kirchmeyer, S.; Lovenich, W.; Merker, U.; Reuter, K. *PEDOT: Principles and Applications of an Intrinsically Conductive Polymer*, 1st ed.; CRC Press: Boca Raton, 2010. https://doi.org/https://doi.org/10.1201/b10318.

(429) Mengistie, D. A.; Chen, C.-H.; Boopathi, K. M.; Pranoto, F. W.; Li, L.-J.; Chu, C.-W. Enhanced Thermoelectric Performance of PEDOT:PSS Flexible Bulky Papers by Treatment with Secondary Dopants. *ACS Appl. Mater. Interfaces* **2015**, *7*, 94–100. https://doi.org/10.1021/am507032e.

(430) Okuzaki, H.; Harashina, Y.; Yan, H. Highly Conductive PEDOT/PSS Microfibers Fabricated by Wet-Spinning and Dip-Treatment in Ethylene Glycol. *Eur. Polym. J.* **2009**, *45*, 256–261. https://doi.org/10.1016/j.eurpolymj.2008.10.027.

(431) Zhou, J.; Li, E. Q.; Li, R.; Xu, X.; Ventura, I. A.; Moussawi, A.; Anjum, D. H.; Hedhili, M. N.; Smilgies, D.-M.; Lubineau, G.; et al. Semi-Metallic, Strong and Stretchable Wet-

Spun Conjugated Polymer Microfibers. *J. Mater. Chem. C* **2015**, *3*, 2528–2538. https://doi.org/10.1039/C4TC02354D.

(432) Kim, Y.; Lim, T.; Kim, C.-H.; Yeo, C. S.; Seo, K.; Kim, S.-M.; Kim, J.; Park, S. Y.; Ju, S.; Yoon, M.-H. Organic Electrochemical Transistor-Based Channel Dimension-Independent Single-Strand Wearable Sweat Sensors. *NPG Asia Mater.* **2018**, *10*, 1086–1095. https://doi.org/10.1038/s41427-018-0097-3.

(433) Kim, Y.; Lund, A.; Noh, H.; Hofmann, A. I.; Craighero, M.; Darabi, S.; Zokaei, S.; Park, J. Il; Yoon, M.-H.; Müller, C. Robust PEDOT:PSS Wet-Spun Fibers for Thermoelectric Textiles. *Macromol. Mater. Eng.* **2020**, *305*, 1900749. https://doi.org/10.1002/mame.201900749.

(434) Sarabia-Riquelme, R.; Andrews, R.; Anthony, J. E.; Weisenberger, M. C. Highly Conductive Wet-Spun PEDOT:PSS Fibers for Applications in Electronic Textiles. *J. Mater. Chem. C* **2020**, *8*, 11618–11630. https://doi.org/10.1039/D0TC02558E.

(435) Sarabia-Riquelme, R.; Shahi, M.; Brill, J. W.; Weisenberger, M. C. Effect of Drawing on the Electrical, Thermoelectrical, and Mechanical Properties of Wet-Spun PEDOT:PSS Fibers. *ACS Appl. Polym. Mater.* **2019**, *1*, 2157–2167. https://doi.org/10.1021/acsapm.9b00425.

(436) Jordan, R. S.; Wang, Y. 3D Printing of Conjugated Polymers. *J. Polym. Sci.* **2019**, *57*, 1592–1605. https://doi.org/10.1002/polb.24893.

(437) Cullen, A. T.; Price, A. D. Fabrication of 3D Conjugated Polymer Structures via Vat Polymerization Additive Manufacturing. *Smart Mater. Struct.* **2019**, *28*, 104007. https://doi.org/10.1088/1361-665x/ab35f1.

(438) Cullen, A. T.; Price, A. D. Digital Light Processing for the Fabrication of 3D Intrinsically Conductive Polymer Structures. *Synth. Met.* **2018**, *235*, 34–41. https://doi.org/10.1016/j.synthmet.2017.11.003.

(439) Hofmann, A. I.; Östergren, I.; Kim, Y.; Fauth, S.; Craighero, M.; Yoon, M. H.; Lund, A.; Müller, C. All-Polymer Conducting Fibers and 3D Prints via Melt Processing and Templated Polymerization. *ACS Appl. Mater. Interfaces* **2020**, *12*, 8713–8721. https://doi.org/10.1021/acsami.9b20615.

(440) Kroon, R.; Hofmann, A. I.; Yu, L.; Lund, A.; Müller, C. Thermally Activated in Situ Doping Enables Solid-State Processing of Conducting Polymers. *Chem. Mater.* **2019**, *31*, 2770–2777. https://doi.org/10.1021/acs.chemmater.8b04895.

(441) Beretta, D.; Neophytou, N.; Hodges, J. M.; Kanatzidis, M. G.; Narducci, D.; Martin-Gonzalez, M.; Beekman, M.; Balke, B.; Cerretti, G.; Tremel, W.; et al. Thermoelectrics:

From History, a Window to the Future. *Mater. Sci. Eng.* **2019**, *138*, 100501. https://doi.org/10.1016/j.mser.2018.09.001.

(442) Liu, J.; van der Zee, B.; Alessandri, R.; Sami, S.; Dong, J.; Nugraha, M. I.; Barker, A. J.; Rousseva, S.; Qiu, L.; Qiu, X.; et al. N-Type Organic Thermoelectrics: Demonstration of ZT > 0.3. *Nat. Commun.* **2020**, *11*, 5694. https://doi.org/10.1038/s41467-020-19537-8.

(443) Hynynen, J.; Kiefer, D.; Yu, L.; Kroon, R.; Munir, R.; Amassian, A.; Kemerink, M.; Müller, C. Enhanced Electrical Conductivity of Molecularly P-Doped Poly(3-Hexylthiophene) through Understanding the Correlation with Solid-State Order. *Macromolecules* **2017**, *50*, 8140–8148. https://doi.org/10.1021/acs.macromol.7b00968.

(444) Untilova, V.; Biskup, T.; Biniek, L.; Vijayakumar, V.; Brinkmann, M. Control of Chain Alignment and Crystallization Helps Enhance Charge Conductivities and Thermoelectric Power Factors in Sequentially Doped P3HT:F4TCNQ Films. *Macromolecules* **2020**, *53*, 2441–2453. https://doi.org/10.1021/acs.macromol.9b02389.

(445) Untilova, V.; Hynynen, J.; Hofmann, A. I.; Scheunemann, D.; Zhang, Y.; Barlow, S.; Kemerink, M.; Marder, S. R.; Biniek, L.; Müller, C.; et al. High Thermoelectric Power Factor of Poly(3-Hexylthiophene) through In-Plane Alignment and Doping with a Molybdenum Dithiolene Complex. *Macromolecules* **2020**, *53*, 6314–6321. https://doi.org/10.1021/acs.macromol.0c01223.

(446) Vijayakumar, V.; Durand, P.; Zeng, H.; Untilova, V.; Herrmann, L.; Algayer, P.; Leclerc, N.; Brinkmann, M. Influence of Dopant Size and Doping Method on the Structure and Thermoelectric Properties of PBTTT Films Doped with F6TCNNQ and F4TCNQ. *J. Mater. Chem. C* **2020**, *8*, 16470–16482. https://doi.org/10.1039/D0TC02828B.

(447) Nogami, Y.; Kaneko, H.; Ishiguro, T.; Takahashi, A.; Tsukamoto, J.; Hosoito, N. On the Metallic States in Highly Conducting Iodine-Doped Polyacetylene. *Solid State Commun.* **1990**, *76*, 583–586. https://doi.org/10.1016/0038-1098(90)90093-Q.

(448) Lu, Y.; Wang, J.-Y.; Pei, J. Strategies To Enhance the Conductivity of N-Type Polymer Thermoelectric Materials. *Chem. Mater.* **2019**, *31*, 6412–6423. https://doi.org/10.1021/acs.chemmater.9b01422.

(449) Wang, S.; Ruoko, T.-P.; Wang, G.; Riera-Galindo, S.; Hultmark, S.; Puttisong, Y.; Moro, F.; Yan, H.; Chen, W. M.; Berggren, M.; et al. Sequential Doping of Ladder-Type Conjugated Polymers for Thermally Stable n-Type Organic Conductors. *ACS Appl. Mater. Interfaces* **2020**, *12*, 53003–53011. https://doi.org/10.1021/acsami.0c16254.

(450) Shi, K.; Zhang, F.; Di, C.-A.; Yan, T.-W.; Zou, Y.; Zhou, X.; Zhu, D.; Wang, J.-Y.; Pei, J. Toward High Performance *n* -Type Thermoelectric Materials by Rational Modification of BDPPV Backbones. *J. Am. Chem. Soc.* **2015**, *137*, 6979–6982. https://doi.org/10.1021/jacs.5b00945.

(451) Krache, R.; Benavente, R.; López-Majada, J. M.; Pereña, J. M.; Cerrada, M. L.; Pérez, E. Competition between α, β, and γ Polymorphs in a β-Nucleated Metallocenic Isotactic Polypropylene. *Macromolecules* **2007**, *40*, 6871–6878. https://doi.org/10.1021/ma0710636.

(452) Blomenhofer, M.; Ganzleben, S.; Hanft, D.; Schmidt, H.-W.; Kristiansen, M.; Smith, P.; Stoll, K.; Mäder, D.; Hoffmann, K. "Designer" Nucleating Agents for Polypropylene. *Macromolecules* **2005**, *38*, 3688–3695. https://doi.org/10.1021/ma0473317.

(453) Kristiansen, M.; Smith, P.; Chanzy, H.; Baerlocher, C.; Gramlich, V.; McCusker, L.; Weber, T.; Pattison, P.; Blomenhofer, M.; Schmidt, H.-W. Structural Aspects of 1,3,5-Benzenetrisamides−A New Family of Nucleating Agents. *Cryst. Growth Des.* **2009**, *9*, 2556–2558. https://doi.org/10.1021/cg900139d.

(454) Lindqvist, C.; Bergqvist, J.; Feng, C.-C.; Gustafsson, S.; Bäcke, O.; Treat, N. D.; Bounioux, C.; Henriksson, P.; Kroon, R.; Wang, E.; et al. Fullerene Nucleating Agents: A Route Towards Thermally Stable Photovoltaic Blends. *Adv. Energy Mater.* **2014**, *4*, 1301437. https://doi.org/10.1002/aenm.201301437.

(455) Sharenko, A.; Treat, N. D.; Love, J. A.; Toney, M. F.; Stingelin, N.; Nguyen, T.-Q. Use of a Commercially Available Nucleating Agent to Control the Morphological Development of Solution-Processed Small Molecule Bulk Heterojunction Organic Solar Cells. *J. Mater. Chem. A* **2014**, *2*, 15717–15721. https://doi.org/10.1039/C4TA03469D.

(456) Treat, N. D.; Nekuda Malik, J. A.; Reid, O.; Yu, L.; Shuttle, C. G.; Rumbles, G.; Hawker, C. J.; Chabinyc, M. L.; Smith, P.; Stingelin, N.; et al. Microstructure Formation in Molecular and Polymer Semiconductors Assisted by Nucleation Agents. *Nat. Mater.* **2013**, *12*, 628–633. https://doi.org/10.1038/nmat3655.

(457) Duong, D. T.; Wang, C.; Antono, E.; Toney, M. F.; Salleo, A. The Chemical and Structural Origin of Efficient P-Type Doping in P3HT. *Org. Electron.* **2013**, *14*, 1330–1336. https://doi.org/10.1016/j.orgel.2013.02.028.

(458) Ma, L.; Lee, W. H.; Park, Y. D.; Kim, J. S.; Lee, H. S.; Cho, K. High Performance Polythiophene Thin-Film Transistors Doped with Very Small Amounts of an Electron Acceptor. *Appl. Phys. Lett.* **2008**, *92*, 63310. https://doi.org/10.1063/1.2883927.

(459) Kang, M.; Yeo, J.-S.; Park, W.-T.; Kim, N.-K.; Lim, D.-H.; Hwang, H.; Baeg, K.-J.;

Noh, Y.-Y.; Kim, D.-Y. Favorable Molecular Orientation Enhancement in Semiconducting Polymer Assisted by Conjugated Organic Small Molecules. *Adv. Funct. Mater.* **2016**, *26*, 8527–8536. https://doi.org/10.1002/adfm.201603617.

(460) Lee, D.-H.; Kang, M.; Lim, D.-H.; Kim, Y.; Lee, J.; Kim, D.-Y.; Baeg, K.-J. Simultaneous Enhancement of Charge Density and Molecular Stacking Order of Polymer Semiconductors by Viologen Dopants for High Performance Organic Field-Effect Transistors. *J. Mater. Chem. C* **2018**, *6*, 5497–5505. https://doi.org/10.1039/C8TC01076E.

(461) Liu, C.; Jang, J.; Xu, Y.; Kim, H.-J.; Khim, D.; Park, W.-T.; Noh, Y.-Y.; Kim, J.-J. Effect of Doping Concentration on Microstructure of Conjugated Polymers and Characteristics in N-Type Polymer Field-Effect Transistors. *Adv. Funct. Mater.* **2015**, *25*, 758–767. https://doi.org/10.1002/adfm.201402321.

(462) Panidi, J.; Kainth, J.; Paterson, A. F.; Wang, S.; Tsetseris, L.; Emwas, A.-H.; McLachlan, M. A.; Heeney, M.; Anthopoulos, T. D. Introducing a Nonvolatile N-Type Dopant Drastically Improves Electron Transport in Polymer and Small-Molecule Organic Transistors. *Adv. Funct. Mater.* **2019**, *29*, 1902784. https://doi.org/10.1002/adfm.201902784.

(463) Scaccabarozzi, A. D.; Basham, J. I.; Yu, L.; Westacott, P.; Zhang, W.; Amassian, A.; McCulloch, I.; Caironi, M.; Gundlach, D. J.; Stingelin, N. High-Density Polyethylene—an Inert Additive with Stabilizing Effects on Organic Field-Effect Transistors. *J. Mater. Chem. C* **2020**, *8*, 15406–15415. https://doi.org/10.1039/D0TC03173A.

(464) Lan, S.; Yan, Y.; Yang, H.; Zhang, G.; Ye, Y.; Li, F.; Chen, H.; Guo, T. Improving Device Performance of N-Type Organic Field-Effect Transistors via Doping with a p-Type Organic Semiconductor. *J. Mater. Chem. C* **2019**, *7*, 4543–4550. https://doi.org/10.1039/C8TC05740K.

(465) Wang, Z.; Zou, Y.; Chen, W.; Huang, Y.; Yao, C.; Zhang, Q. The Role of Weak Molecular Dopants in Enhancing the Performance of Solution-Processed Organic Field-Effect Transistors. *Adv. Electron. Mater.* **2019**, *5*, 1800547. https://doi.org/10.1002/aelm.201800547.

(466) Yoon, S.; Cho, J.; Yu, S. H.; Son, H. J.; Chung, D. S. Effects of Iodine Doping on Small Molecule Organic Semiconductors for High Charge Carrier Mobility and Photoconductivity. *Org. Electron.* **2016**, *34*, 28–32. https://doi.org/10.1016/j.orgel.2016.03.035.

(467) Ma, W.; Shi, K.; Wu, Y.; Lu, Z.-Y.; Liu, H.-Y.; Wang, J.-Y.; Pei, J. Enhanced Molecular

Packing of a Conjugated Polymer with High Organic Thermoelectric Power Factor. *ACS Appl. Mater. Interfaces* **2016**, *8*, 24737–24743. https://doi.org/10.1021/acsami.6b06899.

(468) Basu, A.; Niazi, M. R.; Scaccabarozzi, A. D.; Faber, H.; Fei, Z.; Anjum, D. H.; Paterson, A. F.; Boltalina, O.; Heeney, M.; Anthopoulos, T. D. Impact of P-Type Doping on Charge Transport in Blade-Coated Small-Molecule:Polymer Blend Transistors. *J. Mater. Chem. C* **2020**, *8*, 15638. https://doi.org/10.1039/D0TC03094E.

(469) Wei, Z.; Xi, H.; Dong, H.; Wang, L.; Xu, W.; Hu, W.; Zhu, D. Blending Induced Stack-Ordering and Performance Improvement in a Solution-Processed n-Type Organic Field-Effect Transistor. *J. Mater. Chem.* **2010**, *20*, 1203–1207. https://doi.org/10.1039/B918874F.

(470) Xiong, Y.; Ye, L.; Gadisa, A.; Zhang, Q.; Rech, J. J.; You, W.; Ade, H. Revealing the Impact of F4-TCNQ as Additive on Morphology and Performance of High-Efficiency Nonfullerene Organic Solar Cells. *Adv. Funct. Mater.* **2019**, *29*, 1806262. https://doi.org/10.1002/adfm.201806262.

(471) Tang, C. W.; VanSlyke, S. A. Organic Electroluminescent Diodes. *Appl. Phys. Lett.* **1987**, *51*, 913–915. https://doi.org/10.1063/1.98799.

(472) Hong, G.; Gan, X.; Leonhardt, C.; Zhang, Z.; Seibert, J.; Busch, J. M.; Bräse, S. A Brief History of OLEDs—Emitter Development and Industry Milestones. *Adv. Mater.* **2021**, *33*, 2005630. https://doi.org/10.1002/adma.202005630.

(473) Hiramoto, M.; Kikuchi, M.; Izawa, S. Parts-per-Million-Level Doping Effects in Organic Semiconductor Films and Organic Single Crystals. *Adv. Mater.* **2019**, *31*, 1–15. https://doi.org/10.1002/adma.201801236.

(474) Jiang, Z.; Soltanian, S.; Gholamkhass, B.; Aljaafari, A.; Servati, P. Light-Soaking Free Organic Photovoltaic Devices with Sol-Gel Deposited ZnO and AZO Electron Transport Layers. *RSC Adv.* **2018**, *8*, 36542–36548. https://doi.org/10.1039/C8RA07071G.

(475) Wijeyasinghe, N.; Eisner, F.; Tsetseris, L.; Lin, Y.-H.; Seitkhan, A.; Li, J.; Yan, F.; Solomeshch, O.; Tessler, N.; Patsalas, P.; et al. P-Doping of Copper(I) Thiocyanate (CuSCN) Hole-Transport Layers for High-Performance Transistors and Organic Solar Cells. *Adv. Funct. Mater.* **2018**, *28*, 1802055. https://doi.org/10.1002/adfm.201802055.

(476) Lin, Y.; Adilbekova, B.; Firdaus, Y.; Yengel, E.; Faber, H.; Sajjad, M.; Zheng, X.; Yarali, E.; Seitkhan, A.; Bakr, O. M.; et al. 17% Efficient Organic Solar Cells Based on Liquid Exfoliated WS2 as a Replacement for PEDOT:PSS. *Adv. Mater.* **2019**, *31*,

1902965. https://doi.org/10.1002/adma.201902965.

(477) Cui, Y.; Yao, H.; Zhang, J.; Xian, K.; Zhang, T.; Hong, L.; Wang, Y.; Xu, Y.; Ma, K.; An, C.; et al. Single-Junction Organic Photovoltaic Cells with Approaching 18% Efficiency. *Adv. Mater.* **2020**, *32*, 1908205. https://doi.org/10.1002/adma.201908205.

(478) Lin, Y.; Firdaus, Y.; Isikgor, F. H.; Nugraha, M. I.; Yengel, E.; Harrison, G. T.; Hallani, R.; El-Labban, A.; Faber, H.; Ma, C.; et al. Self-Assembled Monolayer Enables Hole Transport Layer-Free Organic Solar Cells with 18% Efficiency and Improved Operational Stability. *ACS Energy Lett.* **2020**, *5*, 2935–2944. https://doi.org/10.1021/acsenergylett.0c01421.

(479) Liu, Q.; Jiang, Y.; Jin, K.; Qin, J.; Xu, J.; Li, W.; Xiong, J.; Liu, J.; Xiao, Z.; Sun, K.; et al. 18% Efficiency Organic Solar Cells. *Sci. Bull.* **2020**, *65*, 272–275. https://doi.org/10.1016/j.scib.2020.01.001.

(480) Zhang, M.; Zhu, L.; Zhou, G.; Hao, T.; Qiu, C.; Zhao, Z.; Hu, Q.; Larson, B. W.; Zhu, H.; Ma, Z.; et al. Single-Layered Organic Photovoltaics with Double Cascading Charge Transport Pathways: 18% Efficiencies. *Nat. Commun.* **2021**, *12*, 1–10. https://doi.org/10.1038/s41467-020-20580-8.

(481) Bartesaghi, D.; Pérez, I. D. C.; Kniepert, J.; Roland, S.; Turbiez, M.; Neher, D.; Koster, L. J. A. Competition between Recombination and Extraction of Free Charges Determines the Fill Factor of Organic Solar Cells. *Nat. Commun.* **2015**, *6*, 1–10. https://doi.org/10.1038/ncomms8083.

(482) Mihailetchi, V. D.; Blom, P. W. M.; Hummelen, J. C.; Rispens, M. T. Cathode Dependence of the Open-Circuit Voltage of Polymer:Fullerene Bulk Heterojunction Solar Cells. *J. Appl. Phys.* **2003**, *94*, 6849–6854. https://doi.org/10.1063/1.1620683.

(483) Park, M. H.; Li, J. H.; Kumar, A.; Li, G.; Yang, Y. Doping of the Metal Oxide Nanostructure and Its Influence in Organic Electronics. *Adv. Funct. Mater.* **2009**, *19*, 1241–1246. https://doi.org/10.1002/adfm.200801639.

(484) Pfeiffer, M.; Beyer, A.; Plönnigs, B.; Nollau, A.; Fritz, T.; Leo, K.; Schlettwein, D.; Hiller, S.; Wöhrle, D. Controlled P-Doping of Pigment Layers by Cosublimation: Basic Mechanisms and Implications for Their Use in Organic Photovoltaic Cells. *Sol. Energy Mater. Sol. Cells.* **2000**, *63*, 83–99. https://doi.org/10.1016/S0927-0248(00)00022-2.

(485) Chan, C. K.; Zhao, W.; Kahn, A.; Hill, I. G. Influence of Chemical Doping on the Performance of Organic Photovoltaic Cells. *Appl. Phys. Lett.* **2009**, *94*, 1–4. https://doi.org/10.1063/1.3138131.

(486) Babu, B. H.; Lyu, C.; Zhang, H.; Chen, Z.; Li, F.; Feng, L.; Hao, X. T. Modification of

Hole Transport Layers for Fabricating High Performance Non-Fullerene Polymer Solar Cells. *Chinese J. Chem.* **2020**, *38*, 817–822. https://doi.org/10.1002/cjoc.201900462.

(487) Kotadiya, N. B.; Lu, H.; Mondal, A.; Ie, Y.; Andrienko, D.; Blom, P. W. M.; Wetzelaer, G. J. A. H. Universal Strategy for Ohmic Hole Injection into Organic Semiconductors with High Ionization Energies. *Nat. Mater.* **2018**, *17*, 329–334. https://doi.org/10.1038/s41563-018-0022-8.

(488) Helander, M. G.; Wang, Z. B.; Qiu, J.; Greiner, M. T.; Puzzo, D. P.; Liu, Z. W.; Lu, Z. H. Chlorinated Indium Tin Oxide Electrodes with High Work Function for Organic Device Compatibility. *Science.* **2011**, *332*, 944–947. https://doi.org/10.1126/science.1202992.

(489) Lilliedal, M. R.; Medford, A. J.; Madsen, M. V.; Norrman, K.; Krebs, F. C. The Effect of Post-Processing Treatments on Inflection Points in Currentvoltage Curves of Roll-to-Roll Processed Polymer Photovoltaics. *Sol. Energy Mater. Sol. Cells.* **2010**, *94*, 2018–2031. https://doi.org/10.1016/j.solmat.2010.06.007.

(490) Wagenpfahl, A.; Rauh, D.; Binder, M.; Deibel, C.; Dyakonov, V. S-Shaped Current-Voltage Characteristics of Organic Solar Devices. *Phys. Rev. B* **2010**, *82*, 115306. https://doi.org/10.1103/PhysRevB.82.115306.

(491) Ecker, B.; Egelhaaf, H. J.; Steim, R.; Parisi, J.; Von Hauff, E. Understanding S-Shaped Current-Voltage Characteristics in Organic Solar Cells Containing a TiOx Interlayer with Impedance Spectroscopy and Equivalent Circuit Analysis. *J. Phys. Chem. C* **2012**, *116*, 16333–16337. https://doi.org/10.1021/jp305206d.

(492) Hamwi, S.; Meyer, J.; Winkler, T.; Riedl, T.; Kowalsky, W. P -Type Doping Efficiency of MoO3 in Organic Hole Transport Materials. *Appl. Phys. Lett.* **2009**, *94*, 253307. https://doi.org/10.1063/1.3159824.

(493) Kim, D. H.; Kim, T. M.; Jeong, W. I.; Kim, J. J. Rhenium Oxide as an Efficient P-Dopant to Overcome S-Shaped Current Density-Voltage Curves in Organic Photovoltaics with a Deep Highest Occupied Molecular Orbital Level Donor Layer. *Appl. Phys. Lett.* **2012**, *101*, 153303. https://doi.org/10.1063/1.4758681.

(494) Wang, Y.; Luo, Q.; Wu, N.; Wang, Q.; Zhu, H.; Chen, L.; Li, Y. Q.; Luo, L.; Ma, C. Q. Solution-Processed MoO_3:PEDOT:PSS Hybrid Hole Transporting Layer for Inverted Polymer Solar Cells. *ACS Appl. Mater. Inter.* **2015**, *7*, 7170–7179. https://doi.org/10.1021/am509049t.

(495) Maennig, B.; Drechsel, J.; Gebeyehu, D.; Simon, P.; Kozlowski, F.; Werner, A.; Li, F.; Grundmann, S.; Sonntag, S.; Koch, M.; et al. Organic P-i-n Solar Cells. *Appl. Phys. A*

Mater. Sci. Process. **2004**, *79*, 1–14. https://doi.org/10.1007/s00339-003-2494-9.

(496) Cho, N.; Yip, H. L.; Davies, J. A.; Kazarinoff, P. D.; Zeigler, D. F.; Durban, M. M.; Segawa, Y.; Malley, K. M.; Luscombe, C. K.; Jen, A. K. Y. In-Situ Crosslinking and n-Doping of Semiconducting Polymers and Their Application as Efficient Electron-Transporting Materials in Inverted Polymer Solar Cells. *Adv. Energy Mater.* **2011**, *1*, 1148–1153. https://doi.org/10.1002/aenm.201100429.

(497) Kubo, M.; Shinmura, Y.; Ishiyama, N.; Kaji, T.; Hiramoto, M. Invertible Organic Photovoltaic Cells with Heavily Doped Organic/Metal Ohmic Contacts. *Appl. Phys. Express* **2012**, *5*, 092302. https://doi.org/10.1143/APEX.5.092302.

(498) Schueppel, R.; Timmreck, R.; Allinger, N.; Mueller, T.; Furno, M.; Uhrich, C.; Leo, K.; Riede, M. Controlled Current Matching in Small Molecule Organic Tandem Solar Cells Using Doped Spacer Layers. *J. Appl. Phys.* **2010**, *107*, 44503. https://doi.org/10.1063/1.3277051.

(499) Timmreck, R.; Olthof, S.; Leo, K.; Riede, M. K. Highly Doped Layers as Efficient Electron-Hole Recombination Contacts for Tandem Organic Solar Cells. *J. Appl. Phys.* **2010**, *108*, 033108. https://doi.org/10.1063/1.3467786.

(500) Ho, C. H. Y.; Kim, T.; Xiong, Y.; Firdaus, Y.; Yi, X.; Dong, Q.; Rech, J. J.; Gadisa, A.; Booth, R.; O'Connor, B. T.; et al. High-Performance Tandem Organic Solar Cells Using HSolar as the Interconnecting Layer. *Adv. Energy Mater.* **2020**, *10*, 2000823. https://doi.org/10.1002/aenm.202000823.

(501) Gilot, J.; Wienk, M. M.; Janssen, R. A. J. Double and Triple Junction Polymer Solar Cells Processed from Solution. *Appl. Phys. Lett.* **2007**, *90*, 143512. https://doi.org/10.1063/1.2719668.

(502) Meng, L.; Zhang, Y.; Wan, X.; Li, C.; Zhang, X.; Wang, Y.; Ke, X.; Xiao, Z.; Ding, L.; Xia, R.; et al. Organic and Solution-Processed Tandem Solar Cells with 17.3% Efficiency. *Science* **2018**, *361*, 1094–1098. https://doi.org/10.1126/science.aat2612.

(503) Zhang, Y.; Zhou, H.; Seifter, J.; Ying, L.; Mikhailovsky, A.; Heeger, A. J.; Bazan, G. C.; Nguyen, T. Q. Molecular Doping Enhances Photoconductivity in Polymer Bulk Heterojunction Solar Cells. *Adv. Mater.* **2013**, *25*, 7038–7044. https://doi.org/10.1002/adma.201302159.

(504) Zhang, D.; Wang, J.; Zhang, X.; Zhou, J.; Zafar, S. U.; Zhou, H.; Zhang, Y. Sequential Molecular Doping of Non-Fullerene Organic Solar Cells without Hole Transport Layers. *J. Mater. Chem. C* **2019**, *8*, 158–164. https://doi.org/10.1039/c9tc04969j.

(505) Shang, Z.; Heumueller, T.; Prasanna, R.; Burkhard, G. F.; Naab, B. D.; Bao, Z.;

McGehee, M. D.; Salleo, A. Trade-Off between Trap Filling, Trap Creation, and Charge Recombination Results in Performance Increase at Ultralow Doping Levels in Bulk Heterojunction Solar Cells. *Adv. Energy Mater.* **2016**, *6*, 1601149. https://doi.org/10.1002/aenm.201601149.

(506) Yu, R.; Yao, H.; Hong, L.; Gao, M.; Ye, L.; Hou, J. TCNQ as a Volatilizable Morphology Modulator Enables Enhanced Performance in Non-Fullerene Organic Solar Cells. *J. Mater. Chem. C* **2019**, *8*, 44–49. https://doi.org/10.1039/c9tc04892h.

(507) Tang, Y.; Lin, B.; Zhao, H.; Li, T.; Ma, W.; Yan, H. Significance of Dopant/Component Miscibility to Efficient N-Doping in Polymer Solar Cells. *ACS Appl. Mater. Inter.* **2020**, *12*, 13021–13028. https://doi.org/10.1021/acsami.9b21252.

(508) Chen, Z.; Tang, Y.; Lin, B.; Zhao, H.; Li, T.; Min, T.; Yan, H.; Ma, W. Probe and Control of the Tiny Amounts of Dopants in BHJ Film Enable Higher Performance of Polymer Solar Cells. *ACS Appl. Mater. Inter.* **2020**, *12*, 25115–25124. https://doi.org/10.1021/acsami.0c06127.

(509) Yu, S.; Yang, Q.; Yu, W.; Zhang, J.; Liu, J.; Jin, S.; Guo, X.; Li, C. Performance Enhancement of Ternary Polymer Solar Cells Induced by Tetrafluorotetracyanoquinodimethane Doping. *Chem. Mater.* **2019**, *31*, 7650–7656. https://doi.org/10.1021/acs.chemmater.9b02520.

(510) Veysel Tunc, A.; De Sio, A.; Riedel, D.; Deschler, F.; Da Como, E.; Parisi, J.; Von Hauff, E. Molecular Doping of Low-Bandgap-Polymer:Fullerene Solar Cells: Effects on Transport and Solar Cells. *Org. Electron.* **2012**, *13*, 290–296. https://doi.org/10.1016/j.orgel.2011.11.014.

(511) Yan, H.; Tang, Y.; Sui, X.; Liu, Y.; Gao, B.; Liu, X.; Liu, S. F.; Hou, J.; Ma, W. Increasing Quantum Efficiency of Polymer Solar Cells with Efficient Exciton Splitting and Long Carrier Lifetime by Molecular Doping at Heterojunctions. *ACS Energy Lett.* **2019**, *4*, 1356–1363. https://doi.org/10.1021/acsenergylett.9b00843.

(512) Yan, H.; Manion, J. G.; Yuan, M.; García de Arquer, F. P.; McKeown, G. R.; Beaupré, S.; Leclerc, M.; Sargent, E. H.; Seferos, D. S. Increasing Polymer Solar Cell Fill Factor by Trap-Filling with F4-TCNQ at Parts Per Thousand Concentration. *Adv. Mater.* **2016**, *28*, 6491–6496. https://doi.org/10.1002/adma.201601553.

(513) Liu, C.; Li, Z.; Zhang, Z.; Zhang, X.; Shen, L.; Guo, W.; Zhang, L.; Long, Y.; Ruan, S. Improving the Charge Carrier Transport of Organic Solar Cells by Incorporating a Deep Energy Level Molecule. *Phys. Chem. Chem. Phys.* **2017**, *19*, 245–250. https://doi.org/10.1039/c6cp07344a.

(514) Xu, X.; Yu, L.; Yan, H.; Li, R.; Peng, Q. Highly Efficient Non-Fullerene Organic Solar Cells Enabled by a Delayed Processing Method Using a Non-Halogenated Solvent. *Energy Environ. Sci.* **2020**, *13*, 4381–4388. https://doi.org/10.1039/d0ee02034f.

(515) Xu, X.; Feng, K.; Yu, L.; Yan, H.; Li, R.; Peng, Q. Highly Efficient All-Polymer Solar Cells Enabled by p-Doping of the Polymer Donor. *ACS Energy Lett.* **2020**, *5*, 2434–2443. https://doi.org/10.1021/acsenergylett.0c01010.

(516) Zhang, S.; Zhan, L.; Li, S.; Li, C. Z.; Chen, H. Enhanced Performance of Inverted Non-Fullerene Organic Solar Cells through Modifying Zinc Oxide Surface with Self-Assembled Monolayers. *Org. Electron.* **2018**, *63*, 143–148. https://doi.org/10.1016/j.orgel.2018.09.016.

(517) Loiudice, A.; Rizzo, A.; Biasiucci, M.; Gigli, G. Bulk Heterojunction versus Diffused Bilayer: The Role of Device Geometry in Solution p-Doped Polymer-Based Solar Cells. *J. Phys. Chem. Lett.* **2012**, *3*, 1908–1915. https://doi.org/10.1021/jz300754p.

(518) Yan, H.; Tang, Y.; Meng, X.; Xiao, T.; Lu, G.; Ma, W. Achieving High Doping Concentration by Dopant Vapor Deposition in Organic Solar Cells. *ACS Appl. Mater. Inter.* **2019**, *11*, 4178–4184. https://doi.org/10.1021/acsami.8b16162.

(519) Zhang, Y.; Blom, P. W. M. Enhancement of the Hole Injection into Regioregular Poly(3-Hexylthiophene) by Molecular Doping. *Appl. Phys. Lett.* **2010**, *97*, 83303. https://doi.org/10.1063/1.3464560.

(520) Trukhanov, V. A.; Bruevich, V. V.; Paraschuk, D. Y. Effect of Doping on Performance of Organic Solar Cells. *Phys. Rev. B - Condens. Matter Mater. Phys.* **2011**, *84*, 205318. https://doi.org/10.1103/PhysRevB.84.205318.

(521) Zhang, S.; Qin, Y.; Zhu, J.; Hou, J. Over 14% Efficiency in Polymer Solar Cells Enabled by a Chlorinated Polymer Donor. *Adv. Mater.* **2018**, *30*, 1–7. https://doi.org/10.1002/adma.201800868.

(522) Duong, D. T.; Phan, H.; Hanifi, D.; Jo, P. S.; Nguyen, T. Q.; Salleo, A. Direct Observation of Doping Sites in Temperature-Controlled, p-Doped P3ht Thin Films by Conducting Atomic Force Microscopy. *Adv. Mater.* **2014**, *26*, 6069–6073. https://doi.org/10.1002/adma.201402015.

(523) Kim, S. M.; Jang, J. H.; Kim, K. K.; Park, H. K.; Bae, J. J.; Yu, W. J.; Lee, H.; Kim, G.; Loc, D. D.; Kim, U. J.; et al. Reduction-Controlled Viologen in Bisolvent as an Environmentally Stable n-Type Dopant for Carbon Nanotubes. *J. Am. Chem. Soc.* **2009**, *131*, 327–331. https://doi.org/10.1021/ja807480g.

(524) Zhao, W.; Li, S.; Yao, H.; Zhang, S.; Zhang, Y.; Yang, B.; Hou, J. Molecular

Optimization Enables over 13% Efficiency in Organic Solar Cells. *J. Am. Chem. Soc.* **2017**, *139*, 7148–7151. https://doi.org/10.1021/jacs.7b02677.

(525) Yuan, J.; Zhang, Y.; Zhou, L.; Zhang, G.; Yip, H. L.; Lau, T. K.; Lu, X.; Zhu, C.; Peng, H.; Johnson, P. A.; et al. Single-Junction Organic Solar Cell with over 15% Efficiency Using Fused-Ring Acceptor with Electron-Deficient Core. *Joule* **2019**, *3*, 1140–1151. https://doi.org/10.1016/j.joule.2019.01.004.

(526) Sze, S.; Kwok, K. N. *Physics of Semiconductor Devices*; Wiley, **2006**; p. 303.

(527) Meijer, E. J.; Tanase, C.; Blom, P. W. M.; Van Veenendaal, E.; Huisman, B.-H. H.; De Leeuw, D. M.; Klapwijk, T. M. Switch-on Voltage in Disordered Organic Field-Effect Transistors. *Appl. Phys. Lett.* **2002**, *80*, 3838–3840. https://doi.org/10.1063/1.1479210.

(528) Horowitz, G. Organic Field-Effect Transistors. *Adv. Mater.* **1998**, *10*, 365–377. https://doi.org/10.1002/(SICI)1521-4095(199803)10:5<365::AID-ADMA365>3.0.CO;2-U.

(529) Fediai, A.; Symalla, F.; Friederich, P.; Wenzel, W. Disorder Compensation Controls Doping Efficiency in Organic Semiconductors. *Nat. Commun.* **2019**, *10*, 2–8. https://doi.org/10.1038/s41467-019-12526-6.

(530) Brown, A. R.; de Leeuw, D. M.; Havinga, E. E.; Pomp, A. A Universal Relation between Conductivity and Field-Effect Mobility in Doped Amorphous Organic Semiconductors. *Synth. Met.* **1994**, *68*, 65–70. https://doi.org/10.1016/0379-6779(94)90148-1.

(531) Venkateshvaran, D.; Nikolka, M.; Sadhanala, A.; Lemaur, V.; Zelazny, M.; Kepa, M.; Hurhangee, M.; Kronemeijer, A. J.; Pecunia, V.; Nasrallah, I.; et al. Approaching Disorder-Free Transport in High-Mobility Conjugated Polymers. *Nature* **2014**, *515*, 384–388. https://doi.org/10.1038/nature13854.

(532) Kronemeijer, A. J.; Pecunia, V.; Venkateshvaran, D.; Nikolka, M.; Sadhanala, A.; Moriarty, J.; Szumilo, M.; Sirringhaus, H. Two-Dimensional Carrier Distribution in Top-Gate Polymer Field-Effect Transistors: Correlation between Width of Density of Localized States and Urbach Energy. *Adv. Mater.* **2014**, *26*, 728–733. https://doi.org/10.1002/adma.201303060.

(533) Li, J.; Zhao, Y.; Tan, H. S.; Guo, Y.; Di, C.-A.; Yu, G.; Liu, Y.; Lin, M.; Lim, S. H.; Zhou, Y.; et al. A Stable Solution-Processed Polymer Semiconductor with Record High-Mobility for Printed Transistors. *Sci. Rep.* **2012**, *2*, 7541-9. https://doi.org/10.1038/srep00754.

(534) Luzio, A.; Nübling, F.; Martin, J.; Fazzi, D.; Selter, P.; Gann, E.; McNeill, C. R.; Brinkmann, M.; Hansen, M. R.; Stingelin, N.; et al. Microstructural Control Suppresses

Thermal Activation of Electron Transport at Room Temperature in Polymer Transistors. *Nat. Commun.* **2019**, *10*, 3365. https://doi.org/10.1038/s41467-019-11125-9.

(535) Yamashita, Y.; Tsurumi, J.; Hinkel, F.; Okada, Y.; Soeda, J.; Zajączkowski, W.; Baumgarten, M.; Pisula, W.; Matsui, H.; Müllen, K.; et al. Transition Between Band and Hopping Transport in Polymer Field-Effect Transistors. *Adv. Mater.* **2014**, *26*, 8169–8173. https://doi.org/10.1002/adma.201403767.

(536) Cho, J. M.; Higashino, T.; Mori, T. Band-like Transport down to 20 K in Organic Single-Crystal Transistors Based on Dioctylbenzothienobenzothiophene. *Appl. Phys. Lett.* **2015**, *106*, 1–5. https://doi.org/10.1063/1.4921343.

(537) Scaccabarozzi, A. D.; Scuratti, F.; Barker, A. J.; Basu, A.; Paterson, A. F.; Fei, Z.; Solomeshch, O.; Petrozza, A.; Tessler, N.; Heeney, M.; et al. Understanding Charge Transport in High-Mobility p-Doped Multicomponent Blend Organic Transistors. *Adv. Electron. Mater.* **2020**, *6*, 2000539. https://doi.org/doi:10.1002/aelm.202000539.

(538) Waldrip, M.; Jurchescu, O. D.; Gundlach, D. J.; Bittle, E. G. Contact Resistance in Organic Field-Effect Transistors: Conquering the Barrier. *Adv. Funct. Mater.* **2020**, *30*, 1–31. https://doi.org/10.1002/adfm.201904576.

(539) Perinot, A.; Passarella, B.; Giorgio, M.; Caironi, M. Walking the Route to GHz Solution-Processed Organic Electronics: A HEROIC Exploration. *Adv. Funct. Mater.* **2020**, *30*, 1907641. https://doi.org/doi:10.1002/adfm.201907641.

(540) Brondijk, J. J.; Torricelli, F.; Smits, E. C. P.; Blom, P. W. M.; De Leeuw, D. M. Gate-Bias Assisted Charge Injection in Organic Field-Effect Transistors. *Org. Electron.* **2012**, *13*, 1526–1531. https://doi.org/10.1016/j.orgel.2012.04.029.

(541) Bronstein, H.; Chen, Z.; Ashraf, R. S.; Zhang, W.; Du, J.; Durrant, J. R.; Tuladhar, P. S.; Song, K.; Watkins, S. E.; Geerts, Y.; et al. Thieno[3,2-*b*]Thiophene-Diketopyrrolopyrrole-Containing Polymers for High-Performance Organic Field-Effect Transistors and Organic Photovoltaic Devices. *J. Am. Chem. Soc.* **2011**, *133*, 3272–3275. https://doi.org/10.1021/ja110619k.

(542) Khim, D.; Baeg, K. J.; Caironi, M.; Liu, C.; Xu, Y.; Kim, D. Y.; Noh, Y. Y. Control of Ambipolar and Unipolar Transport in Organic Transistors by Selective Inkjet-Printed Chemical Doping for High Performance Complementary Circuits. *Adv. Funct. Mater.* **2014**, *24*, 6252–6261. https://doi.org/10.1002/adfm.201400850.

(543) Xu, Y.; Sun, H.; Shin, E.-Y.; Lin, Y.-F.; Li, W.; Noh, Y.-Y. Planar-Processed Polymer Transistors. *Adv. Mater.* **2016**, *28*, 8531–8537. https://doi.org/10.1002/adma.201601589.

(544) Anthopoulos, T. D.; Anyfantis, G. C.; Papavassiliou, G. C.; de Leeuw, D. M. Air-Stable Ambipolar Organic Transistors. *Appl. Phys. Lett.* **2007**, *90*, 122105. https://doi.org/10.1063/1.2715028.

(545) Park, S.; Kim, S. H.; Choi, H. H.; Kang, B.; Cho, K. Recent Advances in the Bias Stress Stability of Organic Transistors. *Adv. Funct. Mater.* **2020**, *30*, 1904590. https://doi.org/10.1002/adfm.201904590.

(546) Paterson, A. F.; Lin, Y.-H. H.; Mottram, A. D.; Fei, Z.; Niazi, M. R.; Kirmani, A. R.; Amassian, A.; Solomeshch, O.; Tessler, N.; Heeney, M.; et al. The Impact of Molecular P-Doping on Charge Transport in High-Mobility Small-Molecule/Polymer Blend Organic Transistors. *Adv. Electron. Mater.* **2018**, *4*, 1–13. https://doi.org/10.1002/aelm.201700464.

(547) Nikolka, M.; Schweicher, G.; Armitage, J.; Nasrallah, I.; Jellett, C.; Guo, Z.; Hurhangee, M.; Sadhanala, A.; McCulloch, I.; Nielsen, C. B.; et al. Performance Improvements in Conjugated Polymer Devices by Removal of Water-Induced Traps. *Adv. Mater.* **2018**, *30*, 1801874. https://doi.org/10.1002/adma.201801874.

(548) Nikolka, M.; Nasrallah, I.; Rose, B.; Ravva, M. K.; Broch, K.; Sadhanala, A.; Harkin, D.; Charmet, J.; Hurhangee, M.; Brown, A.; et al. High Operational and Environmental Stability of High-Mobility Conjugated Polymer Field-Effect Transistors through the Use of Molecular Additives. *Nat. Mater.* **2017**, *16*, 356–362. https://doi.org/10.1038/nmat4785.

(549) Jarrett, C. P.; Friend, R. H.; Brown, A. R.; de Leeuw, D. M. Field Effect Measurements in Doped Conjugated Polymer Films: Assessment of Charge Carrier Mobilities. *J. Appl. Phys.* **1995**, *77*, 6289–6294. https://doi.org/10.1063/1.359096.

(550) Brown, A. R.; Jarrett, C. P.; de Leeuw, D. M.; Matters, M. Field-Effect Transistors Made from Solution-Processed Organic Semiconductors. *Synth. Met.* **1997**, *88*, 37–55. https://doi.org/10.1016/S0379-6779(97)80881-8.

(551) Abe, Y.; Hasegawa, T.; Takahashi, Y.; Yamada, T.; Tokura, Y. Control of Threshold Voltage in Pentacene Thin-Film Transistors Using Carrier Doping at the Charge-Transfer Interface with Organic Acceptors. *Appl. Phys. Lett.* **2005**, *87*, 153506. https://doi.org/10.1063/1.2099540.

(552) Tada, K.; Harada, H.; Yoshino, K. Field-Effect Mobility of Molecularly Doped Poly(3-Hexylthiophene). *Jpn. J. Appl. Phys.* **1997**, *36*, L718–L720. https://doi.org/10.1143/JJAP.36.L718.

(553) Lim, E.; Jung, B.-J.; Chikamatsu, M.; Azumi, R.; Yoshida, Y.; Yase, K.; Do, L.-M.;

Shim, H.-K. Doping Effect of Solution-Processed Thin-Film Transistors Based on Polyfluorene. *J. Mater. Chem.* **2007**, *17*, 1416–1420. https://doi.org/10.1039/B615720C.

(554) Wei, P.; Oh, J. H.; Dong, G.; Bao, Z. Use of a 1H-Benzoimidazole Derivative as an n-Type Dopant and To Enable Air-Stable Solution-Processed n-Channel Organic Thin-Film Transistors. *J. Am. Chem. Soc.* **2010**, *132*, 8852–8853. https://doi.org/10.1021/ja103173m.

(555) Oh, J. H.; Wei, P.; Bao, Z. Molecular N-Type Doping for Air-Stable Electron Transport in Vacuum-Processed n-Channel Organic Transistors. *Appl. Phys. Lett.* **2010**, *97*, 243305. https://doi.org/10.1063/1.3527972.

(556) Nam, S.; Kim, J.; Lee, H.; Kim, H.; Ha, C.-S.; Kim, Y. Doping Effect of Organosulfonic Acid in Poly(3-Hexylthiophene) Films for Organic Field-Effect Transistors. *ACS Appl. Mater. Inter.* **2012**, *4*, 1281–1288. https://doi.org/10.1021/am300141m.

(557) Hähnlen, T.; Vanoni, C.; Wäckerlin, C.; Jung, T. A.; Tsujino, S. Surface Doping in Pentacene Thin-Film Transistors with Few Monolayer Thick Channels. *Appl. Phys. Lett.* **2012**, *101*, 33305. https://doi.org/10.1063/1.4737214.

(558) Kim, J. H.; Yun, S. W.; An, B.-K.; Han, Y. D.; Yoon, S.-J.; Joo, J.; Park, S. Y. Remarkable Mobility Increase and Threshold Voltage Reduction in Organic Field-Effect Transistors by Overlaying Discontinuous Nano-Patches of Charge-Transfer Doping Layer on Top of Semiconducting Film. *Adv. Mater.* **2013**, *25*, 719–724. https://doi.org/10.1002/adma.201202789.

(559) Soeda, J.; Hirose, Y.; Yamagishi, M.; Nakao, A.; Uemura, T.; Nakayama, K.; Uno, M.; Nakazawa, Y.; Takimiya, K.; Takeya, J. Solution-Crystallized Organic Field-Effect Transistors with Charge-Acceptor Layers: High-Mobility and Low-Threshold-Voltage Operation in Air. *Adv. Mater.* **2011**, *23*, 3309–3314. https://doi.org/10.1002/adma.201101027.

(560) Pacher, P.; Lex, A.; Proschek, V.; Etschmaier, H.; Tchernychova, E.; Sezen, M.; Scherf, U.; Grogger, W.; Trimmel, G.; Slugovc, C.; et al. Chemical Control of Local Doping in Organic Thin-Film Transistors: From Depletion to Enhancement. *Adv. Mater.* **2008**, *20*, 3143–3148. https://doi.org/10.1002/adma.200800058.

(561) Maddalena, F.; Meijer, E. J.; Asadi, K.; de Leeuw, D. M.; Blom, P. W. M. Doping Kinetics of Organic Semiconductors Investigated by Field-Effect Transistors. *Appl. Phys. Lett.* **2010**, *97*, 043302. https://doi.org/10.1063/1.3466903.

(562) Lu, G.; Blakesley, J.; Himmelberger, S.; Pingel, P.; Frisch, J.; Lieberwirth, I.; Salzmann,

I.; Oehzelt, M.; Di Pietro, R.; Salleo, A.; et al. Moderate Doping Leads to High Performance of Semiconductor/Insulator Polymer Blend Transistors. *Nat. Commun.* **2013**, *4*, 1588. https://doi.org/10.1038/ncomms2587.

(563) Wang, C. H.; Gao, X.; Zhong, Y. N.; Liu, J.; Xu, J. L.; Wang, S. D. Controlled Surface Doping for Operating Stability Enhancement in Organic Field-Effect Transistors. *Org. Electron.* **2017**, *42*, 367–371. https://doi.org/10.1016/j.orgel.2016.12.051.

(564) Liu, S.; Billig, P.; Al-Shadeedi, A.; Kaphle, V.; Lüssem, B. Doped Bottom-Contact Organic Field-Effect Transistors. *Nanotechnology* **2018**, *29*, 284001. https://doi.org/10.1088/1361-6528/aab93a.

(565) Hein, M. P.; Zakhidov, A. A.; Lüssem, B.; Jankowski, J.; Tietze, M. L.; Riede, M. K.; Leo, K. Molecular Doping for Control of Gate Bias Stress in Organic Thin Film Transistors. *Appl. Phys. Lett.* **2014**, *104*, 013507. https://doi.org/10.1063/1.4861168.

(566) Liu, S.; Radha Krishnan, R. K.; Dahal, D.; Lüssem, B. Analytic Device Model of Organic Field-Effect Transistors with Doped Channels. *ACS Appl. Mater. Inter.* **2020**, *12*, 49857–49865. https://doi.org/10.1021/acsami.0c12534.

(567) Zhang, F.; Dai, X.; Zhu, W.; Chung, H.; Diao, Y. Large Modulation of Charge Carrier Mobility in Doped Nanoporous Organic Transistors. *Adv. Mater.* **2017**, *29*, 1700411. https://doi.org/10.1002/adma.201700411.

(568) Zhang, F.; Mohammadi, E.; Qu, G.; Dai, X.; Diao, Y. Orientation-Dependent Host–Dopant Interactions for Manipulating Charge Transport in Conjugated Polymers. *Adv. Mater.* **2020**, *32*, 2002823. https://doi.org/10.1002/adma.202002823.

(569) Zessin, J.; Xu, Z.; Shin, N.; Hambsch, M.; Mannsfeld, S. C. B. Threshold Voltage Control in Organic Field-Effect Transistors by Surface Doping with a Fluorinated Alkylsilane. *ACS Appl. Mater. Inter.* **2019**, *11*, 2177–2188. https://doi.org/10.1021/acsami.8b12346.

(570) Barf, M.-M.; Benneckendorf, F. S.; Reiser, P.; Bäuerle, R.; Köntges, W.; Müller, L.; Pfannmöller, M.; Beck, S.; Mankel, E.; Freudenberg, J.; et al. Compensation of Oxygen Doping in P-Type Organic Field-Effect Transistors Utilizing Immobilized n-Dopants. *Adv. Mater. Technol.* **2020**, *n/a*, 2000556. https://doi.org/10.1002/admt.202000556.

(571) Wei, P.; Hu, Y.; Zhu, Y.; Jiang, Y.; Feng, X.; Li, S.; Bu, L.; Yang, X.; Lu, G. Dopant/Semiconductor/Electret Trilayer Architecture for High-Performance Organic Field-Effect Transistors. *Adv. Electron. Mater.* **2018**, *4*, 1800339. https://doi.org/10.1002/aelm.201800339.

(572) Rossbauer, S.; Müller, C.; Anthopoulos, T. D. Comparative Study of the N-Type Doping

Efficiency in Solution-Processed Fullerenes and Fullerene Derivatives. *Adv. Funct. Mater.* **2014**, *24*, 7116–7124. https://doi.org/10.1002/adfm.201401842.

(573) Lee, D.-H.; Yang, D.; Kim, D.-Y.; Baeg, K.-J. Controlled Ambipolar Charge Transport of Polymer Semiconductors by Viologen-Doping for Complementary-like Electronic Circuits. *Org. Electron.* **2018**, *59*, 224–229. https://doi.org/10.1016/j.orgel.2018.04.049.

(574) Lee, D. H.; Kang, M.; Lim, D. H.; Kim, Y.; Lee, J.; Kim, D. Y.; Baeg, K. J. Simultaneous Enhancement of Charge Density and Molecular Stacking Order of Polymer Semiconductors by Viologen Dopants for High Performance Organic Field-Effect Transistors. *J. Mater. Chem. C* **2018**, *6*, 5497–5505. https://doi.org/10.1039/c8tc01076e.

(575) Shin, N.; Zessin, J.; Lee, M. H.; Hambsch, M.; Mannsfeld, S. C. B. Enhancement of N-Type Organic Field-Effect Transistor Performances through Surface Doping with Aminosilanes. *Adv. Funct. Mater.* **2018**, *28*, 1–7. https://doi.org/10.1002/adfm.201802265.

(576) Chueh, C.-C. C.; Li, C.-Z. Z.; Ding, F.; Li, Z. Z.; Cernetic, N.; Li, X.; Jen, A. K. Y. K.-Y. Doping Versatile N-Type Organic Semiconductors via Room Temperature Solution-Processable Anionic Dopants. *ACS Appl. Mater. Inter.* **2017**, *9*, 1136–1144. https://doi.org/10.1021/acsami.6b14375.

(577) Choi, H. H.; Paterson, A. F.; Fusella, M. A.; Panidi, J.; Solomeshch, O.; Tessler, N.; Heeney, M.; Cho, K.; Anthopoulos, T. D.; Rand, B. P.; et al. Hall Effect in Polycrystalline Organic Semiconductors: The Effect of Grain Boundaries. *Adv. Funct. Mater.* **2020**, *30*, 1903617. https://doi.org/doi:10.1002/adfm.201903617.

(578) Ablat, A.; Kyndiah, A.; Houin, G.; Alic, T. Y.; Hirsch, L.; Abbas, M. Role of Oxide/Metal Bilayer Electrodes in Solution Processed Organic Field Effect Transistors. *Sci. Rep.* **2019**, *9*, 1–8. https://doi.org/10.1038/s41598-019-43237-z.

(579) Choi, S.; Fuentes-Hernandez, C.; Wang, C. Y.; Khan, T. M.; Larrain, F. A.; Zhang, Y.; Barlow, S.; Marder, S. R.; Kippelen, B. A Study on Reducing Contact Resistance in Solution-Processed Organic Field-Effect Transistors. *ACS Appl. Mater. Inter.* **2016**, *8*, 24744–24752. https://doi.org/10.1021/acsami.6b07029.

(580) Mathijssen, S. G. J.; Smits, E. C. P.; Van Hal, P. A.; Wondergem, H. J.; Ponomarenko, S. A.; Moser, A.; Resel, R.; Bobbert, P. A.; Kemerink, M.; Janssen, R. A. J.; et al. Monolayer Coverage and Channel Length Set the Mobility in Self-Assembled Monolayer Field-Effect Transistors. *Nat. Nanotechnol.* **2009**, *4*, 674–680. https://doi.org/10.1038/nnano.2009.201.

(581) Suchand Sangeeth, C. S.; Wan, A.; Nijhuis, C. A. Probing the Nature and Resistance of

the Molecule-Electrode Contact in SAM-Based Junctions. *Nanoscale* **2015**, *7*, 12061–12067. https://doi.org/10.1039/c5nr02570b.

(582) Cheng, X.; Noh, Y.-Y.; Wang, J.; Tello, M.; Frisch, J.; Blum, R.-P.; Vollmer, A.; Rabe, J. P.; Koch, N.; Sirringhaus, H. Controlling Electron and Hole Charge Injection in Ambipolar Organic Field-Effect Transistors by Self-Assembled Monolayers. *Adv. Funct. Mater.* **2009**, *19*, 2407–2415. https://doi.org/10.1002/adfm.200900315.

(583) Beebe, J. M.; Engelkes, V. B.; Miller, L. L.; Frisbie, C. D. Contact Resistance in Metal-Molecule-Metal Junctions Based on Aliphatic SAMs: Effects of Surface Linker and Metal Work Function. *J. Am. Chem. Soc.* **2002**, *124*, 11268–11269. https://doi.org/10.1021/ja0268332.

(584) Engelkes, V. B.; Beebe, J. M.; Frisbie, C. D. Length-Dependent Transport in Molecular Junctions Based on SAMs of Alkanethiols and Alkanedithiols: Effect of Metal Work Function and Applied Bias on Tunneling Efficiency and Contact Resistance. *J. Am. Chem. Soc.* **2004**, *126*, 14287–14296. https://doi.org/10.1021/ja046274u.

(585) Darmawan, P.; Minari, T.; Xu, Y.; Li, S.-L. L.; Song, H.; Chan, M.; Tsukagoshi, K. Optimal Structure for High-Performance and Low-Contact-Resistance Organic Field-Effect Transistors Using Contact-Doped Coplanar and Pseudo-Staggered Device Architectures. *Adv. Funct. Mater.* **2012**, *22*, 4577–4583. https://doi.org/10.1002/adfm.201201094.

(586) Minari, T.; Miyadera, T.; Tsukagoshi, K.; Aoyagi, Y.; Ito, H. Charge Injection Process in Organic Field-Effect Transistors. *Appl. Phys. Lett.* **2007**, *91*, 053508. https://doi.org/10.1063/1.2759987.

(587) Wang, S. D.; Minari, T.; Miyadera, T.; Tsukagoshi, K.; Aoyagi, Y. Contact-Metal Dependent Current Injection in Pentacene Thin-Film Transistors. *Appl. Phys. Lett.* **2007**, *91*, 203508. https://doi.org/10.1063/1.2813640.

(588) Liu, C.; Xu, Y.; Li, Y.; Scheideler, W.; Minari, T. Critical Impact of Gate Dielectric Interfaces on the Contact Resistance of High-Performance Organic Field-E Ff Ect Transistors. *J. Phys. Chem. C* **2013**, *117*, 12337–12345. https://doi.org/10.1021/jp4023844.

(589) Lamport, Z. A.; Barth, K. J.; Lee, H.; Gann, E.; Engmann, S.; Chen, H.; Guthold, M.; McCulloch, I.; Anthony, J. E.; Richter, L. J.; et al. A Simple and Robust Approach to Reducing Contact Resistance in Organic Transistors. *Nat. Commun.* **2018**, *9*, 5130. https://doi.org/10.1038/s41467-018-07388-3.

(590) Zojer, K.; Zojer, E.; Fernandez, A. F.; Gruber, M. Impact of the Capacitance of the

Dielectric on the Contact Resistance of Organic Thin-Film Transistors. *Phys. Rev. Appl.* **2015**, *4*, 44002. https://doi.org/10.1103/PhysRevApplied.4.044002.

(591) Borchert, J. W.; Peng, B.; Letzkus, F.; Burghartz, J. N.; Chan, P. K. L.; Zojer, K.; Ludwigs, S.; Klauk, H. Small Contact Resistance and High-Frequency Operation of Flexible Low-Voltage Inverted Coplanar Organic Transistors. *Nat. Commun.* **2019**, *10*, 1119. https://doi.org/10.1038/s41467-019-09119-8.

(592) Liu, C.; Xu, Y.; Noh, Y.-Y. Contact Engineering in Organic Field-Effect Transistors. *Mater. Today* **2015**, *18*, 79–96. https://doi.org/10.1016/j.mattod.2014.08.037.

(593) Kim, C.-H. Contact Resistance in Organic Transistors: Use It or Remove It. *Appl. Phys. Rev.* **2020**, *7*, 031306. https://doi.org/10.1063/5.0005441.

(594) Natali, D.; Caironi, M. Charge Injection in Solution-Processed Organic Field-Effect Transistors: Physics, Models and Characterization Methods. *Adv. Mater.* **2012**, *24*, 1357–1387. https://doi.org/10.1002/adma.201104206.

(595) Gamier, F.; Kouki, F.; Hajlaoui, R.; Horowitz, G. Tunneling at Organic/Metal Interfaces in Oligomer-Based Thin-Film Transistors. *MRS Bull.* **1997**, *22*, 52–56. https://doi.org/10.1557/S0883769400033637.

(596) Kumaki, D.; Umeda, T.; Tokito, S. Reducing the Contact Resistance of Bottom-Contact Pentacene Thin-Film Transistors by Employing a MoOx Carrier Injection Layer. *Appl. Phys. Lett.* **2008**, *92*, 13301. https://doi.org/10.1063/1.2828711.

(597) Schroeder, R.; Majewski, L. A.; Grell, M. Improving Organic Transistor Performance with Schottky Contacts. *Appl. Phys. Lett.* **2004**, *84*, 1004–1006. https://doi.org/10.1063/1.1645993.

(598) Fujimori, F.; Shigeto, K.; Hamano, T.; Minari, T.; Miyadera, T.; Tsukagoshi, K.; Aoyagi, Y. Current Transport in Short Channel Top-Contact Pentacene Field-Effect Transistors Investigated with the Selective Molecular Doping Technique. *Appl. Phys. Lett.* **2007**, *90*, 193507. https://doi.org/10.1063/1.2737418.

(599) Gundlach, D. J.; Jia, L. L.; Jackson, T. N. Pentacene TFT with Improved Linear Region Characteristics Using Chemically Modified Source and Drain Electrodes. *IEEE Electron Device Lett.* **2001**, *22*, 571–573. https://doi.org/10.1109/55.974580.

(600) Minari, T.; Darmawan, P.; Liu, C.; Li, Y.; Xu, Y.; Tsukagoshi, K. Highly Enhanced Charge Injection in Thienoacene-Based Organic Field-Effect Transistors with Chemically Doped Contact. *Appl. Phys. Lett.* **2012**, *100*, 093303. https://doi.org/10.1063/1.3690949.

(601) Yamamura, A.; Sakon, T.; Takahira, K.; Wakimoto, T.; Sasaki, M.; Okamoto, T.;

Watanabe, S.; Takeya, J. High-Speed Organic Single-Crystal Transistor Responding to Very High Frequency Band. *Adv. Funct. Mater.* **2020**, *30*, 1909501. https://doi.org/10.1002/adfm.201909501.

(602) Li, J.; Zhang, X. W.; Zhang, L.; Khizar-ul-Haq; Jiang, X. Y.; Zhu, W. Q.; Zhang, Z. L. Improving Organic Transistor Performance through Contact-Area-Limited Doping. *Solid State Commun.* **2009**, *149*, 1826–1830. https://doi.org/10.1016/j.ssc.2009.07.006.

(603) Miyadera, T.; Minari, T.; Tsukagoshi, K.; Ito, H.; Aoyagi, Y. Frequency Response Analysis of Pentacene Thin-Film Transistors with Low Impedance Contact by Interface Molecular Doping. *Appl. Phys. Lett.* **2007**, *91*, 013512. https://doi.org/10.1063/1.2754350.

(604) Zschieschang, U.; Kang, M. J.; Takimiya, K.; Sekitani, T.; Someya, T.; Canzler, T. W.; Werner, A.; Blochwitz-Nimoth, J.; Klauk, H. Flexible Low-Voltage Organic Thin-Film Transistors and Circuits Based on C 10-DNTT. *J. Mater. Chem.* **2012**, *22*, 4273–4277. https://doi.org/10.1039/c1jm14917b.

(605) Ante, F.; Kälblein, D.; Zschieschang, U.; Canzler, T. W.; Werner, A.; Takimiya, K.; Ikeda, M.; Sekitani, T.; Someya, T.; Klauk, H. Contact Doping and Ultrathin Gate Dielectrics for Nanoscale Organic Thin-Film Transistors. *Small* **2011**, *7*, 1186–1191. https://doi.org/10.1002/smll.201002254.

(606) Tiwari, S. P.; Potscavage, W. J.; Sajoto, T.; Barlow, S.; Marder, S. R.; Kippelen, B. Pentacene Organic Field-Effect Transistors with Doped Electrode-Semiconductor Contacts. *Org. Electron.* **2010**, *11*, 860–863. https://doi.org/10.1016/j.orgel.2010.01.029.

(607) Günther, A. A.; Sawatzki, M.; Formánek, P.; Kasemann, D.; Leo, K. Contact Doping for Vertical Organic Field-Effect Transistors. *Adv. Funct. Mater.* **2016**, *26*, 768–775. https://doi.org/10.1002/adfm.201504377.

(608) Melville, O. A.; Grant, T. M.; Lochhead, K.; King, B.; Ambrose, R.; Rice, N. A.; Boileau, N. T.; Peltekoff, A. J.; Tousignant, M.; Hill, I. G.; et al. Contact Engineering Using Manganese, Chromium, and Bathocuproine in Group 14 Phthalocyanine Organic Thin-Film Transistors. *ACS Appl. Electron. Mater.* **2020**, *2*, 1313–1322. https://doi.org/10.1021/acsaelm.0c00104.

(609) Hamadani, B. H.; Corley, D. A.; Ciszek, J. W.; Tour, J. M.; Natelson, D. Controlling Charge Injection in Organic Field-Effect Transistors Using Self-Assembled Monolayers. *Nano Lett.* **2006**, *6*, 1303–1306. https://doi.org/10.1021/nl060731i.

(610) Park, Y. J.; Cha, M. J.; Yoon, Y. J.; Cho, S.; Kim, J. Y.; Seo, J. H.; Walker, B. Improved

Performance in N-Type Organic Field-Effect Transistors via Polyelectrolyte-Mediated Interfacial Doping. *Adv. Electron. Mater.* **2017**, *3*, 1700184. https://doi.org/10.1002/aelm.201700184.

(611) Kim, Y.; Broch, K.; Lee, W.; Ahn, H.; Lee, J.; Yoo, D.; Kim, J.; Chung, S.; Sirringhaus, H.; Kang, K.; et al. Highly Stable Contact Doping in Organic Field Effect Transistors by Dopant-Blockade Method. *Adv. Funct. Mater.* **2020**, *30*, 2000058. https://doi.org/10.1002/adfm.202000058.

(612) Kim, Y.; Chung, S.; Cho, K.; Harkin, D.; Hwang, W.-T.; Yoo, D.; Kim, J.-K.; Lee, W.; Song, Y.; Ahn, H.; et al. Enhanced Charge Injection Properties of Organic Field-Effect Transistor by Molecular Implantation Doping. *Adv. Mater.* **2019**, *31*, 1806697. https://doi.org/10.1002/adma.201806697.

(613) Dai, A.; Wan, A.; Magee, C.; Zhang, Y.; Barlow, S.; Marder, S. R.; Kahn, A. Investigation of P-Dopant Diffusion in Polymer Films and Bulk Heterojunctions: Stable Spatially-Confined Doping for All-Solution Processed Solar Cells. *Org. Electron.* **2015**, *23*, 151–157. https://doi.org/10.1016/j.orgel.2015.04.023.

(614) Seah, W. L.; Tang, C. G.; Png, R. Q.; Keerthi, V.; Zhao, C.; Guo, H.; Yang, J. G.; Zhou, M.; Ho, P. K. H.; Chua, L. L. Interface Doping for Ohmic Organic Semiconductor Contacts Using Self-Aligned Polyelectrolyte Counterion Monolayer. *Adv. Funct. Mater.* **2017**, *27*, 1606291. https://doi.org/10.1002/adfm.201606291.

(615) Schaur, S.; Stadler, P.; Meana-Esteban, B.; Neugebauer, H.; Serdar Sariciftci, N. Electrochemical Doping for Lowering Contact Barriers in Organic Field Effect Transistors. *Org. Electron.* **2012**, *13*, 1296–1301. https://doi.org/10.1016/j.orgel.2012.03.020.

(616) Zhang, J.; Geng, B.; Duan, S.; Huang, C.; Xi, Y.; Mu, Q.; Chen, H.; Ren, X.; Hu, W. High-Resolution Organic Field-Effect Transistors Manufactured by Electrohydrodynamic Inkjet Printing of Doped Electrodes. *J. Mater. Chem. C* **2020**, *8*, 15219–15223. https://doi.org/10.1039/d0tc02508a.

(617) Elmoughni, H. M.; Menon, A. K.; Wolfe, R. M. W.; Yee, S. K. A Textile-Integrated Polymer Thermoelectric Generator for Body Heat Harvesting. *Adv. Mater. Technol.* **2019**, *4*, 1–6. https://doi.org/10.1002/admt.201800708.

(618) Massetti, M.; Bonfadini, S.; Nava, D.; Butti, M.; Criante, L.; Lanzani, G.; Qiu, L.; Hummelen, J. C.; Liu, J.; Koster, L. J. A.; et al. Fully Direct Written Organic Micro-Thermoelectric Generators Embedded in a Plastic Foil. *Nano Energy* **2020**, *75*, 104983. https://doi.org/10.1016/j.nanoen.2020.104983.

(619) Bubnova, O.; Khan, Z. U.; Malti, A.; Braun, S.; Fahlman, M.; Berggren, M.; Crispin, X. Optimization of the Thermoelectric Figure of Merit in the Conducting Polymer Poly(3,4-Ethylenedioxythiophene). *Nat. Mater.* **2011**, *10*, 429–433. https://doi.org/10.1038/nmat3012.

(620) Hofmann, A. I.; Östergren, I.; Kim, Y.; Fauth, S.; Craighero, M.; Yoon, M.-H.; Lund, A.; Müller, C. All-Polymer Conducting Fibers and 3D Prints via Melt Processing and Templated Polymerization. *ACS Appl. Mater. Inter.* **2020**, *12*, 8713–8721. https://doi.org/10.1021/acsami.9b20615.

(621) Ji, L. *Metal Oxide-Based Thermoelectric Materials*; Elsevier Inc., 2018, 49-72. https://doi.org/10.1016/b978-0-12-811167-3.00003-1.

(622) Watanabe, S.; Ohno, M.; Yamashita, Y.; Terashige, T.; Okamoto, H.; Takeya, J. Validity of the Mott Formula and the Origin of Thermopower in π-Conjugated Semicrystalline Polymers. *Phys. Rev. B* **2019**, *100*, 241201. https://doi.org/10.1103/PhysRevB.100.241201.

(623) Du, Y.; Xu, J.; Paul, B.; Eklund, P. Flexible Thermoelectric Materials and Devices. *Appl. Mater. Today* **2018**, *12*, 366–388. https://doi.org/10.1016/j.apmt.2018.07.004.

(624) Heremans, J. P.; Jovovic, V.; Toberer, E. S.; Saramat, A.; Kurosaki, K.; Charoenphakdee, A.; Yamanaka, S.; Snyder, G. J. Enhancement of Thermoelectric of the Electronic Density of States. *Science* **2008**, *321*, 1457–1461.

(625) Popescu, A.; Woods, L. M. Enhanced Thermoelectricity in Composites by Electronic Structure Modifications and Nanostructuring. *Appl. Phys. Lett.* **2010**, *97*, 2008–2011. https://doi.org/10.1063/1.3464288.

(626) Wang, C.; Sun, K.; Fu, J.; Chen, R.; Li, M.; Zang, Z.; Liu, X.; Li, B.; Gong, H.; Ouyang, J. Enhancement of Conductivity and Thermoelectric Property of PEDOT:PSS via Acid Doping and Single Post-Treatment for Flexible Power Generator. *Adv. Sustain. Syst.* **2018**, *2*, 1–9. https://doi.org/10.1002/adsu.201800085.

(627) Xu, S.; Hong, M.; Shi, X. L.; Wang, Y.; Ge, L.; Bai, Y.; Wang, L.; Dargusch, M.; Zou, J.; Chen, Z. G. High-Performance PEDOT:PSS Flexible Thermoelectric Materials and Their Devices by Triple Post-Treatments. *Chem. Mater.* **2019**, *31*, 5238–5244. https://doi.org/10.1021/acs.chemmater.9b01500.

(628) Jin Bae, E.; Hun Kang, Y.; Jang, K. S.; Yun Cho, S. Enhancement of Thermoelectric Properties of PEDOT:PSS and Tellurium-PEDOT:PSS Hybrid Composites by Simple Chemical Treatment. *Sci. Rep.* **2016**, *6*, 1–10. https://doi.org/10.1038/srep18805.

(629) Scholes, D. T.; Hawks, S. A.; Yee, P. Y.; Wu, H.; Lindemuth, J. R.; Tolbert, S. H.;

Schwartz, B. J. Overcoming Film Quality Issues for Conjugated Polymers Doped with F4TCNQ by Solution Sequential Processing: Hall Effect, Structural, and Optical Measurements. *J. Phys. Chem. Lett.* **2015**, *6*, 4786–4793. https://doi.org/10.1021/acs.jpclett.5b02332.

(630) Hwang, S.; Potscavage, W. J.; Nakamichi, R.; Adachi, C. Processing and Doping of Thick Polymer Active Layers for Flexible Organic Thermoelectric Modules. *Org. Electron.* **2016**, *31*, 31–40. https://doi.org/10.1016/j.orgel.2016.01.007.

(631) Pudzs, K.; Vembris, A.; Rutkis, M.; Woodward, S. Thin Film Organic Thermoelectric Generator Based on Tetrathiotetracene. *Adv. Electron. Mater.* **2017**, *3*. https://doi.org/10.1002/aelm.201600429.

(632) Kluge, R. M.; Saxena, N.; Müller-Buschbaum, P. A Solution-Processable Polymer-Based Thin-Film Thermoelectric Generator. *Adv. Energy Sustain. Res.* **2021**, *2*, 2000060. https://doi.org/10.1002/aesr.202000060.

(633) Liu, J.; van der Zee, B.; Alessandri, R.; Sami, S.; Dong, J.; Nugraha, M. I.; Barker, A. J.; Rousseva, S.; Qiu, L.; Qiu, X.; et al. N-Type Organic Thermoelectrics: Demonstration of ZT > 0.3. *Nat. Commun.* **2020**, *11*, 1–9. https://doi.org/10.1038/s41467-020-19537-8.

(634) Olson, J. R.; Topp, K. A.; Pohl, R. O. Specific Heat and Thermal Conductivity of Solid Fullerenes. *Science* **1993**, *259*, 1145–1148. https://doi.org/10.1126/science.259.5098.1145.

(635) Wang, X.; Liman, C. D.; Treat, N. D.; Chabinyc, M. L.; Cahill, D. G. Ultralow Thermal Conductivity of Fullerene Derivatives. *Phys. Rev. B.* **2013**, *88*, 1–7. https://doi.org/10.1103/PhysRevB.88.075310.

(636) Duda, J. C.; Hopkins, P. E.; Shen, Y.; Gupta, M. C. Exceptionally Low Thermal Conductivities of Films of the Fullerene Derivative PCBM. *Phys. Rev. Lett.* **2013**, *110*, 1–5. https://doi.org/10.1103/PhysRevLett.110.015902.

(637) Lee, W.-Y.; Wu, H.-C.; Lu, C.; Naab, B. D.; Chen, W.-C.; Bao, Z. N-Type Doped Conjugated Polymer for Nonvolatile Memory. *Adv. Mater.* **2017**, *29*, 1605166. https://doi.org/10.1002/adma.201605166.

(638) Yu, T.-F.; Chen, H.-Y.; Liao, M.-Y.; Tien, H.-C.; Chang, T.-T.; Chueh, C.-C.; Lee, W.-Y. Solution-Processable Anion-Doped Conjugated Polymer for Nonvolatile Organic Transistor Memory with Synaptic Behaviors. *ACS Appl. Mater. Inter.* **2020**, *12*, 33968–33978. https://doi.org/10.1021/acsami.0c06109.

(639) Wu, Z.-H.; Sun, W.-J.; Tian, H.-H.; Yu, Z.-F.; Guo, R.-X.; Shao, X.; Zhang, H.-L. 9,10-

Imide-Pyrene-Fused Pyrazaacenes (IPPA) as N-Type Doping Materials for High-Performance Nonvolatile Organic Field Effect Transistor Memory Devices. *Adv. Electron. Mater.* **2019**, *5*, 1800598. https://doi.org/10.1002/aelm.201800598.

(640) Chen, J.; Ma, D. Performance Improvement by Charge Trapping of Doping Fluorescent Dyes in Organic Memory Devices. *J. Appl. Phys.* **2006**, *100*, 034512. https://doi.org/10.1063/1.2234541.

(641) Kang, M.; Khim, D.; Kim, J.; Lee, H. J.; Jo, J. Y.; Baeg, K. J.; Kim, D. Y. Tuning Non-Volatile Memory Characteristics via Molecular Doping of Polymer Semiconductors Based on Ambipolar Organic Field-Effect Transistors. *Org. Electron.* **2018**, *58*, 12–17. https://doi.org/10.1016/j.orgel.2018.03.043.

(642) Wang, W. V.; Zhang, Y.; Li, X.; Chen, Z.; Wu, Z.; Zhang, L.; Lin, Z.; Zhang, H. High Performance Nonvolatile Organic field-effect Transistor Memory Devices Based on Pyrene Diimide Derivative. *InfoMat* **2021**, *3*, 814–822 https://doi.org/10.1002/inf2.12186.

(643) Huang, T.-Y.; Chen, C.-H.; Lin, C.-C.; Lee, Y.-J.; Liu, C.-L.; Liou, G.-S. UV-Sensing Organic Phototransistor Memory Devices with a Doped Organic Polymer Electret Composed of Triphenylamine-Based Aggregation-Induced Emission Luminogens. *J. Mater. Chem. C* **2019**, *7*, 11014–11021. https://doi.org/10.1039/C9TC03607E.

(644) Ling, H.; Lin, J.; Yi, M.; Liu, B.; Li, W.; Lin, Z.; Xie, L.; Bao, Y.; Guo, F.; Huang, W. Synergistic Effects of Self-Doped Nanostructures as Charge Trapping Elements in Organic Field Effect Transistor Memory. *ACS Appl. Mater. Inter.* **2016**, *8*, 18969–18977. https://doi.org/10.1021/acsami.6b03792.

(645) Gedda, M.; Yengel, E.; Faber, H.; Paulus, F.; Kreß, J. A.; Tang, M.; Zhang, S.; Hacker, C. A.; Kumar, P.; Naphade, D. R.; et al. Ruddlesden–Popper-Phase Hybrid Halide Perovskite/Small-Molecule Organic Blend Memory Transistors. *Adv. Mater.* **2021**, *33*, 2003137. https://doi.org/10.1002/adma.202003137.

(646) Yu, Y.; Ma, Q.; Ling, H.; Li, W.; Ju, R.; Bian, L.; Shi, N.; Qian, Y.; Yi, M.; Xie, L.; et al. Small-Molecule-Based Organic Field-Effect Transistor for Nonvolatile Memory and Artificial Synapse. *Adv. Funct. Mater.* **2019**, *29*, 1904602. https://doi.org/10.1002/adfm.201904602.

(647) Chou, Y. H.; Chang, H. C.; Liu, C. L.; Chen, W. C. Polymeric Charge Storage Electrets for Non-Volatile Organic Field Effect Transistor Memory Devices. *Polym. Chem.* **2015**, *6*, 341–352. https://doi.org/10.1039/c4py01213e.

(648) Chen, H.; Zhou, Y.; Han, S. Recent Advances in Metal Nanoparticle-based Floating

Gate Memory. *Nano Sel.* **2021**, *2*, 1245-1265 https://doi.org/10.1002/nano.202000268.

(649) Zheng, C.; Tong, T.; Hu, Y.; Gu, Y.; Wu, H.; Wu, D.; Meng, H.; Yi, M.; Ma, J.; Gao, D.; et al. Charge-Storage Aromatic Amino Compounds for Nonvolatile Organic Transistor Memory Devices. *Small* **2018**, *14*, 1800756. https://doi.org/10.1002/smll.201800756.

(650) Lai, Q.; Zhu, Z.; Chen, Y.; Patil, S.; Wudl, F. Organic Nonvolatile Memory by Dopant-Configurable Polymer. *Appl. Phys. Lett.* **2006**, *88*, 133515. https://doi.org/10.1063/1.2191874.

(651) Zhang, Y.; de Boer, B.; Blom, P. W. M. Controllable Molecular Doping and Charge Transport in Solution-Processed Polymer Semiconducting Layers. *Adv. Funct. Mater.* **2009**, *19*, 1901–1905. https://doi.org/10.1002/adfm.200801761.

(652) Kleemann, H.; Schuenemann, C.; Zakhidov, A. A.; Riede, M.; Lüssem, B.; Leo, K. Structural Phase Transition in Pentacene Caused by Molecular Doping and Its Effect on Charge Carrier Mobility. *Org. Electron.* **2012**, *13*, 58–65. https://doi.org/10.1016/j.orgel.2011.09.027.

(653) Pahner, P.; Kleemann, H.; Burtone, L.; Tietze, M. L.; Fischer, J.; Leo, K.; Lüssem, B. Pentacene Schottky Diodes Studied by Impedance Spectroscopy: Doping Properties and Trap Response. *Phys. Rev. B* **2013**, *88*, 195205. https://doi.org/10.1103/PhysRevB.88.195205.

(654) Wang, B.; Scaccabarozzi, A.; Wang, H.; Koizumi, M.; Nugraha, M. I.; Lin, Y.; Firdaus, Y.; Wang, Y.; Lee, S.; Yokota, T.; et al. Molecular Doping of Near-Infrared Organic Photodetectors for Photoplethysmogram Sensors. *J. Mater. Chem. C* **2021**, *9*, 3129–3135. https://doi.org/10.1039/D0TC05549B.

(655) Daniel Sylvinson, M. R.; Chen, H. F.; Martin, L. M.; Saris, P. J. G.; Thompson, M. E. Rapid Multiscale Computational Screening for OLED Host Materials. *ACS Appl. Mater. Inter.* **2019**, *11*, 5276–5288. https://doi.org/10.1021/acsami.8b16225.

(656) Xu, K.; Sun, H.; Ruoko, T.-P.; Wang, G.; Kroon, R.; Kolhe, N. B.; Puttisong, Y.; Liu, X.; Fazzi, D.; Shibata, K.; et al. Ground-State Electron Transfer in All-Polymer Donor–Acceptor Heterojunctions. *Nat. Mater.* **2020**, *19*, 738–744. https://doi.org/10.1038/s41563-020-0618-7.

(657) Tian, B.; Xu, S.; Rogers, J. A.; Cestellos-Blanco, S.; Yang, P.; Carvalho-de-Souza, J. L.; Bezanilla, F.; Liu, J.; Bao, Z.; Hjort, M.; et al. Roadmap on Semiconductor–Cell Biointerfaces. *Phys. Biol.* **2018**, *15*, 31002. https://doi.org/10.1088/1478-3975/aa9f34.

(658) Rivnay, J.; Owens, R. M.; Malliaras, G. G. The Rise of Organic Bioelectronics. *Chem.*

Mater. **2014**, *26*, 679–685. https://doi.org/10.1021/cm4022003.

Bios

Alberto D. Scaccabarozzi is a Postdoctoral Fellow at the Center for Nanoscience and Technology (CNST) of the Istituto Italiano di Tecnologia in Milan (Italy). He received his PhD from Imperial College London (UK) in 2017 under the supervision of Prof. Natalie Stingelin, followed by postdoctoral appointments at CNST in M. Caironi's group and at King Abdullah University of Science and Technology (KAUST, Saudi Arabia) in Prof. T. D. Anthopoulos' group. His research interests encompass the broad field of organic electronics, in particular the study of structure-processing-property relationships of organic semiconductors for a wide range of devices, especially Organic Field-Effect Transistors (OFETs).

Aniruddha Basu is currently working as a postdoctoral researcher in Prof. Thomas Anthopoulos's group at King Abdullah University of Science and Technology (KAUST), Saudi Arabia. He received his Ph.D. in science, under the supervision of Prof. Satishchandra B Ogale, from National Chemical Laboratory, India in 2017. During his Ph.D. he was working on the development of flexible electronic and electrochemical devices like organic field-effect transistors, quantum dot light-emitting diodes, and micro-supercapacitors. His current research focus includes the development of organic small molecule/ polymer blend systems and molecular doping in those blend systems for organic field-effect transistor and organic electrochemical transistor device applications.

Filip Aniés joined the Heeney Group in 2017 to carry out his Master's Project as part of his undergraduate degree at the Department of Chemistry, Imperial College London. Following his graduation in 2018, Filip was awarded the Sir Geoffrey Wilkinson Studentship Prize, giving him the opportunity to pursue a PhD as a Wilkinson Scholar. Filip's current research focuses on novel dopants and materials for optoelectronic applications.

Jian Liu became a postdoc in the Chalmers University of Technology since June, 2020 where he is working on plastic plasmonic hydrogen sensors. Before joining Chalmers, He was a postdoc in Groningen University and worked on the subject of 'molecular doping of conjugated polymers and organic thermoelectrics'. He received a Ph.D degree in polymer physics and chemistry in Changchun Institute of Applied Chemistry in China. During the PhD study, he

worked on interface engineering of polymer photovoltaics. He coauthored over 30 peer-reviewed papers and his broad interest of research includes organic electronics, new energy generation, and Sensors.

Osnat Zapata Arteaga obtained his Ph.D. in Materials Science from the Universitat Autònoma de Barcelona (2021) under the supervision of Mariano Campoy Quiles. His current research interests focus on the fabrication and characterization of organic materials and devices for energy harvesting applications.

Ross Warren is a Postdoc in Norbert Koch's group at the Humboldt-Universität zu Berlin. He is currently developing new and exciting devices based on doped semiconductors. He enjoys writing, and contributed the simulations and discussion in the 'Physical Processes' section of this work.

Yuliar Firdaus is a researcher at the National Research and Innovation Agency (BRIN) in Indonesia. He completed his Ph.D. from KU Leuven (Belgium) in 2015 under Prof. Mark van der Auweraer, followed by postdoctoral appointments at King Abdullah University of Science and Technology (KAUST, Saudi Arabia) in Prof T.D. Anthopoulos' group. His current research focuses on the device physics and fabrication of next-generation photovoltaics.

Mohamad Insan Nugraha received his PhD (2017) from University of Groningen, the Netherlands. He is currently a postdoctoral fellow in King Abdullah University of Science and Technology (KAUST), Saudi Arabia. His research interest is solution processable optoelectronic and energy harvesting devices, which also includes molecular doping of the devices.

Yuanbao Lin gained his Ph.D. degree in Materials Science and Engineering from King Abdullah University of Science and Technology (KAUST) in 2021. He studied organic photovoltaic under guidance of Thomas D. Anthopoulos from 2018-2021. His current studies are about enhancing the performance and stability of organic solar cells by interface and active layer engineering.

Mariano Campoy-Quiles and his team at the Institute of Materials Science of Barcelona, focus their research efforts on the understanding and development of organic and hybrid

materials for energy and optoelectronic applications, and in particular, through photovoltaic (light-to-electricity) and thermoelectric (heat-to-electricity) technologies. He has been the recipient of a number prestigious of awards, including the Spanish Royal Society of Physics Young Researcher Award in Experimental Physics and an ERC Consolidator Grant by the European Research Council. He is currently the Coordinator of the Materials for Energy and Environment of the main Spanish research funding agency (AEI).

Norbert Koch received a doctorate in solid state physics from Technische Universität Graz in 2000. After two years as postdoc at Princeton University, he was independent junior research group leader at the Department of Physics, Humboldt-Universität zu Berlin, where he was appointed as full professor in 2009. In 2010 his group at the Helmholtz-Zentrum Berlin für Materialien und Energie was established. His research agenda focuses on interfacial phenomena of organic semiconductors, perovskites, and 2D semiconductors.

Christian Müller is a Professor in Polymer Science at Chalmers University of Technology, Sweden. He is a Wallenberg Academy Fellow and a SSF Future Research Leader. Prior to Chalmers, where he has worked since 2012, he completed postdoctoral stays at ICMAB-CSIC, Spain, and Linköping University, Sweden. He holds a Dr.Sc. in Materials Science from ETH Zürich, Switzerland (2008), and a M.Sci. in Natural Sciences from Cambridge University, UK (2004). His research interests include the use of organic semiconductors and polymer blends in the fields of wearable electronics and energy technology.

Leonidas Tsetseris is a Professor in the Department of Physics at the School of Applied Mathematical and Physical Sciences of the National Technical University of Athens (Greece). His field of expertise is Computational Condensed Matter Physics, Materials Science, and Physical Chemistry. Together with his collaborators, he has been using primarily Density Functional Theory calculations and Molecular Dynamics simulations to probe the properties of inorganic electronic materials, organic semiconductors, two-dimensional materials, perovskites and materials used as carrier transport layers in optoelectronic devices.

Martin Heeney is a Professor of Organic Materials Chemistry and Royal Society Wolfson Fellow at Imperial College London. He is a graduate of the University of East Anglia and received his PhD from the same institution in 1999 under the supervision of Prof. Michael Cook. Following eight years in industry, he joined the Materials Department at Queen Mary

University of London as a senior lecturer in 2007 before moving to Imperial College in 2009. His research interests include the design, synthesis and characterisation of solution processed materials for a variety of applications. He has published over 300 research papers, 5 book chapters and over 100 patents. He has been named five times by Thomson Reuters as a HighlyCited researcher in the field of Materials Science, is a recipient of the RSC Corday-Morgan (2013) medal, the RSC Peter Day (2020) award and the Macro group UK medal (2020).

Thomas D. Anthopoulos is a Professor of Material Science at King Abdullah University of Science and Technology (KAUST) in Saudi Arabia. He received his B.Eng. and D.Phil. degrees from Staffordshire University in the UK followed by postdoctoral appointments at the University of St. Andrews (UK) and Philips Research Laboratories (The Netherlands) before joining Imperial College London (UK) from 2006 to 2017. His research interests are diverse and cover the development and application of innovative processing paradigms and the physics, chemistry and application of functional materials and their devices.

SI Section

Doping Approaches for Organic Semiconductors

Alberto D. Scaccabarozzi,[1†*] Aniruddha Basu,[1†] Filip Aniés,[3] Jian Liu,[2] Osnat Zapata-Arteaga,[4] Ross Warren, [5] Yuliar Firdaus,[1,7] Mohamad Insan Nugraha,[1] Yuanbao Lin,[1] Mariano Campoy-Quiles[4] Norbert Koch,[5] Christian Müller,[2] Leonidas Tsetseris,[6] Martin Heeney,[3] Thomas D. Anthopoulos[1*]

1. King Abdullah University of Science and Technology (KAUST), KAUST Solar Center (KSC), Thuwal 23955, Saudi Arabia

2. Department of Chemistry and Chemical Engineering, Chalmers University of Technology, Göteborg 412 96, Sweden

3. Department of Chemistry and Centre for Processable Electronics, Imperial College London, London, W12 0BZ , UK

4. Materials Science Institute of Barcelona, ICMAB-CSIC, Campus UAB, 08193 Bellaterra, Spain

5. Helmholtz-Zentrum Berlin für Materialien und Energie GmbH, Kekulé-Strasse 5, 12489 Berlin, Germany
Institut für Physik & IRIS Adlershof, Humboldt-Universität zu Berlin, 12489 Berlin, Germany

6. Department of Physics, National Technical University of Athens, Athens GR-15780, Greece

7. Research Center for Electronics and Telecommunication, Indonesian Institute of Science, Jalan Sangkuriang Komplek LIPI Building 20 level 4, Bandung 40135, Indonesia

† Authors contributed to this work equally

Corresponding authors: thomas.anthopoulos@kaust.edu.sa; alberto.scaccabarozzi@kaust.edu.sa

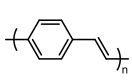

PPV

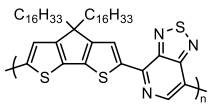

PCPDTPT

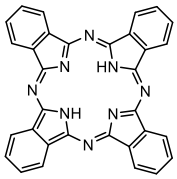

Phthalocyanine

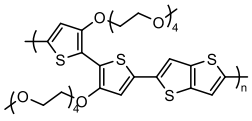

p($g_4$2T-TT)

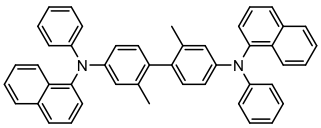

α-NPD

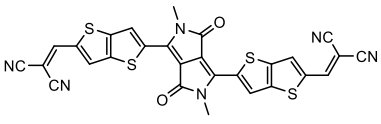

A-DCV-DPPTT

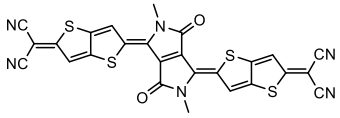

Q-DCV-DPPTT

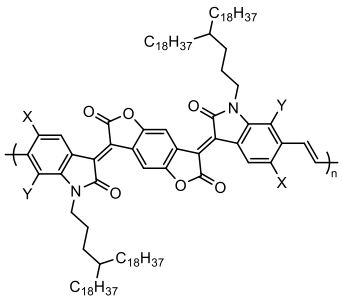

CIBDPPV:
X = Cl, Y = H
FBDPPV:
X = H, Y = F
TBDPPV:
X, Y = H

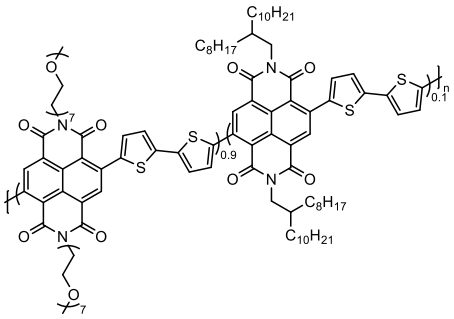

P-90

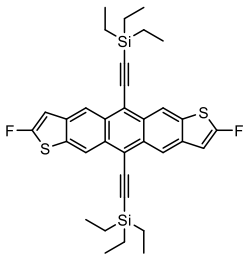

diF-TESADT

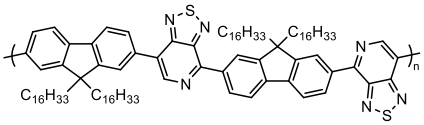

PFPT

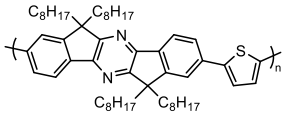

IP-T

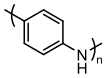

Polyaniline

Polypyrrole

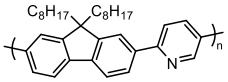

F8Py

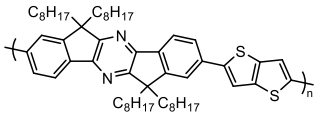

IP-TT

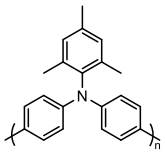

PTAA

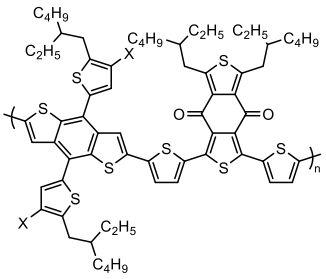

PM6:
X = F
PM7:
X = Cl

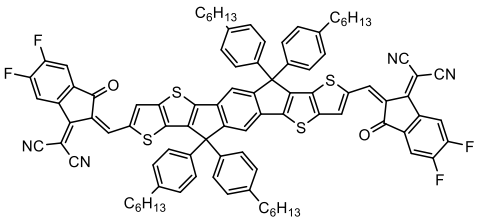

IT-4F

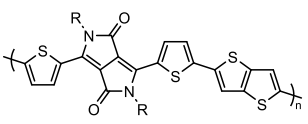

DPPTTT

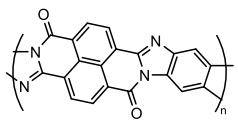

BBL

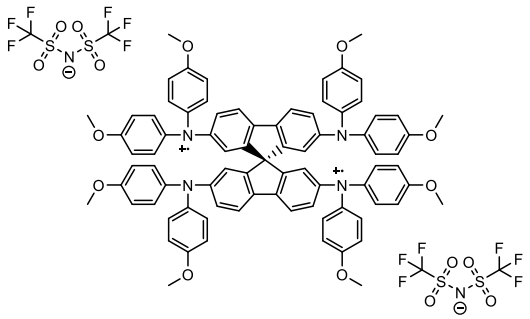

Spiro-OMeTAD(TFSI)$_2$

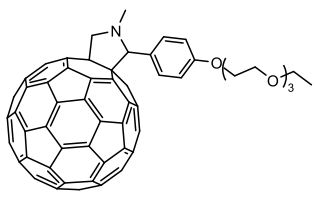

PTEG-1

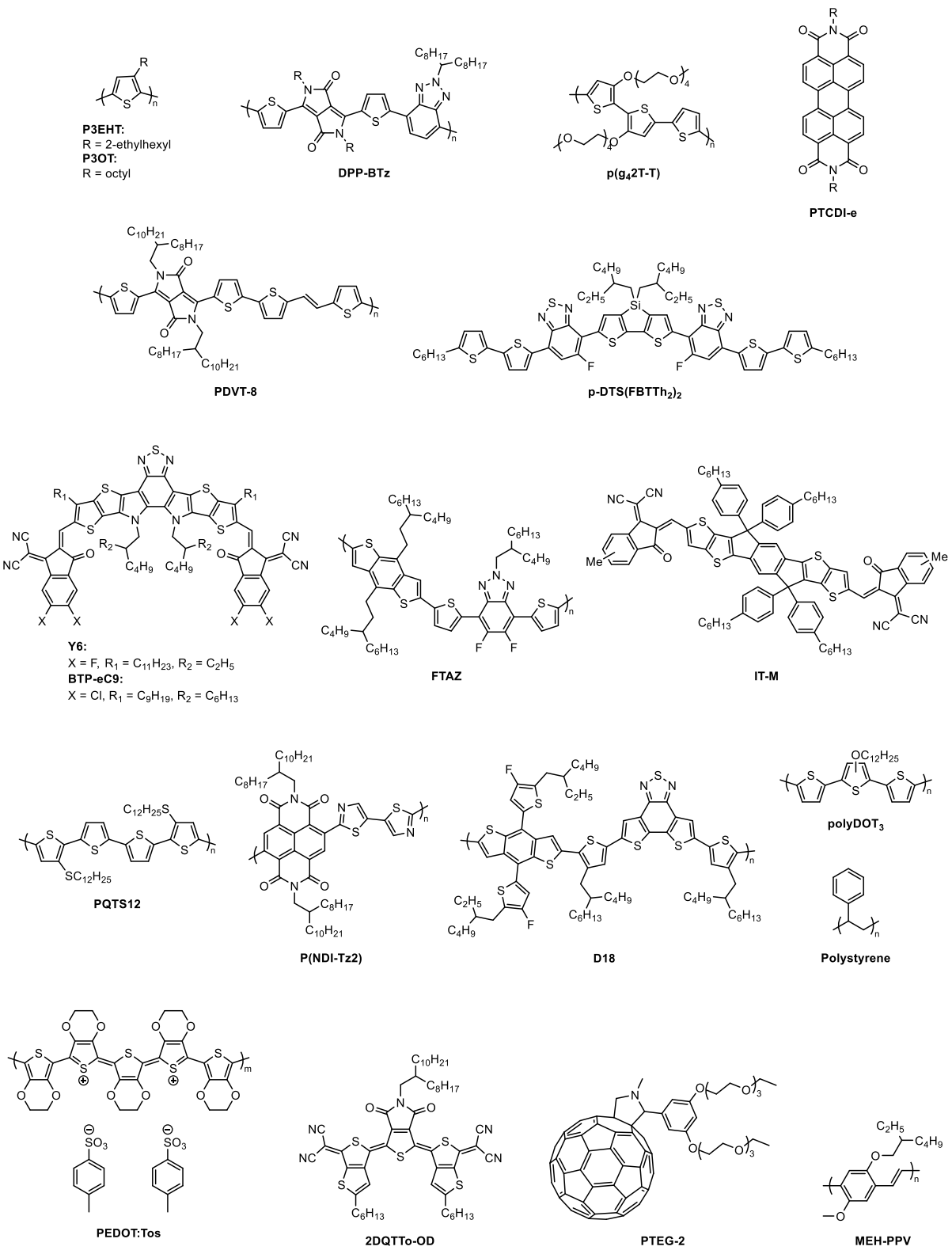

Figure S1: Chemical structure of OSCs mentioned in the main text.

Dopants full names:

F_4-TCNQ: 2,3,5,6-tetra-fluoro-7,7,8,8-tetracyanoquinodimethane

Magic Blue: tris(4-bromophenyl)ammoniumyl hexachloroantimonate

EBSA: 4-ethylbenzenesulfonic acid

TAM: Triaminomethane

N-DMBI: (4-(1,3-dimethyl-2,3-dihydro-1H-benzoimidazol-2-yl)phenyl)dimethyl-amine

BF_3: boron trifluoride

F_6-TCNNQ: hexafluorotetracyanonaphthoquinodimethane

CN6-CP: hexacyano-trimethylene-cyclopropane

TBAF: tetrabutylammonium fluoride

BCF: tris(pentafluorophenyl)borane

ZnCF: bis(pentafluorophenyl)zinc

TTN: tetrathianaphthacene

BEDT-TTF: Bis(ethylenedithio)tetrathiafulvalene

BTQBT: bis(1,2,5-thiadiazolo)-p-quinobis(1,3-dithiole)

$(RuCp^*mes)_2$: pentamethylcyclopentadienyl mesitylene ruthenium dimer

$Mo(tfd)_3$: Molybdenum tris-[1,2-bis(trifluoromethyl)ethane-1,2-dithiolene]

$Mo(tfd\text{-}CO_2Me)_3$: Molybdenum tris(1-(methoxycarbonyl)-2-(trifluoromethyl)ethane-1,2-dithiolene)

$Mo(tfd\text{-}COCF_3)_3$: Molybdenum tris[1-(trifluoroethanoyl)-2-(trifluoromethyl) ethane-1,2-dithiolene]

$Cr_2(hpp)_4$: tetrakis(1,3,4,6,7,8- hexahydro-2H-pyrimido[1,2-a]pyrimidinato)dichromium (II)

$W_2(hpp)_4$: tetrakis(1,3,4,6,7,8- hexahydro-2H-pyrimido[1,2-a]pyrimidinato)ditungsten (II)

$Ru(terpy)_2$: bis(2,2':6',2"-terpyridine)ruthenium

$Ru(t\text{-}but\text{-}terpy)_2$: bis(4,4',4"-tri-tert-butyl-2,2':6',2"-terpyridine)ruthenium

$CoCp_2$: bis(cyclopentadienyl)cobalt(II)

$Rh(C_5HPh_4)_2$: bis(tetraphenylcyclopentadienyl)rhodium(II)

BF_3: Boron trifluoride

$AlMe_3$: Trimethylaluminium

BBr_3: Boron tribromide

TBAOH: tetrabutyl ammonium hydroxide

TMCN3-CP: trimethyl 2,2',2"-(cyclopropane-1,2,3-triylidene)-tris(cyanoacetate)

PEI: polyethylenimine

BBL: poly(benzoimidazobenzophenanthroline)

TDAE: tetrakis(dimethylamino)ethylene

DMBI-BDZC: (12a,18a)-5,6,12,12a,13,18,18a,19-octahydro-5,6-dimethyl-13,18[1′,2′]-benzenobisbenzimidazo[1,2-*b*:2′,1′-*d*]benzo[*i*][2.5]benzodiazocine

DBU: amidines 1,8-diazabicyclo[5.4.0]undec-7-ene

DBN: diazabicyclo(5.3.0)non-5-ene

TBD: 1,5,7-triazabicyclo[4.4.0]dec-5-ene

DQ: diquat

BV: benzyl viologen

NHC: N-heterocyclic carbine

DMImC: 1,3-dimethylimidazolium-2-carboxylate

TPFB: tetrakis(pentafluorophenyl)borate

TrTPFB: trityl tetrakis(pentafluorophenyl) borate

DDB: Dodecaborane

PTPADT-SO_3Na: poly(4-(3′-sulfonatepropoxy-phenyl)bis(4-phenyl)amine-alt-2,2′-bithiophen) sodium

CPDT-BT: cyclopenta-[2,1-b;3,4-b′]-dithiophene-*alt*-4,7-(2,1,3-benzothiadiazole)

FPI: fulleropyrrolidinium iodide

BDOPV: benzodifurandione-centered oligo(p-phenylene vinylene)

TmPyPB: 3,3′-(5′-(3-(pyridin-3-yl)phenyl)-[1,1′:3′,1″-terphenyl]-3,3″-diyl)dipyridine

$NOSbF_6$: Nitrosonium hexafluoroantimonate

EBSA: 4-ethylbenzenesulfonic acid

EBSAc: EBSA capped with an *o*-nitrobenzyl capping moiety

DBSA: dodecylbenzenesulfonic acid

CSA: camphorsulfonic acid

DMDBS: 1,3:2,4-bis(3,4-dimethylbenzylidene)sorbitol

TFP: tetrafluorophthalonitrile

OFN: octafluoronaphthalene

TTF: Tetrathiafulvalene

TMTSF: tetramethyltetraselenafulvalene

DDQ: 2,3-dichloro-5,6-dicyano-1,4-benzoquinone

TMA: 3-(trimethoxysilyl)propan-1-amine

TEDA: *N*-(3-(triethoxysilyl)propyl)ethane-1,2-diamine)

CsF: Cesium fluoride

$TBAPF_6$: tetrabutylammonium hexafluorophosphate

BSA: benzenesulfonic acid

TTF-TCNQ: tetrathiafulvalene-tetracyanoquinodimethane

N-DPBI: 4-(1,3-dimethyl-2,3-dihydro-1H-benzoimidazol-2-yl)-N,N-diphenylaniline

o-MeO-DMBI: 2-(2-Methoxyphenyl)-1,3-dimethyl-1H-benzoimidazol-3-ium

Organic Semiconductors full names:

P3HT: poly(3-hexylthiophene)

4T: quaterthiophene

PBTTT: poly[2,5-bis(3-alkylthiophen-2-yl)thieno(3,2-b)thiophene]

PPV: poly(p-phenylene vinylene)

PCPDTPT: Poly[2,6-(4,4-bis-(2-ethylhexyl)-4H-cyclopenta [2,1-b;3,4-b′]dithiophene)-alt-4,7(2,1,3-benzothiadiazole)]

PCPDTBT: Poly[2,6-(4,4-bis-(2-ethylhexyl)-4H-cyclopenta [2,1-b;3,4-b′]dithiophene)-alt-4,7(2,1,3-benzothiadiazole)]

NDI: naphthalenediimide

C_{60}: Fullerene-C_{60}

p($g_4$2T-TT): poly(3,3'-bis(tetraethylene glycol methyl)-2,2'-dithiophene-thienothiophene)

p($g_4$2T-T): poly(3,3'-bis(tetraethylene glycol methyl)-2,2'-dithiophene-thiophene)

α-NPD: 2,2′-Dimethyl-*N,N′*-di-[(1-naphthyl)-*N,N′*-diphenyl]-1,1′-biphenyl-4,4′-diamine

PDPP(6-DO)$_2$TT: poly[3,6-(dithiophene-2-yl)-2,5-di(6-dodecyloctadecyl)pyrrolo[3,4-c]pyrrole-1,4-dione-alt-thieno[3,2-b]thiophene]

PCBM: [6,6]-Phenyl C_{61} butyric acid methyl ester

diF-TESADT: 2,8-Difluoro-5,11-bis(triethylsilylethynyl)anthradithiophene

TIPS-pentacene: 6,13-Bis(triisopropylsilylethynyl)pentacene

C_{16}IDT-BT: indacenodithiophene-co-benzothiadiazole with copo- lymer with hexadecyl alkyl chains

PFPT: poly-fluorene-pyridylthiadiazole

C_8-BTBT: 2,7-Dioctyl[1]benzothieno[3,2-b][1]benzothiophene

P(NDI2OD-T2): Poly{[N,N′-bis(2-octyldodecyl)-naphthalene-1,4,5,8-bis(dicarboximide)-2,6-diyl]-alt-5,5′-(2,2′-bithiophene)}

DCV-DPPTT: dicyanovinyl- dipyrrolo[3,4-c]pyrrole-1,4-iylidene)bis(thieno[3,2b]thiophene

ClBDPPV: Poly[[5-chloro-1,2-dihydro-1-(4-octadecyldocosyl)-2-oxo-3H-indol-6-yl-3-ylidene]-(1E)-1,2-ethenediyl[5-chloro-1,2-dihydro-1-(4-octadecyldocosyl)-2-oxo-3H-indol-6-yl-3-ylidene][2,6-dioxobenzo[1,2-b:4,5-b']difuran-3,7(2H,6H)-diylidene]]

F8Py: Poly[(9,9-dioctylfluorenyl-2,7-diyl)-alt-(2,6-pyridine)]

PTAA: Poly[bis(4-phenyl)(2,4,6-trimethylphenyl)amine], Poly(triaryl amine)

PBDB-TF: Poly[(2,6-(4,8-bis(5-(2-ethylhexyl-3-fluoro)thiophen-2-yl)-benzo[1,2-b:4,5-b']dithiophene))-alt-(5,5-(1',3'-di-2-thienyl-5',7'-bis(2-ethylhexyl)benzo[1',2'-c:4',5'-c']dithiophene-4,8-dione)]

IT-4F: 3,9-bis(2-methylene-((3-(1,1-dicyanomethylene)-6,7-difluoro)-indanone))-5,5,11,11-tetrakis(4-hexylphenyl)-dithieno[2,3-d:2',3'-d']-s-indaceno[1,2-b:5,6-b']dithiophene

BBL: Poly(benzimidazobenzophenanthroline)

PTEG-1: triethylene glycol monoethyl ether fulleropyrrolidine

P3EHT: poly(3-(2′-ethyl)hexylthiophene)

DPP-BTz: poly[[2,5-bis(2-octadecyl)-2,3,5,6-tetrahydro-3,6-diketopyrrolo[3,4-*c*]pyrrole-1,4-diyl]-alt-(2-octylnonyl)-2,1,3-benzotriazole]

P3OT: Poly(3-octylthiophene-2,5-diyl)

PEDOT:PSS: poly(3,4-ethylenedioxythiophene) polystyrene sulfonate

DPPTTT: Poly[2,5-(2-octyldodecyl)-3,6-diketopyrrolopyrrole-alt-5,5-(2,5-di(thien-2-yl)thieno [3,2-b]thiophene)]

p-DTS(FBTTh$_2$)$_2$: 7,7′-[4,4-Bis(2-ethylhexyl)-4*H*-silolo[3,2-*b*:4,5-*b*′]dithiophene-2,6-diyl]bis[6-fluoro-4-(5′-hexyl-[2,2′-bithiophen]-5-yl)benzo[*c*][1,2,5]thiadiazole]

FBDPPV: Poly[[7-fluoro-1,2-dihydro-1-(4-octadecyldocosyl)-2-oxo-3H-indol-6-yl-3-ylidene]-(1E)-1,2-ethenediyl[7-fluoro-1,2-dihydro-1-(4-octadecyldocosyl)-2-oxo-3H-indol-6-yl-3-ylidene](2,6-dioxobenzo[1,2-b:4,5-b']difuran-3,7(2H,6H)-diylidene)]

PQTS12: poly(bisdodecylthioquaterthiophene)

PTCDI-e: N,N′-di((Z)-9-octadecene)-3,4,9,10-perylene tetracarboxylic diimide

Y6: 2,2'-((2Z,2'Z)-((12,13-bis(2-ethylhexyl)-3,9-diundecyl-12,13-dihydro-[1,2,5]thiadiazolo[3,4-e]thieno[2",3'':4',5']thieno[2',3':4,5]pyrrolo[3,2-g]thieno[2',3':4,5]thieno[3,2-b]indole-2,10-diyl)bis(methanylylidene))bis(5,6-difluoro-3-oxo-2,3-dihydro-1H-indene-2,1-diylidene))dimalononitrile

IT-M: 3,9-bis(2-methylene-((3-(1,1-dicyanomethylene)-6/7-methyl)-indanone))-5,5,11,11-tetrakis(4-hexylphenyl)-dithieno[2,3-d:2',3'-d']-s-indaceno[1,2-b:5,6-b']dithiophene

P(NDI-Tz2): Poly{[N,N′-bis(2-octyldodecyl)-naphthalene-1,4,5,8-bis(dicarboximide)-2,6-diyl]-alt-5,5′-(2,2′-bithiazole)}

BTP-eC9: 2,2'-[[12,13-Bis(2-butyloctyl)-12,13-dihydro-3,9-dinonylbisthieno[2",3":4',5']thieno[2',3':4,5]pyrrolo[3,2-e:2',3'-g][2,1,3]benzothiadiazole-2,10-diyl]bis[methylidyne(5,6-chloro-3-oxo-1H-indene-2,1(3H)-diylidene)]]bis[propanedinitrile]

polyDOT3: poly(β'-dodecyloxy-α,α',-α',α''terthienyl)

MEH-PPV: Poly[2-methoxy-5-(2-ethylhexyloxy)-1,4-phenylenevinylene]

BTP: dithieno[2′′′,3′′′:4′,5′]thieno[2′,3′:4,5]pyrrolo[3,2-*e*:2′,3′-*g*][2,1,3]benzothiadiazole

BO: 2-bultyloctyl